PFC/RR-96-4

Enhanced Probabilistic Decision Analysis for Radiological Confinement Barriers in Tokamak Reactors

Ruxandra P. Golinescu and Mujid S. Kazimi

June 1996

Plasma Fusion Center
Massachusetts Institute of Technology
Cambridge, MA 02139

This work was supported by the U.S. Department of Energy Contract No. DOE-FC02-93-ER-54186.

Enhanced Probabilistic Decision Analysis for Radiological Confinement Barriers in Tokamak Reactors

by

Ruxandra Paula Golinescu

M.S. Electric Power Engineering, Polytechnic Institute of Bucharest, 1988
M.S. Nuclear Engineering, Massachusetts Institute of Technology, 1994

SUBMITTED TO THE DEPARTMENT OF NUCLEAR ENGINEERING IN PARTIAL FULFILLMENT OF THE REQUIREMENTS FOR THE DEGREE OF

DOCTOR OF PHILOSOPHY IN NUCLEAR ENGINEERING
AT THE
MASSACHUSETTS INSTITUTE OF TECHNOLOGY

MAY 1996

Signature of Author: _____
Department of Nuclear Engineering
May 3, 1996

Certified by: _____
Mujid S. Kazimi
Professor of Nuclear Engineering
Thesis Supervisor

Certified by: _____
George Apostolakis
Professor of Nuclear Engineering
Thesis Reader

Accepted by: _____
Jeffrey P. Freidberg
Professor of Nuclear Engineering
Chairman, Committee for Graduate Students

Abstract

Fusion tokamak reactors might become a valuable source of energy for the future if experiments prove that commercial operation is possible under profitable conditions. Safety considerations would also play an important role in future decisions regarding fusion power. Abnormal events can lead to radioactive releases to the environment, and those have to be addressed by designing a confinement strategy. To ensure a defense-in-depth approach, several confinement barriers surrounding the process systems are to be employed.

The objective of the present research project is to develop a methodology using probabilistic risk assessment techniques for evaluating the performance of the design of the radiological confinement barriers of tokamak fusion reactors within the context of a limited allowable risk. Thus, accident sequence models are developed for each of the confinement barriers whose performance should be evaluated. The undesired consequences at each step are radioactive releases from the corresponding confinement barrier.

The first step is to describe the conceivable accident sequences that might lead to failure of the first confinement barrier through various failure modes. Each accident sequence is characterized by a pair of parameters consisting of an annual frequency and a radioactive release. The second step is to continue the branches where the first confinement barrier has failed with accident sequences for the second confinement barrier. These latter accident sequences will end with events expressed in terms of the second confinement barrier failure modes.

A new approach is used in this work for the development of the accident sequences. Combined influence diagram/event tree models are developed instead of the reliance on event trees alone, which is the traditional probabilistic risk assessment tool. This way conditional events and probabilities can be explicitly defined in the influence diagram, which also contains all the frequency, probability and consequence data, while the time sequence is represented in the event tree. Thus, more compact system models are obtained, rather than the usual very large event trees.

A challenge was to find an appropriate form to express the results of the accident sequences analysis for each barrier in a meaningful way that allows comparison of the results to a design requirement for limiting the releases. A complementary cumulative frequency of radioactive releases is proposed, because it takes into considerations important criteria such as: the overall plant risk, the rate at which accident frequency decreases with increasing accident consequences (risk aversion attitude), and the impact of high frequency-low consequence accidents from a public policy stand point.

The International Thermonuclear Experimental Reactor (ITER) was used as a reference design. The Design Description Documents as published in June 1995 contain the confinement strategy analyzed in this project. The current ITER design requirements set radioactive release and dose limits for individual event sequences grouped in categories by frequency. We argue that this form presents drawbacks such as not considering a limit on the plant overall risk, and the difficulty of accounting for event uncertainties in both frequency and consequence. Thus, an analytical form for a limit line is derived having the form of a complementary cumulative frequency of radioactive releases to the environment satisfying the three criteria mentioned above.

After building and analyzing the models for the first and second confinement barriers of ITER, we concluded that a third confinement barrier may be required in order to comply with restrictive design limits on radioactive releases, particularly for events with large uncertainties. However, confidence in this result needs to be gained by improving the failure probability data. A database containing the failure probabilities (conditional or independent) corresponding to various systems failure modes was developed based on the available references, but a comprehensive fault tree analysis was not performed as part of this work.

Finally, a decision model using multi-attribute utility function theory was constructed to help with choosing the type of the ITER tokamak building (the third barrier). Besides safety of the design, other attributes such as construction cost, project completion time, public attitude and technical feasibility were considered. The decision model allows for performing sensitivity analysis on relevant parameters, and for design features of new options for the ITER tokamak building.

Acknowledgments

This report is based on the thesis submitted by the first author to the Department of Nuclear Engineering as part of the requirements of the degree of Doctor of Philosophy at the Massachusetts Institute of Technology. The thesis can be obtained upon request from the MIT libraries.

We gratefully acknowledge the contribution to the thesis by providing valuable information by Lee Cadwallader from INEL, David Petti from EG&G Inc., Steven Piet from ITER-Co-Center in San Diego. Also, the discussions related to safety issues and accident sequences with Andre Poucet from ITER-Co-Center in San Diego and Juergen Raeder from ITER-Co-Center in Garching were very helpful in our work. Dr. Ronald Parker facilitated the opportunity for the first author to spend a month during the summer of 1995 at the ITER Garching Joint Work Site. We appreciate the support provided by the Office of Fusion Energy of the Department of Energy.

The first author would like to thank for the interest in this research project of the following students: Florinel Morosan, Kathryn Hautanen, Boris Lekakh.

Table of Contents

List of Figures

List of Tables

1. Introduction

Fusion, a source of nuclear energy, may become an immense energy resource if the requisite scientific and engineering advances to obtain more energy than required to produce such reaction can be achieved. The temperatures required for controlled thermonuclear fusion are far too large to allow containment by material structures. One major confinement method would employ magnetic fields to hold nuclei in an evacuated space as they undergo the fusion reaction. One type of fusion reactor using magnetic confinement is the tokamak. The nature of the tokamak is well described by this word of Russian origin, roughly translates as: TO - toroidal, KA - chamber, MAK - magnetic.

The potential safety and environmental concerns for tokamaks appear to be of lesser magnitude than those for fission systems. Specific advantages may include lower radionuclide inventory and relative biological hazard, reduced hazard from long-lived wastes, low decay heat, minimal material safeguards requirements.

For tokamaks to be an attractive power solution, a number of issues must be addressed adequately, such as tritium escape in water (as HTO) or air (as HT), activation of materials in plasma chamber, and strong magnetic fields.

This work presents a probabilistic methodology that allows the evaluation of the performance of the radiological confinement barriers for a tokamak reactor. The confinement must function during tokamak operation, maintenance and accidents. A probabilistic approach allows for consideration of all conceivable accidents that can affect the integrity of the confinement barriers. While it is true that a database for frequencies and consequences for fusion reactors is not yet developed, our probabilistic model can be used for sensitivity analysis of various design parameters. Information developed in the analysis could help in making decisions about the allocation of resources for safety improvements. The fusion plant models developed in the assessment provide a basis for evaluating alternative changes to improve safety.

1.1 Background

The two major motivations for developing fusion energy are the potential to be environmentally better than the competition and the potential to secure a virtually unlimited future energy source. In the early stages of development of fusion systems, safety and environmental impact evaluations are somewhat difficult to make. However, they are very useful in directing the design process toward minimizing potential vulnerabilities. To better understand the safety issues of a tokamak reactor, a concise conceptual design presentation is given.

The conceptual reactor for deuterium - tritium (DT) fusion would require features such as: first wall, blanket, shielding, and superconducting magnets. The first wall encloses the plasma-containing

vacuum chamber and absorbs up to 20% of the fusion reaction energy. The moderating-blanket region provides necessary space for tritium breeding with lithium, and absorbs 70% of the fusion energy. It also moderates and reflects neutrons to enhance the breeding of tritium. The shield of iron, lead and probably boron is designed to protect the superconducting magnets and operating personnel from the effects of electromagnetic radiation and neutrons. The magnets must be superconducting to avoid excessive power requirements. Other necessary systems include those for fueling, neutral beam or other heating method, tritium removal and recycle, and conversion of fusion energy to electrical energy.

There would be tremendous temperature differences in tokamak reactors: the extremes of 10^8 K in the DT plasma and 4 K required in the superconducting magnets would present many difficult problems of thermal insulation.

An important research area in fusion reactors is related to the first wall: if plasma interactions lead to vaporization of the first wall, impurities are introduced which have the effect of cooling the plasma and reducing reaction efficiency. Damage and activation of the wall by DT neutrons[1] are also of concern. Selection of first wall material is thus quite important as are design provisions for effective remote repair and maintenance operations.

The basic tokamak houses low fusion energy per unit volume, hence the size must be relatively large. The tokamak devices in operation around the world represent much of the effort toward controlled nuclear fusion. There are a variety of large machines, none of which has yet satisfied the Lawson break-even criterion[2], although certain reactors have achieved one parameter. Many of the devices have not used a DT fuel mixture. However, valuable experience has been gained in system design and operation.

The major drawbacks of the tokamaks are the large size (1000 to 1500 MWe) and the enormous associated capital cost. Because small prototype units are not feasible for physics, a full - scale reactor must be built from non - power - machine experience.

The Tokamak Fusion Test Reactor (TFTR) at Princeton has reached some of the highest temperatures and $n\tau$ values, but not at the same time. TFTR operated on DT for a relatively small number of pulses.

Tore-Supra at Cadarache in France was the first tokamak to use superconducting magnets. The Soviet Union's T-15 followed with superconducting magnets of a different design.

The Doublet III at GA Technologies has achieved high enough plasma pressure for a fusion reactor. Other US tokamak projects include the Advanced Toroidal Facility at Oak Ridge and Alcator C-Mod at MIT.

---

[1] D + T -> He + n

[2] 'Break-even' concept refers to plasma producing as much energy as it consumes. The Lawson criterion for DT plasma break-even requires: T = 8.6 keV ≡ 10^8 K, and $n\tau \equiv 10^{20}$ m^3s, for plasma temperature T, particle density n, and confinement time τ.

The largest fusion machine in the world is the European Economic Community's (EEC) Joint European Torus (JET) at Culham, England. JET has come closest to break-even, and expects to surpass it and to approach ignition[3].

Japan's JT-60 is being used to demonstrate heating concepts. The follow-on Fusion Experimental Reactor (FER) is likely to have similar aims to those of JET.

The Next European Tokamak (NET), planned as a successor to JET, is intended to achieve ignited plasmas routinely and for extended periods (i.e., several minutes). It is also expected to develop and demonstrate fusion reactor technology for superconducting magnets, first wall materials, and a lithium - compound blanket to produce tritium and absorb energy.

The International Thermonuclear Experimental Reactor (ITER) has been planned as a joint project of the EEC, United States, Russian Federation, and Japan under auspices of the IAEA. The overall system is 30 meters high and 30 meters in diameter with a plasma major radius of 8.14 meters, which would make ITER the largest tokamak in the world.

Construction and siting requirements for fusion reactors are expected to be somewhat similar to those for fission systems. Ultimately, regulatory officials will decide what is an acceptable radioactivity confinement for any fusion facility and how much credit it has for reducing postulated public doses. Reference [1-1] gives a survey of existing regulatory documents that refer to fusion facilities.

For fusion to fulfill its goals and become an economical and publicly acceptable major source of energy in the future, the reliable and safe operation of future fusion devices must be proven along with the technical feasibility. At the present time, the design of fusion systems involve large uncertainties about their reliability. Reliability and safety considerations need to be incorporated into the design of fusion machines during all phases of the design. Design decisions should be based on an overall design concept and be reviewed continuously as more detailed information becomes available.

1.2 Objective

The objective of this research project is to develop a methodology using probabilistic risk assessment techniques for evaluating the performance of the radiological confinement barriers of tokamak fusion reactors. Confinement system in this work refers to the confinement structures, as well as the systems designed to mitigate the consequences of accidents, limit the challenge to confinement integrity, reduce the amount of radioactivity available for release, and the systems designed to render the containment spaces habitable.

Functional considerations for selecting a confinement configuration require that the confinement must retain structural integrity and acceptable leak tightness during normal operation,

[3] Ignition refers to self-sustaining hot plasma.

anticipated transients, and design basis and severe accidents, such that the releases to the environment meet the design requirements and safety goals. These considerations require that appropriate pressures and temperatures be selected, and that care be taken to prevent containment leakage or bypass. This can be achieved by proper selection of the design of the penetrations, the confinement isolation system, and the systems required to remove energy released in containment and prevent reaching high values of pressures and temperatures that could cause containment failures. The above translates into consideration of:

- design and ultimate pressure capacity at the corresponding temperature;
- material control (material selection and corrosion protection);
- leakage control (e.g., leakage monitoring);
- penetration design for isolation and minimal leakage under accident conditions, including material selection;
- confinement cooling system design;
- behavior under severe external events (particularly for the last confinement barrier).

The assurance of proper functioning is also achieved by assessing the ability of the confinement systems to perform their intended function in an acceptable manner under a set of unlikely sequence of events.

Probabilistic methods, correlated with deterministic ones, are more appropriate for analyzing a first-of-a-kind design such as a fusion reactor, since they are more able to encompass the multiple uncertainties in parameters and phenomena than the deterministic methods alone could do. In a deterministic approach, consequences are postulated and compared to an upper limit, but the accident mechanism is not always identified and the likelihood of the accident is not estimated. In the probabilistic approach, accident mechanisms are postulated and both the likelihood and consequences are estimated, usually quantified, to provide a measure of total expected risk.

Probabilistic Risk Assessment (PRA) has been successfully used to analyze the risk associated with different nuclear power plant designs. Most PRA studies are performed on plants that are already built and modifications recommended by the PRA studies are generally difficult to make. However, PRA can be effectively incorporated at an earlier stage in the design process. First, qualitative insights gained from previous PRAs are important to the designer. These point out the strengths and weaknesses of existing designs and thus help him direct his efforts. Such qualitative information can be provided at an early stage in the design process. Second, PRA can be used as an interactive quantitative tool for evaluation during design process. By providing a rapid feedback on design performance, the quantitative results of a PRA can be input in overall decision process. Reference [1-2] gives an overview of how to incorporate safety and economical considerations into design decision making. The approach is a risk-based design, suggesting PRA as the basis for decision making in order to enhance fusion safety and plant availability, and for developing a method to compare design options.

PRA is an analytical methodology that identifies and delineates the combinations of events that, if they occurred, would lead to an accident and estimates the frequency of occurrence for each combination of events, and then estimates the consequences. This method involves the development of models of the system, databases giving component failure rates, and baselines of the dominant risk sequences. Generally, three categories of systems or processes are targeted: changes in the hardware of the system, changes in the normal operations of the system, and changes in the off-normal operations of the system.

Although not generally established as legal standards, several countries are moving in the direction of limiting accident probabilistic risk[4]. To the extent that regulatory officials can judge on the basis of risk instead of maximum accidents, the overall effectiveness of design actions to protect against conceivable accidents might be enhanced as effort is concentrated on actually reducing accident risk, rather than concentrating on highly improbable or even inconceivable events.

The goal of this work is to use PRA tools to develop a model that can be used to study the behavior of the radioactivity confinement barriers in tokamak reactors, by evaluating the compliance with the design requirements. The model should:

- consider all the conceivable accident scenarios;
- allow for implementation of design modifications and comparison of different designs of each confinement barrier;
- estimate the number of confinement barriers needed to comply with the design guidelines.

A design guideline for radioactivity releases as consequences of individual accident sequences with the corresponding frequencies is also proposed in the present study. Approaches similar to the Farmer limit line [3-12] have been commonly used, but they do not include important considerations such as overall risk and uncertainties in both frequency and consequence of accident sequences. Previous work showed that the regulation of risk from technological systems should take into account several aspects of risk: overall risk, the rate at which accident frequency decreases with increasing consequences, the impact of high frequency - low consequence accidents. The present study contains a rigorous derivation of a parametric complementary cumulative frequency (CCF) for ITER which complies with all of these requirements. Moreover, CCF allows for the treatment of uncertainties in accident frequencies and consequences unlike the Farmer limit line approach. Therefore, defining the ITER risk limit in a CCF form is more appropriate than the current formulation of the limit line. Chapter 3 contains more details regarding this matter.

An ongoing debate in the ITER safety community is role of the tokamak building as a third confinement barrier. Because it is a very large building, it would be too costly to design it at the standards of the fission power plants containment's. Different options are currently considered, and we

[4] The probabilistic risk is a controversial concept, and will be more thoroughly discussed in Chapter 3.

believe that a decision model considering different attributes such as risk, cost, technical feasibility etc. would provide a useful structures for the decision makers. Such a model is developed in Chapter 8.

1.3 Scope

The International Thermonuclear Experimental Reactor (ITER) is the baseline design considered for developing our model. An important objective of ITER is to demonstrate the potential for safe and environmentally acceptable operation of a power producing fusion reactor. ITER will be by far the largest source of information on which to base the design of subsequent fusion reactors. The ITER major design parameters are given in Table 1-1.

ITER must follow the nuclear regulations of the country which will host the construction site. The country is not decided at this time. Regulatory approval is required before construction, therefore ITER should be designed with a robust safety envelope in order to consider national differences and uncertainties. In order to reflect these requirements in the engineering design, first safety design guidelines should be proposed at an early stage of the design. Due to the fact that large uncertainties exist in the fusion reactor conditions, a probabilistic approach seems to be more suitable for analyzing a particular design.

Underlying the development and implementation of the ITER safety design approach are the following general principles [1-3]:

- make maximum use of the inherent favorable safety characteristics of fusion;
- meet dose/release limits based on International Commission on Radiological Protection (ICRP) and International Atomic Energy Agency (IAEA), and further reduce releases and doses to the public and site personnel to levels as low as reasonable achievable (ALARA);
- minimize the safety role and credit taken in safety analyses and assessments for uncertain plasma physics and experimental in-vessel components.

The ITER radioactivity confinement will be an integrated system, including various confinement zones, and configuration control for each zone. Since the confinement should be as passive as possible, the recommended approach emphasizes natural forces and passive features, minimizing the need for operator or equipment action. The first priority will be the prevention of accidents through the intrinsic features of the facility, quality assurance in design, construction, operation and maintenance, and appropriate provisions for human factors and anomalous events. Safety margins and mitigative features have to be added to protect the public even against extremely rare and unforeseen events. This implies methods for confinement analysis which are suitable for severe accident loading. Severe accidents, as they are defined in the nuclear power industry, are those that result in significant reactor damage and release of radioactivity, but they have a very low probability of occurrence.

The basic approach recommended for containment/confinement of airborne tritium and activation products at ITER is the defense-in-depth strategy which involves the use of multiple barriers.

By ensuring that there are three successive envelopes which have to be breached before radioactivity can be released to the environment, the probability that all three will be unavailable when necessary should be acceptable small. The final (third) barrier could be the building containment.

The tritium processes should be designed to minimize the tritium inventory to the lowest practical level. In addition, process systems should be designed for independent operation to prevent cascading failure propagation. The tritium inventory should be distributed and isolated so that even if all barriers are breached, the maximum inventory released will be a small fraction of site inventory.

Confinement should be provided as close to the tritium source as possible to minimize the spread of activity and to limit the volume of atmosphere which must be monitored and possibly filtered/dried. Confinement barriers should be of sufficient number, strength , specified performance (e.g. leak tightness, decontamination factors etc.) and reliability. In the design of confinement barriers, the principles of redundancy, diversity and independence should be followed. Specifically, in the case of multiple barriers, failure of one barrier should not result in the failure of another barrier.

Chapter 2 presents a more detailed description of the ITER confinement strategy.

Table 1-1: Major Design Parameters of ITER

Nominal Fusion Power	1.5 GW
Nominal Wall Loading	1 MW/m^2
Maximum additional Heating Power	100 MW
Plasma Major Radius (R)	8.14 m
Plasma Minor Radius (a)	2.8 m
Reference Pulse Duration:	
- Inductive pulse flat-top under ignited conditions	1000 s
- Nominal repetition time	2200 s
Total Number of Pulses:	50000
- During the Basic Performance Phase	13000
- During the Enhanced Performance Phase	30000

2. ITER Radiological Confinement Strategy

ITER's operational record will be an important step in the demonstration of the environmental potential of fusion power. ITER's operation will have to involve proper control of any hazardous materials and energy sources that could lead to their releases. By providing multiple independent confinement barriers, the possible releases to the public can be reduced to acceptable limits.

2.1 Hazardous Materials

The major potentially hazardous materials in ITER are tritium, activation products, and beryllium. The first two are radioactive, while beryllium is a chemically toxic material.

Tritium is present in a fusion reactor in the fuel for deuterium-tritium (DT) reactions as sources of thermal energy:

$$^{2}_{1}D+^{3}_{1}T\rightarrow^{4}_{2}He+^{1}_{0}n+17.6\,MeV \qquad (2\text{-}1)$$

Tritium is the most mobile of the ITER radioactive sources, and requires special handling and confinement procedures to prevent it escape. The total tritium inventory on the site may be up to 4 kg (5 kg if carbon is used), which represents an order of magnitude larger inventory than the previous fusion related installations. However, there is also considerable non-fusion related experience, for example, in CANDU reactors, where inventories of similar magnitude are safely handled.

Tritium is active radioactively emitting a weak beta particle with a half-life of 12.3 years. The biological hazard of tritium strongly depends upon its chemical form. Both the gaseous elemental and the oxide form will be present in a fusion reactor. The gaseous elemental forms of tritium (HT, DT or T_2) are relatively difficult to contain and can permeate through most materials. This provides a path for tritium to enter the first wall/divertor coolant streams, where it is converted to the oxide form, whose escape via coolant leaks must be controlled. The oxide form (HTO, DTO, or T_2O) or organic forms of tritium are approximately 10,000 times more hazardous than the elemental form, per gram of tritium taken into the body. The oxide form is readily assimilated and distributed throughout the human body water, while the elemental form is not. The biological half-life of oxidized tritium in the human body is about 10 days and can be reduced by increasing the normal fluid intake.

One significant difference between the fusion and fission reactors is that the fusion fuel is not contained in a compact reactor core, but the tritium is spread among various systems, some of them even in different buildings, and it flows between systems. The hazard is determined by the size of inventory, the extent it can be mobilized, and the chemical form. With the exception of much of the

tritium in plasma facing components and storage, most of the inventories are mobilizable. Figure 2-1 shows the location of major tritium inventories and tritium flows.

The activation products are the result of the interaction of neutrons with high energies - 14.1 MeV from the DT fusion reaction with the structural materials of plasma facing components, and vacuum vessel. It is important to note that the amount and the nature of the activation products is determined by the structural materials that ITER will use. The activation products will produce an intense radioactive field inside the cryostat and vacuum vessel, leading to the requirement for remote maintenance for systems and components inside these structures.

The majority of activation products will be bound in solid metal structures of the in-vessel components. Smaller inventories will be found in structures outside the vacuum vessel or circulating as corrosion products in first wall, blanket, and divertor coolant streams. Some could also be generated in air inside the tokamak building by neutrons streaming through penetrations.

Beryllium might be used as a coating or tiles for the plasma facing components of ITER. Beryllium is a toxic material for humans, a possible carcinogen. In the solid metallic form, beryllium pose little danger, but small particles (usually less than 10 μm) can enter the body through the respiratory tract.

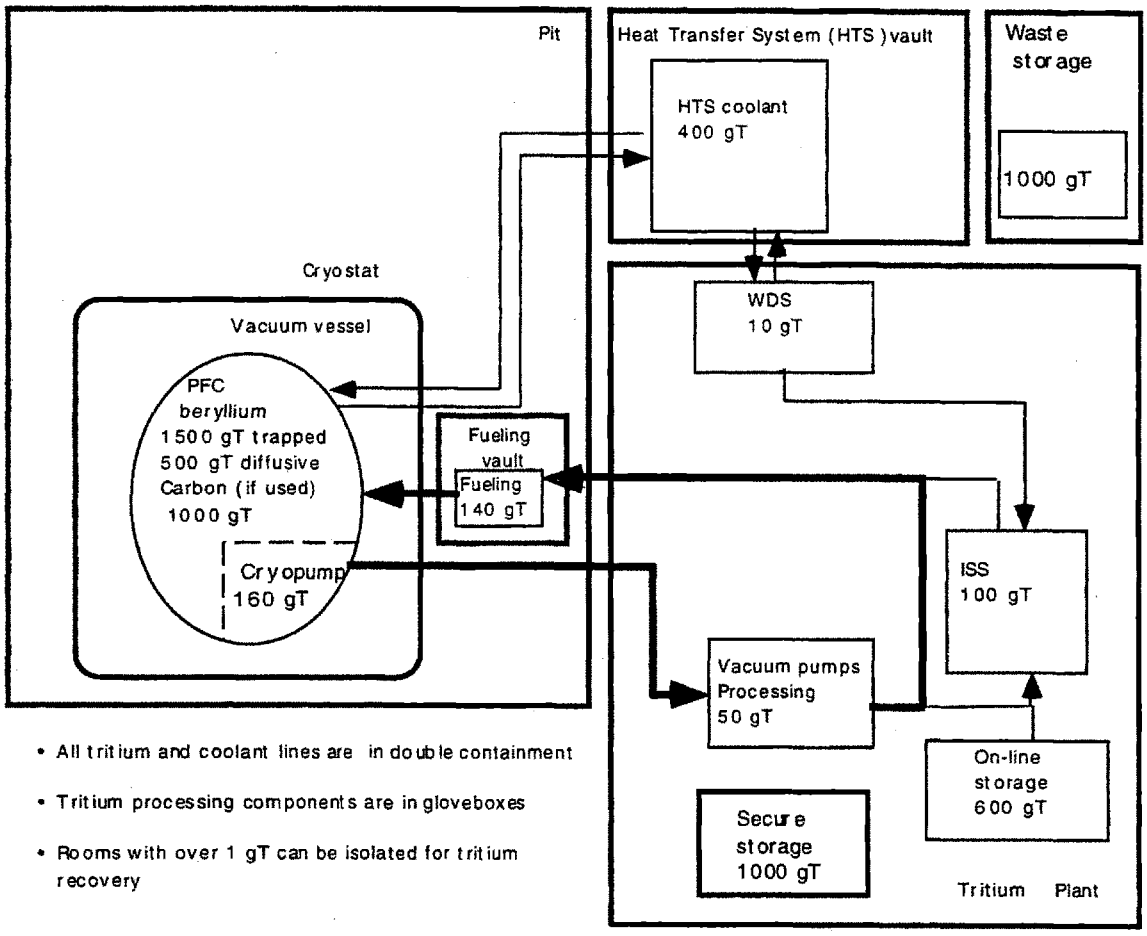

Figure 2-1: Location of Major Tritium Inventories and its Tritium Flows [2-2]

2.2 Confinement of Radioactivity

ITER's confinement design must ensure compliance with the design guideline of permissible releases.[2-3] These values are currently being formulated, and will be reviewed after site selection with respect to the environmental regulations of the country. An important safety related decision, made early in the ITER project, was to shift safety burden from experimental components and uncertainties in physics phenomena to conventional components based on well proven technology. This decision was taken to make the safety case more robust and demonstrable. In this context, it was conservatively determined not to take credit for in-vessel components (e.g. the divertor, the first wall) in formulating a safety strategy for the tokamak, but rather to emphasize confinement and control of energy sources that could damage the confinement (decay heat and fusion power). Consequently, the **major safety functions for the tokamak** are confinement, decay heat removal and plasma power shutdown.

The majority of radioactive inventories in ITER can be found in two buildings: the tokamak building and the tritium plant. Hence, one can describe the confinement strategy for these two buildings separately, since they contain different types and quantities of radioactive inventories. Here, we will only be concerned with the confinement strategy for the tokamak building; it is the one we use to develop our method. Table 2-1 and Figure 2-2 represent the confinement configuration inside the tokamak building.

The first confinement boundary includes the vacuum vessel (VV), the primary heat transport (HTS), the vacuum ports, other penetrations, and isolation valves to segregate the tokamak inventories and energy sources from the tritium plant. The second tokamak confinement boundary includes the HTS vaults, HTS guardpipes, local boxes around cryostat penetrations, the cryostat, and the NBI vaults. It shall enclose the first confinement boundary. Table 2-1 lists the first confinement barriers with the corresponding second confinement barriers enclosing them.

The tokamak building's confinement strategy is complicated because of its compartmentalization. The compartmentalization is motivated by the following:

- Experience in tritium facilities indicates that tanks, piping, gloveboxes, vaults are the way to confine tritium - not buildings.
- The inventories "at risk" differ in type and character at different locations, and the confinement barriers are tailored to each.
- The pressure sources and other threats to confinement barriers differ spatially, and the barriers are tailored to each.
- To operate, the tokamak needs two robust vacuum barriers (vacuum vessel and cryostat), and the confinement strategy makes appropriate use of each.
- Compartmentalization minimizes spread of contamination.

- Compartmentalization means that in an individual accident event sequence, only those compartments involved must operate - the rest are irrelevant.

In conclusion, one of the most important reasons that compartments are used is to segregate the radioactive inventories. Therefore, for events where there is only localized damage, then only one portion of the inventory is released.

It is interesting to note that all confinement barriers during operation have lower pressure than their surrounding volumes. In most accident sequences, this negative pressure is maintained. A large break of liquid helium from the magnet coolants would slowly pressurize the cryostat. This has no public consequences unless there is concurrent mobilization of radioactivity from a coolant line or vacuum vessel failure. However, preliminary calculations for the Non Site-specific Safety Report (NSSR) show that one coolant loop breach into the cryostat gives about 0.8 atmosphere, and the ten loop beyond design basis accident gives significantly higher pressures.[4-13]

Another issue is releasing the overpressure from water breaks. Breaks within the first confinement barrier (vacuum vessel) trigger opening of pressure relief at 0.2 MPa, leading to the suppression tank. The first confinement barrier itself is designed up to 0.5 MPa and calculations show that although 0.2 MPa is exceeded because of the finite blowdown capacity, 0.5 MPa is sufficient even for a break involving all first wall coolant systems. Breaks of the primary HTS, also part of the first confinement barrier, are surrounded by guard pipes inside the CV, and the HTS vault outside the CV. This has several advantages: the guard pipes and vault are more independent from the first barrier than is the cryostat; water blowdown pressure is routed to the vaults, away from other radioactivity sources; magnets are protected. More details about the design of the confinement barriers inside the tokamak building are presented in the following sections.

Table 2-1: Confinement Barriers in Tokamak Building

First Confinement Barriers	**Second Confinement Barriers**
Vacuum Vessel	Cryostat Vessel
Vacuum Vessel NBI[1] Penetration	Neutron Beam Cell
Vacuum Pump Ports and Isolation Valves	Guard Pipe to Tritium Plant
PHTS[2] inside the CV[3]	Guard Pipes and Cryostat Vessel
PHTS inside the HTS[4] Vaults	HTS Vaults
VV[5] Pressure Suppression Tank	Suppression Tank Vault
Diagnostics Windows Isolation Valves	Diagnostics Rooms
Vacuum Vessel Penetrations	Local Boxes

[1] NBI: Neutron Beam Injection
[2] PHTS: Primary Heat Transport System
[3] CV: Cryostat Vessel
[4] HTS: Heat Transport System
[5] VV: Vacuum Vessel

Table 2-2: ITER Design Guidelines for Releases to the Environment [2-3]

	I	II	III	IV
EVENT SEQUENCE CATEGORY	OPERATIONAL EVENTS	LIKELY SEQUENCES	UNLIKELY SEQUENCES	EXTREMELY UNLIKELY SEQUENCES
Category Description	Events and plant conditions planned and required for ITER normal operation, including some faults and events which can occur as a result of the ITER experimental nature.	Event sequences not planned but likely to occur one or more times during the life of the plant but not including category I events.	Event sequences not likely to occur during the life of the plant.	Event sequences not likely to occur during the life of the plant with a very large margin; limiting events for "design basis" (a)
Typical Annual Expected Frequency	list of operational events to be defined explicitly	$f > \sim 10^{-2}/a$	$10^{-4}/a < f < 10^{-2}/a$	$10^{-6}/a < f < 10^{-4}/a$
Release limit for HTO (b)	0.5 g-T/a (c) (not including maintenance to be defined)	1 g-T/event (1 g-T/a integrated over all Category II events)	50 g-T/event	100 g-T/event
Release limit for divertor-first wall activation products (d)	TBD (e)	0.5 g-metal /event (0.5 g /a integrated over all Category II events)	25 g-metal/event	500 g-metal/event

(a) Beyond Category IV, some hypothetical category V events with even lower frequency will be assessed for compliance with the no-evacuation goal and for reducing the associated risk, if necessary; category V events are outside the "design basis."
(b) These are release limits for design purposes, based on the dose limits in General Safety Evaluation Document (GSEDC), assuming atmospheric, elevated release. For tritium in HT form, use 10 times the values shown here. For ground level release, use 10% of the values shown here.
(c) This is a design guideline value of tritium release in routine operation, not including maintenance operation to be defined.
(d) These are release limits for design purposes for 316SS, Cu-alloy, and W at the first wall or divertor, based on the dose limits in GSEDC, assuming atmospheric elevated release. For corrosion products in in-vessel systems, use 10 times the values shown here as a temporary limit until the HTS systems are better defined and assessed. For ground level release, use 10% of the values shown here.
(e) Appropriate release limits for activation products will be estimated later.

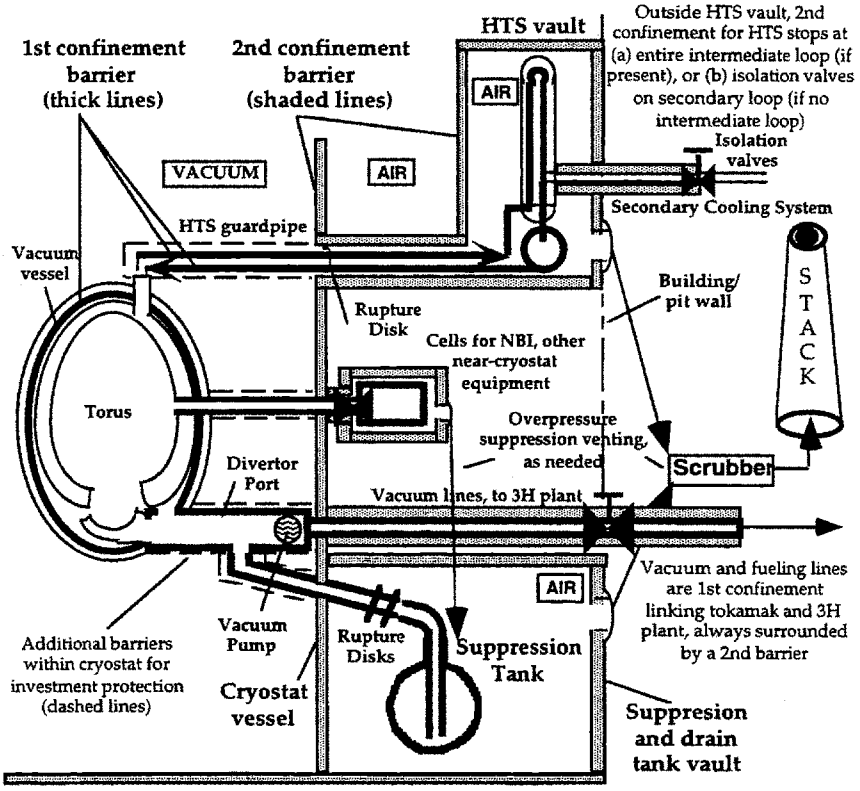

Not shown: fueling lines (similar to vacuum lines), divertor HTS lines (similar to the HTS that are shown), and ECRF/ICRF lines (which extend outside the tokamak building)

Note: most of the penetrations through the cryostat go outside the tokamak building other buildings (HTS, vacuum lines, fueling lines, ECRF, ICRF, and some diagnostics

SJP, June 1, 1995

Figure 2-2: Confinement Strategy inside Tokamak Building [2-3]

2.3 Vacuum Vessel (VV)

2.3.1 General Design Description

The Vacuum Vessel is a part of the Tokamak Basic Machine and provides the primary high vacuum and tritium boundary for the plasma. The main vessel is toroidally shaped and is located inside the cryostat. It is supported from its lower side by steel structures that pass through the cryostat to the concrete floor below. The twenty superconducting magnet toroidal field (TF) coils fit around the vessel and define the details of its outer shape and the space available for ports, supports, and utility connections. The blanket and divertor are mounted on the vessel interior and all loads are transferred through the vessel to the vessel supports. The blanket and divertor provide shielding for the vessel and all three provide shielding for the coils.

The vacuum vessel is divided toroidally into twenty sectors joined by field welding at the central plane of the ports. The vessel has twenty upper, midplane, and lower ports which are used for equipment installation and maintenance, utility feed-throughs, and vacuum pumping. The cover plates for the upper ports of the vacuum vessel are used as feed-throughs for the blanket cooling pipes, a viewing system, and diagnostics. Bellows around the blanket coolant feed-throughs must absorb differential thermal expansion between the blanket and the vacuum vessel, and withstand the high pressures resulting from off-normal conditions. The midplane ports are used for replacement of primary first wall / shield modules, test modules, the ICRF and/or ECRF systems, diagnostics, and installation of remote handling tools. The lower horizontal ports are used for replacement of divertor cassettes and vacuum pumping. Bellows are employed between the port ducts and the cryostat.

The four main sub-components of the vessel system include the main vessel, port assemblies, support structures for in-vessel components, and gravity supports.

The main vessel is made from SS 316 LN and has a double wall structure. The minimum and maximum radii of the vacuum vessel are 4.1 m and 13 m respectively, and the overall height is 14.5 m. The inner and outer shells are made of welded plates, 40 mm in thickness. The inner and outer shells and stiffening ribs between them are joined by welding, which gives the vessel the required mechanical strength. The total thickness of this structure is typically in the range of 0.45 - 0.83 m. One of the major functions of the vacuum vessel is neutron shielding, and the space between the shells will be filled with an array of plate inserts. Water flowing in the space between the plates is required to remove nuclear heat deposition of 3 - 5 MW.

The support structures are used to mechanically support the vessel, blanket, and divertor, and must withstand structural loads due to gravity, earthquakes, and induced electromagnetic loads. Each vessel sector is supported by a single support at the bottom of the sector in an area centered between the TF coils. Once the support extends below the TF coil, "A" - frame structures are used to transfer the load to the cryostat and to the cryostat supports below. The inboard and outboard blanket segments are supported from brackets attached to the inner wall of the vacuum vessel. The support

structures must withstand a large vertical force due to vertical disruption events (VDE), and allow for differential thermal expansion. The divertor cassettes are supported by two rails that extend around the bottom of the vessel.

Figure 2-3 represents one of the twenty segments of the vacuum vessel.

2.3.2 Vacuum Vessel Functions

The primary functions performed by the vacuum vessel are listed below [2-6]:

1. Provide the first confinement barrier around the radioactive materials in the plasma, the in-vessel components and the related loops, and withstand accidents without losing confinement. The VV also provides one of two barriers that separate air from hydrogen that could be generated by accidents inside the VV boundary.
2. Remove nuclear decay heat of all in-vessel components, even in conditions when the other coolants are not functioning.
3. Limit the pressure due to accidents inside the VV using a pressure suppression system (connected to the VV) which is part of the first confinement barrier.
4. Provide a boundary consistent with the generation and maintenance of a high quality vacuum, to create conditions for plasma fusion reaction.
5. Mount in-vessel components and support electromagnetic loads during plasma disruptions and vertical displacement events.
6. Together with the first wall and blanket, maintain a specified toroidal electrical resistance and contribute to plasma stability.
7. Together with the first wall, blanket, and divertor, provide adequate radiation shielding for the superconducting coils.
8. Provide access ports for in-vessel components maintenance equipment, diagnostics and plasma heating methods, and blanket test modules.

The first three functions on the above list are also the Safety Functions of the VV.

To meet its **confinement function**, the VV shall reduce the potential for the release of radioactive materials and ensure that any releases are within prescribed limits during and after operating states and within acceptable limits during and after accident conditions. The design basis for confinement barrier shall take into account all initiating events and loads due to accidents as identified by the safety analyses.

The main vessel is a first strong safety confinement barrier and must be designed to withstand the following **loads** during normal or off-normal operation without losing confinement:

- All possible combinations of internal and external pressure due to off normal conditions such as coolant (water) or cryogenic fluid leakage;
- Electromagnetic loads:

- ◊ during normal operation: experienced as a result of eddy currents in the vessel interacting with the magnetic field crossing them;
- ◊ during faults such as: control failures, power supply failures, bus opens or shorts, magnet faults;
- ◊ vertical displacement events (VDE), plasma disruptions: induced in the vessel as a result of control loss of the plasma;

- Static loads: self-weight and weight of internal components;
- Interaction loads: forces induced on the internal components, blanket back plate and divertor mounts, that are transmitted to the VV during normal or fault conditions;
- Forces applied during installation and removal of in-vessel components; forces to remove failed components may be much higher than for installation due to components deformation, welding, or seizing;
- Natural phenomena such as: seismic loads on the vessel and seismic loads transmitted to the VV from the in-vessel components; wind; floods. These are site-specific loads, and will be evaluated after choosing the ITER site;
- Thermal loads: the normal operating thermal load shall include transient thermal loads during pulsed operation as well as the temperature distribution during bakeout and wall conditioning;
- Loss of coolant loads;
- Hydrogen detonation loads;
- Site-generated missile impact loads.

The list above refers to individual loads, but consideration should be given to the possibility of having combined loads acting simultaneously on the vacuum vessel. In addition, the vacuum vessel is subject to cyclic loading during normal operation. Thermal cycling and unavoidable disruption loads are expected. Cyclic loading can be defined on load-time diagrams so that fatigue analysis can be performed.

The VV and its HTS shall **remove the heat** generated at normal fusion power and, according to its safety function, the decay heat released after operational states (including off-normal burn conditions) and accidents. Heat removal should be as passive as possible. It is suggested to design the HTS to allow for removal of the decay heat by natural coolant circulation.

During normal operation, the total heat deposition in the vacuum vessel is 3 MW with a maximum nuclear heating rate of ~0.04 MW/m^3. The heat load on the vessel due to the decay heat from all in-vessel systems is even higher at 5 MW. The vacuum vessel heat transfer fluid is water for both cooling and baking. The coolant enters through the wall of the divertor port and flows around the vessel and finally exits at a point near the coolant entrance. This design allows all vessel cooling piping to be located on the outside of the cryostat eliminating the need for piping to be double contained and making the addition of instrumentation and leak testing systems much easier. There are two independent cooling loops (100% redundancy) each composed by ten sectors (every other one)

connected in series with a given loop. A valve in the pipe connecting adjacent sectors allows a sector to be isolated for leak testing. The main conditions of the water cooling are summarized in Table 2-3.

Table 2-3: Vacuum Vessel Cooling Parameters

State	Parameter	Value
Normal Operation	Total Heat Load	3 MW
	Maximum Heat Deposition Rate	~0.04 MW/m^3
	Coolant Flow Rate	~65 kg/s (0.065 m^3/s)
	Inlet/Outlet Temperature	~100 C / 111 C
	Coolant Velocity	~0.01 - 0.3 m/s
	Inlet/Outlet Pressure	~2.0/1.9 MPa
	Maximum Vessel Wall Temperature	~160 C
Off-Normal Operation	Total Heat Load	5 MW
	Maximum Heat Deposition Rate	~0.07 MW/m^3
	Coolant Flow Rate (natural convection)	~36 kg/s (0.36 m^3/s)
	Inlet/Outlet Temperature	~150 C / 182 C
	Coolant Velocity	~0.005 - 0.15 m/s
	Inlet/Outlet Pressure	~2.0/1.9 MPa
	Maximum Vessel Wall Temperature	~280 C
Normal Operation	Maximum Heat Up Time	~100 hr.
	Maximum Heat Deposition Rate	~0.0 MW/m^3
	Maximum Inlet Temperature	~200 C
	Inlet/Outlet Pressure	~2.5/2.4 MPa
	Maximum Vessel Wall Temperature	~200 C

During normal operation, the large variation in the flow velocity is caused by the parallel circuit design and the large change in the flow cross-section around the sector.

The **pressure suppression system** is a large tank used to limit the maximum vessel pressure during an off normal event. The connection to the vacuum vessel is by four 1 m^2 ducts located on the bottom of four divertor ports. The ducts, which lead to the suppression tank, are fitted with rupture discs which isolate the tank from the vessel during normal operation.

The vacuum vessel pressure suppression system will be similar to that of a commercial BWR suppression system. The system is foreseen as consisting of 4 relief pipes of 1 m bore, equispaced around the tokamak, which connect to the vacuum vessel at their inlet end and to the suppression tank at the outlet end. The relief pipes have rupture discs to separate the ultra high vacuum environment

inside the vacuum vessel from that of the suppression tank, which will contain water and its vapor at a saturation pressure corresponding to room temperature.

To protect the vacuum vessel and internal components from the effects of premature opening of the rupture discs when not pressure loaded, double disc assemblies are used, one at the vacuum vessel end of the relief pipe and the other at the suppression tank end (a rupture disc assembly is required at the vacuum vessel end to disconnect the relief pipe from the vacuum vessel to avoid interference with the in-vessel gas introduction system dynamics). Both these assemblies have two discs with controlled interspaces for leak monitoring. Additionally the pipe interspace between the disc assemblies is also a controlled interspace. These three interspaces will be evacuated under normal operation conditions to lower the absolute pressure at which the discs open in order the reduce the fluid inertia loading on the internal components of the suppression tank.

The internal components of the suppression tank consist of manifolds which distribute the incoming steam from the 1 m diameter relief pipes into many small bore so-called "organ" pipes, the discharge ends of which are below the free surface of the suppression water. The function of these "organ" pipes is to form a discharging steam jet of small enough diameter so that when it breaks up in the water, the resulting steam bubbles have a short enough collapse (condensation) time to maintain the pressure in the suppression tank at a value close to the prevailing water saturation value. The design is such as to limit the final water temperature, after a loss of in-vacuum coolant event, to 77°C, in line with current BWR suppression practice.

The suppression tank will have pipe connections from the water and gas spaces to the tritium plant, so that tritiated water and non-condensable gases can be routed there for processing. The portion of the suppression system outside the cryostat will be contained in a ferro-concrete cell which will form part of the radiological second barrier.

The instrumentation and control for the VV include monitoring vessel and cooling water temperature, water pressure, and local vessel stresses.

The VV safety assessment should include the analysis of the following events:

Vacuum vessel

- ◊ Overpressure from water LOCAs in the VV;
- ◊ Pressure loads to the VV from rupture of water coolant or cryogen pipes in the cryostat;
- ◊ Temperature transients of in-vessel and VV equipment from LOFAs and from in- and ex-vessel LOCAs;
- ◊ Pressure transients from air ingress into the VV;
- ◊ Electromagnetic loads under disruptions;
- ◊ Mechanical loads to the VV from magnet accidents;
- ◊ Thermal loads to the VV from magnet accidents (such as electrical arcs).

Pressure suppression system

- ◊ Overpressure transients from water LOCAs into the VV which trigger venting.

2.3.3 Vacuum Vessel Interfacing Systems

The VV Interfacing Systems are as follows:

- Magnet Structure : the main vessel will provide the structural mount points where the "A" frame supports will be attached;
- Blanket: the main vessel will provide the structural mount points on the inner skin of the vessel where the blanket support structures will be attached; the VV port assemblies provide the cover plate for the upper port and the feed-throughs and bellows required for blanket cooling;
- Blanket Test Modules: the middle vessel ports will be access ports for these systems;
- Divertor: the main vessel will provide mounting rails along the inner skin of the vessel for divertor attachment. The port extensions for the lower ports will provide a weld interface flange for the divertor feed through flange. The lower port will also have a port opening for the pressure suppression system;
- Thermal Shield: The VV will provide mounting bosses on the outer skin for attachment of the thermal shield.
- Cryostat: the middle and lower vessel port assemblies interface with the cryostat. Extensions and bellows from the cryostat will weld directly to the vessel ports. The lower port will also have a port opening for the pressure suppression system;
- Vacuum Pumping System: the vacuum pump will mount to the shield plug in the lower port. The shield plug will provide the required feed-through holes;
- Diagnostics: Some diagnostics will be mounted directly to the inner wall of the vessel. Some small diagnostic ports may be required for diagnostics.
- Heating and Current Drive Systems: the middle vessel ports will be access ports for these systems;
- Vacuum Vessel Coolant System: the cooling pipes for the vessel and port assemblies will route water for cooling and baking to the vessel sectors.

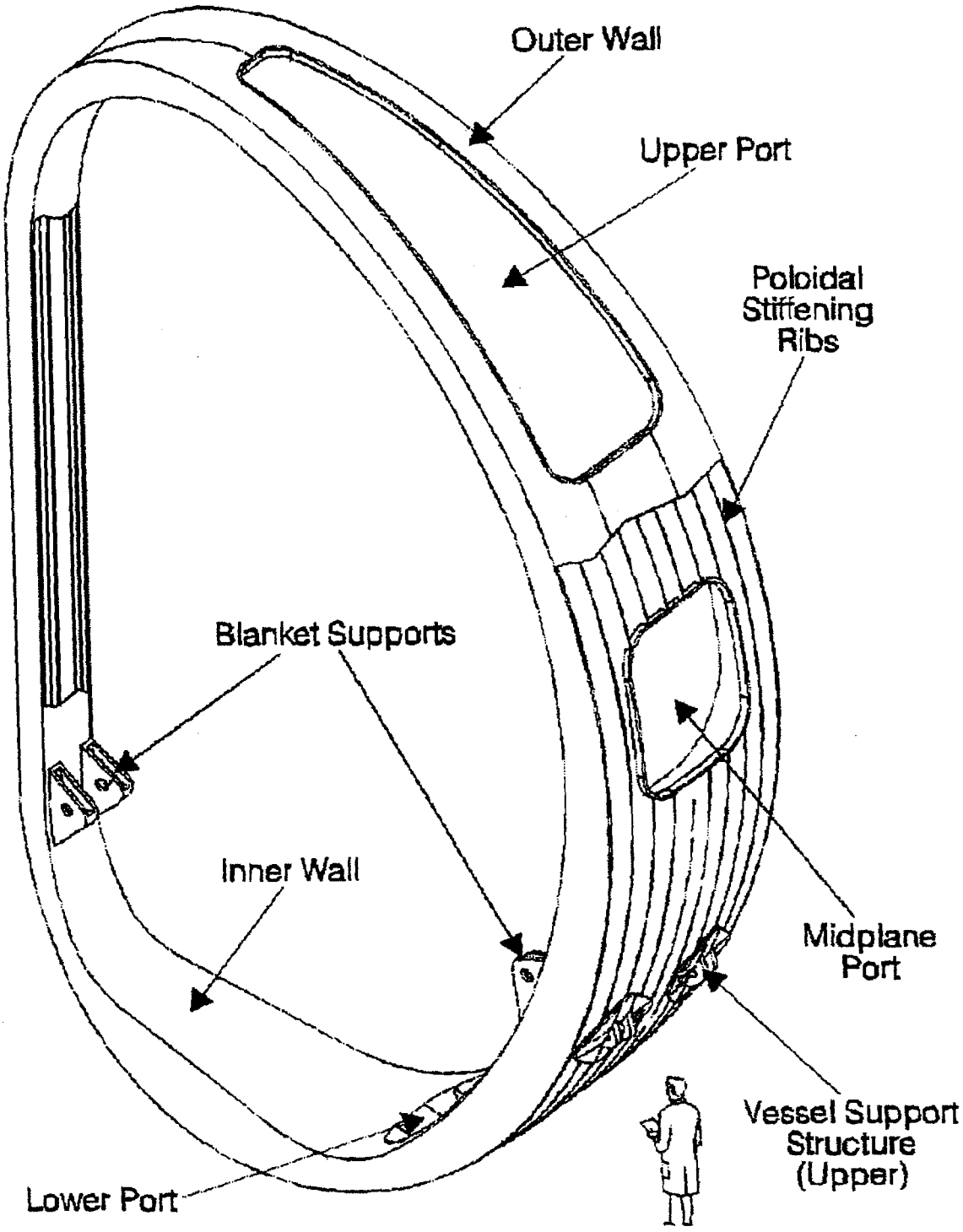

Figure 2-3: ITER Vacuum Vessel Segment

2.4 Cryostat Vessel (CV)

2.4.1 General Design Description

The cryostat is the vacuum vessel containing the ITER tokamak. It consists of a cylindrical section bolted to torispherical heads at top and bottom. The top head is split into flanged concentric sections to permit PF and CS coil removal without removing the entire head. The vessel is made up of two walls connected by horizontal and vertical ribs. The space between the walls is normally filled with helium at slightly above atmospheric pressure, so that any leaks developing in the outer wall are outward and any leaks developing in the inner wall are detected at maximum sensitivity by the cryostat leak detection cryosorption pump. Temporary mitigation of any inner wall leaks (until the next planned machine shutdown) can be obtained by reducing the interspace pressure down to a lower limit of 1 kPa, this pressure being the minimum required to ensure that the inner and outer walls are adequately thermally coupled to limit interwall stresses to acceptable values during a loss of magnet cooling helium event.

The cryostat is 36.5 m outside diameter and height. The inside wall radius is 18 m and the height of the cylindrical section is 20.9 m. The head spherical and knuckle radii are 30 and 3 m, respectively. There is 1.75 m minimum gap between the inner cryostat wall and the machine. The walls are nominally 20 mm thick and the separated by a 200 mm interspace. The interspace region is divided into at least 5 compartments, 3 in the top cover, and one each in the cylinder and in the lower cover.

The cryostat mass is 2165 tones including ribs, flanges, reinforcement and support skirt. Its internal surface area and volume are 5,030 m^2 and 31,400 m^3, respectively. With 12,800 m^3 taken up by the machine, main bellows, and cooling pipe shrouds, the cryostat free volume is 18,600 m^3.

The cryostat design loading is 0.1 MPa (abs) external and 0.2 MPa internal. The latter pressure which would stem from venting of coil helium into the cryostat vacuum due to a fault condition. This helium, which contains no radioactivity, is vented to a stack should internal pressure go above the 0.2 MPa limit.

The cryostat must provide the vacuum for the machine superconducting magnets, form part of the radiological secondary containment, and provide removal of decay heat during beyond design basis events. Also, it must provide access ways and corridors for diagnostic lines of sight, the introduction of additional heating beams and the deployment of remote handling equipment, and provide feed-through penetrations for all the equipment connecting elements of systems outside the cryostat to the corresponding elements inside the cryostat.

The cryostat and all appendages forming part of its vacuum envelope shall be of double wall structure with controlled interspaces for leak detection. This configuration is required to satisfy the CV Safety Function as a Second Tokamak Confinement Boundary. The controlled interspaces help to maintain a satisfactory low leak rate by providing a secondary leak barrier.

The cryostat vessel is designed to withstand all loads applied during the normal and off-normal operational regimes, and at specified accidental and fault conditions. Specific loads are given in Table 2-4.

Table 2-4: Cryostat Operating State Parameters

Parameter	Value
External pressure (absolute)	0.1 MPa
Nominal max internal pressure	0.2 MPa
Max interspace pressure	0.2 MPa
Min interspace pressure	0
Free internal volume	18,600 m^3
Normal temperature	300 K
Maximum temperature	500 K
Minimum temperature	4.5 K
Maximum in/out wall ΔT	40 K

During normal operation the temperature of the cryostat metallic structure will remain close to room temperature. Under design basis accident conditions of loss of magnet or primary heat transport system coolant, the cryostat metallic structure may be subject to transient contact by low temperature (4.5 K) or high temperature (up to 500 K) fluids.

The nominal pressure inside the Cryostat Vessel at the start normal operation conditions shall be less than 10^{-3} Pa total gas pressure with the partial pressure of residual air or nitrogen not to exceed 10% of the total.

The position of the CV in the tokamak pit is represented in Figures 2-5 and 2-6.

2.4.2 Cryostat Vessel Functions

The CV safety functions are as follows:

1. Provide the second confinement barrier for radioactive materials in the loops and in the torus;
2. Provide a barrier for air to separate it from hydrogen that could be generated by accidents in the torus boundary;
3. Limit the pressure due to accidents inside the CV;
4. Provide thermal shielding for the superconducting magnets during normal operation;
5. Provide first barrier during some maintenance operations on the torus boundary.

The cryostat should be designed to withstand the following individual **loads**:

- Static load: the weight of the cryostat and all supported hardware;

- Normal operating pressure and thermal load;
- Interaction loads imposed by other components during normal or fault conditions:
  - ◊ Disruptions and VDE: interaction loads on the cryostat from the vacuum vessel and in-vessel hardware;
  - ◊ Vacuum Vessel: loads on the cryostat due to the vacuum vessel transient response to design basis accidents;
  - ◊ Magnet system: loads on the cryostat due to the magnet system transient response to design basis accidents;
- Natural phenomena hazard loads: earthquake, wind, flood;
- Site-generated missile impact load;
- Cryogen evaporation load.

Combined loads and cyclic loads (thermal and disruption loads) should also be considered in the cryostat vessel design.

The cryostat overpressure protection system will consist of two relief paths connected in parallel. The first will comprise a remote operated vacuum valve (operated from the ITER main control room). This valve is used to mitigate overpressures which build slowly following loss of magnet helium coolant into cryostat vacuum. The helium efflux temperature is in the region of 55 K and for the design basis spillage the cryostat pressure just after the spillage is less that an atmosphere absolute, building slowly thereafter on a time scale of hours. In these circumstances, the helium is vented to stack when the pressure inside the cryostat exceeds atmospheric. In this way, opening of the rupture disc, and its subsequent replacement are avoided. The second overpressure protection element is a rupture disc, the discharge line from which is connected directly to the stack. This protects against overpressures which build quickly, following for example, the rapid volatilization of air ice which had been frozen on the magnet structures after an undetected air in-leakage, and which had fallen off after a coil quench. Subsequent to such an event, the rupture disc would have to be replaced.

Instrumentation and Controls are required for the cryostat vacuum system, the interspace leak detection system, the air ice detection system and the cryostat overpressure protection system.

The **cryostat safety analysis** should include but not be limited to the following events:

- ◊ Over pressure transients from cryogen release;
- ◊ Over pressure from water LOCA in the cryostat;
- ◊ Overpressure from water LOCA in the vacuum vessel propagating into the cryostat;
- ◊ Pressure transients from air breaks into the cryostat;
- ◊ Risk of ozone explosions;
- ◊ Ice buildup;
- ◊ Arcing from magnets and busbars;
- ◊ Internal and external missiles.

2.4.3 Cryostat Vessel Interfacing Systems

Cryostat Interfacing Systems are as follows:

- Superconducting coils and structures (vacuum and thermal);
- Heat Transport System (secondary containment and leak mitigation);
- Vacuum vessel (pressure suppression);
- Tritium Plant (detritiation systems);
- All systems using cryostat penetrations (Diagnostics, additional heating, HTS etc.);
- Remote handling;
- Vacuum leak detection (magnet performance and detection of accident precursors);
- CODAC (integrated control and interlocking).

2.5 Primary Heat Transfer Systems (PHTS)

The PHTS consists of pipework containing the pressurized water coolant, valves, pumps, heat exchangers, pressurizes, drain tanks, a blow down tank and associated instrumentation and auxiliary equipment. During plasma operation, the PHTS transfer heat generated in components (first wall, blanket shield, vacuum vessel, divertor, auxiliary heating systems, test blanket modules, diagnostics) to the environment (air, water) via Secondary Heat Transfer Systems (SHTS) or directly to cooling towers, or air. The total heat load to be dissipated during a plasma pulse is in the order of 2.6 GW. In between pulses, the PHTS remove decay heat from the plasma facing components (first wall including baffles and limiters, divertor) as well as shield and vacuum vessel. The expected maximum decay heat generation at plasma shutdown is < 25 MW, decreasing after one day to less than 5 MW.

The PHTS also provide the baking function[1] of the in-vessel components and the vessel itself (up to 200°C or higher consistent with saturation pressure) as well as the temperature control function for the coolant feed streams to keep the components within a specified temperature window.

Due to the build-up of activated corrosion products and permeation of tritium through the first wall into coolant, the PHTS, especially the loops serving first wall including baffles and limiters, as well as divertor, will gradually build up radioactive inventory. To keep the activity to acceptably low levels, the affected PHTS loops will be connected to a chemical control system (to scrub suspended activation products and to inhibit corrosion) as well as to a water detritiation plant. PHTS loops with anticipated higher levels of activated corrosion products and tritium are expected to require a secondary loop in order to avoid that a heat exchanger tube failure results in unacceptable environmental release. It is

[1]In-vessel components and the inner vessel walls will require periodic surface conditioning to maintain acceptable plasma operating conditions.

assumed that the divertor and first wall (including baffles and limiters), and the blanket test modules will have secondary loops.

With respect to overall functional requirements, the PHTS loops can be divided into three categories:

1. loops that remove the heat deposited during plasma pulses, and provide baking and temperature inlet control function as well as decay heat removal (all in-vessel components and systems located in main ports, e.g. test blanket modules etc.);
2. the VV PHTS loops which, in addition to the functions above, also provide heat removal safety function, i.e. decay heat removal, when all other loops are not available for this function;
3. loops that simply provide a heat removal function during operation but have no baking or decay heat removal function (NBI, certain diagnostics etc.).

At the time of publication of the present work, no design work has been undertaken for the heat transfer systems in the category 3. As far as categories 1 and 2 are concerned, the layout of the loops will probably not change; however, the thermohydraulic parameters are not yet frozen. We will present here the description and parameters of categories 1 and 2 as given in the Design Description Documents published in June 5, 1995.

2.5.1 First Wall and Shield Blanket PHTS

The FW/SB PHTS is divided into four loops. Two of these loops include all the baffle and limiter modules, whereas the other two include only "normal" blanket modules. The former, due to high heat fluxes, dominate the pressure drop requirement, and to reduce the overall amount of coolant required, the flow through blanket modules with less heat input will be appropriately throttled (baffle, limiter and other coolant flows). Each loop serves ten inboard and ten outboard sectors comprising each of three outboard and two inboard arrays of blanket modules. The present pipework layout work is based on routing all these pipes from their connection point to the FW/SB arrays to the HTS vaults where they are manifolded into headers and collectors. These are then connected to the heat exchanger and the pump. The pump, heat exchanger and pipework diameter are all being sized for the maximum heat load. Within the vault, the PHTS pipe diameter is 1,200 mm, and the approximate size of the intermediate heat exchangers is 4.5 m diameters, 14.2 m high. Integrated in the first wall are the ICRF antennae and ECH mirror assembly. Their power loading is very similar to the FW/SB modules, and their cooling is integrated in parallel with blanket modules.

Due to the large variation in heat input in the individual blanket modules, both temporal and geometrical during a pulse, the overall temperature increase of the coolant will be below 40°C, which results in large loop components. Due to build up of activated corrosion products and the gradual tritiation of the coolant due to permeation of tritium through FW material, the use of a secondary, intermediate loop is being considered in the present design.

Baking will be achieved by heating up the water by the pump power combined with bypassing of the heat sink, the intermediate heat exchanger. This requires also good thermal insulation of all the loop components. During detailed design it will be decided whether additional external heating will be required, by means of electrical heaters in a bypass of the main loop, in order to arrive within an acceptable time frame at the baking temperature which will be 200 - 220°C for an inlet pressure of 3 MPa.

During an operational period, the FW components should be maintained within a prescribed temperature window despite the pulsed nature of plasma operation. Temperature control is intended to be achieved by controlled bypassing of the heat exchanger. During the dwell time (between pulses), only a trickle stream needs to be cooled commensurate with the decay heat deposited in the FW. Due to the fact that the FW components have a high thermal capacity, valve activation may be slow thereby avoiding any cavitation problems.

The use of the large pumps is not economically justifiable for removal of decay heat and control of temperatures during extended interpulse periods. Hence it is intended to fit small (possibly in the range of 20 kW or so) pony motors for this mode of operation. These could be also powered by emergency power, if required. The large thermal capacity of the FW/SB should be amenable to start up of the pony motors one or two hours after failure of site power. While not a mandatory requirement, establishment of natural convection for removal of decay heat would be considered a safety advantage and the detailed loop design will consider this issue. Maintaining regular forced circulation is also important during long shutdown periods for maintaining good chemistry control of the coolant throughout the loop.

The main loop data are listed in Table 2-5 and Table 2-6 for the loops serving "normal" blanket modules and those serving baffle, limiter modules respectively.

Table 2-5: Main Data for FW/SB PHTS Loops 1 and 3 (only normal modules)

Parameter	Value
Thermal Power/Loop	603 MW
Coolant Inlet Temp.	100 °C
Coolant Outlet Temp.	134C
Coolant Inlet Pressure	3.0 MPa
In-Vessel Pressure Drop	0.1 MPa
In-Vessel Water Holdup	102 m^3
Number of Loops	2 Loops
Flow Rate/Loop	4195 kg/s
Loop Pipe Diameter (*1)	1.2 m
Pressure Drop (*2)	0.56 MPa
Total Water Holdup (*3)	842 m^3
Pumping Power/Loop	3.5 MW
Pump Size	3.2 m-D x 6.7 m-H
Heat Exchanger:	
- HX Size	4.5 m-D x 14.2 m-H
- Heat Transfer Surface	11430 m^2/Loop
- Tube Number	12520 Loop
Pressurizer Size	3.2 m-D x 8.5 m-H

(*1) Fluid velocity : v = approx. 4.0 m/s

(*2) Total pressure drop including In-vessel components, Heat exchanger and piping

(*3) Assumed Pipe length : (Loop) = 40 m/Loop, (Sub-1) = 40 m/Loop, (Sub-2) = 7000 m/Loop

Table 2-6: Main Data for FW/SB PHTS Loops 2 and 4 (including baffles, limiters, ICRF, ECH)

Parameter	Value
Thermal power/Loop	358 MW
Coolant inlet temp.	100 °C
Coolant outlet temp.	122 °C
Coolant inlet pressure	3.0 MPa
In-vessel pressure drop	0.3 MPa
In-vessel water holdup	41 m^3
Number of Loops	2 Loops
Flow rate/Loop	3860 kg/s
Loop pipe diameter (*1)	1.2 m
Pressure drop (*2)	0.7 MPa
Total water holdup	745 m^3
Pumping power/Loop	4.0 MW
Pump size	3.3 m-D x 6.9 m-H
Heat exchanger:	
- Size	4.3 m-D x 12.5 m-H
- Heat transfer surface	8520 m^3/ Loop
- Tube number	11460 / Loop
Pressurizer size	3.1 m-D x 8.0 m-H

(*1) Fluid velocity : v = approx. 3.6 m/sec

(*2) Total pressure drop including In-vessel components, Heat exchanger and piping

(*3) Assumed pipe length : (Loop) = 40 m/Loop, (Sub-1) = 40 m/Loop, (sub-2) = 7000 m/ Loop

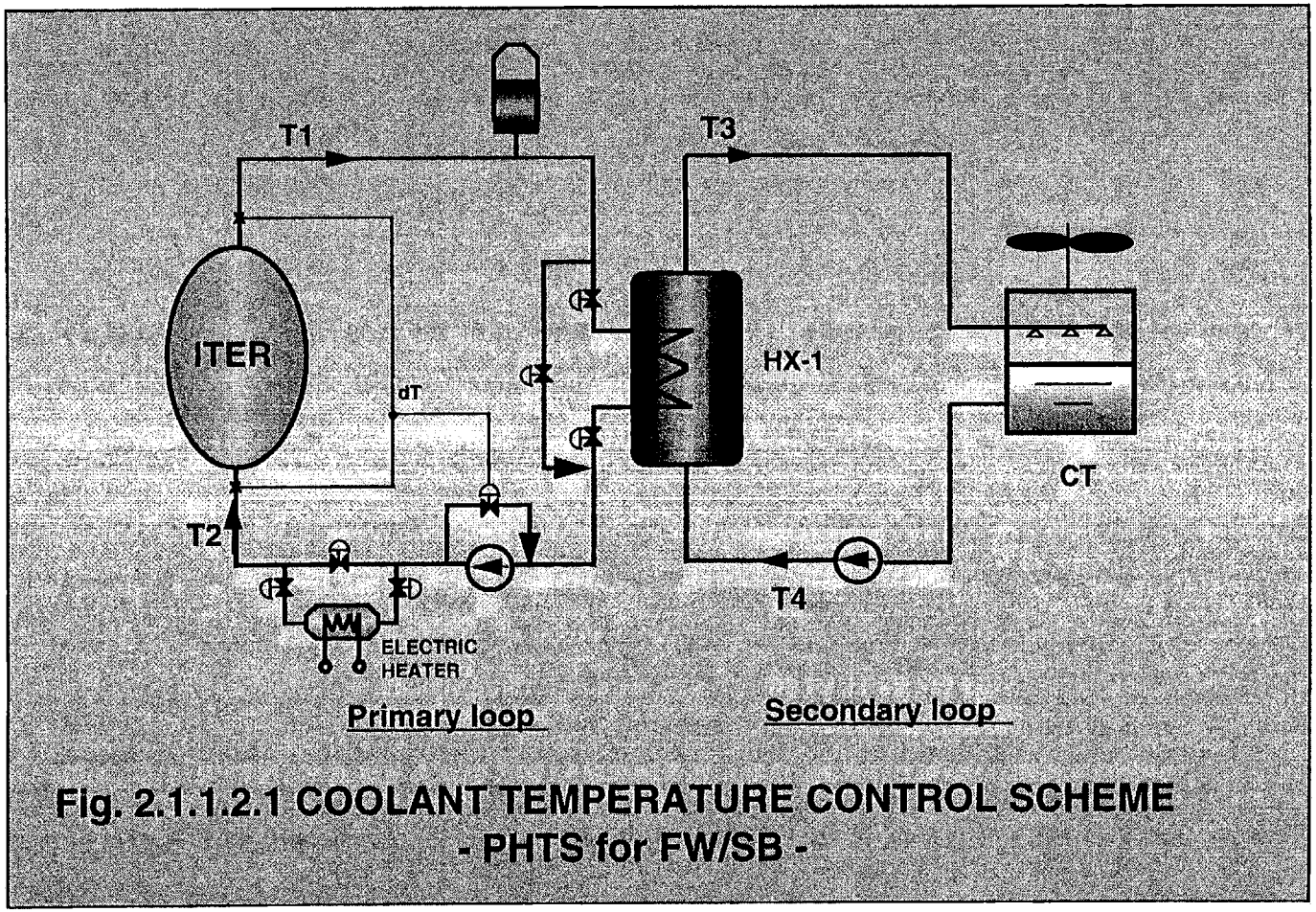

Figure 2-4: FW/SB PHTS and SHTS [2-5]

2.5.2 Divertor PHTS

Four loops have been selected as this allows a single very large pump per loop. Also this division into loops does match the quadrant of individual modules that would be replaced (if required) through a single maintenance port, so that this would allow replacement of a complete quadrant of divertor cassettes without having to drain the other quadrants.

Several options for the routing of pipework from the divertor ports to the HTS vaults are still under consideration. Components for two loops are located in each of the two vaults. The pipes to each individual cassette are approximately 150 mm in diameter. The diameter of the combined pipes to the pump and heat exchanger is approximately 600 mm. Due to the very high heat loads on components of the divertor cassettes, high pressure drop and flow requirements exist and therefore large and powerful pumps are required (2.2 MW) as well as a high coolant inlet pressure (4 MPa).

The heat exchangers between the primary and secondary coolants have been tentatively sized. They will be of the tube and shell type with floating end developed for PWRs for improved inspectability and minimization of exposure of maintenance personnel.

The high pumping power coupled with good thermal insulation of the pipework and other loop components may suffice for baking the divertor cassettes without use of external heat source. It does, of course, require valves to bypass the intermediate heat exchanger in this mode of operation. Controlled bypass valves will be required for cassette inlet temperature control in any case.

Having two identical loops side by side in each vault opens up the possibility of interconnecting the loops by non-automatic valves so that pump and/or heat exchanger of one loop could be used for both loops simultaneously in case this is required for maintenance or other operation. Such an interconnection will not allow, however, full power operation but some reduced power operation may be feasible. During non operation period, the Divertor PHTS still has to remove decay heat. It would not be very economic to run the large pumps for this, and hence it is planned to have additional small pony motors that provide the power for the pumps to generate forced circulation under these conditions. With the heat exchanger positioned at a level some 25 - 35 m above the cassettes, it is likely that natural circulation will develop as well.

The very high thermal flux in certain position dictates the use of copper components wetted by coolant in the cassettes, which may produce erosion and corrosion products. A dedicated chemical and volume control system will be required and the present design assumes the use of a secondary, intermediate loop.

The main loop parameters are given in Table 2-7. The loop layout, temperature control, etc. is more or less identical to that of the FW/SB PHTS loops.

Table 2-7: Main Data for Divertor PHTS Loop

Parameter	Value
Thermal Power	400 MW
Coolant Inlet Temp.	150 °C
Coolant Outlet Temp.	175 °C
Coolant Inlet Pressure	4.0 MPa
In-Vessel Pressure Drop	0.85 MPa
In-Vessel Water Holdup	42 m^3
Number of Loops	4 Loops
Flow Rate	3690 kg/s
Loop Pipe Diameter (*1)	0.6 m
Pressure Drop (*2)	1.53 MPa
Total Water Holdup (*3)	281 m^3
Pumping Power	2.2 MW / Loop
Pump Size	2.7 m-D x 6.0 m-H
Heat Exchanger:	
- Size	1.9 m-D x 6.7 m-H
- Heat Transfer Surface	900 m^2 /Loop
- Tube Number	192/Loop
Pressurizer Size	1.8 m-D x 5.0 m-H

(*1) Fluid velocity : v = approx. 4.0 m/sec

(*2) Total pressure drop including In-vessel components, Heat exchanger and piping

(*3) Assumed pipe length : (Loop)=20m/Loop,(Sub-1)=20 m/ Loop, (Sub-2) = 2400 m/Loop

2.5.3 Vacuum Vessel PHTS

The VV PHTS is divided in two loops. Each of two independent loops serves half each VV sector (1/20 - th of VV), so that, in case of failure of a complete loop, the other loop can take over its duty. Each loop will be designed for removing the full in-vessel decay heat (< 5 MW after one day) by natural convection. The thermal capacity of the in-vessel components is such that removal of decay heat could be disrupted for several hours without adverse effects on components. Normal removal of heat would be by forced circulation as this will allow to achieve the temperature control function.

To bake the vessel at 200 °C will require heating of the coolant by external means. Electrical heaters mounted inside a bypass line of the main loops are envisaged for this purpose.

To keep the water inlet temperature during normal operation at a reasonably constant value, bypassing, probably using three - way control valves, of the heat exchanger will be required. The loop

pumps will be located in the vaults together with the valves and heaters. The two water to air heat exchangers are intended to be positioned on top of adjacent buildings. This gives a high height difference between the vacuum vessel and the heat sink which is promoting natural convection. For each of the two loops, the pipe diameter will be approximately 100 mm, the pump will have a power of 50 kW.

It should be noted that double containment around the VV PHTS pipework is not strictly necessary, as the VV itself will be designed and built to a stringent code of practice forming barrier number one and therefore the PHTS pipework and components provide the second barrier. Consequently, the VV PHTS does not have to be secondary contained, thereby allowing the HXs to be positioned outside the HTS vaults. The main VV HTS loop data are given in Table 2-8.

The requirement that the VV PHTS must be available under all circumstances as it is a safety system for decay heat removal is covered by simplicity and redundancy. Simplicity is given by the natural convection capability, and redundancy by having two loops each of which able to transfer passively the full decay heat burden. It should be noted that the total decay heat will fall to approximately 1 MW a few days after shutdown. The very large thermal capacity of the in-vessel components and the vessel itself could then allow interruption of the cooling function of the VV PHTS and all other PHTS loops probably for days or even weeks without adverse effect. This shows that, while eventually heat needs to be dissipated, the so-called safety function of the VV PHTS in this respect is not comparable to that of the emergency cooling system of a fission reactor.

Table 2-8: Main Data for VV PHTS Loop

	Normal Operation	Off-Normal Operation
Thermal Power/Loop	1.5 MW	5 MW
Coolant Inlet Temp.	100 °C	100 °C
Coolant Outlet Temp.	111 °C	195 °C
Coolant Inlet Pressure	2.0 MPa	2.0 MPa
In-Vessel Pressure Drop	0.1 MPa	0.04 MPa
In-Vessel Water Holdup	425 m^3	425 m^3
Number of Loops	2 Loops	1 Loop
Flow Rate/Loop	32 kg/s	12.35 kg/s
Loop Pipe Diameter (*1)	0.15 m	0.15 m
Pressure Drop (*2)	0.1 MPa	0.04 MPa
Total Water Holdup (*3)	~725 m^3	~725 m^3
Pumping Power/Loop	0.5 MW	-
Pump Size	0.6 m-D x 2.4 m-H	-
Heat Exchanger (*4):		
- Size	12 m-L x 6.5m-W	~ 12 m-L x 6.5m-W
- Heat Transfer Surface	9135 m^2/Loop	9135 m^2/Loop
Pressurizer Size	2.7 m-D x 7.7 m-H	2.7 m-D x 7.7 m-H

(*1) Fluid velocity : v = approx. 1.9 m/sec

(*2) Total pressure drop including In-vessel components, Heat exchanger and piping

(*3) Assumed pipe length : 230 m/Loop

(*4) Air Cooled Type HX

2.5.4 Blowdown Tank and Refilling System

Short term malfunctions may lead to the pressure relief valves of the PHTS loops being actuated. To catch the released water/steam mixture, it is intended to install a blowdown tank, common to all PHTS systems, alongside the drain tanks at the lower pit level. The tank will be partially filled with water into which the incoming water/steam mixture will be injected. Tentative sizing is based on 20 m^3 tank volume.

2.6 PHTS's Secondary Confinement

Within the cryostat, PHTS pipework is secondary contained for reasons of machine protection, i.e. to ensure that primary pipework leaks do not cause failure of in-cryostat component (particularly coils). Outside the cryostat, the PHTS is secondary contained for a different reason: it is a requirement that there shall be always at least two barriers between plasma and environment. As discussed in Section 2.2, it is difficult to claim safety barrier credit for the first wall and hence the requirement for at least two barriers leads to the need to envelope the PHTS by a second barrier. The pipework penetrating through the cryostat are therefore enclosed by a secondary pipe. As such an individual envelope is very difficult to apply to large components like pumps, heat exchangers, etc., it has been decided to locate these inside special rooms - vaults, which form the secondary barrier. These vaults are inside the Reactor Hall along the East and West side of the pit. These positions give the shortest pipe lengths between first wall components and the large PHTS components.

A large ex-vessel LOCA within the secondary pipework to the HTS vaults or within the vaults will cause flashing to steam of the released water and, depending on the loop hold up, could rapidly cause overpressurization of the secondary containment provided by the HTS vaults which have a design pressure of 0.17 MPa.

To prevent overpressurization and to reduce to low levels environmental release of radioactive material (activated corrosion products and tritium) contained within the coolant, it is intended to connect to each vault a filter vent system which are connected to the vaults by large diameter ducts (several meters diameter) and rupture or blow panels.

Different concepts of filter vent or vent systems have been developed for water-cooled power plants (PWR/BWR) including pressure suppression pool, gravel beds and ice condensers. Although design conditions for the ITER filter vent system are quite different from those for PWR/BWR, similar design technology will be applicable.

The configuration of a water pool/bed type filter vent system is relatively simple and composed of low pressure blow panels and/or rupture discs, high throughput vent duct, high speed steam distributor, high efficiency steam condenser (water pool), HEPA filters, and isolation valves. A preliminary sizing of a filter vent system has been made for the ITER HTS vaults based on obsolete PHTS parameters. The location of the system should be as close as possible to the vaults to minimize friction losses in the duct. The systems have been tentatively sized an located inside the Reactor Hall building, adjacent to (just North of) the HTS vaults.

A preferred alternative from a safety point of view is to relief the overpressure into a suppression tank, but that is less likely due to the very large tank volumes required to mitigate a guillotine break of a large pipe of the FW or Divertor loop.

2.7 Tokamak Building (TB)

2.7.1 General Design Description

The primary functions performed by the tokamak building are to house, support, protect and provide a suitable environment, and control access to the components and systems which are located inside the building. In addition, the building provides some general services such as lighting, power, and fluids. The building has also been assigned some of the functions which contribute to the protection of the safety of workers and the public.

The Tokamak Building is located in the center of the hypothetical site. It is composed of three contiguous halls with the Tokamak Hall at the center, the Assembly Hall at the south end and the Laydown Hall at the north end. Tokamak Hall is structurally attached to the Tritium Building at the east end and to the Electrical Termination Building at the west end for the purpose of being structurally stable. At the east and west sides of the Assembly Hall, there are Tokamak Services Buildings and at the east side of the Laydown Hall, there are Hot Cell and Radwaste Buildings. Figures 2-5 and 2-6 represent the TB layout and cross-section.

The Tokamak Hall consists of the cryostat pit and crane hall. The structure of the Tokamak Hall is reinforced concrete. The bottom of the pit basemat is -53 m relative to nominal grade. The thickness of the basemat is 6 m. The pit is configured as a cylinder with 67 m inside diameter and 2 to 3 m variable thickness from the basemat to -9 m below grade level. From -9 m to grade, the pit has a square shape, 67 m inner dimension with 2 m thickness wall.

The above-grade portion is the crane hall with a square shape, 71 m outer dimension, and 61 m height. At the east and west sides in the crane hall, there are **vaults to accommodate Heat Transport System**. The crane hall is composed of frame structure in the east-west direction, which is arranged on a 6.9 m pitch, and wall structure in the north-south direction. The frame consists of steel reinforced concrete columns with the dimensions of 2 m width and 3.5 m depth and structural steel trusses with 8 m depth. To make the frame stable, the adjacent buildings, Tritium and Electrical Termination Buildings, are structurally attached to the Tokamak Hall. Those buildings are steel reinforced concrete structures and are symmetrical. The dimensions of both buildings are 71 m north-south length, 30 m east-west width, -11.5 m depth and 35 m height from the grade.

ITER buildings or rooms are classified into the following four zones:

1. WHITE ZONE: This includes offices and control rooms where the ventilation rates are decided by the conventional standards.
2. GREEN ZONE: This comprises the radiation working areas which includes general working and cell operating face zones within a building handling radioactive materials but which should not become contaminated under normal conditions.

3. AMBER ZONE: This includes service and maintenance areas for process equipment, cells and so on. These zones can be contaminated when cell doors are opened, cell roof blocks removed for transfer of materials, maintenance and similar purpose. Access between amber and green zones should be under controlled conditions using interlocks and the transition zones where necessary.
4. RED ZONE: This comprises the internal cave or cell areas which are closed off from all access under normal working conditions and which can be contaminated by the operations carried out in the zone.

The areas in the Tokamak Buildings are assigned to the following classification.

- Cryostat extension vault and HTS vaults — Red Zone
- Tokamak pit and Laydown basement — Amber Zone
- Tokamak and Laydown crane halls — Green Zone
- Assembly crane hall and basement — White Zone

2.7.2 Tokamak Building Functions

The TB functions are the following:

- **Accommodate Equipment**

The largest single component in the building is the 40 m diameter cryostat which is centered in the pit. The pit also contains all the components which must be in close proximity to the cryostat, such as diagnostics, plasma heating, plasma fueling, remote maintenance equipment, and a large number of service penetrations in the cryostat.

- **Protect Components from External Hazards**

The building provides the resistance to the seismic load, wind load, snow load, tornado and wind generated missiles as required. The magnitude of each load is determined by the site conditions and the classification of the building. Because the building is not a strong safety barrier in the regulatory sense, protection is provided if the building does not collapse or damage the equipment under design basis conditions. The building must also continue to function as a ventilation system boundary, directing all exhaust air to the stack.

- **Tritium Control**

The entire Tokamak building does not have a containment function, however the Heat Transport System (HTS) vaults within the Tokamak building do have a confinement function. Primary coolant system equipment and other components containing tritium will have confinement systems (e.g. HTS vaults with vent-scrubbers) built around them. Additional tritium bearing equipment is located in the pit area which will have a separate (higher velocity) ventilation system at negative pressure relative to the rest of the building. This system will safely handle any small leaks from the confinement systems or chronic releases during maintenance when confinement is breached. The crane hall and the other

areas, which do not include tritiated equipment have a conventional ventilation system because tritium leakage to these areas during machine operation is very unlikely. If tritium does enter the crane hall area during major (open cryostat) maintenance of the machine, the ventilation system is reconfigured and it is exhausted through the stack. This approach to tritium control by the ventilation systems requires that tritiated components (such as Divertor cassette, Shield/Blanket segments, etc.) removed from the machine must be placed in sealed containers to prevent the release of tritium to the building atmosphere.

- **Provide Radiation Shielding**

During the operating phase, there is protection against activated material inside the cryostat because the cryostat is surrounded by a reinforced concrete bioshield. The bioshield is a load bearing structural member supporting the floor slabs in the pit. Therefore while the Tokamak Hall does not have a biological shielding function, the pit structures and crane hall floor have a major shielding function. Additional shielding during tokamak operation is provided for the radiation leakage from the penetrations of the cryostat/bioshield and from high energy N^{16} radiation from the primary coolant loops. The Assembly and Laydown Halls have no shielding function. During maintenance activities, activated components such as Shield/Blanket, Divertor, Diagnostic equipment, etc. will be transported using casks. The building does not have the shielding function for the top access ports, but provides shielding for components removed from horizontal access ports in the cryostat pit. Casks (top access) may be transported using building cranes or on special trolleys that carry casks to the Hot Cells. Containers with irradiated components from horizontal access ports are remotely moved around the pit to a tunnel connecting with the Hot Cells.

A project requirement which applies to all design solutions is that the building and components whose design interacts with the building (e.g. cryostat, lifting device(s), remote maintenance casks, etc.) shall be evaluated to ensure that the minimum total project cost solution is obtained consistent with the requirements for the building and the interfacing components.

Table 2-9: Tokamak Building Compartments Parameters

Area	Volume (m^3)	Pressure (cm H_2O)
Tokamak & Laydown Area Crane Hall	430,000	atmospheric
HTS Vault (No. 1)	17,000	-2
HTS Vault (No. 2)	17,000	-2
Tokamak Pit (Outside bioshield)	85,000	-2
Tokamak Pit (Inside bioshield excluding Cryostat)	TBD	-3
Laydown Basement	23,000	-2
Assembly Hall	300,000	atmospheric
Assembly Basement	36,000	atmospheric

2.7.3 Tokamak Building Interfacing Systems

The TB Interfacing Systems are given in Table 2-10.

Table 2-10: Tokamak Building Interfacing Systems

Interfacing System Requirement including parameters	Feature which responds to interfacing requirement including parameters
The dimensions of the cryostat are 36.48 m diameter and 34 m height. The cryostat does not have a shielding function.	The Tokamak pit is sized to accommodate the cryostat. There are 1.2 m thick cylindrical concrete bioshield walls and 1 m thick concrete slab around the Cryostat to provide shielding function.
Ex-vessel LOCA primary loop blowdown to HTS vault.	All HTS vault walls, slabs, penetrations and doors must withstand 70 kPa pressure and each HTS sub-vault has rupture disk to adjacent sub-vault. Sub-vault with highest steam blowdown load has connecting duct to vent/scrubber.
Vacuum pumping systems	The building provides required space for the system.
Secondary heat transfer systems	The building provides required space for the piping.
Additional heating power supplies	The building provides required space for the cable.
Neutral beam injection	The building provides required space for the system.
Radiological protection	Some parts of the walls and slabs are seized to satisfy required shielding function.

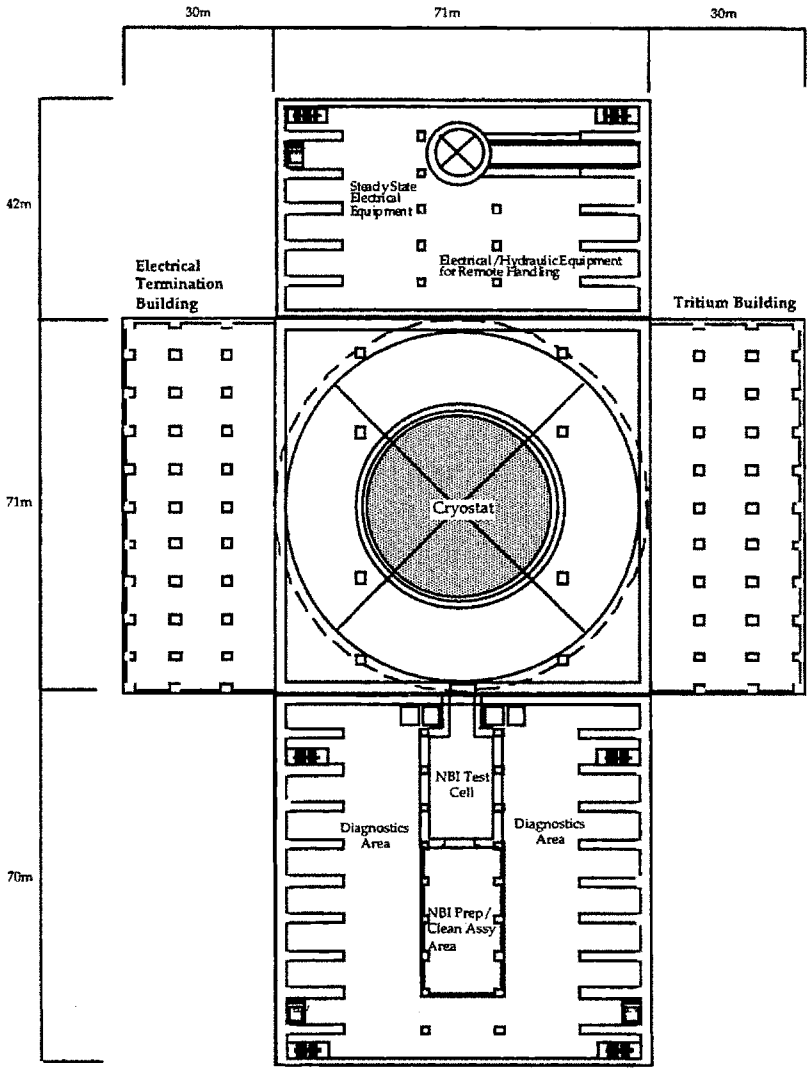

Title: Tokamak Building Floor Plan (EL-9 m)		
Subject Index : 6.2	WBS: 6.2.A	Rev.: 0
WBS: Tokamak Building		
Originator: K. Ishimoto	Date: April 1, 1995	
Object Type: Sketch	Sketch Number : 6.2.A-003	

Figure 2-5: Tokamak Building Floor Plan Elevation 9 m [2-4]

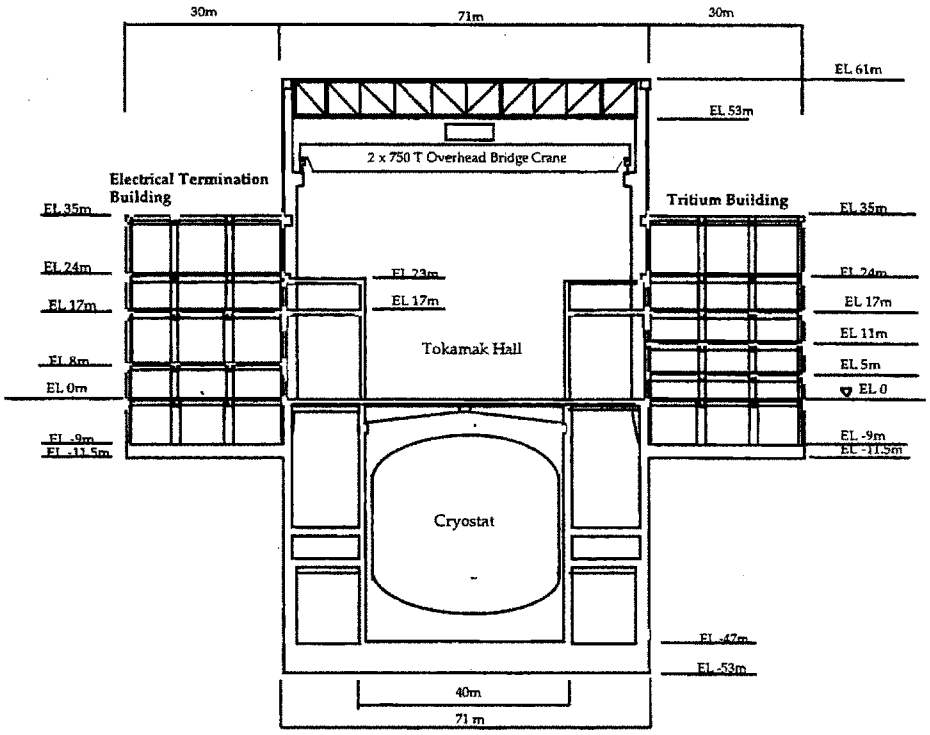

Title: Tokamak Building Section (A-A)		
Subject Index : 6.2	WBS: 6.2.A	Rev.: 0
WBS: Tokamak Building		
Originator: K. Ishimoto	Date: April 1, 1995	
Object Type: Sketch	Sketch Number : 6.2.A-005	

Figure 2-6: Tokamak Building Cross Section [2-4]

3. Method Development

This chapter describes the methodology developed for evaluating the performance of the radiological confinement barriers of a tokamak reactor, using ITER as a baseline design. The methodology includes several steps, some of them already well established in PRA studies, others being new approaches proposed for solving similar problems encountered in PRA studies. Finally, these methods are integrated to meet the objective of the present study.

The steps involved can be delineated as follows:

- Define the objectives of the study;
- Acquire and understand the fusion plant information;
- Determine safety functions and systems required for success;
- Identify a set of accident initiating events;
- Develop all conceivable accident scenarios starting with the initiating event and ending with failure of the first confinement barrier to retain radioactive releases;
- Develop containment models for the second confinement barriers and attach them to the accident sequences ended with failure of first confinement barrier;
- Recommend appropriate requirements concerning radioactive releases to the environment;
- Compare radioactive releases from each confinement barrier against the proposed requirements;
- Perform sensitivity analysis on confinement barrier parameters to evaluate their performance and the number of boundaries required to comply with the proposed requirements;
- Build a decision model for choice of tokamak building type.

The first step in performing a probabilistic risk assessment is the task of accident sequence definition and system modeling. This task begins with a definition of the objectives of the study and the acquisition of a substantial amount of information of plant design and operation. Recognizing the objective is important because the level of truncation in the analysis of various systems and sequences will depend on the desired product, which could be design optimization, estimation of public risk to provide information on the value of plant modifications aimed at reducing the risk level, selection of optimal testing frequencies, etc. For the present study, the objective is presented in Chapter 1 Section 2. Based on PRA methods, the objective is to develop a methodology to assess the performance of each radiological confinement barrier. The ITER is still in the design phase, so our methodology should be capable of performing sensitivity analysis to identify design weaknesses and recommend design remedies. Thus, the method could be used for comparing competing designs. At this stage in ITER design, basic information (such as design descriptions, preliminary safety analysis reports, and piping diagrams) is available, but the lack of detailed design and operational information limits the level of detail that can be included in the study. Detailed information on support system requirements,

instrumentation, and operational and maintenance procedures is not available, and will not be available until the plant is completed.

Design information about ITER is presented in this study as follows: general information in Chapter 1 Section 3, radiological confinement barriers in Chapter 2, and a system block diagram in Chapter 3 Section 1. The system block diagram was developed to understand the role of various systems in a fusion power plant, as well as interfaces and interactions among the systems, in terms of energy and materials (e.g., coolant, particles) flows.

In any PRA study, it is necessary to define a "freeze point", a time after which design or operational changes are not incorporated into the PRA until it is finished the first time. We chose the "freeze time" for our study to be June 5, 1995, when the first version for ITER Design Description Documents were made available to the ITER community. Declaring a freeze point does not usually eliminate the responsibility of updating the model to include subsequent design changes, but that is outside the scope of this thesis. We hope that the way we developed the models and the way they are presented in this thesis will facilitate an eventual updating in a convenient manner.

The task then progresses through the identification of required safety functions and accident initiating events. Chapter 3 Section 2 contains a description of the method employed - Master Logic Diagram, and a list of the initiating events identified and grouped by the systems where they occur. The grouping of initiators defines of number of accident sequences models required and simplifies the analytical process, because models are typically developed for groups of initiating events with similar characteristics rather than individual initiating events.

Then, the response of the plant to the identified group of initiating events must be evaluated. Detailed information on safety functions, systems, dependent-failure mechanisms and operational schemes is required to identify responses and define criteria for successfully meeting the challenges to plant safety. The common tool used in PRA studies for this part of the analysis is the event tree. The event tree construction is an inductive process requiring considerable iteration. Usually, the first step is to develop functional models which are then converted into system models. This is done by identifying the systems that satisfy the various functions and reconstructing the event tree accordingly. The ITER Early Safety and Environmental Characterization Study [3-1] presents functional event trees for selected initiating events. We used those as a basis for developing systems models, but we chose to employ a new approach for sequence development: the influence diagram/event tree combined model. This method and the advantages of using it are presented in Chapter 3 Section 3. It produces an inductive plant model that is consistent with the methods chosen for quantifying the frequency and the consequences of the sequences. It is desired to keep the models as flexible as possible to accommodate changes in the design, and even use for other objectives.

In order to meet the objectives of the study which is concerned with the confinement barriers, the analysis is performed in three consecutive steps: develop accident sequences for the failure of the first barrier, then for the failure of the second barrier, and finally for the third barrier, and present the results for each confinement barrier. The form of results presentation is discussed in Chapter 3 Section

4, and naturally, it has to be similar to the regulatory requirements formulation, so that the results for each barrier can be compared against the regulatory requirements (see Chapter 3 Section 5). Consequently, an assessment of the number of barriers sufficient to comply with the requirements can be performed. The required number of barriers is directly dependent on the their design, since different designs reflect different probabilities of failures for the confinement systems.

In PRA analysis, success (or failure) states for systems depicted on the event trees must then be defined to allow the development of system models. Deterministic analyses may be required in some cases to define the success states realistically. These definitions, converted to statements of undesired events, constitute the top events of the logic models used to analyze specific system failure modes. Deductive system logic models are constructed to determine the causes of system failure. The fault trees must include not only component failures but also the effects of testing, maintenance, and human errors on system performance. The structure of the trees is also influenced by the techniques used for dependent failure analysis and the scope of the overall analysis. This work is usually the result of a team of safety analysts, and it is not the goal of the present study to perform a rigorous analysis of the ITER systems. Rather, we present an analysis to a degree that defines the approach and demonstrates its applicability. As an example, we developed a fault tree with the top event 'DIV PHTS fails to remove decay heat', which is presented in Appendix D, but all the other events in the accident sequences are assigned estimated values, some based on literature as specified in Appendix D, and others based on engineering judgment. To gain more confidence in results, a more thorough system analysis should be undertaken by a safety team.

3.1 Systems Block Diagram

Before the detailed analytical work, it is necessary to become familiar with the design and operation of the plant, to help insure that function and system dependencies are appropriately considered. In important activities such as defining success criteria, care must be exercised not to use information that cannot be properly documented and justified. A significant task is the identification and listing of the front-line systems (i.e., the systems that directly perform the safety functions and thereby have a direct impact on the course of potential accident) and the support, or auxiliary systems that are associated with each front-line system. Since an understanding of the interactions between systems and the dependence of one system on another is vitally important, and overview of system operations should be performed to identify dependencies among systems, and a systems block diagram is a good tool for performing this analysis.

Moreover, a preliminary system analysis can be a vital step in the search for initiators, helping to ensure completeness in the definition of accident sequences. Plant familiarization provides baseline information for starting the definition of accident sequences and the modeling of plant systems. Initial

requirements for the types and number of influence diagram/event tree models can be developed and documented, key systems are identified, and their success criteria is defined.

The ITER systems block diagram is presented in Figure 3-1. It is a conceptual representation of the systems and their interfaces, as opposed to Figure 2-2 in Chapter 2 that gives a physical representation. Materials, energy, and coolant flows between systems are pictured as described in the legend. A short description of the systems follows, inspired by references [3-5] and [3-6].

The major components of the tokamak are the toroidal and poloidal **magnets**, which confine, shape and control the plasma inside the evacuated torus. The magnet coil systems include 20 toroidal field (TF) coils, 7 poloidal field (PF) coils, the central solenoid (CS) and the mechanical structure. The magnets are superconducting and cryogenically cooled; they are powered from the grid via a large AC/DC power supply. The TF coils provide a constant magnetic field to stabilize the plasma. The PF coils provide the magnetic field which changes over time to control the plasma position and shape. The CS provides the majority of the magnetic flux change needed to initiate the plasma, generate the plasma current, and maintain current during burn time. The mechanical structure integrates the TF coils, PF coils, and CS into the mechanical system for electromagnetic and gravity loads equilibration.

Inside the vacuum vessel are internal, removable components; these include the **first wall** (FW), the **shield/blanket** (SB) modules, and **divertor** (DV) cassettes. The blanket system, acting as a shield, removes the surface heat flux from the plasma, reduces the activity in the vacuum vessel structural material for the ITER fluence, and, in combination with the vacuum vessel, protects the superconducting magnets from excessive nuclear heating and radiation damage. The main components of the blanket system are as follows:

1. a structural toroidal shell, called back plate;
2. combined First Wall and Shield modules attached to the back plate; and
3. manifolds welded to the back plate that supply cooling water to the modules from the primary heat transport.

The main function of the divertor system is to exhaust impurities and reaction products from the plasma (material flow). As the main interface component under normal operation between the plasma and material surfaces, it must tolerate high heat loads while at the same time provide shielding for the vacuum vessel and magnet coils in the vicinity of the divertor. The main components of the divertor systems are:

- the divertor cassette body which provides a mechanical support;
- the inner and outer targets, which are high heat flux components;
- the dome, located below the separatrix X-point, to baffle neutrals and shield the wings from plasma interaction;
- the support pads mounted at the bottom of the cassette to provide locking and alignment of the divertor cassettes;

- earth straps connecting the cassettes with each other, the baffles and the vacuum vessel to prevent arcing and provide defined current paths;
- the divertor to blanket back plate gas seal to prevent backstreaming of target gas into the plasma chamber;
- the cooling pipe interface connecting the divertor cassettes to the radial cooling pipes at each divertor port;
- special diagnostic cassettes providing access for optical diagnosis.

The **additional heating and current drive systems**, capable of driving part of the plasma current, are provided to bring the plasma to ignition, to help in controlling the DT burn and extending it to steady-state. These systems are as follows: Ion Cyclotron Radio Frequency (ICRF), Electron Cyclotron Radio Frequency (ECRF), and Neutron Beam Injection (NBI) systems. Two main auxiliary heating methods envisaged for heating to ignition temperatures are the injection of energetic neutral beams (NBI system) and the resonant absorption of radio frequency (RF) electromagnetic waves. The beams (NBI) used for heating have to be composed of neutral particles because ions would be reflected by the magnetic fields. Ions must first be produced and accelerated, then neutralized by charge exchange in a gas target and the unwanted residual ions removed. In the plasma, the neutral particles become charged again so that they can be confined by the magnetic fields. They are then slowed by collisions with the plasma particles giving up their energy in the process.

There are several types of RF heating, the three principal ones involving waves around the ion cyclotron frequency, the electron cyclotron frequency, and the lower hybrid frequency. The high-frequency waves are generated by oscillators outside the torus. The design of the system must be such that the waves propagate to the central region of the plasma and are then get absorbed by the charged particles of the plasma, which in turn collide with other plasma particles, thus increasing the temperature.

Particle control in ITER is achieved by fueling in the divertor and main chamber and by active pumping in the divertor. The primary functions of the **fueling system** are to inject DT fuel and other impurity gases into the vacuum vessel at the required fueling rate and response time to maintain the fusion power at the required level, and to provide impurity pellets to rapidly terminate the discharge. The fueling system will use a combination of gas puffing and pellet injection to achieve and maintain ignited DT plasmas. For gas puffing, a system of reservoirs, manifolds and injection valves will deliver hydrogenic (H, D, T) and other gases (for divertor radiation enhancement and wall conditioning) at two poloidal elevations: the top of the plasma and in the divertor chamber, and toroidally to five discrete locations. A separate delivery system will deliver reactive gases to the vacuum vessel as required for wall conditioning. The centrifuge pellet injector design consists of multiple hydrogenic extruders feeding a rotating wheel. The pellet injectors will be located external to the cryostat and will interface with the torus via a flight tube. A torus interface valve will be provided to isolate the pellet injector from the

machine. A separate pellet injector is provided to reliably and quickly deliver impurity pellets to the torus for discharge termination in response to a precursor signal of a VDE.

The **torus primary pumping system** is based on 16 cryogenic pumps, independently controlled to allow individual pumps to be regenerated, shut down in the event of failure or to regulate the pumping speed of the torus. Each pump will be located in the pump port directly behind the divertor. The pump is designed to pump impurities, hydrogenic species and helium on separate pumping surfaces and provide the capability to regenerate the hydrogenic species separately allowing direct recycling to the fuel re-injection system. A flap valve, mounted on the inlet to the pump is provided to allow regulation of pumping speed and total regeneration of the pump. A second flap valve and movable shroud are provided to allow regeneration of the hydrogenic pumping panels.

The external pumping for each of the three NBI enclosures are independent systems. The high vacuum pumping subsystem is used to pump trace of helium during NBI operations.

The fueling and pumping systems are part of the ITER fuel cycle, and are connected to the Tritium Processing Building, located adjacent to the tokamak building. The **tritium plant** processes the torus exhaust, separates the tritium and deuterium, and returns them to the fueling system. The tritium plant also detritiates the heat transport system coolant and the atmosphere in spaces where potential contamination can occur. Lastly, it provides the torus and attached spaces with inert gas for maintenance operations, and detritiates the gas upon exhaust.

The heat deposited in the internal components and the vessel is rejected to the environment via a set of heat transport systems designed to preclude releases of tritium and other radionuclides to the environment. Portions of the heat transport systems are also used to heat the inside of the vessel to bakeout temperatures above 200°C for impurity control. The heat transport system is comprised of: the primary heat transport systems (PHTSs), secondary heat transport systems (SHTSs), chemical and volume control systems (CVCSs), and the heat rejection systems.

The **power supply system** consists of the pulse power supply system and the steady-state power supply system. The pulse power supply system provides electrical power to the TF and PF superconducting magnets, and the auxiliary heating and current drive systems. Steady-state power supply system is for the plant electrical equipment which requires a steady supply of alternating current power.

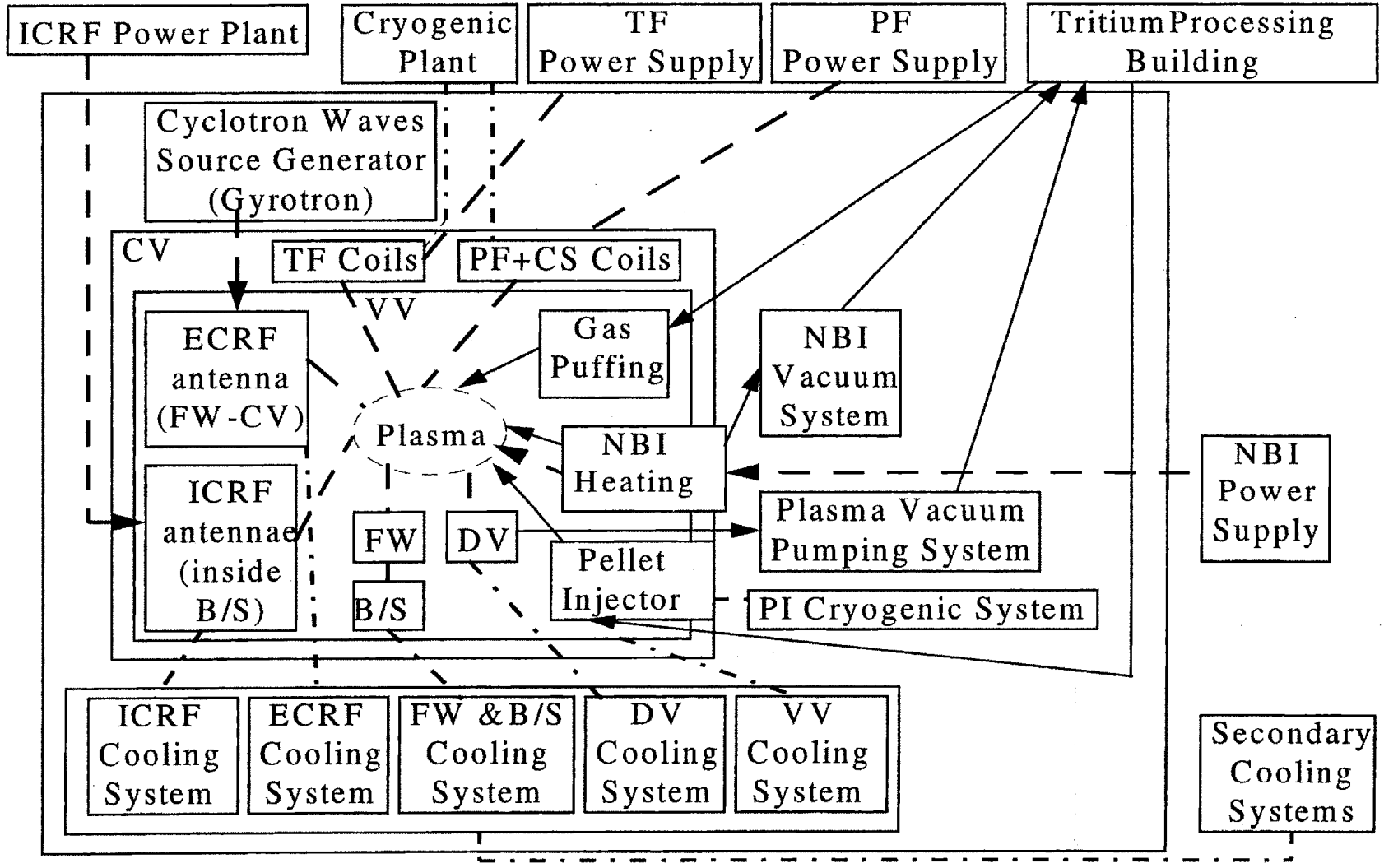

Figure 3-1: ITER Tokamak Building Systems Blocks Diagram

[*Legend:* full line for materials, dash line for energy, and dot-dash line for coolant (water or cryogenics)]

3.2 Initiating Events Identification

The objective of event tree development is to define a comprehensive set of accident sequences that encompasses the effects of all realistic and physically possible potential accidents involving the reactor core. By definition, an initiating event is the beginning point in the sequence. Hence, a comprehensive list of accident initiating events must be compiled to ensure that the event trees properly depict all important sequences.

The selection of initiating events for inclusion in event trees consists of two steps:

- Definition of possible events;
- Grouping of identified initiating events by the safety function to be performed or combinations of system responses.

A clear understanding of the general safety functions and features incorporated into the ITER plant design, supplemented by the preliminary system reviews presented in the previous section, provide the initial information necessary to select and group the initiating events.

Two approaches can be taken for identifying the accident initiating events. One is a comprehensive engineering evaluation, where the available information is evaluated and a list of initiating events is compiled based on the engineering judgment derived from the evaluation. This is called Failure Modes and Effects Analysis (FMEA), and is used by the ITER safety team. FMEA is a tabular approach, where typical headings identify the system and component under analysis, possible failure modes, the effect of failure an estimate of the criticality, the estimated probability of failure, mitigators, and possibly the support systems.[3-2] Another approach is the Master Logic Diagram, which more formally organizes the search for initiating events by constructing a top-level logic model and then deducing the appropriate set of initiating events. In this study, the later is used.

3.2.1 Master Logic Diagram for ITER

A summary fault tree, or master logic diagram (MLD), can be constructed to guide the selection and grouping of accident initiating events and to ensure completeness. Figures 3-2 and 3-3 show the ITER Master Logic Diagram (MLD).

The event "Excessive offsite release" of radionuclides is the top event. The events in the MLD are identified by the level they appear in the tree, with the top being level 1. The use of levels is an ordering technique to assist in locating events by approach to an offsite release. The strategy is to achieve completeness of events by level.

"Excessive offsite release", level 1, can result from either (OR gate) an excessive release from the tokamak building or from other building containing systems with radioactive inventories. Since these and only these release paths exist at ITER power plant, first step of level 2 is

complete. The scope of the present study encompasses only the accidents in the tokamak building, thus we do not develop the branch of "Excessive releases from non-tokamak building"[1]. Although there is an inherent linkage between the tokamak building and the tritium plant (e.g., fueling, vacuum pumping), that is neglected in the current work assuming that it has a small contribuition to the overall plant risk. A second step of level 2 follows from the "Excessive releases from the tokamak building", which can come either (OR gate) from the vacuum vessel, or from the primary heat transfer systems, or from other systems containing radioactive inventories and situated inside the tokamak building. Level 2 is now complete.

Level 3 refers to the confinement barriers. An excessive release from the vacuum vessel would require vacuum vessel failure, cryostat vessel and/or extensions failure, and tokamak building failure (AND gate). Similarly, an excessive release from the primary systems would require failure of the PHTS piping or equipment, failure of piping guard pipes or heat transfer system vault, and tokamak building failure. Other systems in tokamak building contain relatively small amounts of radioactive materials compared with the vacuum vessel and primary heat transport systems, therefore, we disregard them for now.

For these events to occur, some of the safety functions would have to fail. Thus, failure of the vacuum vessel could be caused by events such as: insufficient heat removal and chemical energy control, insufficient magnetic energy control, insufficient overpressure control, insufficient plasma control or support. Similarly, the failure of the cryostat vessel and its extensions could be the result of: insufficient control of overpressure caused by water or cryogenic fluid spills, insufficient air leakage control, insufficient radioactive inventories cleanup. The inclusion of safety functions completes level 4.

When the diagram reaches level 5, equipment failures or misoperations that could threaten each safety function are identified. A comprehensive listing of such events defines all important accident initiating events.

External events such as earthquakes, tornado, fires, floods, have not been included in this MLD for simplicity reasons.

Reference [3-3] developed a MLD for INTOR, as being representative for tokamak reactors, and it was the main reference we used for developing the ITER MLD.

[1] The rhomboid under a rectangle containing the event name means that the event is not developed further due to lack of sufficient information, or lack of interest for the purpose of the respective study.

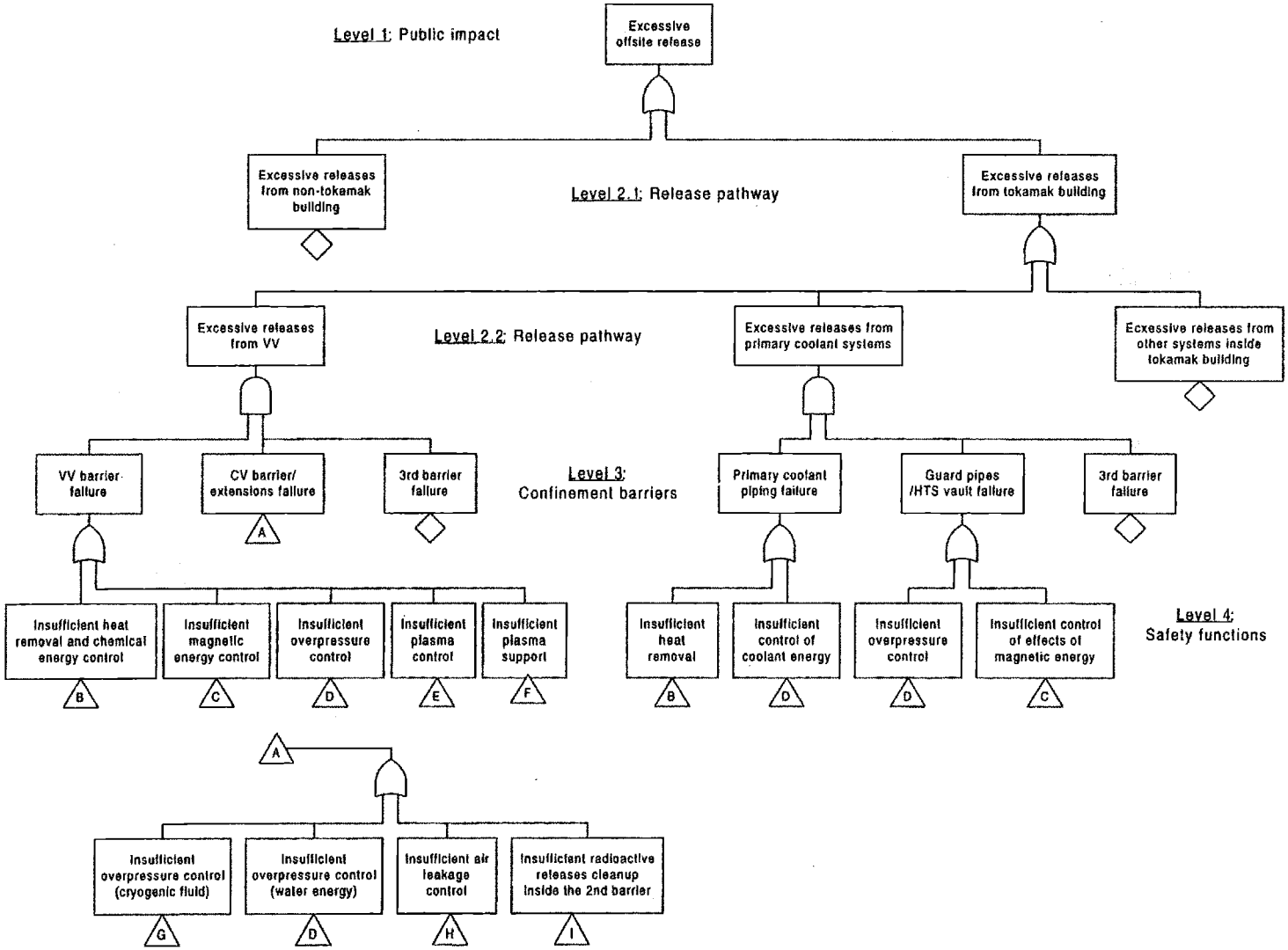

Figure 3-2: ITER Master Logic Diagram

Level 5: Initiating events

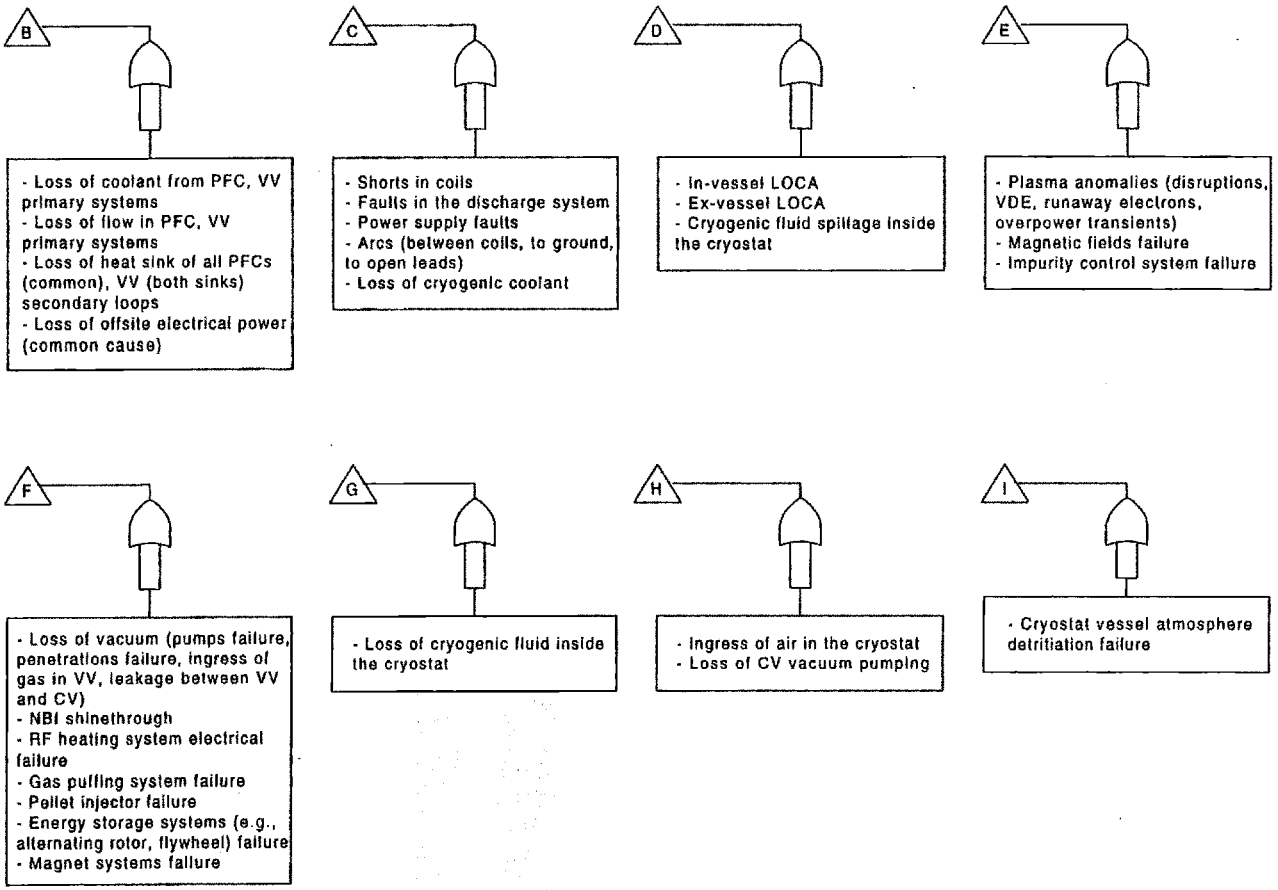

Figure 3-3: ITER Master Logic Diagram (cont.)

3.2.2 Initiating Event Categories

The initiating events defined by the MLD are already grouped by the safety function they most threaten. Figure 3-4 contains the list of initiating events grouped by the systems where they start. Chapter 5 presents accident sequences using the influence diagram/event tree model for all of these initiating events. However, only one IE in each category will be included in our model for simplicity reasons, and those IEs are shown in bold letters in Figure 3-4. The methodology we developed allows for the addition of an indefinite number of initiating events.

Initiating Events List

1. COOLANT ACCIDENTS:
   - 1.1 LBV1: Small in-vessel LOCA from FW/SB system
   - 1.2 LDO1: Ex-vessel LOCA in the divertor loop
   - 1.3 **LFO2: Ex-vessel LOCA of the FW/SB coolant loop**
   - 1.4 LFO3: Heat exchanger tube rupture in a FW/SB loop
   - 1.5 LFV99: Large in-vessel LOCA from FW/SB loops
   - 1.6 LGC: Generalized rupture of coolant lines in cryostat
   - 1.7 FF2: Loss of flow in a FW/SB coolant loop
   - 1.8 HB99: Loss of heat sink to divertor, blanket, and FW
2. MAGNETS ACCIDENTS:
   - 2.1 **MPO1: TF coil overcurrent**
   - 2.2 MPO2: CS/PF Coil Overcurrent
   - 2.3 MS: TF coil case failure from initial defect
   - 2.4 MAC: Short between busbars outside the cryostat
   - 2.5 MI: Insulation failure (Turn and Pancake arcs)
   - 2.6 MCC1: Cryogen leaks in cryostat
3. FUEL SYSTEM ACCIDENTS:
   - 3.1 **TVP1: Vacuum pump process boundary failure**
   - 3.2 TGP3: Failure of gas puffing valves in open position
4. PLASMA ACCIDENTS:
   - 4.1 **OP: Overpower transient**
5. LOSS OF VACUUM ACCIDENTS:
   - 5.1 VCL: Large leakage of air in the cryostat
   - 5.2 **VCS: Small leakage of air in the cryostat**
6. LOSS OF AUXILIARY SYSTEMS:
   - 6.1 **LOSP: Loss of offsite power**

Figure 3-4: ITER Initiating Event Categories

3.3 Accident Sequences Development using Influence Diagram/Event Tree Models

Given an IE, the question is asked: What plant systems or actions are involved in responding to this IE? In the fission power plant, where the goal is often to calculate the core meltdown frequency, the accident sequences are developed to the point where the core is damaged (this means that the first confinement barrier - the fuel cladding - has been breached); then, several core damage states are defined. Thus, many event sequences will lead to the same damage state. By equivalence, we will develop our ETs to the point where the first confinement barrier is breached. From the point of view of consequences, instead of damage states, we evaluate releases of radioactive inventories.

The Event Tree (ET) analysis was first introduced in the nuclear industry by the NRC WASH-1400, and has been used in the PRAs sponsored by the NRC and by utility PRAs. The ET analysis is an analytical tool that can be used to organize, characterize, and quantify potential accidents in a methodical manner. An ET models the sequence of events that results from a single initiating event, by postulating the success and failure of the mitigating systems and continue through all alternate paths, considering each consequence as a new initiating event.

The basic steps to constructing an event tree include the following:

1. list all possible initiating events;
2. identify functional system responses;
3. identify support system responses;
4. group initiating event with all responses;
5. define accident sequences: each system response has a corresponding branch that indicates whether or not it was successful; at the end of each sequence is an indication of the consequences that can be expected;
6. probabilities can be assigned to each step in the event tree to arrive at total probability of occurrence for each accident sequence.

The technique can be exhaustively thorough, while having two theoretical limits:

- the presumption that all system events have been anticipated;
- the presumption that all consequences of those events have been explored.

A potential disadvantage is that event trees can appear very impressive but contain serious errors. Care must be taken to thoroughly review the resulting tree against system descriptions, assumptions, and judgment factors.

In an actual ET, either systems or functions can serve as headings. There is considerable latitude as to the definition of event headings, but they have to be consistent with actual plant-response modes and to ensure that the heading can be precisely related to system-success criteria that can be translated for system-fault modeling. The placement of events across the tree is based on either the

time sequence in which they occur, proceeding from left to right, or some other logical order reflecting operational interdependence.

In general, if there are n event headings representing system functional responses, there are 2^n potential sequence associated with each initiating event. Because of the logic inherent in the ET process, only meaningful sequences are retained for further evaluation and illogical sequences are eliminated during the development of the tree, thus greatly reducing the total number of sequences to be evaluated.

The functions that must be performed to control the sources of energy in the plant and the radiation hazard are called "safety functions". The concept of safety functions forms the basis for selecting accident-initiating events and delineating potential plant responses. Generally, safety functions are defined by a group of actions that confinement barriers failure or minimize radionuclide releases. Such actions can result from the automatic or manual actuation of a system, from passive system performance, or from the natural feedback inherent in the design of a plant.

ITER Safety Functions are presented in Figure 3-5.[3-5][2] Within the design, major lines of defense are identified and an achievable reliability target is allocated to each such that the overall plant event sequence meets category release limits. The limiting accident cases are specified more or less independently for each line of defense as the basis for defining the reliability targets. By integrating the safety role of these lines of defense, an acceptable level of risk can be expected.

The confinement approach includes provision of multiple barriers, for example:

- vacuum vessel/cryostat;
- process lines/glove boxes;
- the ventilation system to ensure elevated releases for accidents.

For heat removal, the lines of defense involve:

- multiple normal heat removal paths and systems provided for machine operation;
- two independent loops of the vacuum vessel cooling systems;
- natural circulation capability of the vacuum vessel cooling system (should power be lost);
- the possibility of cooling the machine by introducing gas into the cryostat.

For fusion power, the lines of defense involve:

- normal plasma control and interlocks;
- safety fusion power shutdown system;
- the inherent characteristics of nuclear fusion, whereby impurities introduced into the plasma by off normal conditions act to terminate the plasma.

The ET technique was actually inspired by the decision trees used in decision analysis. A decision tree is a graphical representation of the decisions, uncertainties and values in a problem. The

[2] "General Design Requirements Document (GDRD)" and "General Safety and Environmental Design Criteria (GSEDC)" are chapters of [3-5].

nodes in the decision tree display all the possible combinations of decision and chance event states and show the impact (value) of each combination. There are two kinds of nodes: decision nodes and chance nodes. Each node has branches that represent possible sates, and chance node branches have associated probabilities. Thus, the ET is a decision tree which only has chance nodes, and those usually have only two possible states: success and failure. The probability of these two states adds to one, and hence it is sufficient to give the probability of either one state. In our analysis, we define the events in terms of system success, and supply the probability of system failure.

An alternative way of solving decision problems is the influence diagram, which is a graphical structure for modeling uncertain variables and decisions and explicitly revealing probabilistic (functional or system) dependence and the flow of information. It is an intuitive framework to formulate problems in a network representation, which includes all the components of a decision problem - decisions, uncertainties, and values - and the relationships among them. The rectangle indicates a decision node, the rounded rectangle is a value node, and a circle represents a chance node. The arrows between the nodes represent conditioning - the probabilities and values associated with the states of the conditioned event depend on the states of the conditioning event. The detailed data about the variables are stored within the nodes, so the diagram graph is compact and focuses attention on the relationships among the variables.

The major advantage of influence diagrams is an unambiguous representation of probabilistic and value dependencies. The directional arcs between chance nodes clearly indicate dependence; absence of arcs indicate independence. Hence, influence diagrams can graphically represent much larger models than decision trees can, because each additional influence diagram variable requires only a node and appropriate arcs, whereas a new decision tree variable typically requires multiplying the number of branches.

The disadvantage of the influence diagrams is that they are structurally symmetric in the sense that every scenario includes the same sequence of decisions and chance events. That leads to difficulties when trying to develop an influence diagram from an inherently asymmetric problem. In this case, it is possible to assign probabilities of 0 and 1 to set the state of an event, but that is not a convenient representation of accident sequences for a power plant. Influence diagrams also do not have a natural way to represent the results, an are difficult to debug and validate.

The use of influence diagrams in risk management was explored in [3-7] and [3-8]. The authors introduce the concept of conditional influence diagrams as an alternative to decision trees in risk management, and emphasize the advantage of the influence diagrams of being more compact, and displaying the dependencies among variables in a visible and understandable format.

References [3-9] and [3-10] offer a comprehensive description of methods to evaluate the influence diagram, pointing out that the influence diagram not only fosters good communications among people who are developing, analyzing, and using a model, but also it is a convenient structure for computer manipulation and solution procedures.

Decision trees have two main limitations in practical applications. First, they become very large very quickly, making them difficult to display and intimidating to work with. Second, they do not show probabilistic and value dependencies very well - although probabilities on the branches of one event can depend on the state of a previous event, there is no easy way to identify which previous event is conditioning the current probabilities.

As we discussed in previous paragraphs, traditional decision trees and traditional influence diagrams are very useful tools for modeling many problems. However, when trying to work on realistic problems, their limitations may seriously affect the models. In conclusion, it is far simpler and much clearer to use combined models with both an influence diagram and a decision tree to develop accident sequences for each initiating event. The model is described in Figure 3-6. The software we used to build and analyze the ITER models for the selected initiating events is called DPL (Decision Programming Language), and it provides a synthesis of decision trees and influence diagrams, allowing for capture of the benefits of each without having to obide by the limitations.[3-11] In DPL, the influence diagram (ID) and the event tree (ET) of a model - each contains only part of the model and requires the other for a complete picture of the analysis. The ID defines the events involved in the accident sequences and the relationships among them. Here, too, the data - the failure probabilities, the frequency of the initiating event, and the consequences in terms of radioactive inventories releases - are entered. This diagram does not contain information on the actual sequence of the events; as a result, ID of a combined model can be more compact than a traditional ID. The ET shows the chronology of the events that were defined in the ID. Because all the Probabilities and data are entered in the ID, the tree does not display this information. As a result, ET of a combined model is much more compact than a traditional ET.

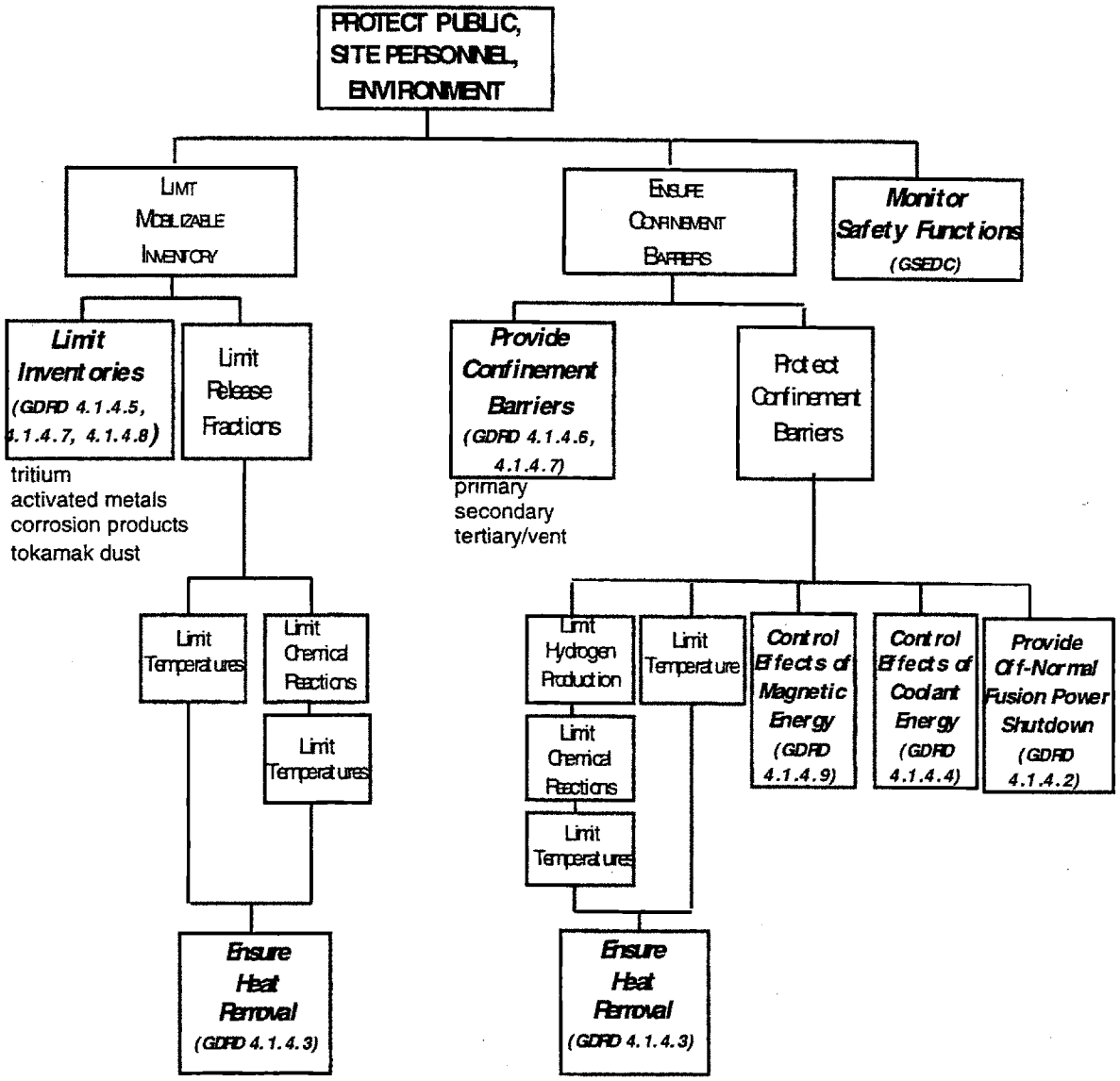

cvg May 26, 1995

Figure 3-5: ITER Safety Functions [3-5]

Influence Diagram/Event Tree Model

- Influence Diagram:
  - definition of the events and their relationships (conditioning relations)
  - data: event probabilities and releases associated with accident sequences
- Event Tree:
  - chronology of the events
  - easy to handle the asymmetries

Advantages: much larger models, unambiguous representation of probabilistic and value dependencies

Figure 3-6: The Influence Diagram/Event Tree Model

3.4 Method of Evaluating Performance of Confinement Barriers

ITER confinement strategy refers to multiple confinement barriers around any process system containing radioactive inventories. The reason is to preclude unacceptable radiological doses in case of normal operation and accidents. Since ITER is a first-of-a-kind machine, uncertainties both in physics and engineering are unavoidable. These reflect uncertainties in the frequency and consequence of each accident sequence. Thus, a probabilistic methodology for evaluating the performance of each confinement barrier can be an important tool for the design process. The goal of the present research is to develop a methodology that presents the results of accident sequence analysis for each confinement barrier individually. That allows sensitivity analysis for failure modes of each confinement barrier to be performed, which can be then used as a decision aid for choosing the most appropriate design.

In the fission power plants' Probabilistic Risk Assessment (PRA), the system analysis goal is to calculate the probability of core meltdown frequency potentially leading to radioactive releases to the environment. Thus, the accident sequences are developed up to the point where the core is damaged, and a few core-damage states are defined. Several event sequences can lead to the same damage state. In other words, damage of the reactor core means that the first confinement barrier - the fuel cladding - has been breached. By equivalence, we will develop the present event trees down to the point where the first confinement barrier integrity is lost due to one of the failure modes considered. Instead of damage states, values of radioactive releases such as tritium or activation products are considered.

For a multiple barrier confinement strategy, the analysis should have as many steps as the barriers required to comply with the ITER design requirements. These are given in Table 2-2 in Chapter 2. That table presents various radioactive release limits for individual event sequences according to the frequency of the sequence. The straight forward approach would have the following steps:

1. Analyze all the conceivable accident scenarios leading to possible damage of the first confinement barrier, and obtain a list of triplets $<s_i, f_i, c_i>$, where s_i is a scenario description, f_i is the frequency of that scenario (per year), and c_i is the consequence (i.e., radioactive release from the first confinement barrier) of that scenario. Build a frequency-consequences graph including those points along with the limit line based on Table 2-2; if there are points above the limit line, then a second confinement barrier is needed;
2. Develop containment models for the second confinement barrier representing its possible failure modes. Attach those models to the corresponding accidents sequences, and obtain a new set of frequency-consequence points representing scenarios for failure of the second confinement barrier. These points represented on the same graph from step 1 will correspond to lower

frequencies and consequences (due to confinement barrier retention factor); if there are still points above the limit line, then a third confinement barrier is required, and so on.

The position of the points representing scenarios on the frequency-consequences graph ultimately depends on the design parameters of the confinement barriers, which affect their probability of failure and retention factors.

The approach delineated above is similar to the European approach known as the ENEA Fusion Plant Safety Assessment (EFPSA), based on a "semi-probabilistic methodology" [3-24]. That is consistent with the limit line for ITER given in Table 2-2, which the authors of reference [3-24] call 'risk curve'. The only difference would be that we look at each confinement barrier independently instead of only comparing releases to the environment against the design limit.

'Risk' regulation is a very controversial concept. Approaches to the regulation of risk from technological systems, such as nuclear power plants, in which potential accidents may result in a broad range of adverse consequences must take into account several aspects of risk. Each country solves this problem in a different way, defining regulatory limits by employing more or less probabilistic criteria. Generally, probabilistic safety objectives or criteria for maintaining the public health level are of a political nature and therefore often phrased in broad terms. An extensive literature search was performed during this project to review the risk concepts and their use in the regulatory process.[3-2, 3-12 to 3-25] While most authors refer to 'risk' as the probability times consequences of an event, others believe that a single number is not a broad enough concept to communicate the idea of risk. In case of multiple scenarios, the probability times consequence view would correspond to the expected consequence per unit time:

$$R = \sum_{i=1}^{n} f_i \, c_i \qquad (3\text{-}1)$$

where R is the risk, f_i is the frequency of scenario i, c_i is the consequence of scenario i, and there are n conceivable scenarios.

In 1967, Farmer wrote a paper [3-12] which pulled together many of the issues over which safety regulators and analysts have been struggling ever since. Farmer suggested that the right format for capturing the results of a safety evaluation should be a "probability-consequence diagram". Farmer limit line can be used as a safety criterion by defining a limit on the frequencies for a given level of consequences. Several authors interpreted the Farmer limit line in different ways. For example, Cox and Baybutt [3-17] explain that the Farmer limit line sets acceptability criteria only for the risk due to individual accident sequences. Meleis and Erdmann [3-27] consider that Farmer criterion specifies upper limits for the releases of iodine (^{131}I) in accident situations of a given frequency. In response, Farmer published the definition of the Farmer limit line.[3-28] He defined a function g(C) such as the probability dP(C) that a release will occur in the interval C to C+dC is as follows:

$$dP(C) = g(C)\, dC \tag{3-2}$$

The Farmer limit line is defined by the following equation, since Farmer used logarithmic rather than linear scales:

$$dP(C) = F(C)\, d(\log_{10} C) \tag{3-3}$$

In logarithmic scales, the line of constant risk (risk = frequency times consequence) has a slope equal to -1. Consideration of risk aversion lead Farmer to propose a line of slope -1.5. In the low consequences range, the line is curved to control nuisance releases. The exact location of the line is adjusted in accordance with the requirements of the regulatory agencies or public opinion.

Kaplan and Garrick [3-15] introduced a graphical representation in a logarithmic scale of the first-level definition of risk as the set of triplets:

$$R = \{< s_i, f_i, c_i >\}, \quad i = 1,2,\ldots,n \tag{3-4}$$

Furthermore, if the consequences c_i obey the ordering relationship:

$$c_1 \leq c_2 \leq c_3 \leq \ldots \leq c_n \tag{3-5}$$

a cumulative frequency can be calculated as shown in Table 3-1. This is another way to represent the risk by the so called "risk curves", which is the complementary cumulative frequency of consequences[3] (CCF) of consequences plotted against the consequences in logarithmic scales. $CCF(c_0)$ is the frequency of events with consequences greater than or equal to c_0. WASH-1400 is a well known example of presenting the results in the CCF form [3-16]. Risk curves can be built both when using point estimates and probability distribution functions for the frequencies and consequences of the accident scenarios, so that the propagation of uncertainties is possible in this approach. Some other advantages are presented in [3-18].

---

[3] $F(y) = \sum_{x \leq y} f(x)$, where f(x) is the cumulative frequency (CF) function, and x is the release for each accident sequence. CCF = 1 - CF.

Table 3-1: Scenario List with Cumulative Frequency

Radioactive Releases (x_i)	Frequency (f_i)	Complementary Cumulative Frequency (CCF_i)
x_1	f_1	$CCF_1 = CCF_2 + f_1$
x_2	f_2	$CCF_2 = CCF_3 + f_2$
.	.	.
.	.	.
.	.	.
x_i	f_i	$CCF_i = CCF_{i+1} + f_i$
.	.	.
.	.	.
.	.	.
x_{n-1}	f_{n-1}	$CCF_{n-1} = CCF_n + f_{n-1}$
x_n	f_n	$CCF_n = f_n$

We decided to represent the results from the analysis of each confinement barrier by a CCF of consequences. In the quantitative representation of the CCFs, it is important to affirm the following assumption: the scenarios should be chosen so that they are mutually exclusive[4], meaning that the simultaneous occurrence of two or more scenarios is practically impossible. This is intuitively true when the scenarios follow from the same initiating event, but it is not necessarily the case when the scenarios are caused by distinct initiating events.

The result of running the ID/ET model of each initiating event in DPL [3-11] is a frequency histogram of consequences. DPL does not offer the choice of explicitly seeing the list of scenarios with corresponding consequence and frequency, but it sums the frequencies corresponding to the same consequence. This is just a step forward towards calculating the CCF of consequences for each confinement barrier.

DPL has the option of exporting the histogram data to another application such as a spreadsheet package (i.e., EXCEL or LOTUS 1-2-3). In the present work, we export the frequency histogram for each IE in EXCEL in a .csv file format. For a number of n IEs, n EXCEL files will be generated and they have to be combined in a single CCF for the given confinement barrier. This is an exhaustive operation which is performed in several steps as shown in Figure 3-8:

- link each .csv file with the corresponding IE's worksheet in the EXCEL file for the first confinement barrier IEs_1st.xls;[5]

[4] For two mutually exclusive events A and B, Pr(A or B) = Pr(A) + Pr(B). If A and B are not mutually exclusive, Pr(A or B) = Pr(A) + Pr(B) - Pr(A and B), where Pr(A and B) = Pr(A)Pr(B) if the events are independent, and Pr(A and B) = Pr(A) Pr(B|A) = Pr(A|B) Pr(B) if the events are dependent.

[5] EXCEL allows Dynamic Data Exchange (DDE) between cells in separate workbooks, and separate worksheets in the same workbook. If two cells are linked, one being the source and the other the target information, when the value of the source changes, EXCEL automatically updates the value of the target.

- a 'data advanced filter' operation is performed on each histogram to cut the frequencies lower than 10^{-8}/yr;[6]
- the worksheet are linked together in a pivot table that adds frequencies corresponding to the same release value, to calculate the overall frequency histogram for the first confinement barrier;
- The frequency-consequence table is sorted by releases in increasing order in preparation for the CCF calculation;[7]
- the overall CCF for the first confinement barrier is calculated according to the Table 3-1, and it is represented graphically in a scattered plot on a log-log scale.

Eventually, the same steps are performed for the second and third confinement barriers, except that the .csv input files are obtained by running the DPL ID/ET models that include the second and third confinement barriers models respectively.

Instead of performing all these steps manually for a large number of times required for sensitivity analysis, a Visual Basic macro was created for the EXCEL operations and a button was assigned to it. The macro for the first confinement barrier CCF calculation is attached in Appendix A.

Sensitivity analysis entails the determination of how rapidly the output of the analysis changes with respect to variations in the input. Sensitivity analysis can be particularly useful in this study for assessing the impacts of different failure modes on confinement barriers.

[6] ITER has a proposed cut-off frequency for the design basis accidents of 10^{-6}/yr.

[7] The 'data sort' operation is not very reliable, and it has to be done in a separate worksheet than the one containing the pivot table.

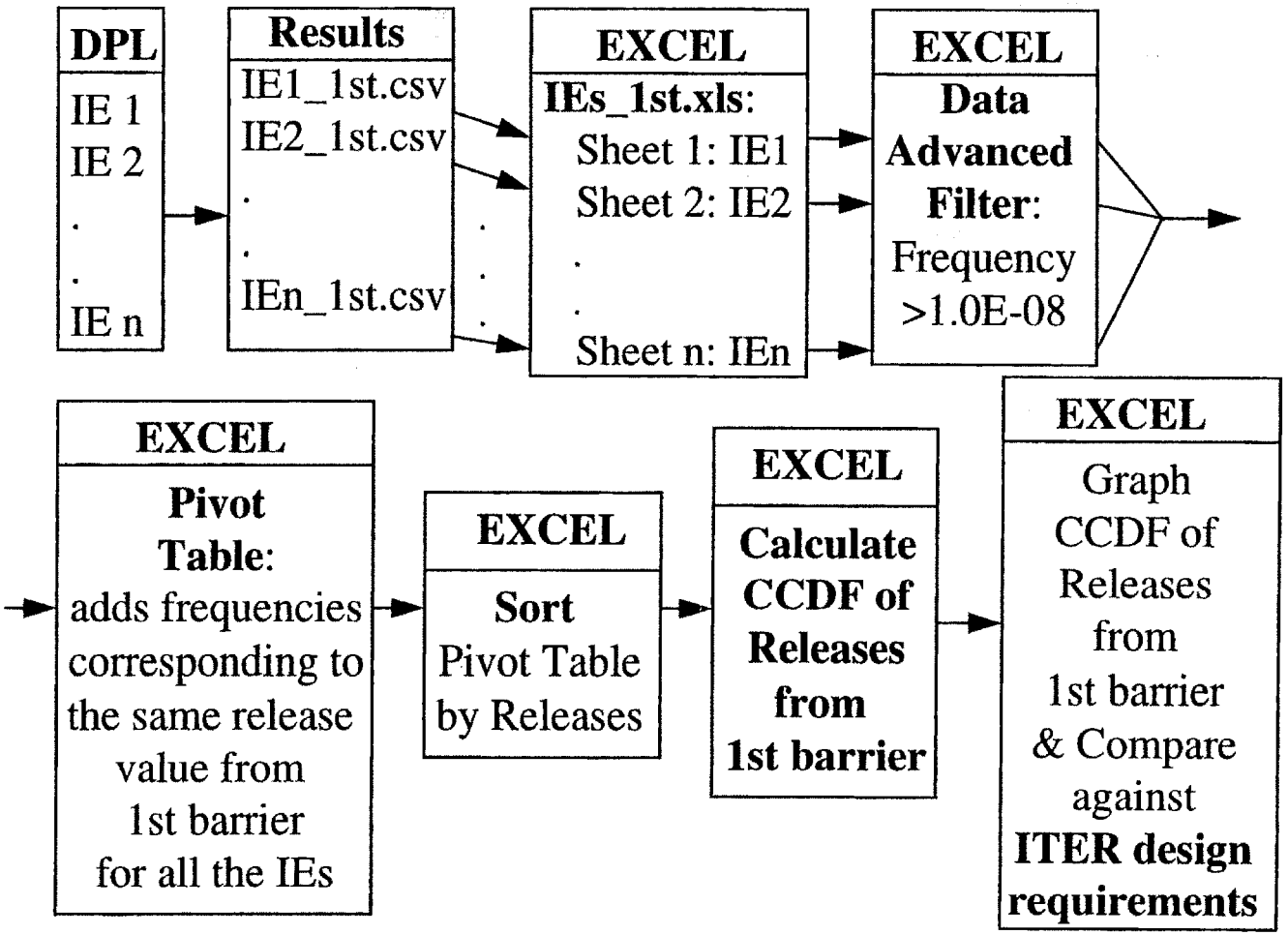

Figure 3-7: Schematic Presentation of Methodology Workflow

3.5 Uncertainty Analysis Considerations

Uncertainty analysis is an integral part of a risk assessment. There are uncertainties in every step of a PRA, and some of them may be large. Whether qualitative or quantitative in nature, the analysis should consider uncertainties in the data base, uncertainties arising from assumptions in modeling, and the completeness of the analysis. To the extent possible, these uncertainties should be propagated through the analysis. Where this is impractical, a sensitivity analysis provides insight into the possible range of results, and this is what we choose to do in the present work.

This section will give an overview of reasons the uncertainty analysis is important, and a suggestion for the integration of the frequencies and uncertainties in the risk curve.

The uncertainty analysis addresses those factors that cause the results of the analysis to be uncertain, due to a variety of causes. The causes of uncertainty fall into three basic categories: uncertainties in the parameter values[8], uncertainties in modeling[9], and uncertainties in the degree of completeness[10]. Parameter uncertainty may be quantitatively analyzed using standard propagation methods such as the Moments Methods or Monte Carlo simulation method.[3-26]

A concise method of displaying the uncertainties in the overall results of a PRA is to represent a series of CCFs. The risk will then be represented by a family of CCF curves that could represent, for instance, the best estimate and the upper and lower bounds. If a full uncertainty analysis were done, it would be possible to produce a series of curves at different probability levels.

When considering the parameter uncertainties, each accident sequence s_i could be associated a probability distribution function (PDF) for frequency and another one for consequence. Using the CCF definition, the CCFs of consequences for all the accident scenarios can be calculated and plotted on a log-log scale as in Figure 3-8. Figure 3-8 gives $\text{Probability}(c \geq c_i | s_i)$ for three scenarios: i = 1, 2, 3. Each of these consequence CCF has an associated frequency PDF, thus, at each value of consequences c_i, a PDF for the overall $CCF(c_i)$ can be obtained. Monte Carlo simulation can propagate the uncertainties through the equation (3-4) to obtain a PDF for the CCF at each value of consequences. Then, the mean values of these PDFs at each c_i can be calculated resulting in the best estimate of the risk curve: $CCF_{50\%}(c_i)$. Similarly, lower and upper bounds risk curves can be obtained by calculating the 10-th and 90-th percentiles of the PDFs respectively.

---

[8] The values of the input parameters are not exactly known. Data limitations or uncertainties in component failure rates require the use of probability distributions or interval estimates to model frequencies for the IEs and probabilities for system failures, as well as consequences.

[9] Basic assumptions about accident sequences, system failure modes, and the application of the quantification formulas may not be correct.

[10] Important failure modes can be overlooked. The scope of the risk assessment may preclude the analysis of all the IEs, the required information may not be available to the analyst, or the quantification process may truncate sequences with large consequences-low frequency that sum to a significant frequency.

$$CCF(c_i) = \text{Frequency}\ (c \geq c_i) \qquad (3\text{-}6)$$

$$CCF(c_i) = \sum_{\text{all } s_i} \text{Probability}\ (c \geq c_i \mid s_i) \cdot \text{Frequency}\ (s_i)$$

where Probability$(c \geq c_i \mid s_i)$ = CCDF of consequences for scenario s_i

and Frequency (s_i) = frequency distribution for scenarios$_i$

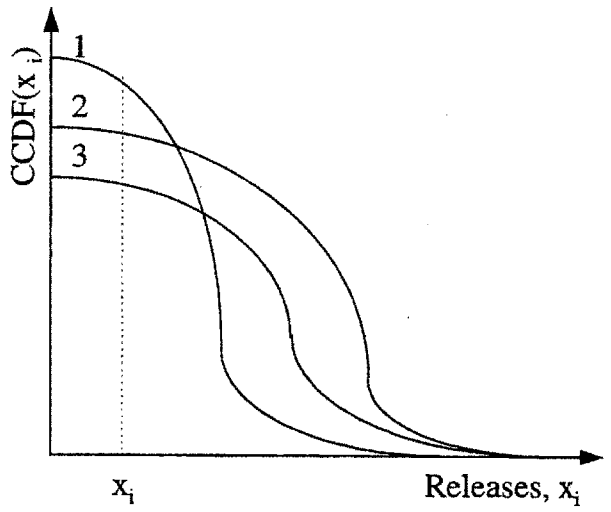

Figure 3-8: CCDFs of Releases Corresponding to Three Initiating Events

The current version of the DPL does not offer the option of associating a PDF to the probability of system failure, therefore uncertainty analysis can not be performed directly. The task of propagating uncertainties through the model is not undertaken in the present study.

3.6 Proposed Limit Line for Risk

The ITER project must set its working limits for release of hazardous substances in such a way that the design does not have to be significantly modified after the site selection. The current ITER design guideline of radioactivity releases sets acceptability criteria only for the risk due to individual accident sequences, and does not provide a limit for the overall plant risk. This creates an important limitation to the methodology, because a large concentration of accident sequences near the limit line could lead to unacceptable overall risk, despite the adequately low risk posed by each individual sequence. Another problem is the treatment of uncertainties. Since ITER is a first-of-a-kind machine, uncertainties both in physics and engineering are unavoidable. As the ITER design develops further and the system safety analysis step is reached, propagation of uncertainties will become more important, but the current ITER design requirement does not allow for a convenient integration of uncertainties. This section proposes a parametric form for the risk limit lines to be used as ITER design assessment tool.

The safety analysis results presented in the risk curves form will have to be compared against a safety criterion in the CCF form. We derive a parametric form for a CCF limit line, which accounts for three criteria:

1. the overall plant risk;
2. the rate at which accident frequency decreases with increasing accident consequences (risk aversion attitude);
3. impact of high frequency-low consequence accidents.

For ITER, five event categories have been defined (see Table 2-2). The classes of event sequences are based on the expected annual occurrence frequency of the event sequence. A dose/release limit per event sequence is established for each events category.

A CCF limit line with appropriately chosen parametric form for fission reactors was proposed based on the three requirements delineated above.[3-17] In the present work, the current ITER design guideline of releases was used to determine the slope and position of the limit line. First, a limit line in the form of a frequency distribution of releases was obtained and then integrated to lead to the desired CCF limit line.

Criterion 2 is concerned with risk aversion, which refers to the greater importance attached by the public to single catastrophic accidents as opposed to a large number of small accidents with similar total consequences. We can account for the risk averse attitude by requiring that accident sequence frequencies to decrease faster than the accident consequences increase. In other words, the following condition should hold:

$$c\,f(c) \text{ is a decreasing function of } c \text{ for all } c \geq c_0 \qquad (3\text{-}7)$$

where c are the consequences (low consequences $c < c_0$ will be treated separately) and f(c) is the frequency histogram of the consequences.

It can be proven that, in a normal (non-logarithmic scale), a function f(c) satisfying the conditions:

$$f(c) < f_0(c) \tag{3-8}$$

$$\frac{df}{dc} < \frac{df_0}{dc}, \text{ where } \frac{df}{dc} < 0, \frac{df_0}{dc} < 0, \text{ and } c \cdot f_0(c) = \text{constant} \tag{3-9}$$

for all $c \geq c_0$, also satisfies condition (3-7). Figure 3-10 shows the f(c) function which gives a decreasing risk in c as opposed to $f_0(c)$ corresponding to a constant risk.

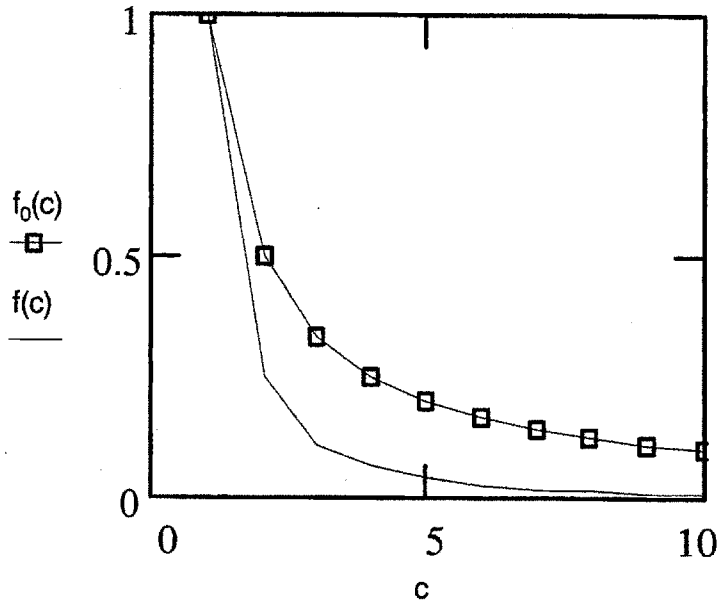

Figure 3-9: Frequency-consequence diagram in non-logarithmic scale

In a logarithmic scale, functions $f_0(c)$ and f(c) above are shown in Figure 3-11. In this case, f(c) should comply with the following conditions:

$$\log f(c) < \log f_0(c), \tag{3-10}$$

$$\frac{d\log f(c)}{d\log c} < \frac{d\log f_0(c)}{d\log c} = -1, \qquad (3\text{-}11)$$

where $\frac{d\log f(c)}{d\log c} < 0, cf_0(c) = constant,$

for all $c \geq c_0$. Conditions (3-10) and (3-11) are not sufficient to give us a function f(c) verifying condition (3-7). However, by imposing that:

$c^2 f(c)$ is a decreasing function of c for all $c \geq c_0$, (3-12)

It can be shown that condition (3-7), as well as (3-10) and (3-11) are satisfied. Hence, (3-12 is a stronger requirement than (3-7 on the function f(c). Thus, to ensure the risk averse attitude in a log-log scale, we can now conclude that f(c) could have the form:

$f(c) = k \cdot c^{-a}$, where $a > 2$, for all $c \geq c_0$, (3-13)

and k is a positive constant. However, we will also include in this study the cases when a = 1 (no risk aversion), a = 2, and 1 < a < 2. We analyze these situations because we do not know if the current ITER limit line has included or not risk aversion in its definition. It is therefore interesting to provide a family of frequency distribution of releases corresponding to different risk aversion attitudes, among which the regulatory committee could chose the one reflecting its views.

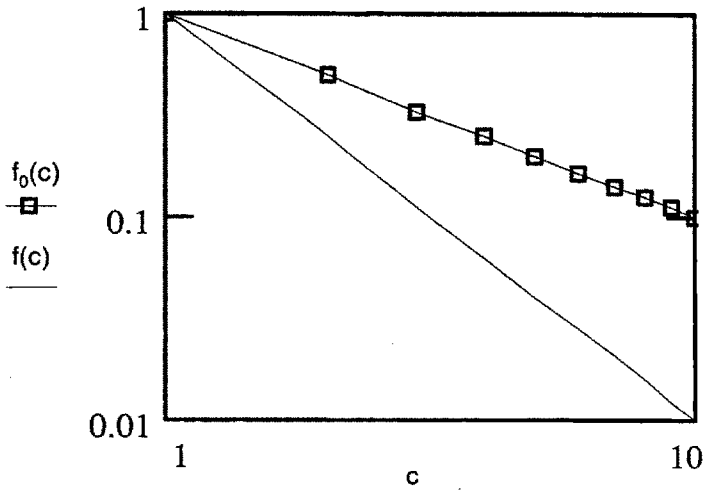

Figure 3-10: Frequency-consequence diagram in logarithmic scale

Let us next consider the impact of the high frequency - low consequence accident sequences. Farmer [3-12] proposed a transition in the slope at a certain value of consequences (called the nuisance value) to minimize the frequency of small consequences. In other words, even very small consequences, close to zero, are desired to have a frequency not higher than a chosen k_1. Its value can be derived by imposing a maximum acceptable value for the risk R_0 due to high frequency - low consequence accidents only.

The complete form of the frequency distribution function of consequences is:

$$f(c) = \begin{cases} k_1, \text{ for } c < c_0 \\ k_2 \cdot c^{-a}, \text{ for } c \geq c_0 \end{cases}. \tag{3-14}$$

An overall risk limit R_{tot} is used to determine the positive parameter k_2, and the risk limit R_0 on low consequence - high frequency accidents is used to determine k_1. In a mathematical form, conditions (3-15) and (3-16) are used to determine the parameters k_1 and k_2, while considering three separate cases for the value of parameter a:

1. $a = 1$;
2. $a = 2$;
3. $1 < a < 2$ or $a > 2$.

$$\int_0^{c_0} cf(c)dc = R_0, \tag{3-15}$$

$$\int_0^{\infty} cf(c)dc = R_{tot}. \tag{3-16}$$

k_1 is derived from equation (3-15) and does not depend on the value of a:

$$k_1 = \frac{2R_0}{c_0^2} \tag{3-17}$$

k_2 is derived from equation (3-16) and depends on the value of a:

Table 3-2: Values of k_2 as a function of a

	a = 1	**a = 2**	**1 <a < 2 or a > 2**
k_2	$\left(R_{tot} - k_1 \frac{c_0^2}{2}\right)\left(\frac{1}{c_{max} - c_0}\right)$	$\left(R_{tot} - k_1 \frac{c_0^2}{2}\right)\left(\frac{1}{\ln(c_{max} - c_0)}\right)$	$\left(\frac{2-a}{c_{max}^{2-a} - c_0^{2-a}}\right)\left(R_{tot} - k_1 \frac{c_0^2}{2}\right)$

The values for the risk limits R_0 and R_{tot} were calculated using the proposed ITER design tritium releases guidelines (Table 2-2). The data in that table can be plotted in a frequency -

consequence form in Figure 3-12. The overall risk limit is the overall expected value of consequences per year:

$$R_{tot} = \int_0^{\infty} c\, f_{ITERlim}(c)dc\,, \tag{3-18}$$

and the risk limit for the low consequence accidents can be calculated by changing the upper limit of the integral in (3-18):

$$R_0 = \int_0^{c_0} c\, f_{ITERlim}(c)dc\,, \tag{3-19}$$

where $f_{ITERlim}$ is the annual frequency function of HTO releases in grams given in Figure 3-12.

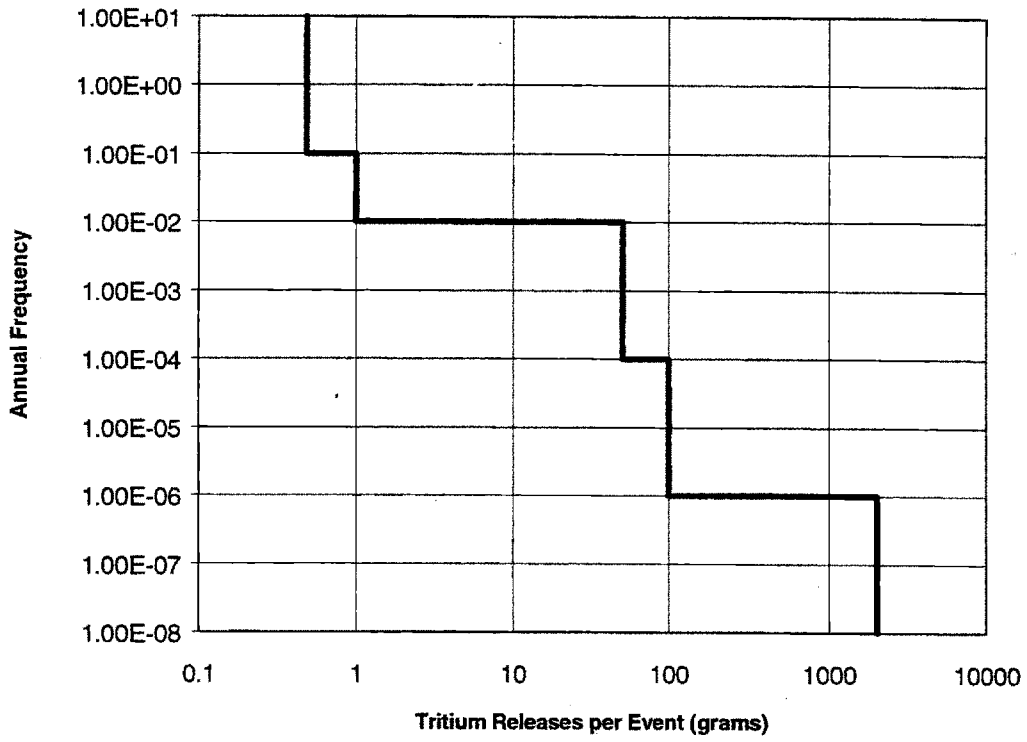

Figure 3-11: ITER Design Guideline for HTO Releases

For the ITER case, we assigned to c_0 the value of the tritium release limit for operational events category (category I) (0.5 grams).

The parametric form for the limit line as a frequency distribution of tritium releases as obtained for ITER is presented in equation (3-20), and a selection of k_2 parameters for five a values is also given:

$$f(c) = \begin{cases} 10, \text{ for } c < 0.5 \\ k_2 \cdot c^{-a}, \text{ for } c \geq 0.5 \end{cases} \quad (3\text{-}20)$$

where $k_2(a = 1) = 0.0036$, $k_2(a = 1.5) = 0.1175$, $k_2(a = 2) = 1.791$,
$k_2(a = 3) = 7.4524$, $k_2(a = 4) = 7.4515$.

In conclusion, a large set of pairs (a, k_2) defining the proposed limit line given in equation (3-20) is available for the respective regulatory commission to choose from, corresponding to the desired conservatism. The set of parametric forms for the proposed frequency distribution function of consequences can now be compared against the frequency - consequence graph for ITER as given by the current design guidelines (Figure 3-12).

The CCF form is derived by using its definition[11] as following:

$$\bar{F} = \int_c^{\infty} f(c)dc \quad (3\text{-}21)$$

Therefore, the parametric form of the proposed CCF for the three cases corresponding to parameter a is as following:

1. $$\bar{F}(c) = \begin{cases} k_1(c_0 - c) + k_2 \ln(c_{max} - c_0), & \text{for } c < c_0 \\ k_2 \ln(c_{max} - c), & \text{for } c \geq c_0 \end{cases}, \text{ for } a = 1, \quad (3\text{-}22)$$

2. $$\bar{F}(c) = \begin{cases} k_1(c_0 - c) + k_2\left(\frac{1}{c_0} - \frac{1}{c_{max}}\right), & \text{for } c < c_0 \\ k_2\left(\frac{1}{c} - \frac{1}{c_{max}}\right), & \text{for } c \geq c_0 \end{cases}, \text{ for } a = 2, \quad (3\text{-}23)$$

[11] The upper limit of the integral is actually c_{max}, because $\int_{c_{max}}^{\infty} f(c)dc = 0$.

3. $$\bar{F}(c)=\begin{cases} k_1(c_0-c)+\dfrac{k_2}{a-1}\left(\dfrac{1}{c_0^{a-1}}-\dfrac{1}{c_{max}^{a-1}}\right), & \text{for } c<c_0 \\ \dfrac{k_2}{a-1}\left(\dfrac{1}{c^{a-1}}-\dfrac{1}{c_{max}^{a-1}}\right), & \text{for } c\geq c_0 \end{cases}, \qquad (3\text{-}24)$$

for $1 < a < 2$ or $a > 2$, and k_2 given in Table 3-2.

This function is the proposed CCF of consequences limit line for ITER, and a family of CCF lines for different risk aversion attitudes is represented in Figure 3-13.

In conclusion, we have proposed a CCF as a limit line for ITER. We believe that a CCF of consequences is a suitable tool for constraining the risk from a fusion power plant. Quantitative risk standards can be imposed, while being sufficiently flexible to allow the designers and regulators to take into account several important aspects of risk: the overall risk limit, the risk averse attitude, the impact of high frequency - low consequence accident sequences. The CCF limit is obtained by integrating a proposed frequency distribution limit line shown in Figure 3-13. From to comparison of the frequency distribution with no risk aversion against the current ITER limit line it can be concluded that the ITER limit line has already some risk aversion attitude incorporated in its formulation. That is, the limit line with a risk aversion corresponding to a = 1.5 fits the inclination of the ITER line more closely than the line with a = 1. However, we propose the limit line with a = 3, due to the reasons explained in equations (3-7) to (3-12).

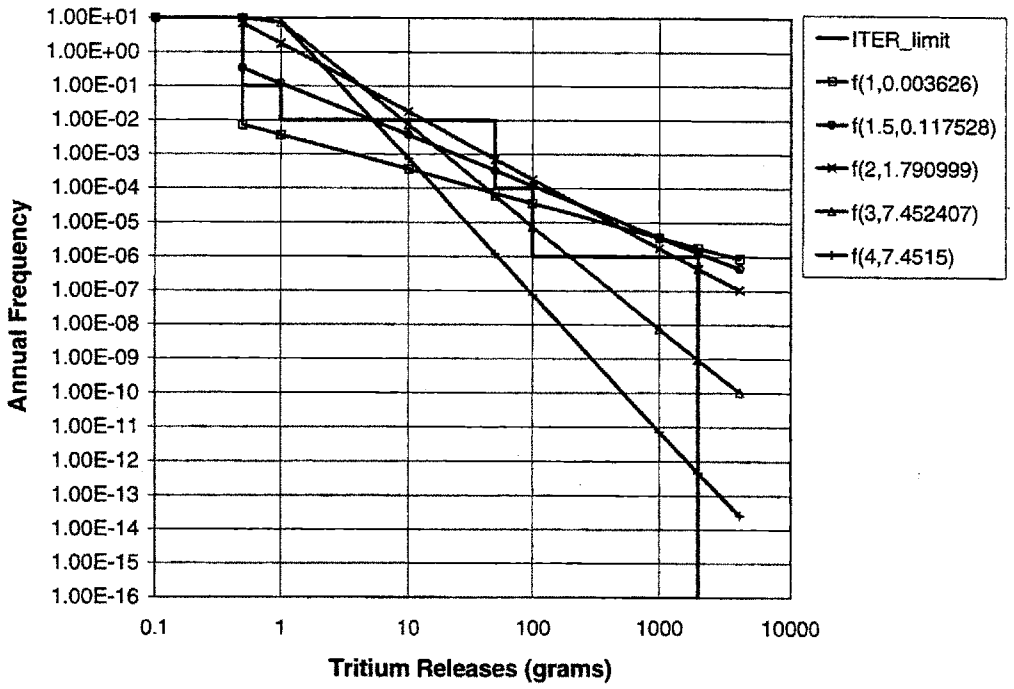

Figure 3-12: Proposed parametric frequency distribution of tritium releases for ITER compared against the ITER design guideline releases[12]

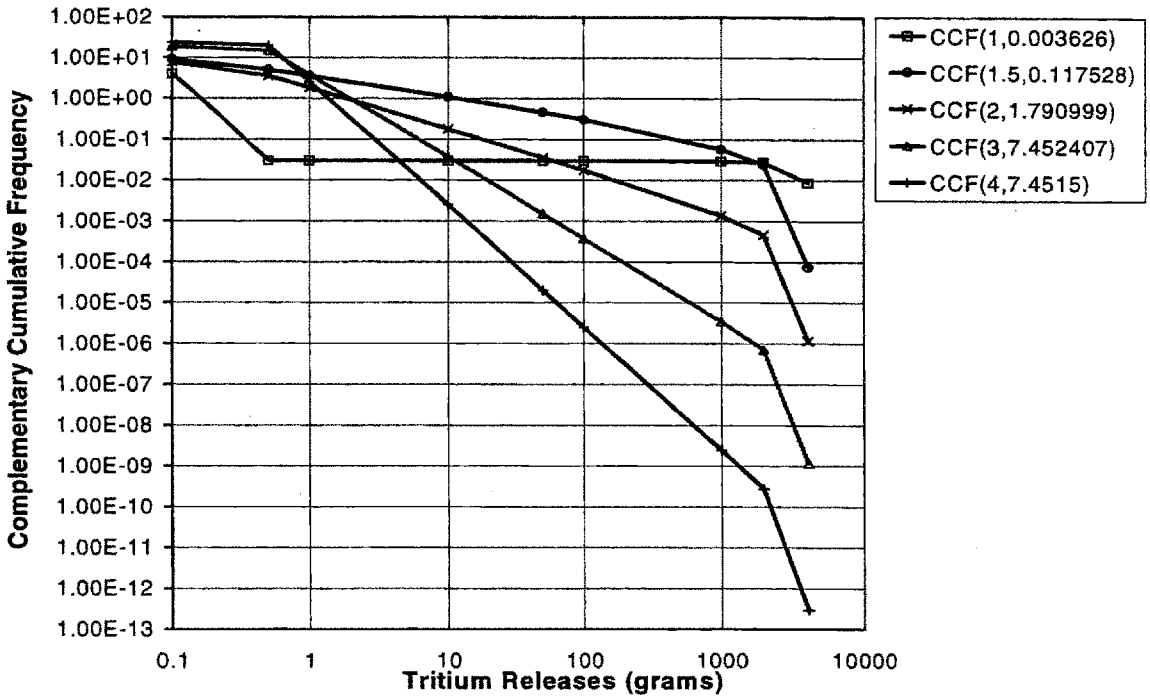

Figure 3-13: Proposed parametric CCF of tritium releases for ITER

[12] The legend refers to f(c) as a function of (a, k_2).

4. Analysis of Accident Sequences that affect the Integrity of the First Confinement Barrier[1]

The purpose of the Accident Analysis is to evaluate the effect of postulated events that develop into accidents. The analysis determine potential initiating events that could lead to various accidents involving the release of hazardous materials. Based on the materials and energy involved, the physical parameters of the immediate environment can be determined. Between the hazardous material and the affected target (i.e., environment, public), there usually are several barriers in the form of safety-related systems. The challenges to the barriers are those physical conditions posed by the accident. It should be determined whether or not the barriers will fail when challenged by the conditions resulting from the accident.

The identification and delineation of combinations of events that might lead to release of hazardous material or other undesired events is the first step of any Probabilistic Risk Assessment (PRA) performed for nuclear fission power plants. In that field, the PRAs focus is on severe core damage or core melt accidents, as they pose the greatest potential risk to the public. Therefore, the qualitative result is a list of all conceivable core-melt sequences, which are developed down to the point where the core has reached a damage state (PRA Level 1). The quantitative analysis at the PRA Level 1 consists of evaluating the frequencies of occurrence and the particular damage state of each accident sequence. The following step is to evaluate the response of the containment, and the transport and release of the radionuclides from the core to the environment (PRA Level 2).

In a fusion power plant, the fuel is not confined in a reactor core as in a fission power plant, but is recirculated through various systems, part of which are located outside the tokamak reactor building. Thus, there is no such concept as "core damage". Between the process and the environment, several confinement barriers should be provided, so that radioactive releases to the environment in any conceivable accident situation are kept under prescribed design limits.

The safety requirements for the ITER design recommend at least two robust confinement barriers such as the vacuum vessel and cryostat with extensions, when significant radiological hazards exist. Although there are other systems connected to the vacuum vessel which might be contaminated by tritium, we will only evaluate the performance of the vacuum vessel, the cryostat, and the tokamak building as confinement barriers, for the purpose of developing a methodology.

The accident sequence analysis contains two parts:

1. the qualitative analysis, consisting of the development of the accident sequences using an influence diagram/event tree model;

---

[1] Only six initiating events will be analyzed in this chapter, the rest will be attached Appendix B. The reason is that the construction of our probabilistic model is based only on these six events, eventually allowing for the inclusion of the others. However, this last part is outside the scope of the present study.

2. the quantitative analysis, referring to the estimation of probabilities of occurrence of various events, data base design, and radioactive releases evaluation.

The first step of the qualitative analysis refers to accident sequences which stop when the first confinement barrier is damaged. The second step consists in modeling the behavior of the second confinement barrier, given that the first barrier failed. In case the releases out of the second barrier are higher than the design limits, a third barrier will be required, and its performance will be evaluated.

Our main reference was ESECS [4-1] Chapter 6 "Analysis of Accident Sequences". ESECS used Failure Modes and Effects Analysis (FMEA) as a systematic method to identify the initiating events. At the time the analysis was performed, not enough system design information was available to develop a system based FMEA. Therefore, a functional FMEA was performed. Also, the document presents the functional event trees for a set of initiating events. A functional event tree orders and depicts the safety functional responses that mitigate the initiating event. The headings of the function event tree are statements of safety functions required. The problem with function event trees is that some functions are quite complex and may be provided by many combinations of systems. The success of each function can then be expressed in terms of system engineered safety systems, and support systems success.

As we developed the accident sequences after the ITER Design Description Documents became available, our approach was to describe accident sequences in the form of influence diagram/event tree (ID/ET) models, while using the function event trees of the ESECS [4-1] as a starting point.

The previous chapter on method development describes the Master logic Diagram as the tool used in the present work for developing a comprehensive list of initiating events for a fusion power plant. For accident analysis, we selected a set of initiating events also considered in ESECS, for the purpose of comparison.

Developing accident sequences for a system as complex as a nuclear power plant is a considerable team effort, and the results depend on the expertise and the subjective judgment of a particular team. Since the ITER project has a powerful safety team, our work considered their results to the extent possible in analyzing the accident sequences. The main differences between our approach and the ITER safety team approach are:

- we developed system accident sequences as opposed to function event trees;
- we used influence diagram/event trees instead of event trees;
- we developed separate modules for initiating events affecting different systems, then integrated their effects on the systems with common interfaces. Thus, the accident is propagated from one system to another.

These issues are more thoroughly explained in the "Method Development" chapter.

In the following paragraphs, phenomena characteristic to fusion reactors will be mentioned such as: disruptions, runaway electron damage, electromagnetic loads. Brief definitions are given here to explain the effect of these phenomena on the plasma facing components.

- **Disruptions**: Disruptions of plasma in ITER will result in significant transient heat loads on the in-vessel components and appreciable electrodynamical stresses on the first wall, divertor and surrounding structures.
- **Runaway electron damage**: Disruptions of the ITER ignited plasma have capability to vaporize a large amount of plasma-facing material, and result in the fast decay of a plasma current, which will induce a strong electric field and produce significant runaways. In addition, the large plasma current of 20–24 MA will enhance the possibility of runaway electrons produced by the avalanching mechanism. The ITER plasma design will probably incorporate features to reduce the effect of runaways, such as placement of sacrificial elements - poloidal and/or toroidal limiters (low Z) to blunt the effects of runaways on the FW. Since the flux is largest at the magnetic axis, runaways will be somewhat peaked and not produced in the scrape-off layer (SOL) or at plasma edge. It should be noted that the energy in the runaways which carry the current is only a few percent of the pre-collapse plasma thermal energy. It must be expected that the runaway electrons will be deposited by flux penetration on the inboard first wall, unless for example the vertical control pushed the plasma to the divertor. To the extent that they remain directed along the field line and reasonably uniform spatially, this may not be a problem, since the energy is only a few percent of thermal quench, and the expected energies are low 10-15 MeV. It is important to note that RAE is a toroidally symmetric phenomenon, capable of producing simultaneous damage to all the cooling loops of the FW or DIV.
- **Electromagnetic loads**: Plasma disruption causes electromagnetic loads whose effect on the PFC and VV in ITER depends on design details such as geometry, electrical connections, wall thickness, etc. Reference [4-6] presents results of plasma disruption simulations calculating 3-D electrical response of VV and PFC.

The initiating events are grouped into six categories using the criterion of the system where the event occurs. Some of these systems do not contain radioactive inventories, but they have interfaces with systems which do have radioactive inventories. We tried to model the propagation of an accident from a system to another in the present work. This chapter only analyzes the six initiating events shown in bold face in Figure 3-4, since they are the ones included in the confinement barriers model we developed. The model should eventually be completed with all the other conceivable accident situations in order to give meaningful results for ITER design, but that is outside the scope of the present study.

4.1 LFO2: Ex-vessel LOCA in a FW/SB coolant loop

The IE is the rupture of a medium size pipe (about 160 mm diameter) located inside the FW/SB HTS vault or in the guard pipe leading from the VV to the vault. The accident sequences which might develop are modeled in Figures 4-1 and 4-2.

Following the rupture, the cooling loop depressurizes rapidly, and most of the water coolant of the damaged loop is depleted. Thus, the RI of that loop are out of the first confinement barrier (PHTS loop) into the HTS vault.

Different loop parameters (e.g. pressure, flow) are suitable for detecting the accident conditions and for triggering a safety plasma shutdown (an indicative time of 10 seconds can be considered for detection and intervention of this safety system). Here the question arises if the plasma shutdown will be done actively before the end of the pulse by the intervention of the safety shutdown system, or passively due to the impurity or water ingress from the broken loop. The challenged shutdown system is not necessarily the fast one, but it might be one of the interlock systems as well. There is sufficient time available before any consequences occur, therefore the plasma shutdown is not as critical here as it is for LDO1.[2,3]

The main difference between LFO2 and LDO1 comes from this time issue: even if the safety shutdown fails, there is a probability that the FW tubes of the broken loop do not melt before the end of the pulse. We again assume that success of the safety shutdown system assures that FW tubes of damaged loop do not fail.[4] Moreover, the total water holdup per loop is about 400 m^3 for FW/SB, as opposed to a DIV loop of about 70 m^3; the pressure being approximately the same (3.5 MPa), the HTS vault will be much more challenged in the LFO2 then in the LDO1 case.

Nevertheless, the failure of active plasma shutdown systems, including detection and correct communication of the IE, is an aggravating event. It can lead to overheating of in-vessel components. There are ongoing studies to determine the temperature at which the plasma burn will be terminated passively by:

- impurity ingress of evaporated beryllium atoms for hot parts of the first wall, or
- water ingress from the FW loop following failure of tubes from the damaged loop due to melting or thermal stresses.

When the shutdown is caused by impurity ingress, the disruption may affect the PFCs integrity by RAE or electromagnetic loads. The effect can be an extended in-vessel LOCA with or without

---

[2] The heat-up of the first wall, assuming continued burning of the plasma, was calculated [4-5] and the results showed that there would be 100-200 seconds before the first wall would reach melting temperatures.

[3] LDO1 accident sequences analysis is included in Appendix B.

[4] L. Cadwallader pointed out that the ITER plasma shutdown system will result in a disruption. Although not a severe disruption, it may not be prudent to assume no first wall tube damage if the plasma shutdown system successfully actuates. A damage spectrum for the tubes might be more appropriate.[4-13]

bypass. It will be with bypass whenever the FW integrity is affected, because we make the following assumption: whenever FW surface is damaged, the FW tubes of the damaged loop will fail with 100% probability since their condition is more critical. In conclusion, impurity ingress may lead three types of accident sequences:

1. no in-vessel LOCA: PFCs are not damaged (VV might only fail due to electromagnetic loads);
2. extended in-vessel LOCA, but no bypass: FW not damaged, but DIV damaged (VV might fail due to: electromagnetic loads, or overpressure if RDs fail);
3. extended in-vessel LOCA, with bypass: FW damaged, DIV damaged or not (VV might be damaged by any of the three causes enumerated in the previous section). In this case, the bypass sequence is of concern since RI from the plasma chamber have a way to pass both VV and CV into the HTS vault.

When the shutdown is caused by water ingress, that means that a small in-vessel LOCA with bypass occurred. Coolant ingress - induced plasma disruptions are likely to be two or three times more intense than typical disruptions, and perhaps even more severe than other density limit disruptions caused by wall impurities. That disruption can cause more damage to PFCs leading to an extended in-vessel LOCA, so the final result is similar to type 3 sequences above. The magnitude of releases depend on the degree of damage to the PFCs.

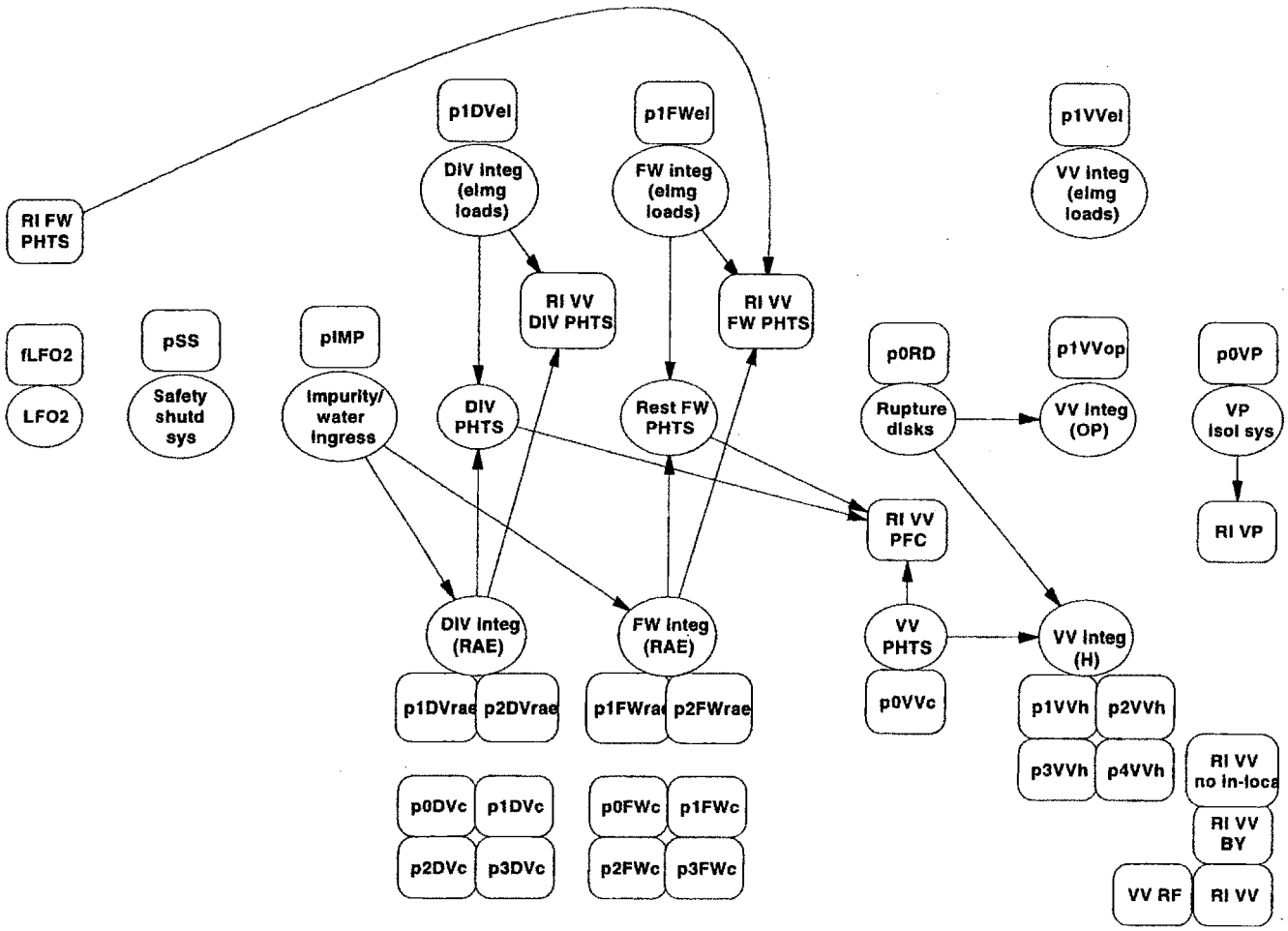

Figure 4-1: Influence Diagram for the Initiating Event LFO2

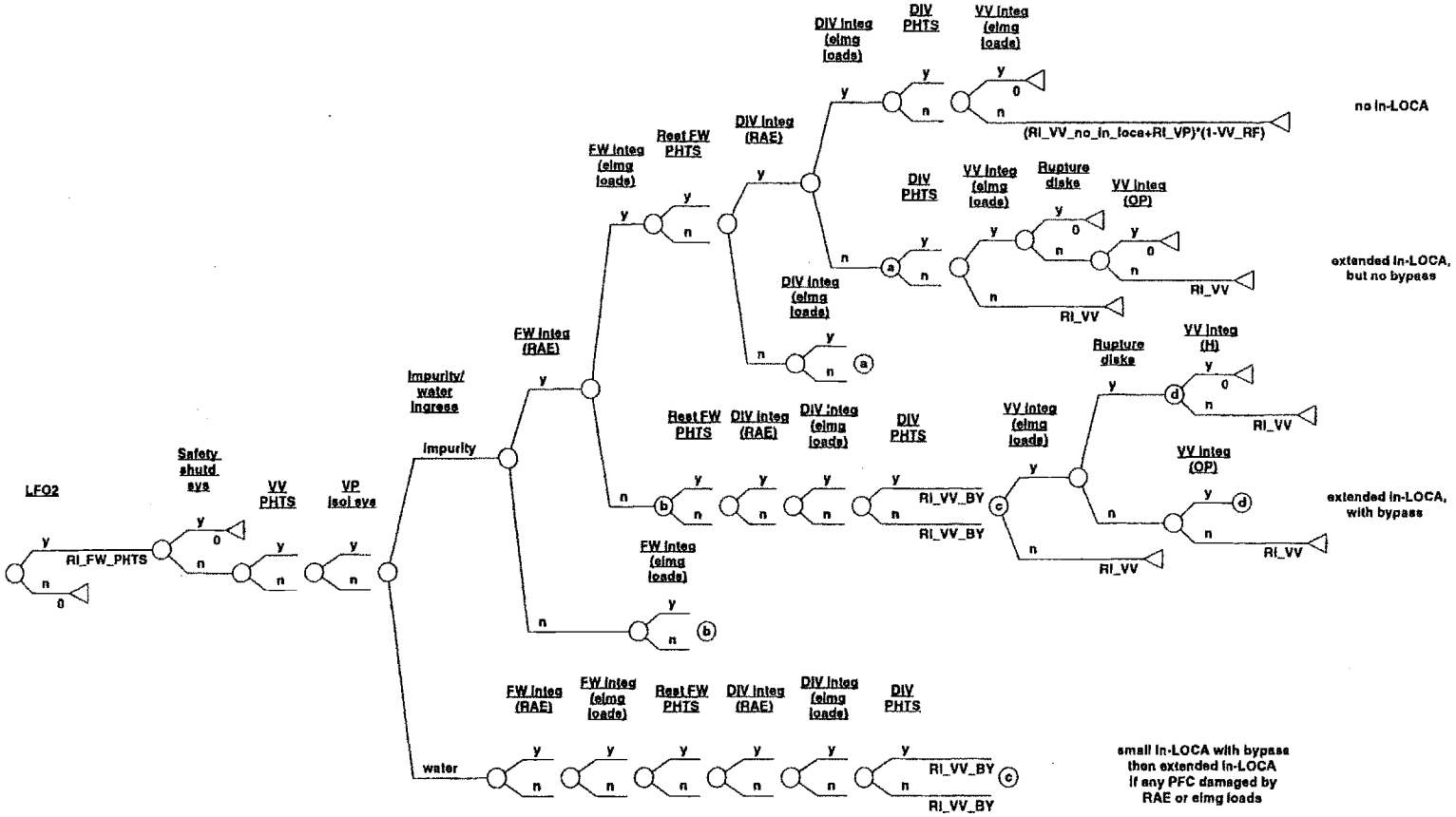

Figure 4-2: Event Tree for the Initiating Event LFO2

4.2 MPO1: TF coil overcurrent

Two causes could lead to this IE: power supply control failure, or TF shorted coil. We will look here at the second case, because it is the most severe accident for a TF coil. The MPO1 ID/ET model is presented in Figures 4-3 and 4-4. On two of the ET branches, plasma disruption could occur. The disruption event leads to accident sequences described in Figures 4-5 and 4-6.

A TF shorted coil sees a rapid current increase due to inductive coupling from the other coils. The whole coil can be considered to quench simultaneously as the critical conditions are approached. Continued supply of power in the kV range will eventually overheat the coils. However, the coil resistance is such that even at 2 kV, supply of power for several minutes does not cause excessive temperatures.

In the event of a fast discharge, much of the helium is expelled from the coils: at higher temperature, helium becomes gas and its pressure increases considerable resulting in a pressure wave that could damage the conductor. A system of relief valves and a relief tank is designed to capture the helium coolant.

The safety systems that should be activated by MOP1 are the following:

- **TF quench detection system**: this system should send signals to the other safety systems;
- **Safety shutdown system of plasma**: its prompt operation is very important before TF magnet discharge; otherwise a disruption follows, possibly damaging PFCs and VV;
- **TF fast discharge system**: even if the TF discharge system does not work, TF coils will quench by themselves, but in a longer time;
- **CS discharge system and PFs discharge systems**. The PF coils have separate power supply systems. All of these coils need to be discharged in order to avoid mutual forces between magnet systems that could cause coil displacement, missile generation, that could damage VV, and PHTSs;
- **helium expulsion system** (relief valves and tank); if this system fails, TF coil integrity could be lost due to overpressure. This event is not sufficient to damage structure, but local arcs could be generated (if TF coil has not been yet discharged). Arcing can be an issue even if the TF coil did not fail structurally.

By definition, **arcing** is a luminous discharge of current that is formed when a strong current jumps a gap in a circuit or between two electrodes. Arcing can impair VV structure, and VV and PFCs PHTSs. During arcing destructive process, some structural part (for instance, shear key[5] or objects forgotten in the CV during maintenance) can become loosen and be accelerated by magnetic field

[5] A newer design provides for keys constructed of non-magnetic stainless steel, so there is no longer any concern about ferromagnetic induced motion of shear keys.[4-13]

variations, if the magnet system have not yet been discharged. The missiles can damage VV structure, as well as PHTSs pipes inside the CV.

For the accident sequence of success for all the safety systems enumerated above (except for the helium relief system leading to loss of the TF coil integrity), we assume helium leakage is contained in the TF coil case. Since all the coils were discharged, no danger of shorts or arcs exist.

If any of the CS and PFs coils is not discharged, coil displacement and acceleration of loose objects are threats to the integrity of VV and PHTSs pipes inside CV. For simplification, we consider that the same happens when TF's fast discharge system fails. We assume that the VV probability of failure due to coil displacement and missile generation is dependent on the magnet systems might have been discharged since the forces and magnetic fields are different. The same applies to PHTSs inside the CV, but that would complicate the model too much. In fact, PHTSs pipes are smaller components than VV, and they contain smaller RI quantities, thus we can afford to ignore them for the time being.

Basically, when safety shutdown works, damage to VV and PHTSs can only come from outside of VV, directly caused by the magnets. When safety shutdown fails, events very similar to the LOFA accidents add up to the above ones. Some sequences also include in-vessel LOCA accident. Care has to be used in evaluating the consequences so that they add up to at most maximum conceivable value; for instance, when some of the RI mobilizable in the VV were escaped via bypass, and a missile breaks through the VV thereafter, the remaining RI in the VV have to be considered.

When the fast safety shutdown system fails, a disruption is expected due to the loss of magnetic confinement since TF quench is spreading automatically (even if TF fast discharge system fails). This disruption can damage the PFCs via run-away electrons (RAE) or electromagnetic loads, leading to an in-vessel LOCA. The sequences in that case are very similar to the LOFA sequences. However, we will represent them here in a simplified way by excluding the dependencies between damage to PFCs and the PFCs PHTSs. It is reasonable to do this since we have already described these sequences in the LOFA case; and, if included here, sequences with lower probability would be obtained since they are following from the magnets accidents.

When TF quench detection system fails, no signal will be sent to the other safety systems: **safety shutdown**, and **magnets discharge** systems. Therefore, those will not operate. The frequency of such a sequence is very small, clearly in the area of BDBA, so we will not develop the sequences further.

The ID/ET model for the MOP1 is considerably large, and it might be difficult to estimate some of the event probabilities in the way the events are now defined. However, the events can always be changed as more data become available. The model developed here is the most comprehensive one that exist at this time. It has put together all the information about possible accidents that could be found in the ITER documents as well as the European study (SEAFP).[4-1, 4-3, 4-16]

A good way to solving the problem of large models is separating the ID/ET model into several **modules.** Each module represents the accident sequences for an IE in a certain system (i.e., magnet

system, plasma chamber), or an IE which might be the result of an accident in a different system (i.e., disruption caused by a magnet quench). What this means is solving independent parts of a large ID/ET separately, and reducing them to a chance event with the same frequency distribution of consequences. Then, introducing that chance event in the MPO1 model (converted into DPL code) on the branches where it could occur. So, instead of having the initial large number of accident sequences on that branch, only a representative number of sequences will be chosen.[6] To exemplify the concept, we calculated the frequency distribution and the corresponding cumulative distribution function (CCDF) of releases for the disruption initiating event. Then, the disruption ID/ET model is reduced to a single chance event with six possible states with a corresponding CCDF, represented by 'ccdf_red' in Figure 4-7. That shows that ccdf_red is an close envelope of the original CCDF.

DPL has a feature that makes the above concept possible by taking an independent 'module' of the ET apart and using the 'Reduction' command. That way the module is transformed into a chance event with a maximum of six states with the same expected value as the initial module. The comparison of the frequencies histograms of the module with its associated chance event shows that the latter is an envelope of the first, and therefore the same is valid for the associated complementary cumulative distribution functions. Furthermore, in the initial ID/ET model, the module is removed from the ET part, then the file is converted to DPL code, and, in the sequence part of the code, on the branches were the module was previously, the lottery on the chance event representing the module is introduced. Consequently, the number and the length of the accident sequences in this newly obtained ID/ET model is much smaller, the program runs faster, and now information is lost.

We believe that the use of modules is valuable in building the event trees for a device like ITER where systems like magnets, containing no RI, can produce defects that can damage other systems containing RI. That way we can build modules of ET for separate systems, and then link them at their interfaces.

---

[6] 'Representative' is defined as an envelope of the sequences in the initial module of the ET.

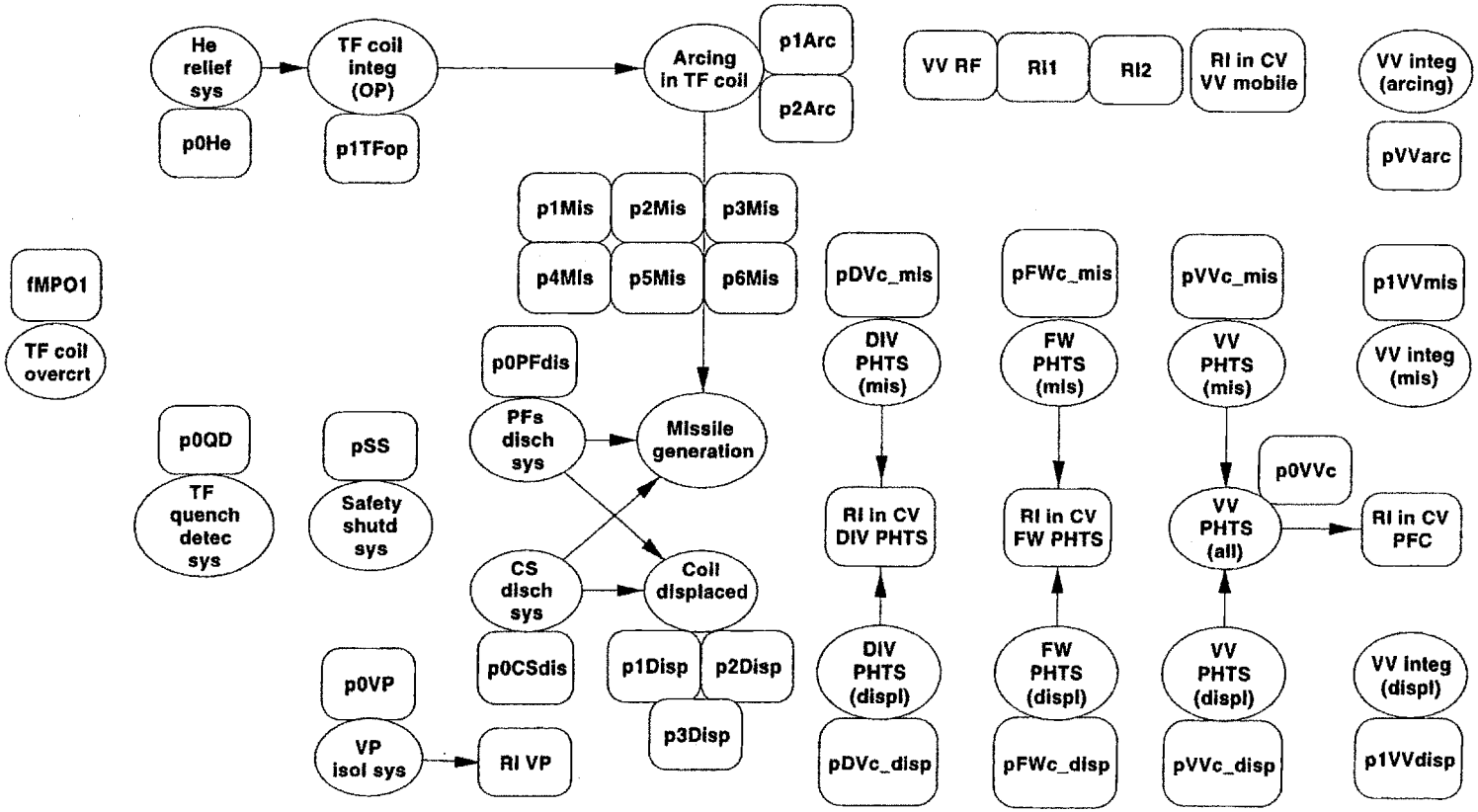

Figure 4-3: Influence Diagram for the Initiating Event MPO1

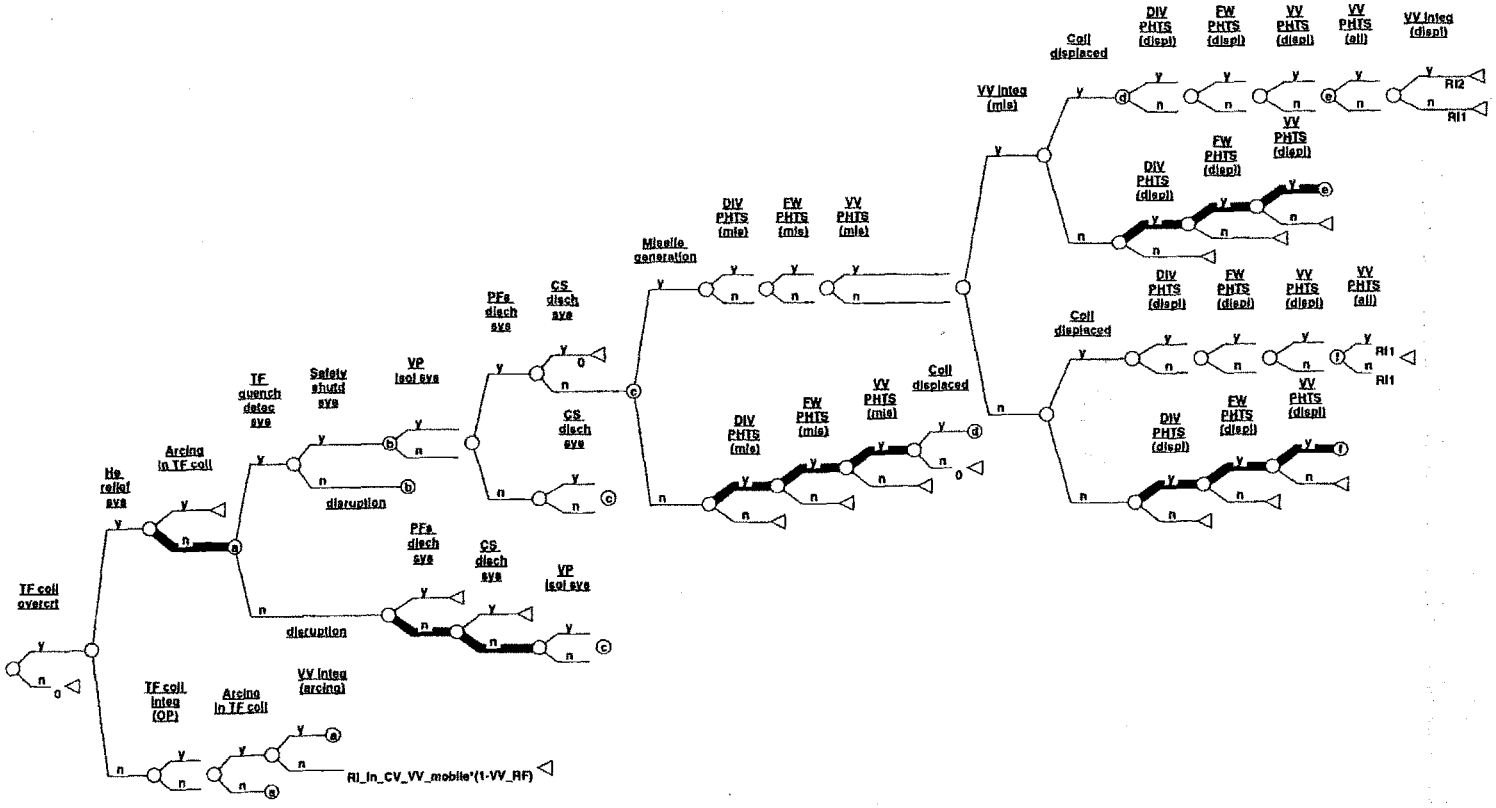

Figure 4-4: Event Tree for the Initiating Event MPO1

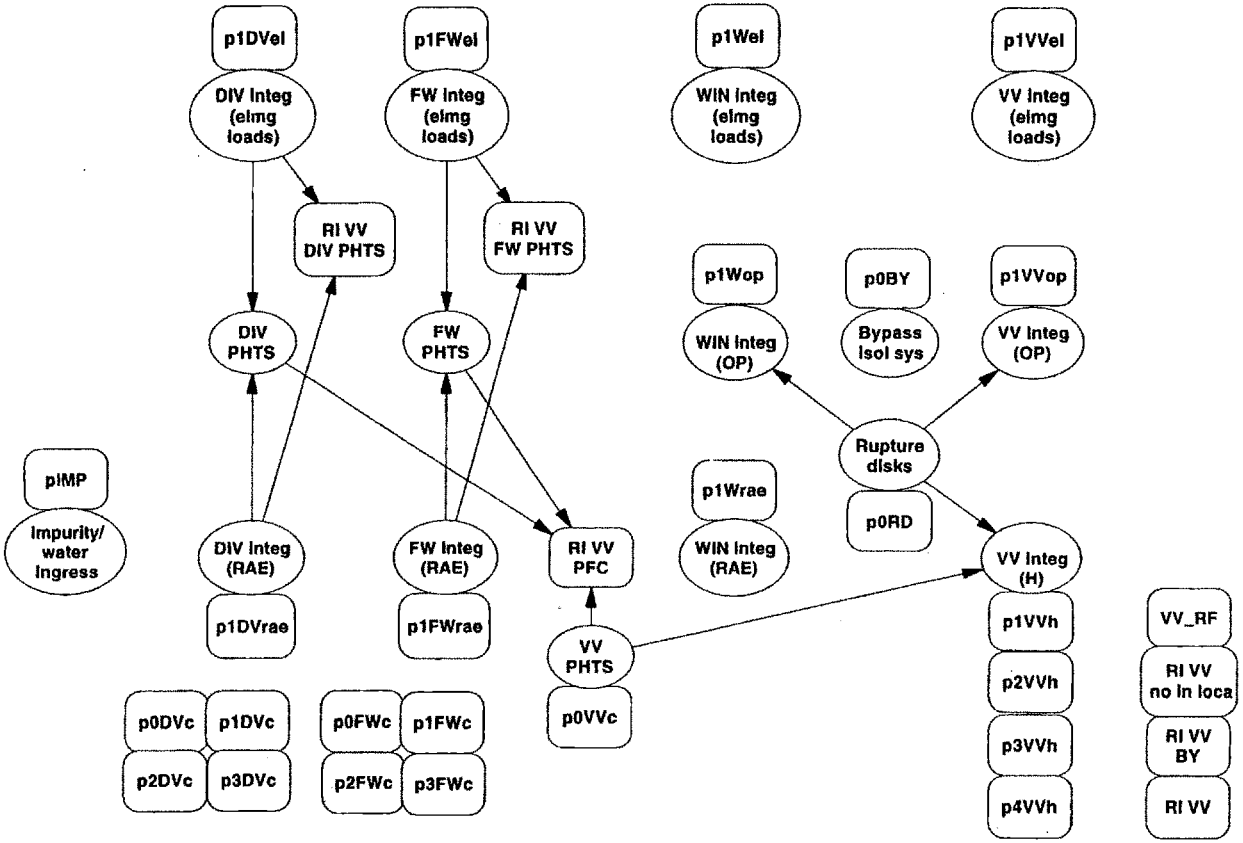

Figure 4-5: Influence Diagram for the Disruption Event

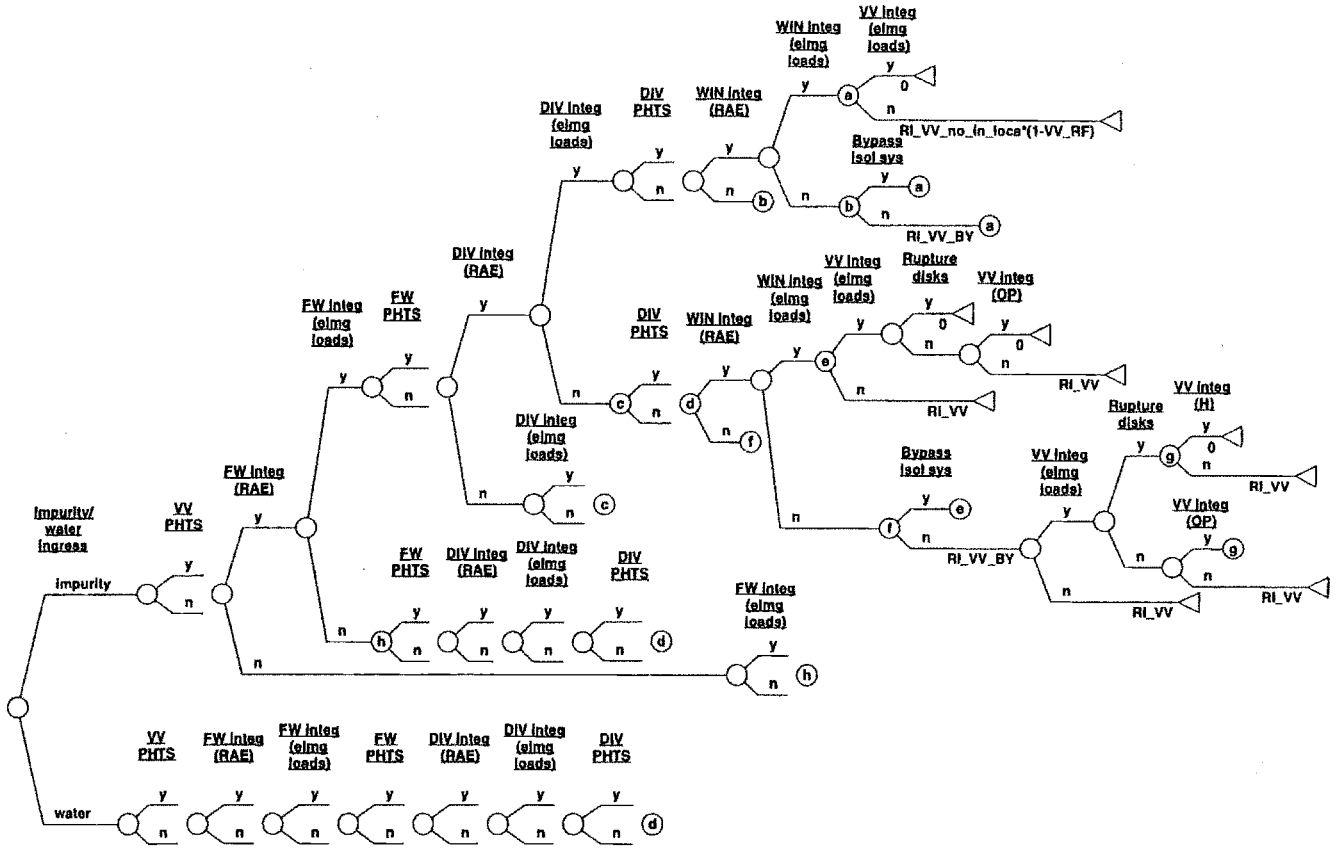

Figure 4-6: Event Tree for the Disruption Event

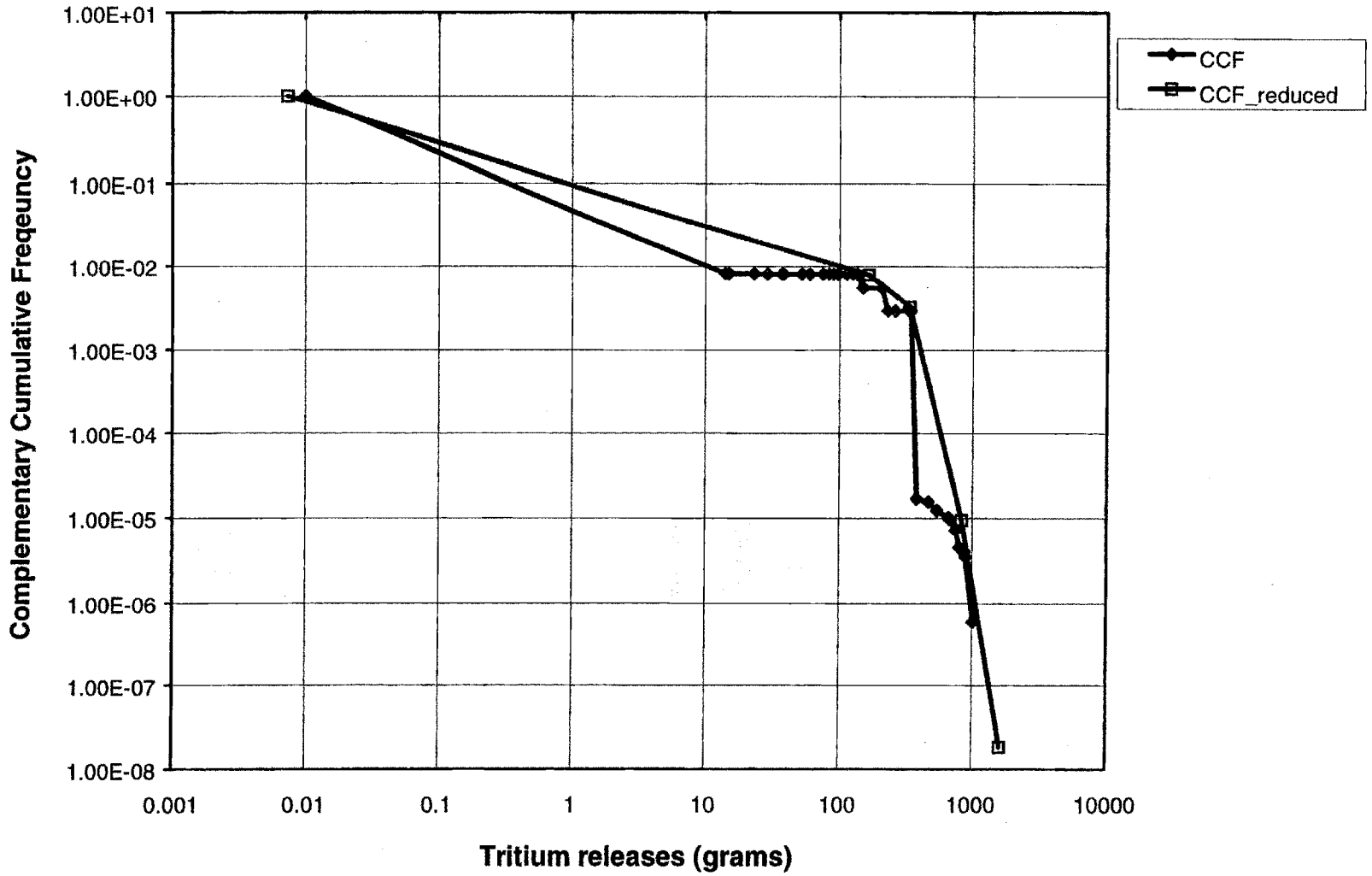

Figure 4-7: Complementary Cumulative Frequency (CCF) of Tritium Release from the First Confinement Barrier for the Disruption Event: Complete Model versus Reduced Chance Event

4.3 TVP1: Vacuum pump process boundary failure

Failure of the cryogen lines inside the pump process boundary is accompanied by a large release of tritium, deuterium and cryogen into the divertor section of the torus. This will cause a disturbance and possibly a plasma disruption, but no direct tritium release. The disruption, in turn, could lead to an in-vessel LOCA, which would pressurize the vacuum vessel and the process piping connected to the vacuum pumps. If process piping isolation fails, then tritium handling equipment outside of the vacuum vessel will become pressurized and could fail.

A typical configuration of vacuum pump regeneration at power involves two pumps regenerating and two pumps pumping. The vacuum pumps are passive components, and are fully within the vacuum vessel boundary. However, during regeneration, the pumps are directly connected to the DT return header and the gas puffing header, which are in turn connected to two lines that penetrate the vacuum vessel boundary and the cryostat boundary. One is the line supplying DT from fuel storage, and the other is the line delivering DT to the isotope separation system. Hence, failure of the vacuum pump boundary, during regeneration, is similar to a failure in the headers to which it is connected. And, failure of the headers is similar to failure of the lines that connect the headers to equipment outside the vacuum vessel and cryostat. Thus, failures in the two lines are representative of failures occurring anywhere in between them.

Two systems are challenged by this IE: **the break isolation towards the tritium plant**, and **the safety plasma shutdown**. If the safety shutdown fails, a disruption will terminate the plasma due to impurity or water ingress, so there is a probability that in-vessel LOCA will occur. We again used the concept of modules by reducing the sequences following a disruption to a single chance event with a corresponding probability distribution function, and attaching that event to the TVP1 sequences where the safety shutdown fails.

Figures 4-8 and 4-9 describe the ID/ET model for TVP1 without disruption.

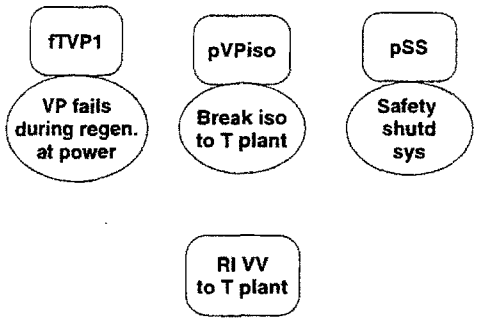

Figure 4-8: Influence Diagram for the Initiating Event TVP2 without Disruption

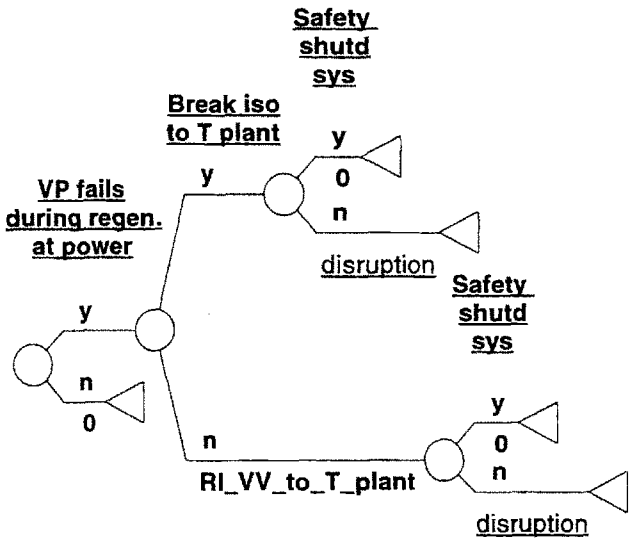

Figure 4-9: Event Tree for the Initiating Event TVP1 without Disruption

4.4 OP: Overpower transient

The overpower event caused by thermal instability is referred to as an abnormal plasma occurrence in nuclear fusion reactors. Thermal instability of the plasma causes the density and temperature to deviate from the steady-state values, which results in deviations of the heat fluxes and neutron wall loads to the core internal structures. Positive fluctuations in plasma parameters, e.g. plasma temperature, will cause elevated fusion power within several seconds, which will result in a beta-limit disruption. Such an abrupt positive thermal excursion may increase damage to plasma facing components. On the other hand, negative fluctuations will reduce fusion power, which will eventually shut down the plasma with a density-limit disruption.

According to studies of thermal instability of plasma, the instability increases when the plasma temperature is low and the Q value is high. By contrast, it has been reported that around beta limit, thermal instability of plasma may be suppressed by a decrease in the performance of the plasma confinement, which will not reach beta-limit disruption. However, the behavior of plasma around the beta limit is not clear at present. Therefore, to evaluate ITER safety conservatively, it is necessary to include an accident sequence in which thermal excursion due to thermal instability of the plasma will result in a beta-limit disruption.[4-21]

Overpower events of plasma may be triggered by abnormal actions of fueling and external heating. Overpower transients could lead to partial or general overheating of plasma facing components which, if not terminated by shutdown, could lead to in-vessel LOCA. The difference from the in-vessel LOCAs discussed previously is that the temperature of the plasma facing components would become higher in case of OP, and therefore the consequences are more severe (higher radioactive inventories releases).

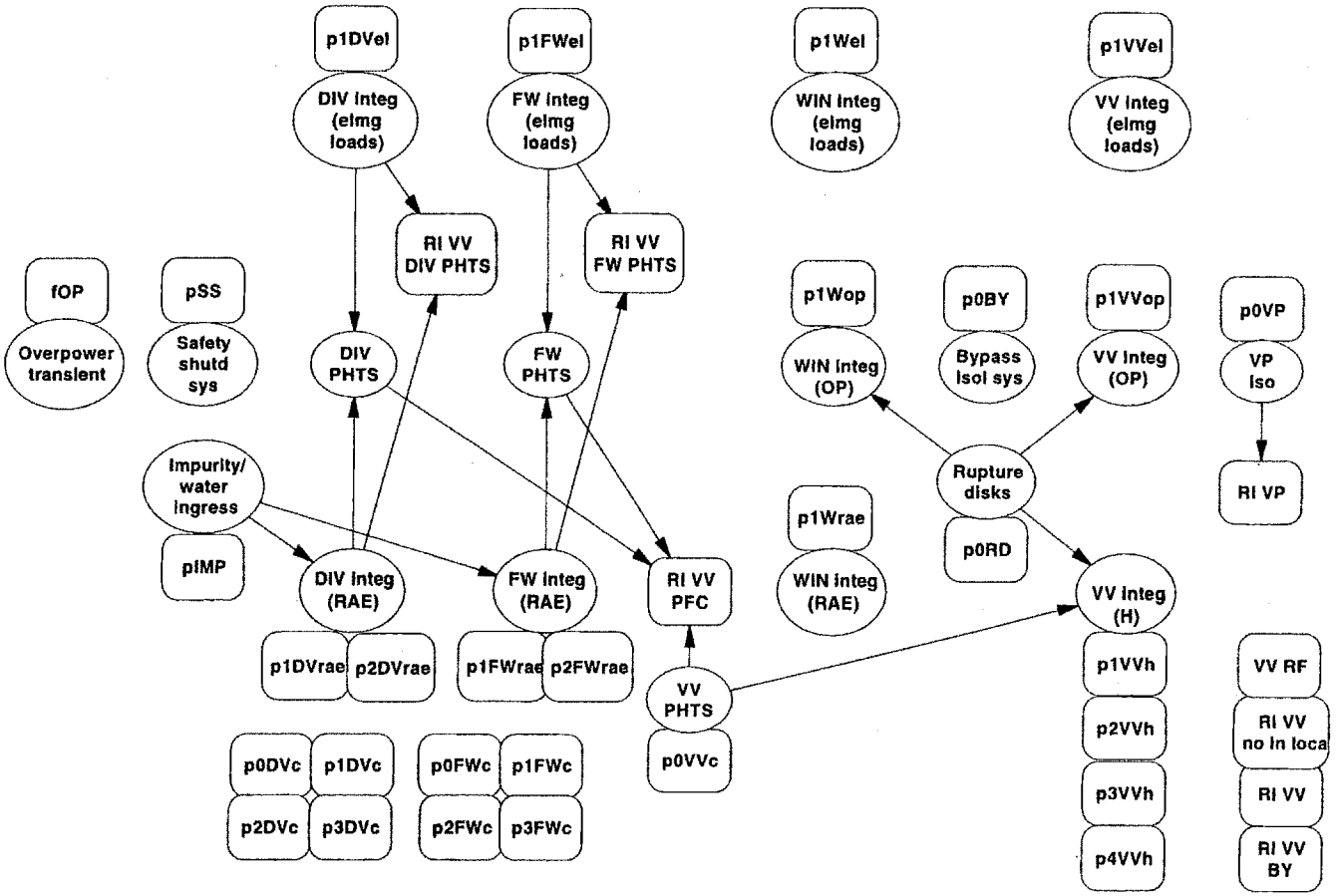

Figure 4-10: Influence Diagram for the Initiating Event OP

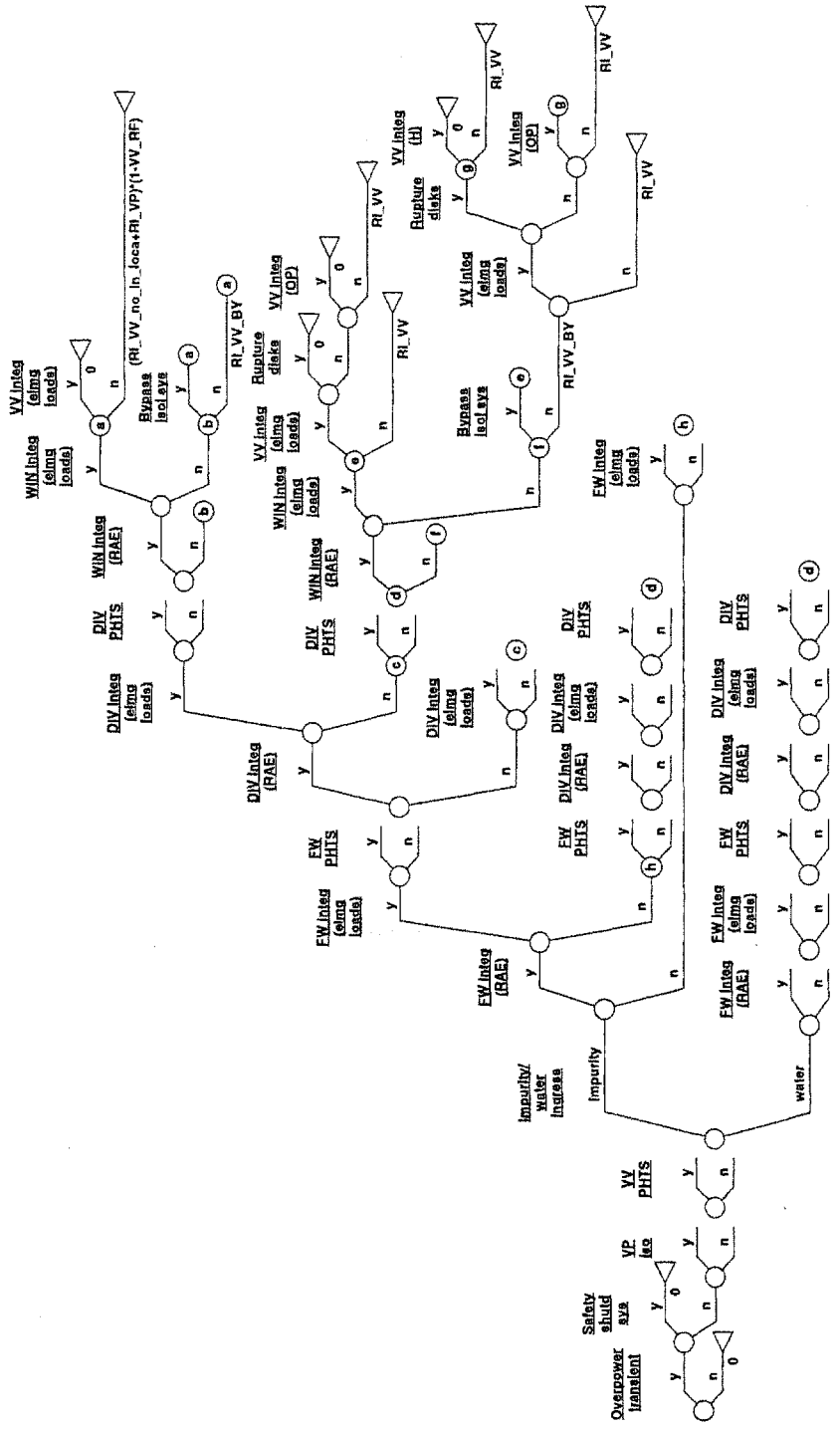

Figure 4-11: Event Tree for the Initiating Event OP

4.5 VCS: Small leakage of air in the cryostat vessel

Small leaks could lead to air freezing on the cold surfaces in the cryostat, so the coil cooling systems could be able to maintain the vacuum in the cryostat by condensing the incoming air. This frozen air would lead to two safety concerns:

- in case of an event like a magnet quench, the frozen air could be vaporized again and pressurize the cryostat (loss of vacuum in CV) if present in sufficient quantities. This effect will be studied when looking at the CV performance;
- formation of ozone in the frozen air could lead to an explosion hazard that can affect the VV and PHTSs integrity.

Ozone is generated from oxygen according to the reaction:

$$3O_2 = 2O_3 + Q \qquad (4\text{-}1)$$

with Q = −144 kJ/mole of ozone

The energy required for the reaction is provided by neutron and gamma radiation. One of the main sources of oxygen in the ITER cryostat is air in-leakage and condensation on cryogenic surfaces. Air condensation and accumulation of solid air on cryogenic surfaces strongly depends on the amount of air in-leakage into the cryostat, and the presence of inadequately shielded cryogenic surfaces inside the cryostat area.

The mechanisms of the formation and decomposition of zone are not fully known, particularly with regard to:

- the production rate of O_3 from oxygen, as a function of the gamma or neutron deposited energy;
- the amount and concentration of O_3 that constitute an explosion hazard;
- the energy threshold to initiate decomposition and the effects of impurities in reducing this energy.

Most of the reported ozone explosion accidents are related to LN_2 systems in the presence of significant oxygen contamination. O_3 explosions were reproduced experimentally in LN2 and oxygen systems. In such experiments it was found that O_3 explosions can occur when the O_3 concentration in liquid phase is 4% or higher. Conversely, in most of the recorded explosion accidents, the amount of oxygen which was initially contained in the nitrogen as impurity was apparently incapable of producing sufficient O_3 to cause concern. Therefore, some mechanism of O_3 concentration must be hypothesed to have the risk of an explosion, e.g. by evaporation, perhaps on localized parts of the cryogenic circuits where liquid gas equilibrium exists. Another cause of explosion can be the presence of impurities that catalyze the decomposition of O_3, thus reducing the minimum concentration required to produce an explosion.[4-20]

Detonations of O_3 in solid phase have not been recorded, but solid O_3 can become liquid by the effect of heating. The pressurization with consequent heating of the cryostat can e generated by:

- an air injection prior to access for scheduled or unscheduled maintenance;
- an accidental air or water inlet to the cryostat due to the failure of a sealing component;
- the failure of leak tightness with a consequent loss of coolant from a fluid system (LN_2 or liquid helium).

One way to detect leaks is to monitor the cryostat pressure. However, the pressure inside the cryostat will rise only when the leak rate is larger than 20 g/s; because of smaller leak rates, the cold surfaces of the magnets will act as cryopumps. Indeed, estimations in reference [4-20] have shown that for a temperature of 80 K, a pressure inside the cryostat of 10 Pa, and a cold (cryogenic) surface of 4000 m^2, the condensation capability is about 20 g/s. If the air in leakage is above 20 g/s, then the pressure inside the cryostat will rise. With rising pressure, the condensation capability increases also until a maximum condensation rate of 65 g/s is reached. At this rate, the condensation causes a heat flux which is above the threshold at which the magnets quench. From the previous considerations, a leak rate of 20 g/sec would be difficult to detect by pressure measurement and would a priori not lead to quenching of the magnets.

VCS can lead to magnets quench, an event which is analyzed separately in a module, reduced to a chance event, and incorporated on the branch showed in the Figure 4-13. The quench model itself contains the disruption event on some branches, and again the module concept is used for simplification. Figures 4-15 and 4-16 represent the quench model.

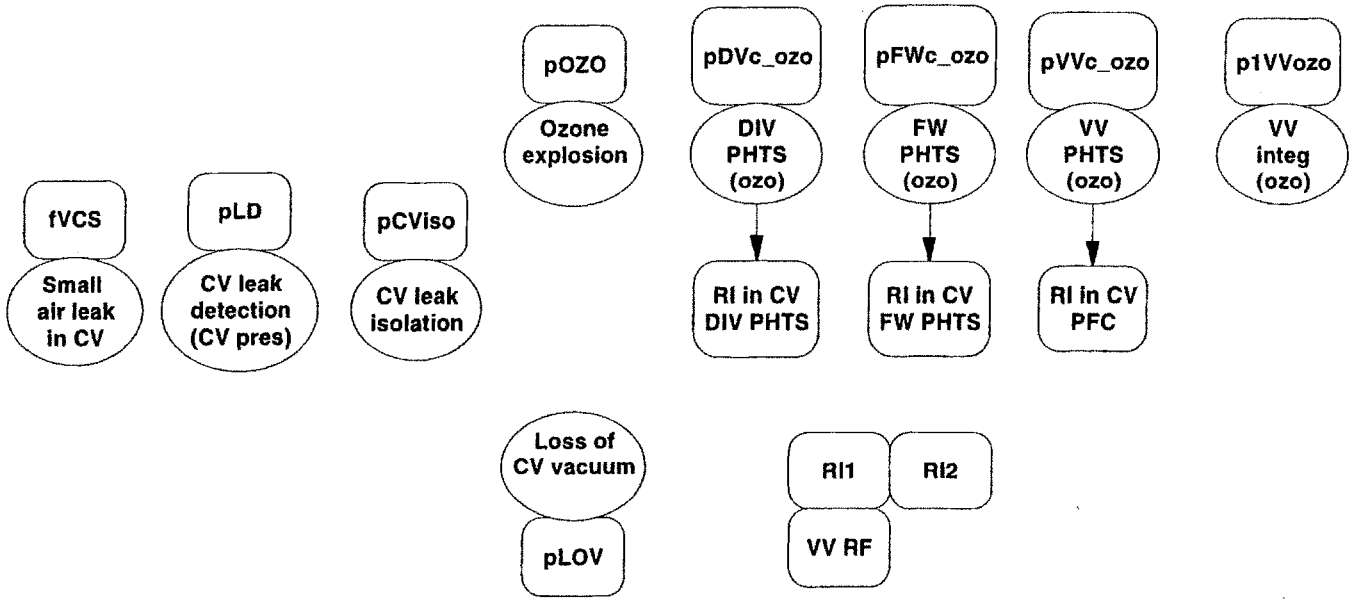

Figure 4-12: Influence Diagram for the Initiating Event VCS without Quench

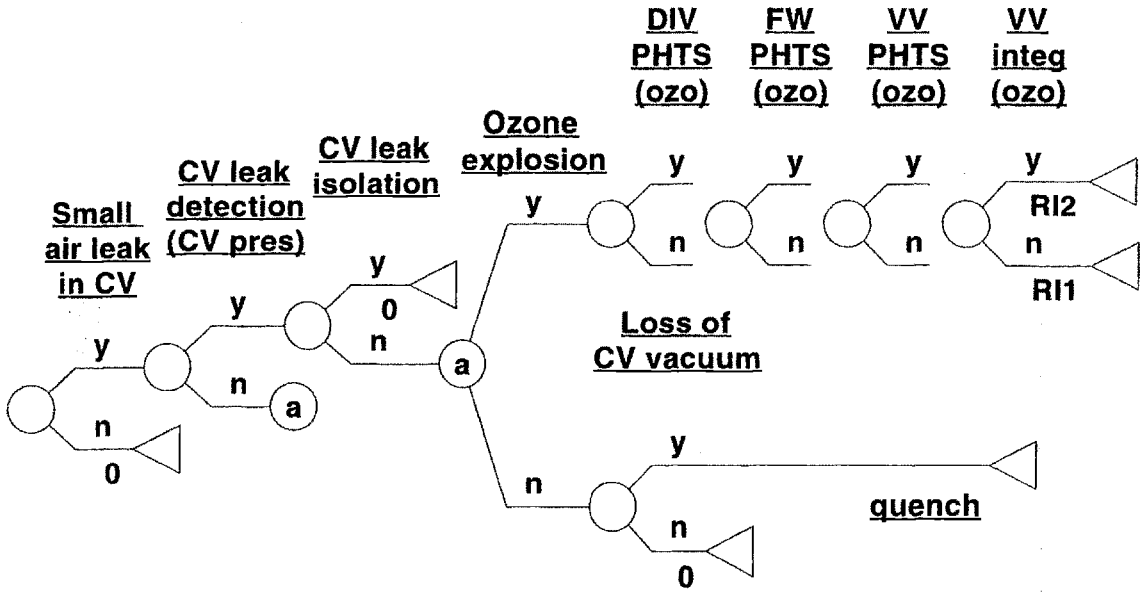

Figure 4-13: Event Tree for the Initiating Event VCS without Quench

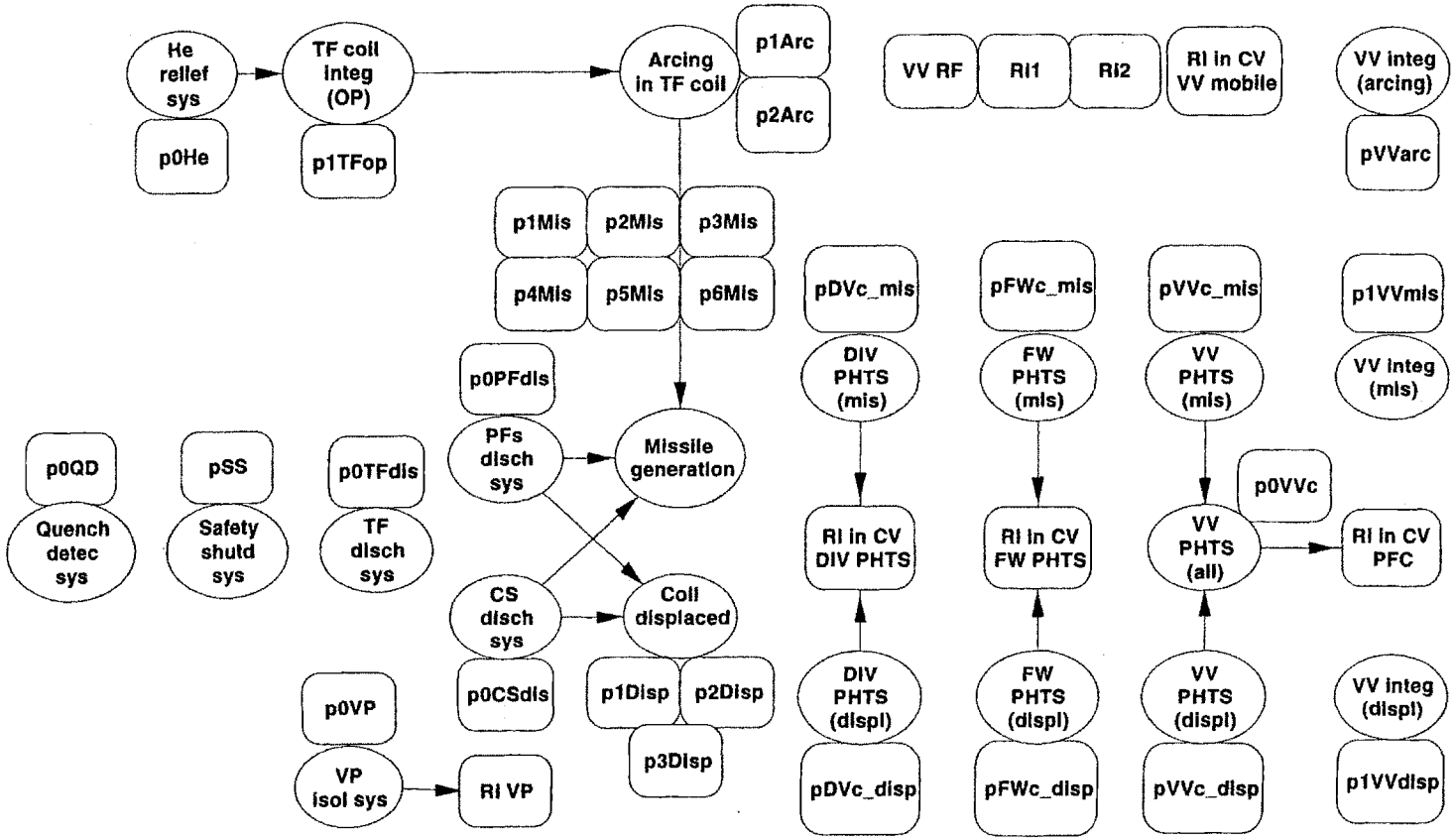

Figure 4-14: Influence Diagram for the Quench Event without Disruption

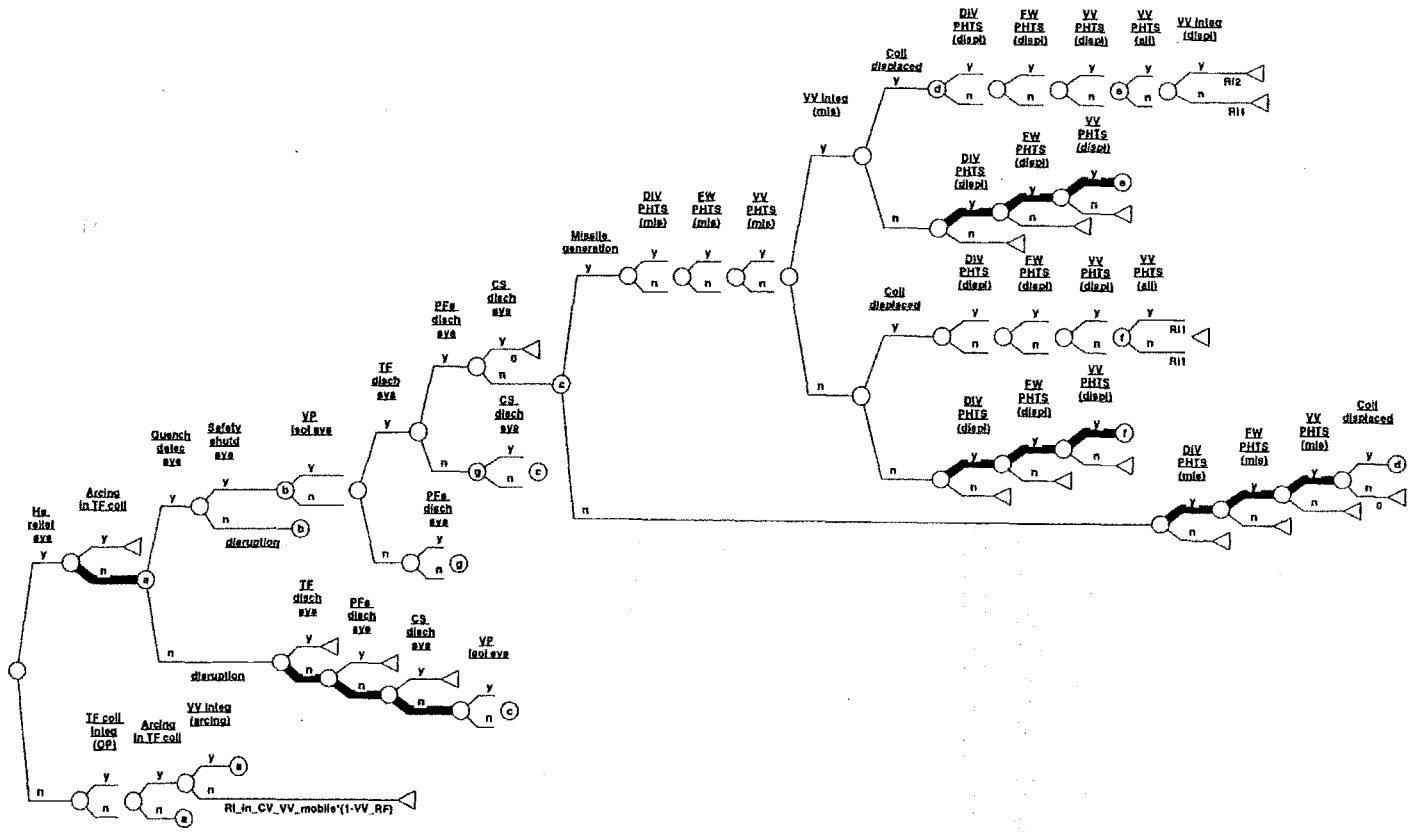

Figure 4-15: Event Tree for the Quench Event without Disruption

4.6 LOSP: Loss of offsite power

On-site power supply will be provided in ITER to keep the plant in a safe state in case of offsite power loss. Pony motors might serve to accomplish the decay heat removal function.

Loss of off-site power data for power plants indicate that the frequency of this initiating event is between 10^{-3}/a to 10^{-6}/a, depending on the duration of the loss of power: the higher value is for short duration events (typically under 2 h), and the lower value for events with a duration up to 10 h.

Should ITER suffer a complete station blackout, loss of plasma control will lead to plasma shutdown due to the unstable plasma position. To keep the confinement function intact, all active systems involved in confinement have to be designed as fail safe, i.e. in case of power loss they should automatically get into a safe state. Decay heat will be either removed by natural circulation or evaporation of the primary coolant. The vacuum vessel cooling loop should be designed for natural circulation up to the ultimate heat sink. This will be sufficient to keep the first wall temperature below 500°C.

In order to develop a meaningful ID/ET model for this IE, we will consider the power supply design described in SEAFP [4-24]. An emergency power supply (on-site generators and batteries) will back up the external power supply for the following systems: cryogenics, decay heat removal, tritium process, safety related instrumentation and control loads. However, the magnet related loads are powered only from the external grid. Thus, LOSP will lead to a severe plasma disruption which challenges the integrity of the PFCs structures and also of the superconductors (electromagnetic forces, induced high voltage).

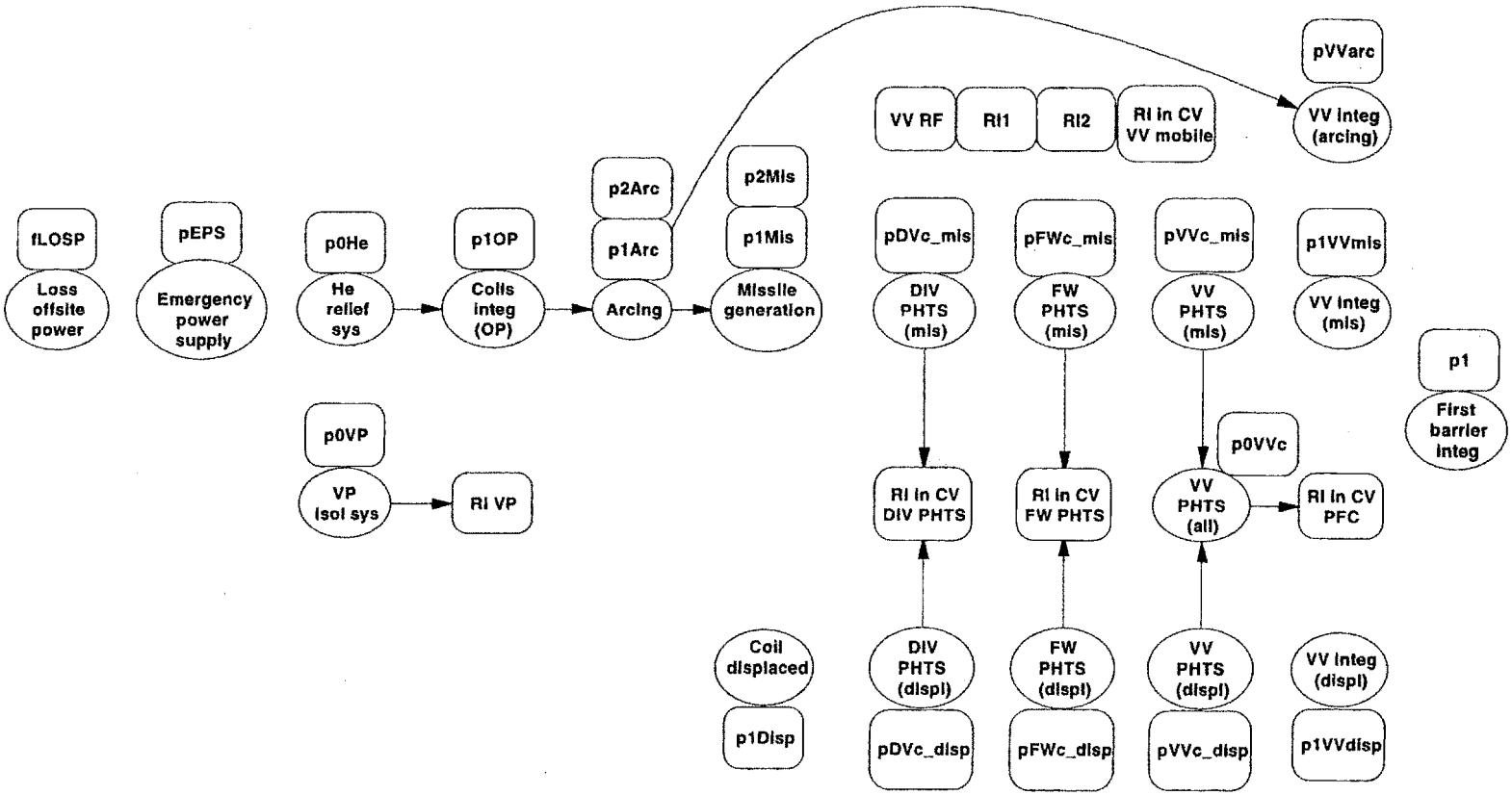

Figure 4-16: Influence Diagram for the Initiating Event LOSP

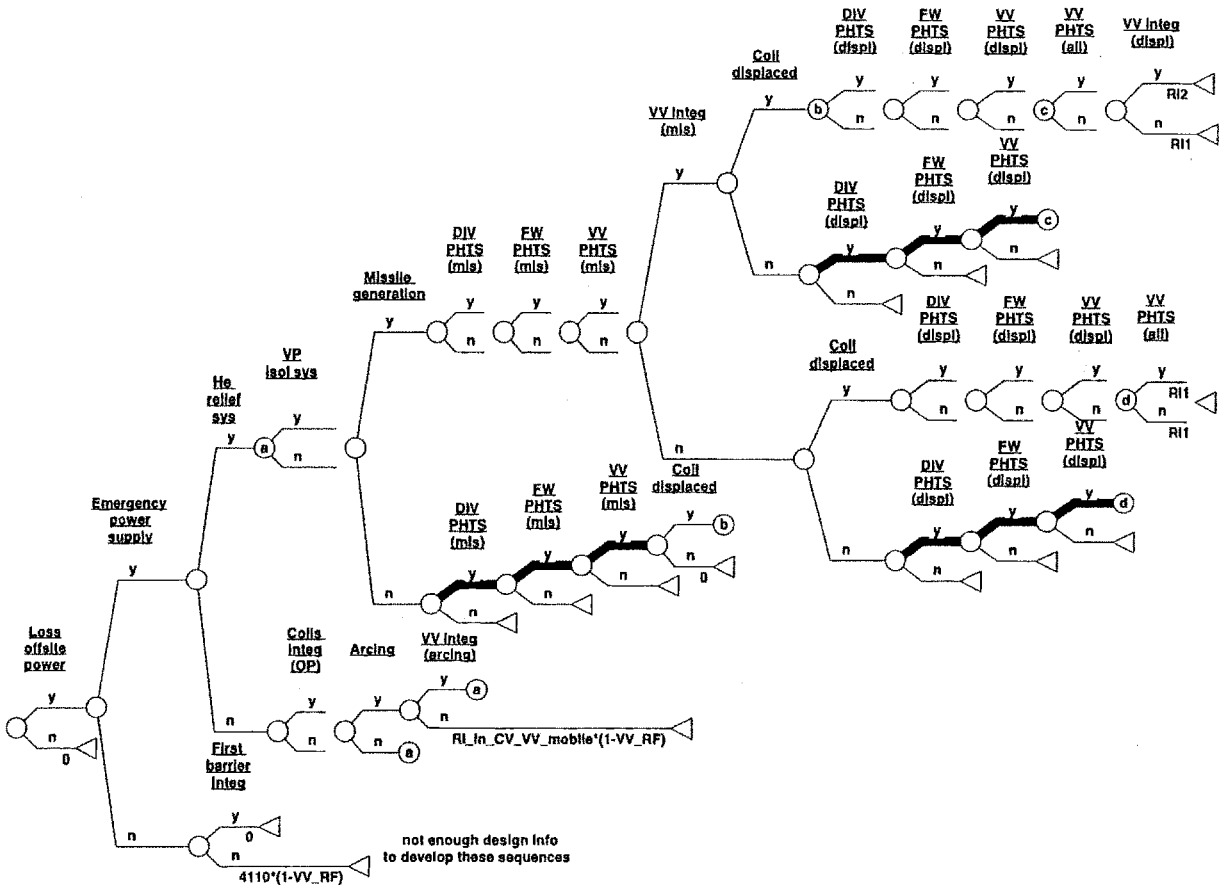

Figure 4-17: Event Tree for the Initiating Event LOSP

5. Containment models for the Second Confinement Barriers

By considering the success of failure of active plant systems, the influence diagrams/event trees described in the previous section trace an accident sequence from an initiating event, through the failure of the first confinement barrier which is the process system. In fission power plants, the system event tree branches end with a stable condition with intact fuel or the onset of core damage. The containment event tree is developed to describe the progression of an accident sequence from the start of core melt to the release of radionuclides after containment failure, and it is attached to the final branch points of system trees.

In a fusion power plant, the fuel (tritium) as well as other radioactive inventories are localized or flowing among different systems, so they are not concentrated in the reactor core as in a fission plant. Thus, the confinement strategy is more complicated as described in Chapter 2. As a result, the system event trees end points include integrity or damage of many different parts of the first confinement barrier. Those parts have different corresponding parts of the second confinement barriers as given in Table 2-1. Therefore, several containment event trees have to be developed for these parts of the second confinement barriers.

One initiating event can lead to accident sequences that affect different parts of the confinement barriers, hence multiple containment event trees for the second confinement barrier should be included in the same ID/ET model for any given IE.

The various containment failure mechanisms may be structured with a containment event tree. In addition to considering the gross behavior of the structure (yield and ultimate-strength levels), special consideration should be given to localized conditions, such as: electrical penetrations and major openings, major discontinuities, interactions with surrounding structures. The containment may fail as a result of overpressure, overtemperature, hydrogen explosion. In the fusion case, specific events are: missile generation in the magnetic field, magnet coil displacement, ozone explosion, arcing leading to melting.

The common practice in fission power plants PRA is grouping system event trees sequences by release categories, a process called 'binning'. Two approaches have been used for binning: probability screening and the development of plant-damage bins.[4-19] In the former approach, trial sequences are selected using point estimates to identify those with the highest frequencies having realistic accident processes. The physical process for these sequences are evaluated. If the results of the analysis indicate that the spectrum of potential accident consequences is not well represented (e. G., there are no sequences that fall into the large release categories), the level of discrimination is reduced and more sequences are analyzed. One problem with this approach is that it requires iteration and some judgment in deciding when the process is complete.

In the latter approach, the analyst develops groups of system sequences referred to as "plant-damage bins", "plant-damage states", or "plant event sequence categories". The categories are identified by the characteristics of the system sequence that affect the release of radionuclides to the environment. All system sequences within a bin are assumed to have the same containment tree, in that the branching probabilities are the same, and the end points are assigned to the same radionuclide release categories. The second approach is suitable for use in our ID/ET models for the ITER power plant with one difference: instead of assigning the same release categories to the end points, we propagate the radionuclides releases corresponding to each branch by multiplying it with the containment retention factor (RF). In order to do this, the containment models will be built into the ID/ET models for the first confinement barrier as it is shown in Appendix C.

By considering the success or failure states of the active plant systems, the ID/ET models described in Chapter 4 trace the accident sequence from the initiating event to the point were the first confinement barrier is damaged. The containment models for the second confinement barrier (and eventually for the third confinement barrier if one is required) are developed to describe the progression of the accident sequences from the first confinement failure to the release of radionuclides from the second confinement after its failure.

Figure 5-1 shows the containment event tree used on the Reactor Safety Study [4-18] from the Pressurized Water Reactor (PWR). The headings were events postulated to lead to containment failure. However, it might be appropriate to include in the containment event tree events that significantly change accident sequences without failing the containment. The basic procedure is to order the events from most severe to least, so that subsequent events are compounding. For example, CRVSE is the worst thing. If it occurs, overpressure, hydrogen explosion, etc., do not matter. However, if CRVSE does not occur and containment isolation is successful, a hydrogen explosion might occur or it might not.

Although it is comparatively easy to draw these event trees, quantifying the probabilities is something else. Since the events are basically physical processes which may or may not occur, the probabilities of these events happening are basically judgmental. Because of the uncertainties in the prediction of physical processes, it is sometimes not possible to state with complete confidence which pathway an accident sequence will take. The branching probability in this sense represents a lack of knowledge about the physical processes that are involved.

The approach used in the present work is similar to the 'plant-damage binning': we looked at accident sequences which end with similar damage states of the first confinement barrier, we developed containment event trees for the second confinement barrier, and attached them to the corresponding branches.

One example is shown in Figures 5-2 and 5-3 representing the influence diagram and event tree model for the cryostat vessel failure corresponding to branches where the vacuum vessel failed and there is an in-vessel LOCA. The in-vessel LOCA may come from different cooling systems, and

the vacuum vessel may fail due to different failure modes, which results in a family of branches to be continued with the same cryostat vessel event tree. The probabilities of the events in the cryostat vessel ID/ET do not change from branch to branch. However, the consequences in terms of radioactive inventories released from the VV and called RI_VV do vary for different accident sequences, because each is the sum of conditional values depending on the events of the accident sequence:

$$RI\_VV = RI\_VP + RI\_VV\_PFC + RI\_VV\_DIV\_PHTS + RI\_VV\_FW\_PHTS \quad (5\text{-}1)$$

where RI_VP is the tritium in the vacuum pumps mobilized in the VV if the vacuum pumps are not isolated, RI_VV_PFC is the tritium in the plasma facing components mobilized in the VV depending on the performance of the PFC cooling systems, RI_VV_DIV_PHTS and RI_VV_FW_PHTS are tritium in the coolant released into the VV in case the respective PHTS caused in-vessel LOCA. In conclusion, we need to include the second confinement barriers ID/ET models in the same DPL files containing the first confinement barriers models.

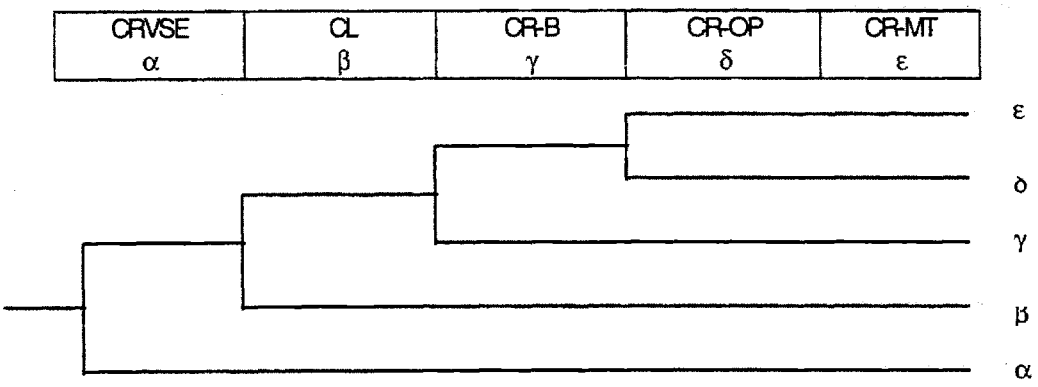

CRVSE	Containment failure from in-vessel steam explosion
CL	Containment isolation failure
CR-B	Containment failure from hydrogen combustion
CR-OP	Containment failure from overpressurization
CR-MT	Containment failure through basemat penetration

Figure 5-1: Example of Containment Event Tree [4-18]

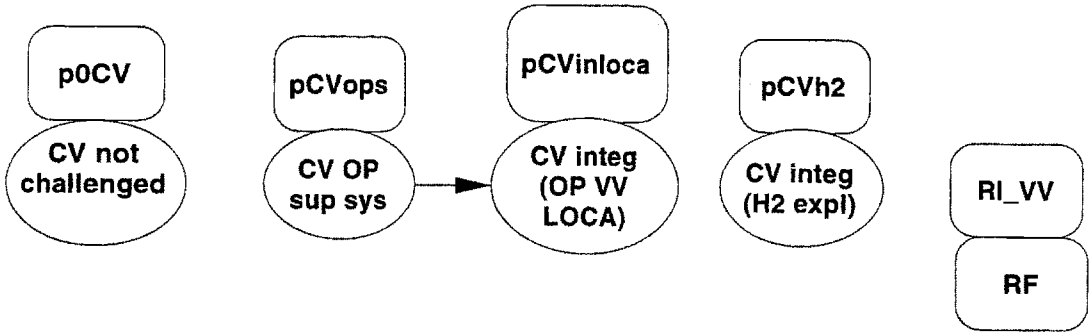

Figure 5-2: Cryostat Vessel Influence Diagram

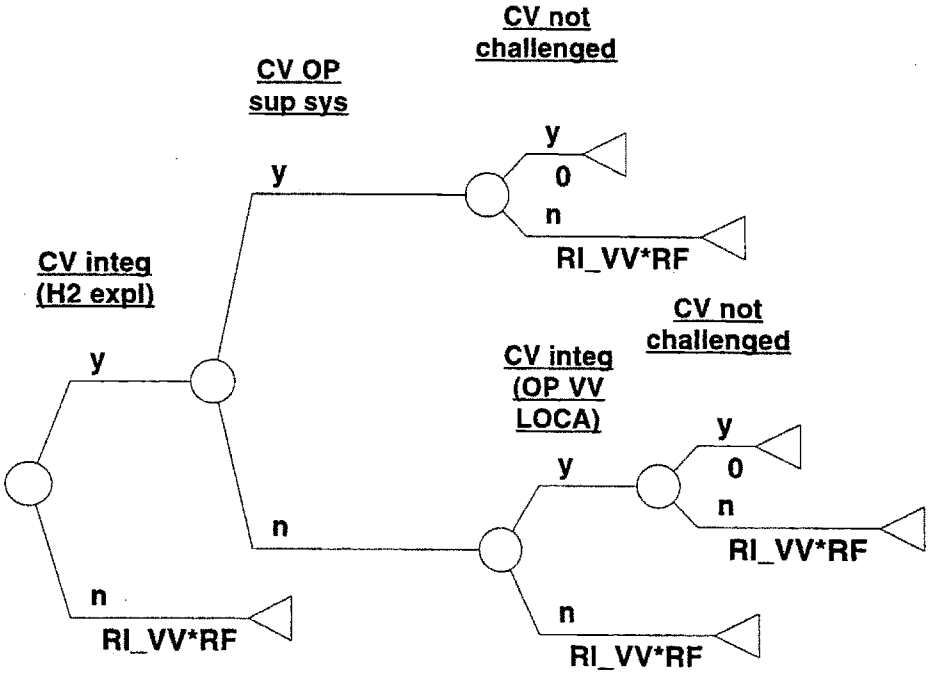

Figure 5-3: Cryostat Vessel Event Tree

One of the most important types of cryostat vessel failure involves overpressurization caused by a loss of water coolant inside the vacuum vessel combined with the VV failure, loss of water coolant inside the cryostat from the PHTS pipes, or loss of cryogen coolant in the cryostat. The pressure level at which the containment would fail can be calculated but only within some range of uncertainty, and the same is true for the pressure history inside the cryostat. To determine failure probability for a specific accident sequence, a curve that shows the probability of failure as a function of pressure can be developed. For example, at the design pressure, the probability of failure is near zero; at the ultimate strength of the structure, the probability of failure is equal to 1. In defining the rest of the curve, the material properties should be considered, the uncertainties in analyzing failure level of the structures, and the possibility of construction defects.

If hydrogen production is involved in a particular containment sequence, it is appropriate to include a conditional probability of hydrogen combustion. The conditions resulting in combustion can be described with uncertainties, and a probability of combustion can be estimated.

The analysis of the physical processes is outside the scope of the present work. We defined several failure modes of the cryostat vessel as given in Table C-3, and we combined them in five models depending on the accident sequences for the first confinement barrier they are attached to. The accident sequences models for the six selected initiating events including the second confinement barrier are included in Appendix C.

6. Database Analysis: Initiating Event Frequencies, Failures Rates, Radioactive Releases

6.1 General Concepts

The quantification of accident sequences requires a component-data base, which is developed by compiling data, selecting reliability models, establishing the parameters for those models, and then estimating the probabilities of component failures and the frequencies of initiating events. The data available for a tokamak fusion reactor is very scarce, and moreover, ITER is different than the existent experimental tokamak reactors in dimensions and new technologies involved. The most difficult task involves estimating data for components characteristic to fusion tokamak reactors, while generic nuclear industry data can be used for heat transport systems, electric equipment and other systems for which operating experience data is available.

The development of a data base for accident sequence quantification is a multi-step process involving collection and analysis of data, and the evaluation of appropriate reliability models. It produces tables that specify the quantity to be used for each event in the fault and event trees. The primary events can be analyzed with four types of models: component-failure models, test-contribution models, maintenance-contribution models, and initiating-events models. The first three of these models provide estimates of the probability that a plant element cannot accomplish its design function because it has failed, is being tested, or is being maintained. The model for initiating events provides the estimated frequency of the specific event of interest.

Component-failure models can be divided into two general types: time-related models and demand models. Time-related models are used in situations such as:

- components in standby mode, which are not used until needed or tested, and they could fail while in the standby mode;
- components in standby mode whose failure is detected immediately and they are returned to service after a specific period of time;
- components which fail during operation before completing their mission;[1]
- components are recovered in a certain period of time from their failure.

In most PRA studies, the exponential model is the most commonly used time-to-failure distribution. It is not only because it is a simple model, but also many reliability studies have found empirical grounds for the use of the exponential distribution. The probability that the event has occurred by time t is given by the equation:

[1] It should not be assumed that the failure rate during operation is the same as the failure rate in standby. Also, failure to start and failure to continue running after starting are mutually exclusive events.

$$p(t)=1-e^{-\lambda t} \tag{6-1}$$

The parameter λ is the failure rate, and is expressed in units of failures per unit time.

The demand model is appropriate for components that are in a dormant state until the moment of need, when they are switched on. It is used to describe the failure of a component at the time of a demand for its use.

For ITER, a cut-off frequency of 10^{-6}/a is used to determine accident sequences, i.e., sequences with an estimated frequency lower than this cut-off are not included within design basis.

Test- and maintenance-contribution models are usually considered in the fault tree analysis since they contribute to the component unavailability should a demand occur.

The probability that a component will be in testing when a demand occurs P_T is the frequency of the test f_T multiplied by the average duration of the test L_T, normalized by the time between the start of tests ΔT_T.

$$P_T = \frac{f_T(\text{tests/month}) \cdot L_T(\text{hr/test})}{\Delta T_T(\text{hr/month})} \tag{6-2}$$

A maintenance act is considered to be any unscheduled activity that causes a component or a system to be taken out of service for repair, but this repair may vary from very simple to very complex. The evaluation of the maintenance contribution is similar to that of testing, except that maintenance acts occur randomly in time, whereas for tests, the time is fixed. The probability that a component is in maintenance when a demand occurs can be estimated as follows:

$$P_M = \frac{f_M(\text{maintenance acts/month}) \cdot L_M(\text{hr/maintenance})}{1+f_M L_M} \tag{6-3}$$

where f_M is the average frequency of required maintenance, and L_M is the average length of the maintenance.

Initiating events are the occurrences that initiate accident sequences. The desired measure for such events is frequency. A plant may experience tens of these events per year or only one in 10,000 years.

The events in the accident sequences occur either randomly in time, or randomly at each challenge. Thus, data will be either in number of events in time T, or number of events in n demands. For events involving components in safety systems, the quantity of interest is the probability that the component cannot perform its intended function when the initiating event occurs.

The data-gathering task is to obtain the information needed for estimating the event-model parameters described above:

1. the number of failures in time or the number of demands for reliability models;
2. the frequency and duration of tests for systems and components;
3. the frequency and duration of maintenance on components;
4. the frequency of initiating events.

At this time, there is not enough data to consider tests and maintenance for ITER, hence, we will only consider the first and the last issues on this list. Moreover, unavailability due to tests or maintenance are usually considered at the fault tree level that calculates the failure probability for specific systems. In the present work, we gather failure probabilities for systems from existing references for fusion experimental reactors, data reports, and previous risk assessments for nuclear power plants. When more design information will be available for ITER, detailed fault tree analysis should be performed.

The references that we used for data collection are as follows:

- L. C. Cadwallader, S. J. Piet, "1989 Failure Rate Screening Data for Fusion Reliability and Risk Analysis", EGG-FSP-8709, September 1989: This document contains failure rate screening data for application to fusion components. The screening values are generally fission or aerospace industry failure rates estimates that can be extrapolated for use by fusion systems designers, reliability engineers and risk analysts. Failure rates estimates for tritium systems, liquid metal-cooled systems, gas-cooled systems, water-cooled systems, vacuum systems, plasma heating systems, and containment systems are given. Preliminary system availability, system level failure rates estimates, and selected initiating event frequency estimates are presented.[5-11]
- R. Buende, "Reliability and Availability Assessment of the Next European Torus", *Fusion Technology*, Vol. 14, Page 197, 1988: This paper discusses reliability and availability targets envisaged for the Next European Torus (NET) operation, describes and performs a failure modes, effects, and criticality analysis (FMECA) of the overall plant and of major components (toroidal field coil system, plasma heating system, protection, instrumentation, and control system, first wall and blanket and the cooling system).[5-10] The conclusions section of the paper presents a table (Table V) with system failure rates and corresponding mean downtime (MDT).
- G. Cambi, G. Cavallone, T. Palma, "Accident Scenarios for The In-Vessel Plant Area of NET-II/ITER", NET Task SEA 4.1, ENEA-DISP, 1991: The paper presents the summary of the risk evaluation for the main accident scenarios associated with failures originated in the In-Vessel Plant Area of NET-II/ITER. The risk assessment performed represents the first part of a probabilistic risk assessment dedicated to the accident scenario identification and to the corresponding risk quantification for a tokamak experimental fusion machine like NET/ITER. The study is mainly finalized to identify the most severe accident scenarios related to failures of the in-vessel systems, with respect to the public hazards, and to quantify them in terms of risk to the public.[5-12]

- Early Safety and Environmental Characterization Study (ESECS), ITER EDA, S 81 RE 95-06-01 W 1.1, June, 1995: Chapters 6 and 7 of ESECS present the results of accident analysis which demonstrate that the consequences of the event sequences do not exceed the corresponding limits established for the various sequences categories. Postulated sequences of events are divided between those that are within the "design basis" (chapter 6) and those "beyond the design basis" (chapter 7). Engineering judgment is used to categorize sequences, with 10^{-6}/a as a guide value for cut-off of "design basis".[5-1]

6.2 Database Development

The accident sequence models were developed using influence diagrams/event trees in Decision Programming Language (DPL), as explained in Chapter 3. DPL models can be dynamically linked to spreadsheets (EXCEL or Lotus 1-2-3): as DPL analyzes a model, it can send parameters to the spreadsheet and ask for calculated or just stored values back. As the same system failure event can occur in many accident sequences corresponding to different initiating events, it is important to make sure that the data used in different initiating event models are consistent with each other. Linking an event as it occurs in different DPL models to the same spreadsheet cell takes care of the consistency issue. If the value of an event failure rate is changed in the spreadsheet, all the DPL models will update it when running.

All the accident events involved in the sequences are defined in the influence diagram part of the DPL model as chance events expressing the success/integrity of the system. Each chance event has usually two states: yes (success) and no (failure). The failure has a probability of occurrence given as a point estimate value between 0 and 1, and is shown in a value node. This value node is linked to the spreadsheet model, which means that it is defined as a DPL-import variable: the spreadsheet cell returns its output to the DPL analysis. The probability of system success is automatically calculated by DPL as 1 minus the probability of system failure.

There are systems whose probability of failure depends on the output of other events in the accident sequences (which can occur before or after the system itself is challenged). The dependency is represented in the DPL influence diagram by arrows from the conditioning events towards the conditioned event. Several probability nodes will be associated with the conditioned event, and they represent conditional probabilities given specific states of conditioning events.

Our EXCEL 5.0 database is constructed in the form of a two-column table with the events name and the corresponding frequencies for initiating events, and probability of failure for systems failures. The failures are either failures on demand or failures to accomplish the mission for a specific duration. The failure database and the explanation of the data is presented in Appendix D.

The consequence data in terms of radioactive inventories released from the confinement barriers are also defined as value nodes, and they may also be dependent on some system states. They are attached in the event tree model to the appropriate branches. The present work concentrates on tritium releases, but the same model could be applied for any other radioactive inventory. In chapter 2, an overview of tritium characteristics and locations of major inventories and flows was presented. In this section, the concern is focused on the amount of tritium in the torus and in the cooling systems. Chapter 2 of ESECS [4-1] gives a comprehensive description of tritium processes.

The tritium inventory in the torus is composed of tritium in the plasma and divertor gas, tritium on the cryopanels of the vacuum pumps, and tritium in the plasma facing components.

The tritium in the plasma and divertor gas target does not contribute significantly to the inventory that could be mobilized in case of an accident since it is only a few grams. (This low in-plasma inventory is also one reason that there cannot be a runaway fusion reaction since there is inadequate fuel present.)

The inventory on the cryogenic panels of the vacuum pumps can become mobile in any accidental condition in which these panels would heat-up (for example, gas ingress or steam ingress in the vacuum vessel). If the vacuum pumps are only regenerated after the end of burn, the total inventory on the hydrogen panels of all vacuum pumps is the inventory that is injected in one burn-cycle minus the amount that is burned, or approximately 130 g-T. If some of the pumps could be regenerated during the burn, then the total inventory could be less than this. In the rest of this report. we conservatively assume that the inventory is 130 g-T. Besides this inventory, the vacuum pumps also collect tritiated impurities such as tritiated water and organics (if carbon is used in the machine). The tritium content collected in a 1000 s burn from these is estimated to be 6-8 g, and the regeneration could be less frequent than for the hydrogen panels. Assuming regeneration every fourth cycle, the inventory would add up to 30 g-T. This leads to a total inventory on the vacuum pumps of 160 g-T, all of which would be mobile in hot, oxidizing accident conditions.

Tritium in the plasma facing components is the most important inventory and the one that has the largest uncertainty. Depending on the material, there are several dominant mechanisms for tritium to be in (or on) plasma facing components:

- for metals the dominant mechanism is implantation with associated diffusion of tritium into the bulk material;
- for carbon it is tritium co-depositing with carbon materials onto surfaces;
- tritium breeding in beryllium (or boron) in near-plasma materials.

The inventories in Table 6-1 are the values used in the present work: the total inventory base case or only the mobilizable inventory depending on the temperature and the integrity of the respective plasma facing component. The uncertainty in these values is large but will be reduced substantially as the ITER R&D program progresses. For now, the best estimate is about 2 kg-T total with about 500 g-T that could potentially be mobilized.

Table 6-1: Tritium Inventory in Beryllium PFC Material

Component	Total Inventory Base Case (g-T)	Mobilizable inventory Base Case (g-T)	Reduction due to Surface Barrier	Reduction due to Erosion	Inventory due to breeding (g-T)
First Wall	900	40	100%	none	130
Limiter and Baffle	400	100	none	50%	60
Divertor Components	1900	600	50%	75%	180

7. Evaluation of Confinement Barriers Performance

The probabilistic model developed in the previous chapters is used to evaluate the safety performance of the first and second confinement barriers. The Vacuum Vessel (VV) and the Cryostat Vessel (CV) respectively are the most significant parts in the current ITER confinement strategy, and therefore, a sensitivity analysis of their failure modes is performed in this chapter.

The failure probabilities corresponding to the failure modes of the first confinement barrier are included in the first and second confinement barrier DPL models, while those corresponding to the second barrier only affect the model of the second barrier.

A reference case is considered with the database parameters as given in Table D-3, Appendix D. The failure modes and retention factors corresponding to the VV and the CV are enumerated from 1 to 23. The first step is to run the DPL accident sequence models for a low and a high value of each of the 23 probabilities of failure, changing them one by one, while keeping all the other values at their reference levels. The goal is to study the influence of that particular failure mode on the overall complementary cumulative frequency (CCF) of tritium releases. The low (l) and high (h) values are arbitrarily chosen equal to 10^{-6} and 0.1 respectively. This is a very large range, so if there is no variation of the CCF between these values for a particular failure mode of a confinement barrier, it can be concluded that this failure mode does not affect the overall safety of the plant.

It is important to realize that the development of the accident sequences is a subjective work, so the list of failure modes considered might be different for different models. However, if we assume that all the conceivable failure modes of the confinement barriers have been defined, the sensitivity analysis presented here can be used to perform a ranking of the most important failure modes.

The overall frequency distribution of radioactive releases is analyzed with BestFit [8-13], which gives statistical parameters such as: minimum and maximum consequence, mode[1], mean, standard deviation, variance, skewness[2], and kurtosis[3].

The notations to differentiate among PDFs and CCFs of radioactive releases for various parameter values are as follows: #l_b1, #l_b2, #h_b1, #h_b2, where "#" is the failure mode number (from 1 to 23) as given in Table D-3, 'l' and 'h' are the low and high values of the probability of failure, 'b1' and 'b2' are barriers 1 and 2. The reference case for barriers 1 and 2 is represented by 0_b1 and

[1] Mode is the value with the highest probability of occurrence.

[2] Skewness of a distribution gives an indication of the degree of asymmetry. A distribution which is symmetrical about the mean leads to a value of skewnesss equal to zero (i.e., normal distribution). Negative values show a distribution peak to the right of the mean, and positive values a peak to the left of the mean.

[3] Kurtosis of a distribution describes the extent to which a distribution is peaked. Normal probability distribution function has a kurtosis of 3, and is taken as a standard measure. A distribution with kurtosis smaller than 3 has a flatter top than the normal distribution. A distribution with a kurtosis greater than 3 has a more peaked top than a normal distribution.

0_b2. When a failure mode has a corresponding probability close to the low or high values, that case is not run any more. The results are grouped in three sections: VV failure modes, CV failure modes, and retention factors. The statistical parameters of the PDFs of tritium releases determine those failure modes to which the model is sensitive, and the corresponding CCF of tritium releases is plotted for those cases along with the reference graphs and the ITER tritium release limit. When the reference probabilities of failure are very close to the low or to the high values considered, it is not useful to run the model, particularly if no sensitivity to that failure mode is observed for the other end of the range. The statistics that differ from the reference one are highlighted in the figures below.

7.1 Sensitivity Analysis for First Confinement Barrier Failure Modes

There are ten vacuum vessel failure modes defined in the present accident sequences model. Possible failure causes include: electromagnetic loads, overpressure following in-vessel LOCA, hydrogen explosion inside the vacuum vessel, arcing, missile generation, displaced magnet coil, ozone explosion inside the cryostat vessel. The probabilities of integrity loss of the vacuum vessel as we defined them are conditional probabilities; for example, given an event such as arcing has occurred, the probability that the vacuum vessel fails due to arcing is estimated.

The PDF and CCF of tritium releases was calculated when changing each of the ten probabilities of failures to the low and then to the high values as defined above, while keeping all the other probabilities constant. The statistics analysis shows that only two failure modes have an actual impact on the PDF of tritium releases, while all the others do not have any significant effect. The two failure causes are arcing (number 7) and displaced magnet coil (number 9), both magnet system related events. Hence, it is important that the vacuum vessel design has provisions to avoid being affected by events in the magnet systems. Moreover, if the magnet systems design allow for a decrease in the probability of failure due to those causes, that would also decrease the frequency of the accident sequences that include the vacuum vessel failure due to arcing or displaced coil.

For the arcing case, Figure 7-3 presents the complementary cumulative frequency of tritium releases for the first and second confinement barriers for the vacuum vessel failure due to arcing. The reference value of the failure probability is 0.01. It is interesting that changing the probability to 10^{-6} does not have a very significant effect on decreasing the accident frequencies; however, by increasing the probability with only one order of magnitude to 0.1, the curves for both the first and second barriers are shifted to upper frequencies quite significantly. Therefore, there is no benefit in trying to improve the design in order to lower the probability of failure due to arcing, but care should be taken so that the probability of failure does not increase above the current value.

The failure probability of the vacuum vessel due to a displaced coil has little effect on the second barrier complementary cumulative frequency function, while the first confinement barrier

function varies quite significantly. The low value of the probability is again 10^{-6}, but the high value is 0.9 (because the reference value is 0.5).

What captures our attention in this case is that for the low case, the complementary cumulative frequency for the first and second barriers intersect one another in the region of 500 - 800 grams of tritium (Figure 7-4). Intuitively, such a fact should not happen since the presence of a second confinement barrier should lower the consequences in terms of both frequency and release. However, due to the fact that CCF is a cumulative function, it might happen that, by introducing an additional confinement barrier, more accident sequences leading to the same radioactive release are possible. When adding all these frequencies corresponding to the same consequences, there might be points where the CCF for the second confinement barrier is above the one for the first barrier, which happens in our case.

A simplified example shown in Figure 7-1 and 7-2 demonstrates the statements above mathematically. For the case when there is only one confinement barrier (i.e., the vacuum vessel), two accident sequences are possible: one without any consequences, and the other with a probability of pVV and release of X_grams. When a second confinement barrier is introduced (i.e., the cryostat vessel), which has two possible failure modes, there are four possible accident sequences: two of them with no consequences, and the other two with the probabilities as given in Figure 7-2 and the same consequence X_grams. Thus, the release X_grams will have a cumulative probability of occurrence equal to the sum of the probabilities of the two accident sequences:

$$\begin{aligned} Pr(X\_grams) &= pVV(1 - pCV\_1)pCV\_2 + pVV(pCV\_1) = \\ &= pVV[(1 - pCV\_1)pCV\_2 + pCV\_1] \end{aligned} \qquad (7\text{-}1)$$

Equation (7-1) implies that Pr(X_grams) can be lower or higher than pVV, depending on the probabilities of failure of the cryostat vessel: [pCV_1 + pCV_2 - pCV_1.pCV_2] < or > 1.

In conclusion, when an additional confinement barrier is included in the confinement strategy, the failure probabilities corresponding to its possible failure modes should be reasonably low, so that the situation encountered above does not occur.

The Primary Heat Transport Systems (PHTSs) of the Plasma Facing Components (PFCs) of ITER are also part of the first confinement barrier. Because the accident sequences models developed in the present study are symmetrical with regard to the divertor and first wall PHTSs, sensitivity analysis is performed only on selected failure modes for the divertor PHTS. The failure causes of interest are as follows: runaway electrons damage, electromagnetic loads, missile generation, displaced coil, and ozone explosion in the cryostat vessel. The results, as presented in Tables 7-5 and 7-6 and plotted in Figures 7-5 and 7-6, show almost no sensitivity of the model to those failure modes.

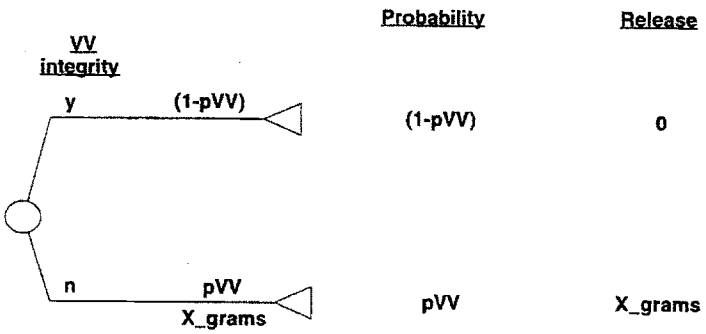

Figure 7-1: Probability versus Radioactive Releases from First Barrier

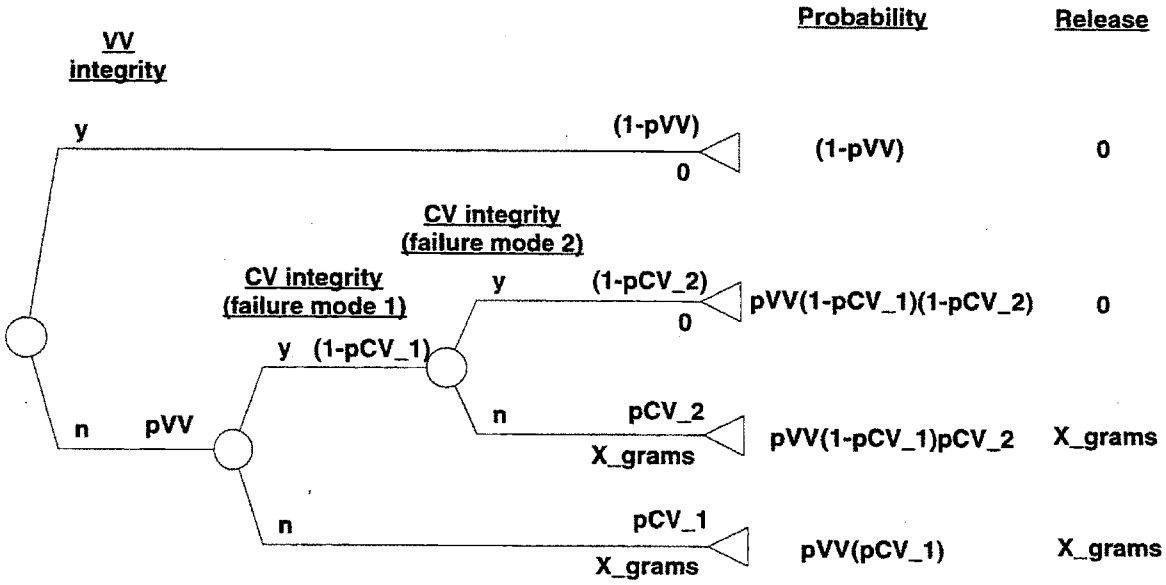

Figure 7-2: Probability versus Radioactive Releases from Second Barrier

	A	B	C	D	E	F	G	H	I	J	K
1	**0_b1**	Input Data		**0_b2**	Input Data					**l -> p(i) = 1.0E-06**	
2	Minimum=	0		Minimum=	0					**h -> p(i) = 0.1**	
3	Maximum=	3699		Maximum=	2673						
4	Mode=	1.125		Mode=	0.84375						
5	Mean=	2.878102		Mean=	0.867413						
6	Std Deviati	38.87469		Std Deviati	12.24945						
7	Variance=	1511.241		Variance=	150.0489						
8	Skewness=	22.9602		Skewness=	55.99461						
9	Kurtosis=	766.1326		Kurtosis=	4398.47						
10											
11	**1l_b1**	Input Data		**1l_b2**	Input Data		**1h_b1**	Input Data		**1h_b2**	Input Data
12	Minimum=	0		Minimum=	0		Minimum=	0		Minimum=	0
13	Maximum=	3699		Maximum=	2673		Maximum=	3699		Maximum=	2673
14	Mode=	1.125		Mode=	0.84375		Mode=	1.125		Mode=	0.84375
15	Mean=	2.8781		Mean=	0.867413		Mean=	2.885896		Mean=	0.86742
16	Std Deviati	38.87435		Std Deviati	12.24946		Std Deviati	38.87956		Std Deviati	12.24939
17	Variance=	1511.215		Variance=	150.0492		Variance=	1511.62		Variance=	150.0474
18	Skewness=	22.95773		Skewness=	55.9946		Skewness=	22.95033		Skewness=	55.99874
19	Kurtosis=	765.786		Kurtosis=	4398.466		Kurtosis=	765.3753		Kurtosis=	4399.869
20											
21	**2l_b1**	Input Data		**2l_b2**	Input Data						
22	Minimum=	0		Minimum=	0						
23	Maximum=	3699		Maximum=	2673						
24	Mode=	1.125		Mode=	0.84375						
25	Mean=	2.878089		Mean=	0.867411						
26	Std Deviati	38.87442		Std Deviati	12.24944						
27	Variance=	1511.22		Variance=	150.0488						
28	Skewness=	22.95994		Skewness=	55.99925						
29	Kurtosis=	766.0865		Kurtosis=	4399.986						
30											

Table 7-1: Statistical Parameters for PDF of Tritium Releases
for Sensitivity on VV Failure Modes

	A	B	C	D	E	F	G	H	I	J	K
31	**3l_b1**	Input Data		**3l_b2**	Input Data		**3h_b1**	Input Data		**3h_b2**	Input Data
32	Minimum=	0		Minimum=	0		Minimum=	0		Minimum=	0
33	Maximum=	3699		Maximum=	2673		Maximum=	3699		Maximum=	2673
34	Mode=	1.125		Mode=	0.84375		Mode=	1.125		Mode=	0.84375
35	Mean=	2.878101		Mean=	0.867413		Mean=	2.878091		Mean=	0.867413
36	Std Deviati	38.87466		Std Deviati	12.24944		Std Deviati	38.87453		Std Deviati	12.24943
37	Variance=	1511.239		Variance=	150.0488		Variance=	1511.229		Variance=	150.0485
38	Skewness=	22.96018		Skewness=	55.99463		Skewness=	22.96087		Skewness=	55.99465
39	Kurtosis=	766.1291		Kurtosis=	4398.476		Kurtosis=	766.2258		Kurtosis=	4398.484
40											
41	**4l_b1**	Input Data		**4l_b2**	Input Data		**4h_b1**	Input Data		**4h_b2**	Input Data
42	Minimum=	0		Minimum=	0		Minimum=	0		Minimum=	0
43	Maximum=	3699		Maximum=	2673		Maximum=	3699		Maximum=	2673
44	Mode=	1.125		Mode=	0.84375		Mode=	1.125		Mode=	0.84375
45	Mean=	2.878102		Mean=	0.867413		Mean=	2.878102		Mean=	0.867413
46	Std Deviati	38.87469		Std Deviati	12.24945		Std Deviati	38.87469		Std Deviati	12.24945
47	Variance=	1511.241		Variance=	150.0489		Variance=	1511.241		Variance=	150.0489
48	Skewness=	22.9602		Skewness=	55.99462		Skewness=	22.9602		Skewness=	55.99461
49	Kurtosis=	766.1326		Kurtosis=	4398.47		Kurtosis=	766.1326		Kurtosis=	4398.468
50											
51	**5l_b1**	Input Data		**5l_b2**	Input Data						
52	Minimum=	0		Minimum=	0						
53	Maximum=	3699		Maximum=	2673						
54	Mode=	1.125		Mode=	0.84375						
55	Mean=	2.878099		Mean=	0.867413						
56	Std Deviati	38.87463		Std Deviati	12.24944						
57	Variance=	1511.237		Variance=	150.0488						
58	Skewness=	22.96019		Skewness=	55.9946						
59	Kurtosis=	766.1298		Kurtosis=	4398.473						
60											

Table 7-2: Statistical Parameters for PDF of Tritium Releases
for Sensitivity on VV Failure Modes (Table 7-1 cont.)

	A	B	C	D	E	F	G	H	I	J	K
61	6l_b1	Input Data		6l_b2	Input Data						
62	Minimum=	0		Minimum=	0						
63	Maximum=	3699		Maximum=	2673						
64	Mode=	1.125		Mode=	0.84375						
65	Mean=	2.878102		Mean=	0.867413						
66	Std Deviati	38.87469		Std Deviati	12.24945						
67	Variance=	1511.241		Variance=	150.0489						
68	Skewness=	22.9602		Skewness=	55.99461						
69	Kurtosis=	766.1326		Kurtosis=	4398.47						
70											
71	7l_b1	Input Data		7l_b2	Input Data		7h_b1	Input Data		7h_b2	Input Data
72	Minimum=	0		Minimum=	0		Minimum=	0		Minimum=	0
73	Maximum=	3699		Maximum=	2673		Maximum=	3699		Maximum=	2673
74	Mode=	1.125		Mode=	0.84375		Mode=	1.125		Mode=	0.84375
75	Mean=	2.871625		Mean=	0.851615		Mean=	3.462465		Mean=	0.911222
76	Std Deviati	38.58299		Std Deviati	11.80918		Std Deviati	59.40001		Std Deviati	16.2528
77	Variance=	1488.647		Variance=	139.4567		Variance=	3528.362		Variance=	264.1536
78	Skewness=	22.15476		Skewness=	56.64655		Skewness=	38.89352		Skewness=	91.2984
79	Kurtosis=	673.6569		Kurtosis=	4369.255		Kurtosis=	1976.268		Kurtosis=	1.19E+04
80											
81	8l_b1	Input Data		8l_b2	Input Data						
82	Minimum=	0		Minimum=	0						
83	Maximum=	3699		Maximum=	2673						
84	Mode=	1.125		Mode=	0.84375						
85	Mean=	2.81472		Mean=	0.867268						
86	Std Deviati	38.17572		Std Deviati	12.24584						
87	Variance=	1457.385		Variance=	149.9606						
88	Skewness=	23.39791		Skewness=	56.01565						
89	Kurtosis=	799.2622		Kurtosis=	4402.274						
90											

Table 7-3: Statistical Parameters for PDF of Tritium Releases
for Sensitivity on VV Failure Modes (Table 7-2 cont.)

	A	B	C	D	E	F	G	H	I	J	K
91	9l_b1	Input Data		9l_b2	Input Data		9h_b1	Input Data		9h_b2	Input Data
92	Minimum=	0		Minimum=	0		Minimum=	0		Minimum=	0
93	Maximum=	3699		Maximum=	2673		Maximum=	3699		Maximum=	2673
94	Mode=	1.125		Mode=	0.84375		Mode=	1.125		Mode=	0.84375
95	Mean=	1.487338		Mean=	0.86401		Mean=	3.990802		Mean=	0.870448
96	Std Deviati	16.70668		Std Deviati	12.15429		Std Deviati	49.94178		Std Deviati	12.33037
97	Variance=	279.1132		Variance=	147.7268		Variance=	2494.182		Variance=	152.0379
98	Skewness=	45.97089		Skewness=	56.40709		Skewness=	18.05512		Skewness=	55.62711
99	Kurtosis=	4952.508		Kurtosis=	4469.689		Kurtosis=	455.1232		Kurtosis=	4337.821
100											
101	10l_b1	Input Data		10l_b2	Input Data						
102	Minimum=	0		Minimum=	0						
103	Maximum=	3699		Maximum=	2673						
104	Mode=	1.125		Mode=	0.84375						
105	Mean=	2.8781		Mean=	0.867412						
106	Std Deviati	38.87468		Std Deviati	12.24944						
107	Variance=	1511.24		Variance=	150.0488						
108	Skewness=	22.96021		Skewness=	55.99466						
109	Kurtosis=	766.1334		Kurtosis=	4398.476						
110											

Table 7-4: Statistical Parameters for PDF of Tritium Releases
for Sensitivity on VV Failure Modes (Table 7-3 cont.)

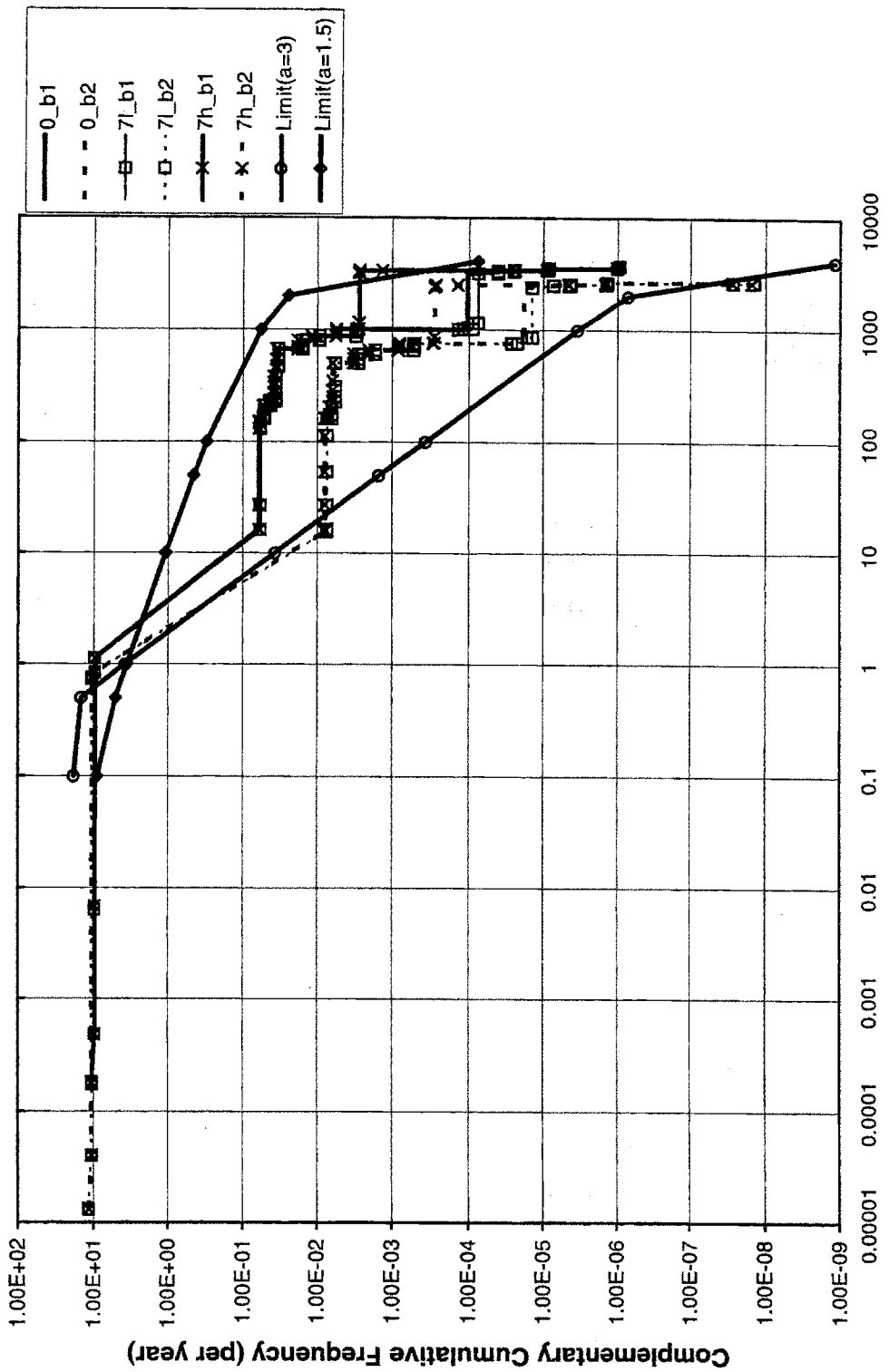

Figure 7-3: Sensitivity of CCF of Tritium Releases to the Probability of Failure of the Vacuum Vessel due to Arcing

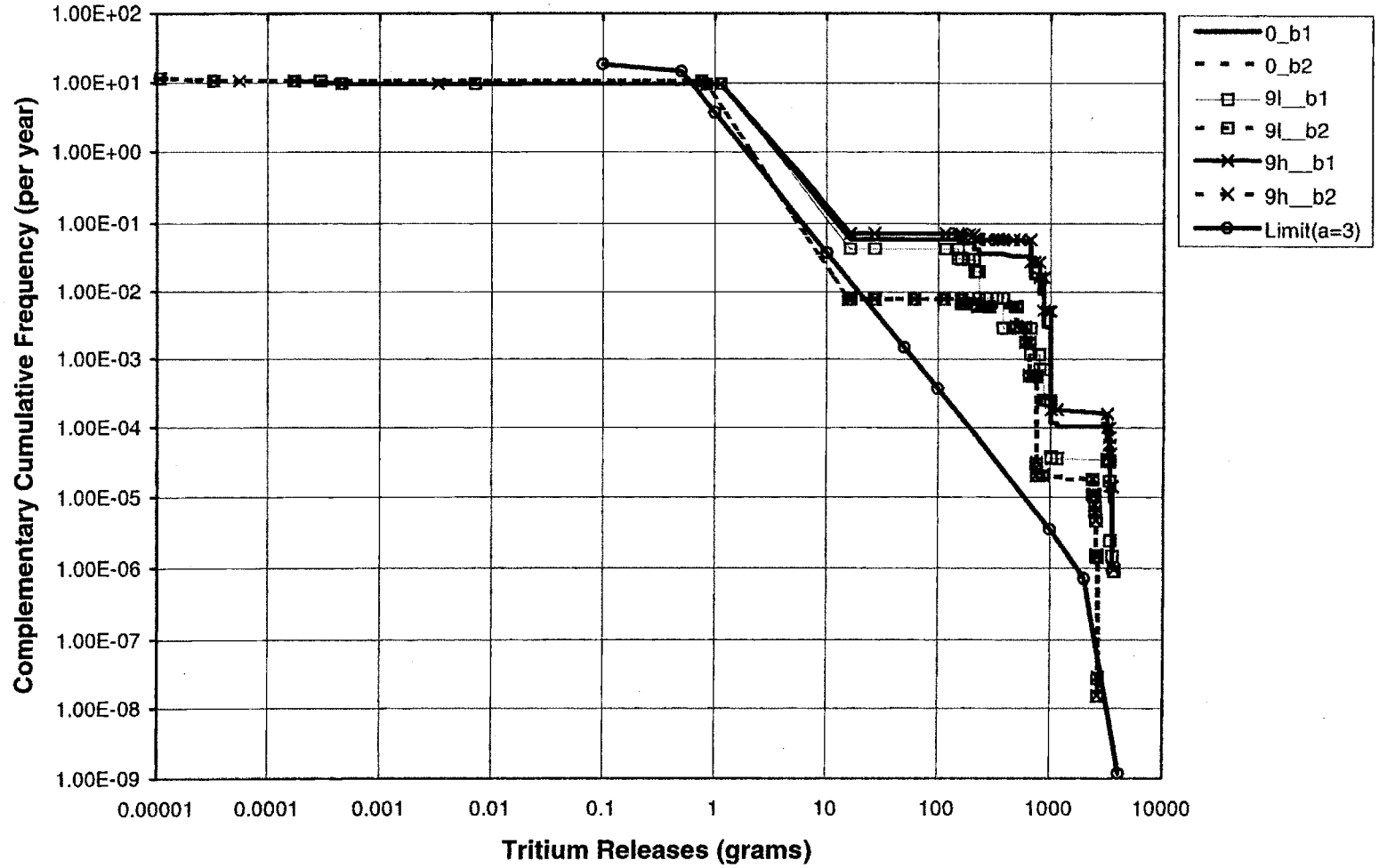

Figure 7-4: Sensitivity of CCF of Tritium Releases to the Probability of Failure of the Vacuum Vessel due to Displaced Magnet Coil

	A	B	C	D	E	F	G	H	I	J	K
1	**0_b1**	Input Data		**0_b2**	Input Data					**l -> p(i) = 1.0E-06**	
2	Minimum=	0		Minimum=	0					**h -> p(i) = 0.1**	
3	Maximum=	3699		Maximum=	2673						
4	Mode=	1.125		Mode=	0.84375						
5	Mean=	2.878102		Mean=	0.867413						
6	Std Deviati	38.87469		Std Deviati	12.24945						
7	Variance=	1511.241		Variance=	150.0489						
8	Skewness=	22.9602		Skewness=	55.99461						
9	Kurtosis=	766.1326		Kurtosis=	4398.47						
10											
11	**24l_b1**	Input Data		**24l_b1**	Input Data		**24h_b1**	Input Data		**24h_b2**	Input Data
12	Minimum=	0		Minimum=	0		Minimum=	0		Minimum=	0
13	Maximum=	3699		Maximum=	2673		Maximum=	3699		Maximum=	2673
14	Mode=	1.125		Mode=	0.84375		Mode=	1.125		Mode=	0.84375
15	Mean=	2.875767		Mean=	0.86743		Mean=	2.945136		Mean=	0.87189
16	Std Deviati	38.84658		Std Deviati	12.24501		Std Deviati	39.66926		Std Deviati	12.45799
17	Variance=	1509.056		Variance=	149.9403		Variance=	1573.65		Variance=	155.2016
18	Skewness=	22.96897		Skewness=	55.97656		Skewness=	22.70938		Skewness=	55.69727
19	Kurtosis=	767.0592		Kurtosis=	4398.209		Kurtosis=	739.2456		Kurtosis=	4293.848

Table 7-5: Statistical Parameters for PDF of Tritium Releases
for Sensitivity on PHTS Failure Modes

	A	B	C	D	E	F	G	H	I	J	K
21	**25l_b1**	Input Data		**25l_b2**	Input Data						
22	Minimum=	0		Minimum=	0						
23	Maximum=	3699		Maximum=	2673						
24	Mode=	1.125		Mode=	0.84375						
25	Mean=	2.878113		Mean=	0.867581						
26	Std Deviati	38.87466		Std Deviati	12.25223						
27	Variance=	1511.239		Variance=	150.1171						
28	Skewness=	22.95967		Skewness=	55.96732						
29	Kurtosis=	766.0646		Kurtosis=	4394.65						
30											
31	**26l_b1**	Input Data		**27l_b1**	Input Data		**28l_b1**	Input Data		**29l_b1**	Input Data
32	Minimum=	0		Minimum=	0		Minimum=	0		Minimum=	0
33	Maximum=	3699		Maximum=	3699		Maximum=	3699		Maximum=	3699
34	Mode=	1.125		Mode=	1.125		Mode=	1.125		Mode=	1.125
35	Mean=	2.878079		Mean=	2.855154		Mean=	2.735718		Mean=	2.878079
36	Std Deviati	38.87408		Std Deviati	38.59895		Std Deviati	37.12516		Std Deviati	38.87408
37	Variance=	1511.194		Variance=	1489.879		Variance=	1378.278		Variance=	1511.194
38	Skewness=	22.95984		Skewness=	23.05409		Skewness=	23.47135		Skewness=	22.95984
39	Kurtosis=	766.0877		Kurtosis=	776.8366		Kurtosis=	826.7571		Kurtosis=	766.0877

Table 7-6: Statistical Parameters for PDF of Tritium Releases
for Sensitivity on PHTS Failure Modes (Table 7-5 cont.)

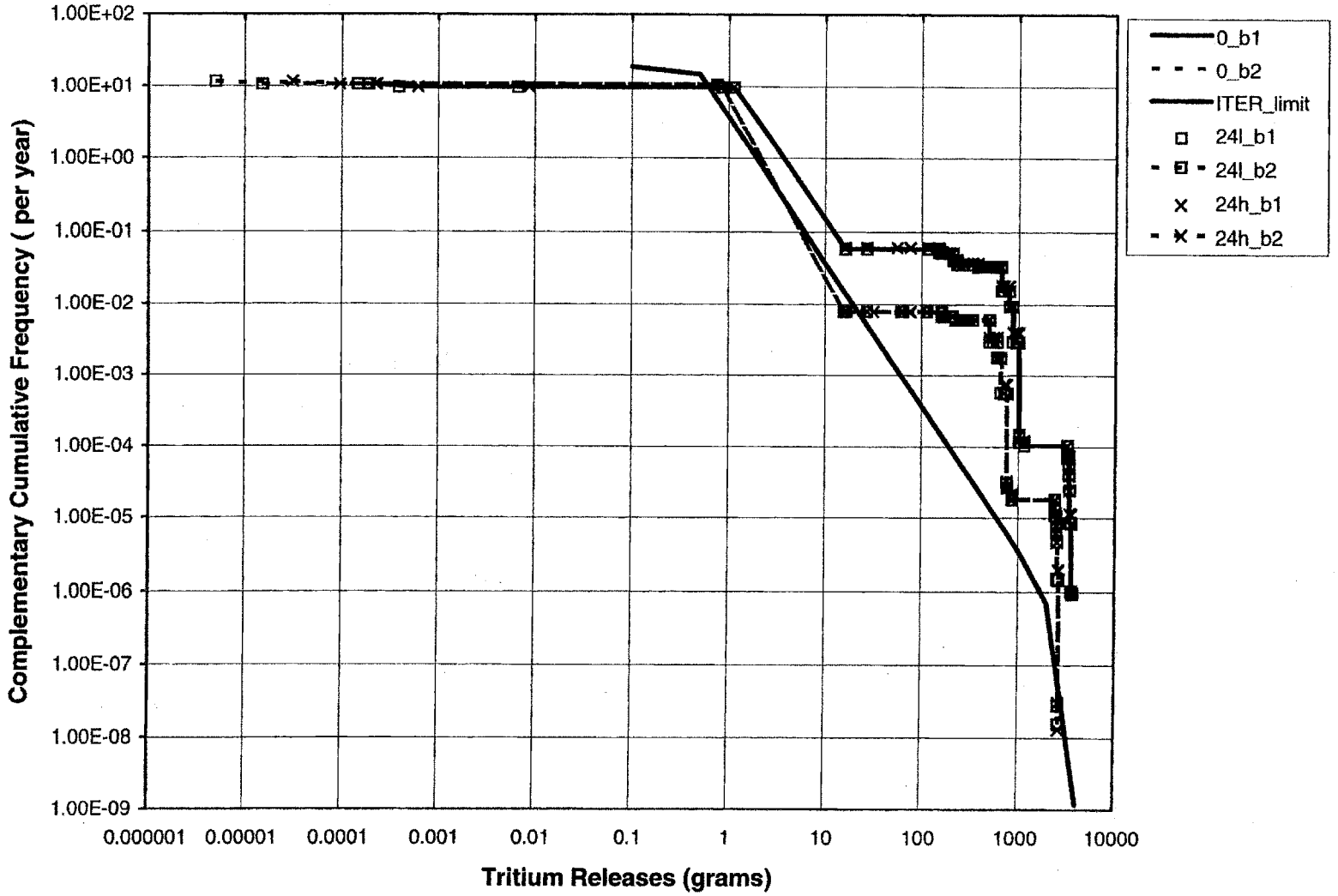

Figure 7-5: Sensitivity of CCF of Tritium Releases to the Independent Probability of Failure of the Divertor PHTS

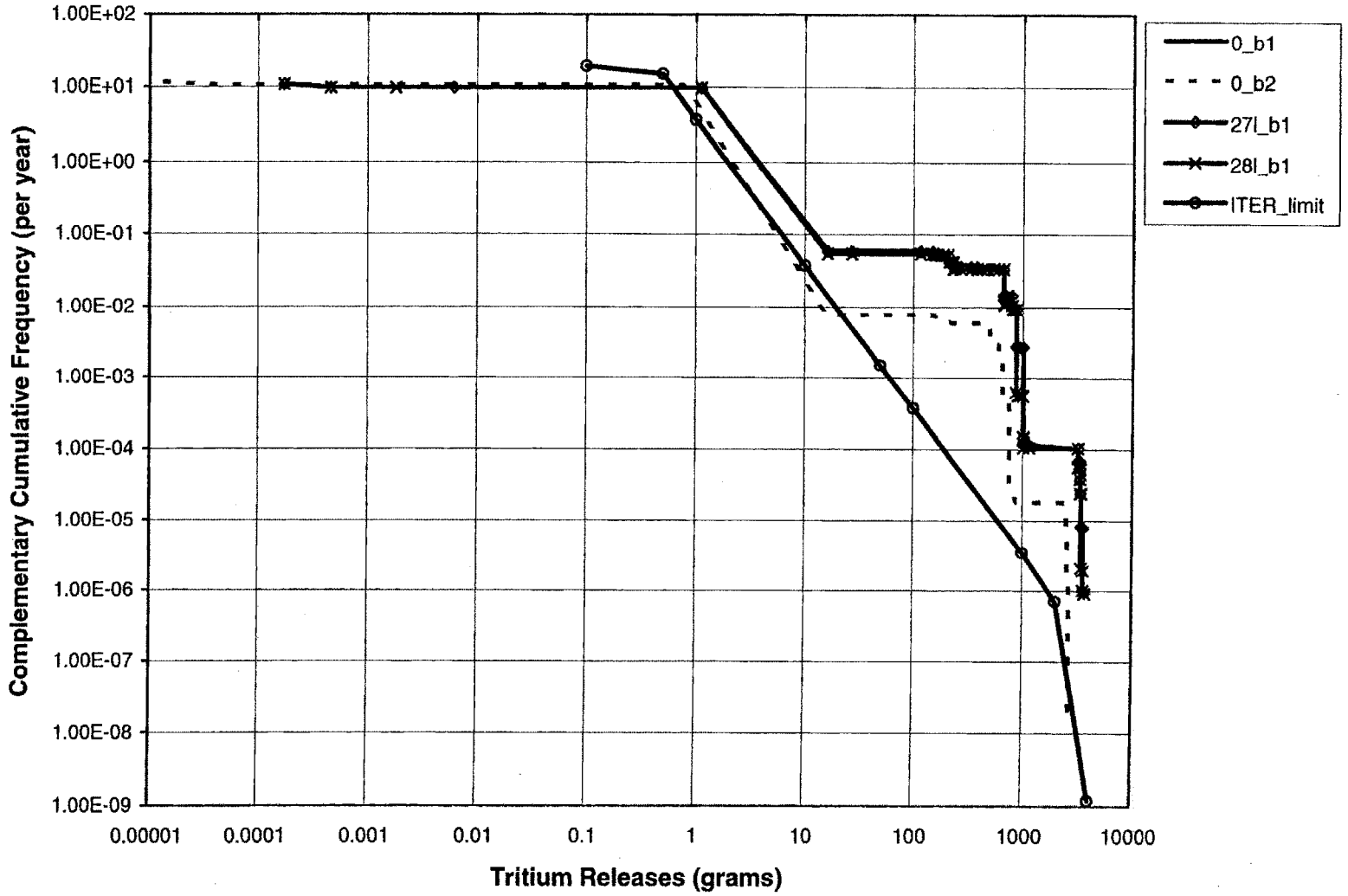

Figure 7-6: Sensitivity of CCF of Tritium Releases to the Probability of Failure of the Divertor PHTS due to Missile Generation or Displaced Coil

7.2 Sensitivity Analysis for Second Confinement Barrier Failure Modes

The most important component of the second confinement barrier for ITER strategy is the cryostat vessel. Eleven failure modes are considered for the cryostat vessel (numbers 11 to 21 in Table D-3, Appendix D); some of the accident events as defined are conditional and some are independent. Naturally, these failure modes are only included in the accident sequence DPL models for the second confinement barrier, which considerably decreases the DPL and EXCEL run time to obtain the complementary cumulative frequency (CCF) of tritium releases. Four failure modes affect the CCF of releases from the second confinement barrier in this case: arcing (number 12), missile generation (number 15), displaced magnet coil (number 16), and failure of the cryostat vessel without off-normal challenge (number 18). Tables 7-7 to 7-9 present the statistical parameters of the PDFs of tritium releases when sensitivity analysis is performed on the failure probabilities. Figures 7-7 to 7-10 include the CCF of releases for the four failure modes mentioned above.

The conditional failure probability of the cryostat vessel due to arcing (event number 12) given that arc was produced has a reference value of 0.1. The low and the high values for which the model was run are 10^{-6} and 0.9 respectively. As Figure 7-7 shows, decreasing the conditional probability by a factor of 10^{-5} lowers the CCF curve for the second barrier by less than a factor of 10^{-1} in the range of 20 to 900 grams of tritium releases where most of the accident sequences belong. However, the CCF is still above the prescribed ITER limit. When the failure probability of CV due to arcing is increased to 0.9, the CCF for second confinement barrier overlaps with the CCF for the first barrier, implying no advantage from a safety point of view for the presence of a second barrier. Therefore, the CV and magnet systems design should be such that the probability of failure should not be more than 0.1, but the gain in CCF curve is not considerable if the probability of this failure mode is decreased below the reference value.

For missile generation and displaced magnet coil (numbers 15 and 16, respectively), the reference value for the CV conditional failure probabilities is the same and equal to 0.01. The model was run for three other values: 10^{-6}, 0.1, and 1. For the low value, there is practically no change in the CCF of tritium releases, meaning that no effort should be made to decrease the probability for those failure modes. When the probability is increased by one factor of magnitude to 0.1, an increase of CCF by a factor of 3 in the range of 20 to 3000 grams of tritium is observed. When increasing the probability from 0.1 to 1, the CCF for second barrier jumps considerably, in some points above the CCF for the first barrier. Care should be taken that the conditional probability of failure of CV for these two failure modes does not go above 0.1.

The failure of the CV without being challenged by any off-normal causes is an independent event (number 18), having a reference probability of 10^{-3}. By decreasing this probability to 10^{-6}, no gain

in CCF of tritium releases is observed at all. The CCF curve is more sensitive to an increase of the probability to 0.1, although not significantly (Figure 7-10).

	A	B	C	D	E	F	G	H	I	J	K
1	**0_b1**	Input Data		**0_b2**	Input Data		**l -> p(i) = 1.0E-06**				
2	Minimum=	0		Minimum=	0		**h -> p(i) = 0.1**				
3	Maximum=	3699		Maximum=	2673						
4	Mode=	1.125		Mode=	0.84375						
5	Mean=	2.878102		Mean=	0.867413						
6	Std Deviati	38.87469		Std Deviati	12.24945						
7	Variance=	1511.241		Variance=	150.0489						
8	Skewness=	22.9602		Skewness=	55.99461						
9	Kurtosis=	766.1326		Kurtosis=	4398.47						
10											
11	**Events 11 to 21 only affect barrier 2 performance.**										
12											
13	**11l**	Input Data					**12l**	Input Data		**12h**	Input Data
14	Minimum=	0					Minimum=	0		Minimum=	0
15	Maximum=	2673					Maximum=	2666.25		Maximum=	2774.25
16	Mode=	0.84375					Mode=	0.84375		Mode=	0.84375
17	Mean=	0.867424					Mean=	0.671679		Mean=	2.433557
18	Std Deviati	12.24988					Std Deviati	5.520199		Std Deviati	33.22661
19	Variance=	150.0595					Variance=	30.4726		Variance=	1104.007
20	Skewness=	55.99756					Skewness=	112.2346		Skewness=	20.99612
21	Kurtosis=	4399.393					Kurtosis=	1.81E+04		Kurtosis=	617.0509
22											
23	**13l**	Input Data		**13h**	Input Data		**14l**	Input Data		**14h**	Input Data
24	Minimum=	0		Minimum=	0		Minimum=	0		Minimum=	0
25	Maximum=	2673		Maximum=	2673		Maximum=	2673		Maximum=	2673
26	Mode=	0.84375		Mode=	0.84375		Mode=	0.84375		Mode=	0.84375
27	Mean=	0.867413		Mean=	0.867413		Mean=	0.867413		Mean=	0.867606
28	Std Deviati	12.24945		Std Deviati	12.24945		Std Deviati	12.24945		Std Deviati	12.2541
29	Variance=	150.0489		Variance=	150.049		Variance=	150.0489		Variance=	150.163
30	Skewness=	55.99461		Skewness=	55.99459		Skewness=	55.99461		Skewness=	55.97452
31	Kurtosis=	4398.47		Kurtosis=	4398.467		Kurtosis=	4398.47		Kurtosis=	4395.568
32											

Table 7-7: Statistical Parameters for PDF of Tritium Releases
for Sensitivity on Second Confinement Barrier Failure Modes

	A	B	C	D	E	F	G	H	I	J	K
33	**15l**	Input Data		**15h**	Input Data		**15h_1**	Input Data		**15h_0.1(17=e-6)**	
34	Minimum=	0		Minimum=	0		Minimum=	0		Minimum=	0
35	Maximum=	2673		Maximum=	2774.25		Maximum=	2774.25		Maximum=	2774.25
36	Mode=	0.84375		Mode=	0.84375		Mode=	0.84375		Mode=	0.84375
37	Mean=	0.848358		Mean=	1.038514		Mean=	2.749248		Mean=	1.038511
38	Std Deviati	11.77142		Std Deviati	15.9078		Std Deviati	35.77483		Std Deviati	15.90769
39	Variance=	138.5662		Variance=	253.058		Variance=	1279.838		Variance=	253.0544
40	Skewness=	58.30007		Skewness=	42.97324		Skewness=	18.96072		Skewness=	42.97332
41	Kurtosis=	4784.505		Kurtosis=	2546.433		Kurtosis=	487.7932		Kurtosis=	2546.461
42											
43	**16l**	Input Data		**16h**	Input Data		**16h_1**	Input Data		**16h_0.1(17=e-6)**	
44	Minimum=	0		Minimum=	0		Minimum=	0		Minimum=	0
45	Maximum=	2673		Maximum=	2774.25		Maximum=	2774.25		Maximum=	2774.25
46	Mode=	0.84375		Mode=	0.84375		Mode=	0.84375		Mode=	0.84375
47	Mean=	0.848358		Mean=	1.038514		Mean=	2.749248		Mean=	1.038511
48	Std Deviati	11.77142		Std Deviati	15.9078		Std Deviati	35.77483		Std Deviati	15.90769
49	Variance=	138.5662		Variance=	253.058		Variance=	1279.838		Variance=	253.0544
50	Skewness=	58.30007		Skewness=	42.97324		Skewness=	18.96072		Skewness=	42.97332
51	Kurtosis=	4784.505		Kurtosis=	2546.433		Kurtosis=	487.7932		Kurtosis=	2546.461
52											
53	**17l**	Input Data		**17h**	Input Data		**18l**	Input Data		**18h**	Input Data
54	Minimum=	0		Minimum=	0		Minimum=	0		Minimum=	0
55	Maximum=	2673		Maximum=	2673		Maximum=	2673		Maximum=	2774.25
56	Mode=	0.84375		Mode=	0.84375		Mode=	0.84375		Mode=	0.84375
57	Mean=	0.867411		Mean=	0.871186		Mean=	0.865583		Mean=	1.054296
58	Std Deviati	12.24935		Std Deviati	12.34212		Std Deviati	12.20408		Std Deviati	16.23077
59	Variance=	150.0465		Variance=	152.3279		Variance=	148.9396		Variance=	263.438
60	Skewness=	55.99479		Skewness=	55.57914		Skewness=	56.19598		Skewness=	42.61175
61	Kurtosis=	4398.535		Kurtosis=	4331.876		Kurtosis=	4430.804		Kurtosis=	2539.035
62											

Table 7-8: Statistical Parameters for PDF of Tritium Releases
for Sensitivity on Second Confinement Barrier Failure Modes (Table 7-7 cont.)

	A	B	C	D	E	F	G	H	I	J	K
63	**19l**	Input Data		**19la_0.01**	Input Data		**20l**	Input Data		**20h**	Input Data
64	Minimum=	0		Minimum=	0		Minimum=	0		Minimum=	0
65	Maximum=	2673		Maximum=	2673		Maximum=	2673		Maximum=	2673
66	Mode=	0.84375		Mode=	0.84375		Mode=	0.84375		Mode=	0.84375
67	Mean=	0.867411		Mean=	0.867411		Mean=	0.867413		Mean=	0.867413
68	Std Deviati	12.24935		Std Deviati	12.24935		Std Deviati	12.24945		Std Deviati	12.24943
69	Variance=	150.0465		Variance=	150.0465		Variance=	150.0489		Variance=	150.0485
70	Skewness=	55.9948		Skewness=	55.99479		Skewness=	55.9946		Skewness=	55.99462
71	Kurtosis=	4398.536		Kurtosis=	4398.535		Kurtosis=	4398.467		Kurtosis=	4398.488
72											
73	**21l**	Input Data									
74	Minimum=	0									
75	Maximum=	2673									
76	Mode=	0.84375									
77	Mean=	0.867412									
78	Std Deviati	12.24944									
79	Variance=	150.0488									
80	Skewness=	55.99466									
81	Kurtosis=	4398.476									
82											

Table 7-9: Statistical Parameters for PDF of Tritium Releases
for Sensitivity on Second Confinement Barrier Failure Modes (Table 7-8 cont.)

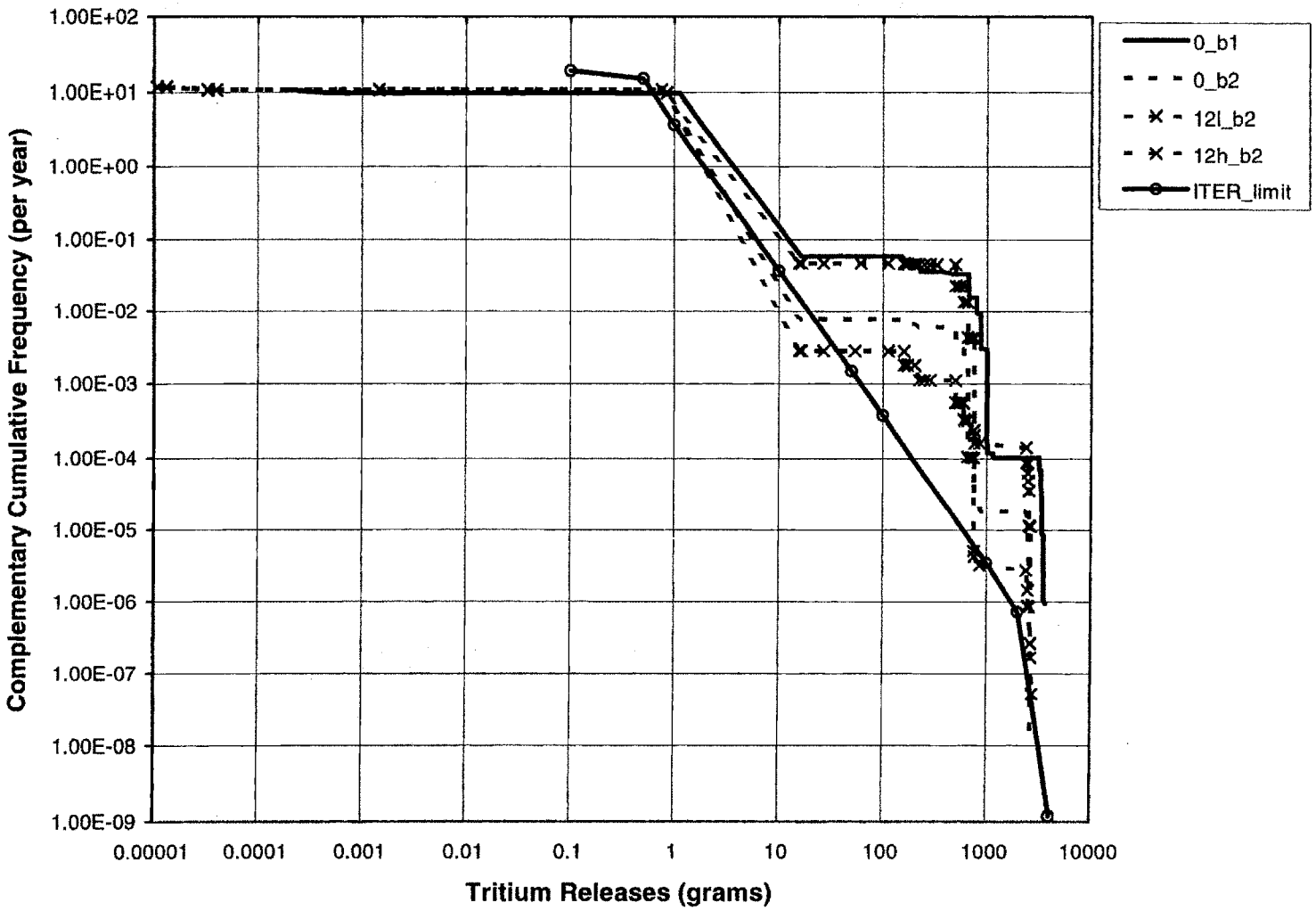

Figure 7-7: Sensitivity of CCF of Tritium Releases to the Probability of Failure of the Cryostat Vessel due to Arcing

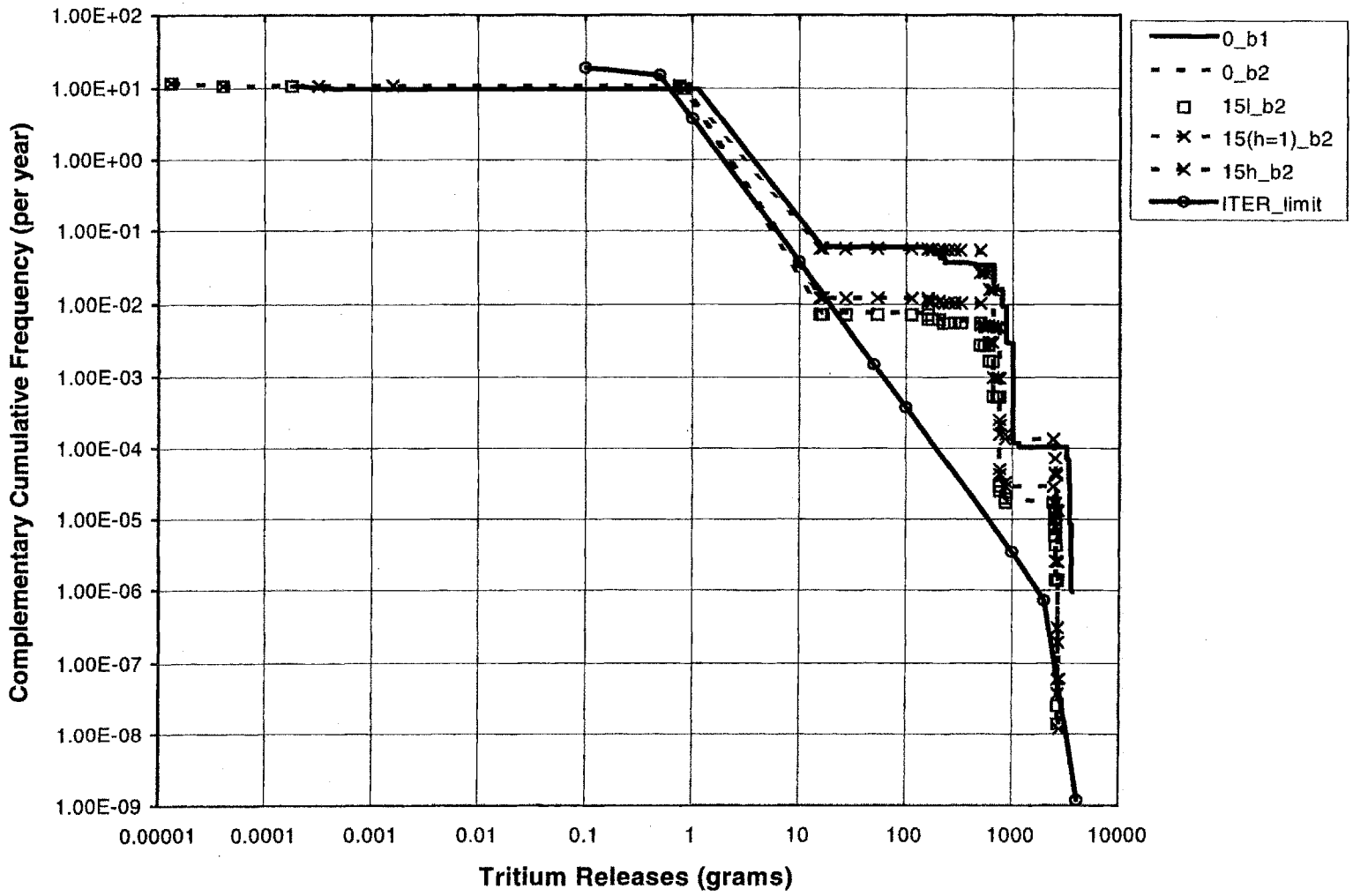

Figure 7-8: Sensitivity of CCF of Tritium Releases to the Probability of Failure of the Cryostat Vessel due to Missile Generation

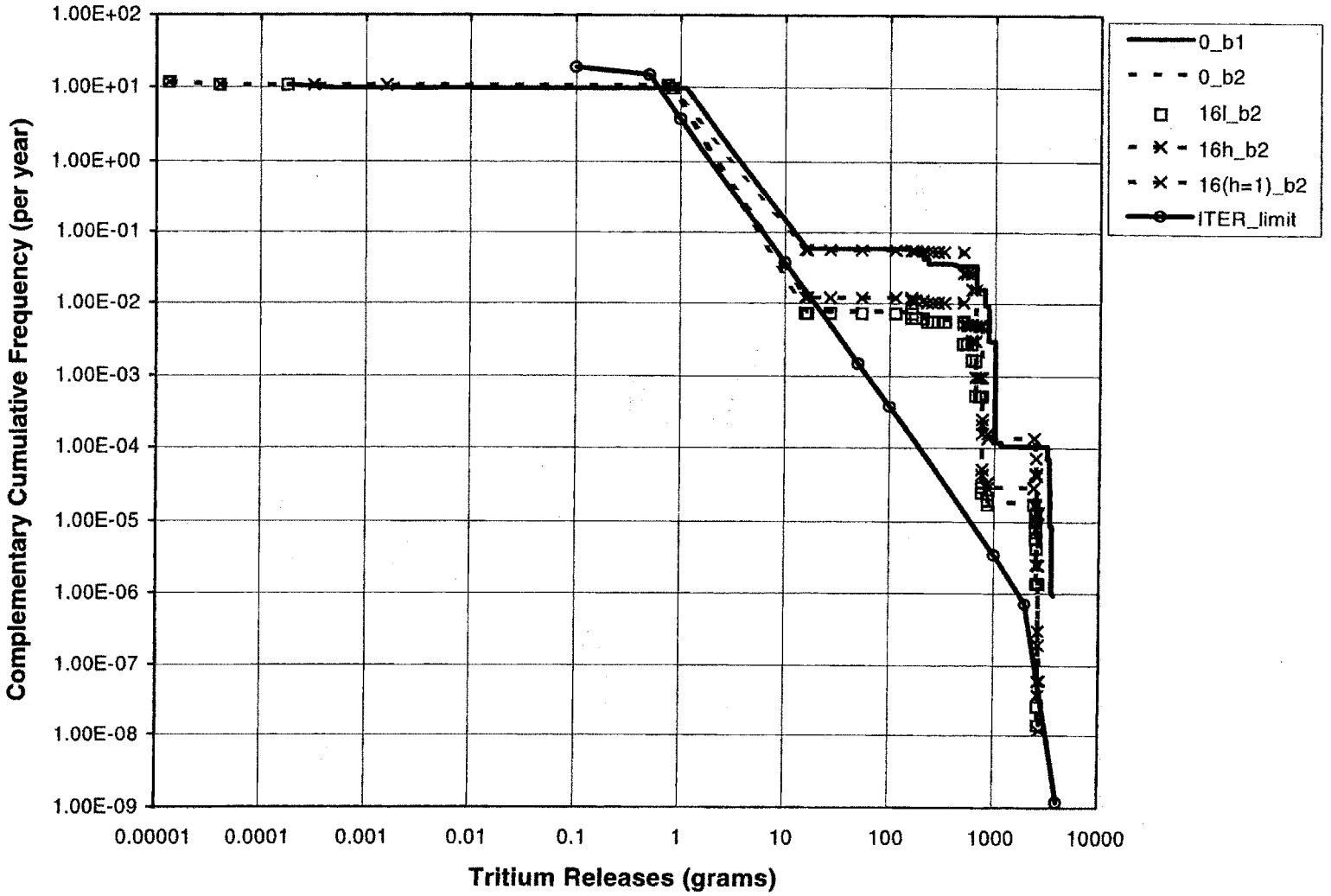

Figure 7-9: Sensitivity of CCF of Tritium Releases to the Probability of Failure of the Cryostat Vessel due to Displaced Coil

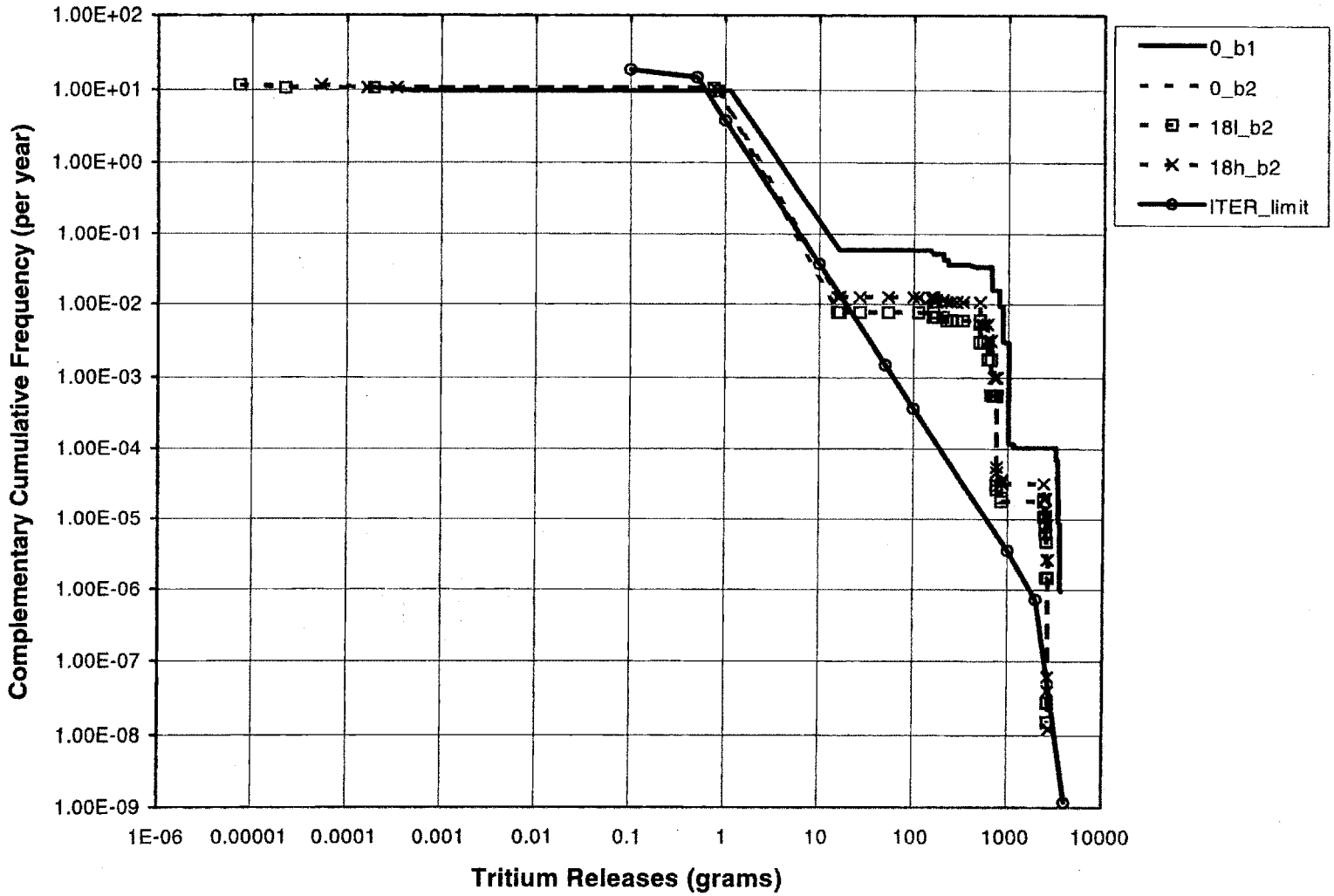

Figure 7-10: Sensitivity of CCF of Tritium Releases to the Probability of Failure of the Cryostat Vessel (without being challenged by off-normal events)

7.3 Sensitivity Analysis for Confinement Barriers Retention Factors

The judgmental reference values used in this study for the retention factors of the vacuum vessel and the cryostat vessel are 0.1 and 0.25 respectively. Sensitivity analysis is performed for the low and high values of 0 and 0.9 for each of the retention factors.

Let us first analyze the vacuum vessel retention factor. For accident sequences with frequencies higher than 10^{-6}/year, a reduction of the retention factor to zero (meaning that all radioactive releases escape the first confinement barrier if its integrity is lost) will lead to an increase of tritium releases by hundreds of grams; for instance, the maximum release increases from 3700 to 4110 grams. This is a significant amount of tritium, although the change of CCF curve in Figure 7-11 does not look impressive. If both the first and the second confinement barriers failed, a retention factor of zero for the vacuum vessel causes the maximum tritium release from the second barrier to increase from 2670 to 2970 grams.

When the VV retention factor is equal to 0.9, the maximum release from the first confinement barrier is decreased to 411 grams, and from the second confinement barrier if both barriers fail to only 297 grams (Figure 7-12). The CCF curve for the second confinement barrier is still not entirely under the ITER limit, but it is much closer to satisfying the design requirements. However, a retention factor of 0.9 might not be a realistic value, or might increase the cost of designing and constructing such a vessel by an unreasonable amount of money.

The cryostat vessel retention factor only affects the second barrier model. Decreasing it from 0.25 to 0 leads to an increase of tritium releases from the second barrier of about 900 grams (from 2673 to 3564 grams). A value of 0.9 for the CV retention factor leads to a maximum release of 356 grams, a very important reduction in radioactive releases. However, the maximum release is higher than in the case of a VV retention factor increase to 0.9 (356 versus 297 grams). Also, there are more points corresponding to possible consequences above the ITER limit line in Figure 7-13 than in Figure 7-12. The conclusion might be that the design effort of increasing the retention factor for the VV rather than for the CV is more justified. Another argument to sustain that conclusion is that the vacuum vessel is smaller than the cryostat vessel and contains a higher vacuum during normal operation, so the vacuum vessel is already designed for more severe conditions that the cryostat vessel.

We also looked at the effect of increasing both retention factors to 0.9 simultaneously, to observe if the second confinement barrier CCF curve is below the ITER limit in that limit case. Figure 7-14 shows that this is not the case, although the number of points above the ITER limit is significantly decreased. However, the maximum possible release is 222 grams, only 70 grams lower (25%) than the case when only the VV retention factor is 0.9, and the CV retention factor is 0.25.

In conclusion, the vacuum vessel and the cryostat vessel retention factors highly influence the complementary cumulative frequency of tritium releases. More analysis should be performed to observe if their increase combined with the decrease of the failure probability of various confinement

failure modes can bring the second barrier CCF curve under the ITER recommended limit. In that case, a third strong confinement barrier would not be required.

	A	B	C	D	E	F	G	H	I	J	K
1	**0_b1**	Input Data		**0_b2**	Input Data						
2	Minimum=	0		Minimum=	0						
3	Maximum=	3699		Maximum=	2673						
4	Mode=	1.125		Mode=	0.84375						
5	Mean=	2.878079		Mean=	0.867581						
6	Std Deviati	38.87411		Std Deviati	12.25223						
7	Variance=	1511.197		Variance=	150.1171						
8	Skewness=	22.95998		Skewness=	55.96731						
9	Kurtosis=	766.1062		Kurtosis=	4394.65						
10											
11	**22l_b1**	Input Data		**22l_b2**	Input Data		**22h_b1**	Input Data		**22h_b2**	Input Data
12	Minimum=	0		Minimum=	0		Minimum=	0		Minimum=	0
13	Maximum=	4110		Maximum=	2970		Maximum=	411		Maximum=	297
14	Mode=	0		Mode=	0		Mode=	0		Mode=	0
15	Mean=	6.577159		Mean=	0.745481		Mean=	4.832938		Mean=	0.186642
16	Std Deviati	59.46365		Std Deviati	14.75392		Std Deviati	25.92403		Std Deviati	3.85347
17	Variance=	3535.926		Variance=	217.6782		Variance=	672.0551		Variance=	14.84923
18	Skewness=	13.95785		Skewness=	42.73373		Skewness=	7.148311		Skewness=	27.455
19	Kurtosis=	320.0764		Kurtosis=	2785.078		Kurtosis=	67.69108		Kurtosis=	954.1195
20											
21	**23l_b2**	Input Data		**23h_b2**	Input Data		**22a23h_b2**				
22	Minimum=	0		Minimum=	0		Minimum=	0			
23	Maximum=	3564		Maximum=	356.4		Maximum=	222			
24	Mode=	0		Mode=	0		Mode=	0			
25	Mean=	0.874511		Mean=	0.180924		Mean=	0.032581			
26	Std Deviati	18.42803		Std Deviati	3.27383		Std Deviati	1.936423			
27	Variance=	339.5924		Variance=	10.71796		Variance=	3.749735			
28	Skewness=	40.42368		Skewness=	29.36746		Skewness=	94.67389			
29	Kurtosis=	2477.531		Kurtosis=	1094.365		Kurtosis=	9185.987			
30											

Table 7-10: Statistical Parameters for PDF of Tritium Releases
for Sensitivity on Confinement Barriers Retention Factors

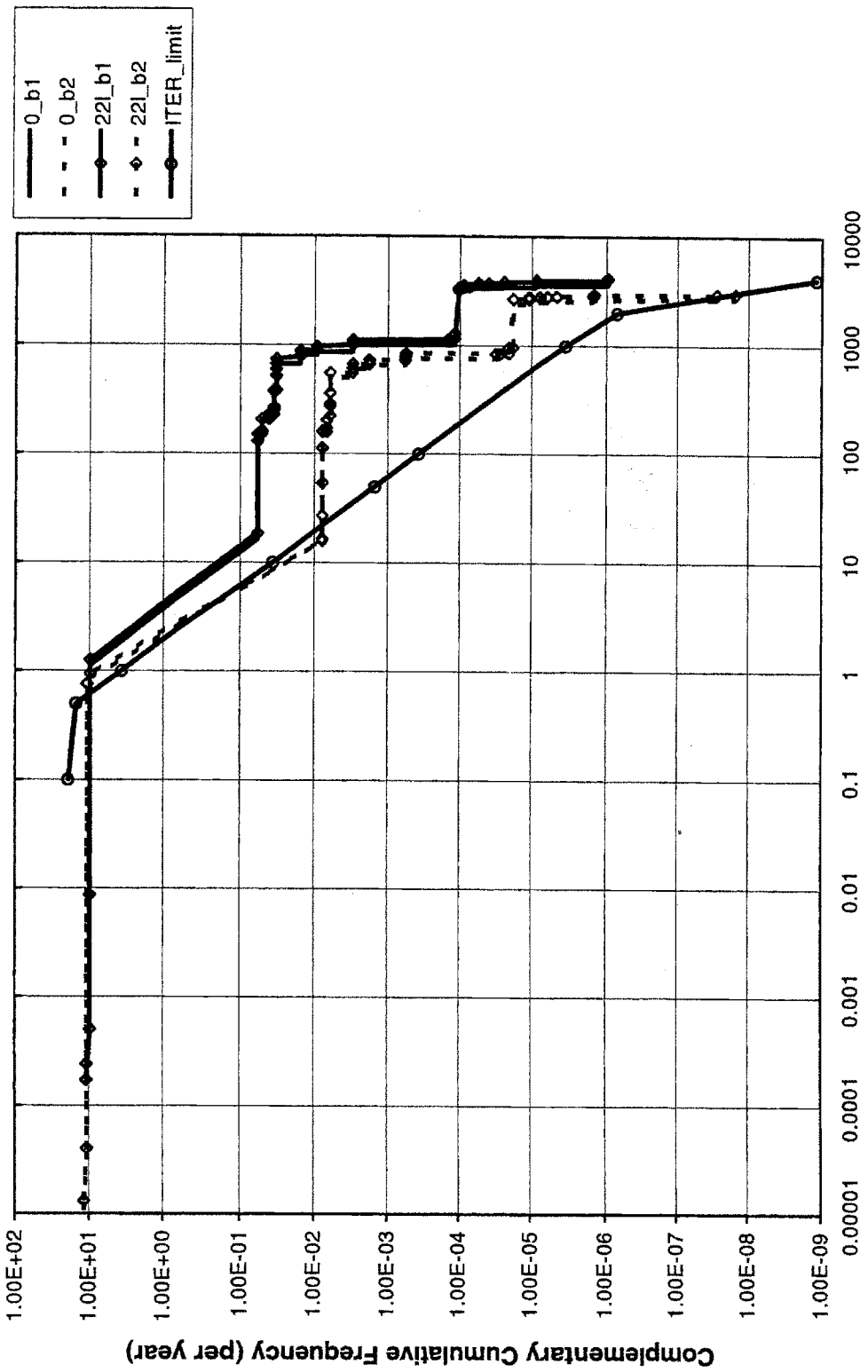

Figure 7-11: Sensitivity of CCF of Tritium Releases to the Vacuum Vessel Retention Factor (low limit)

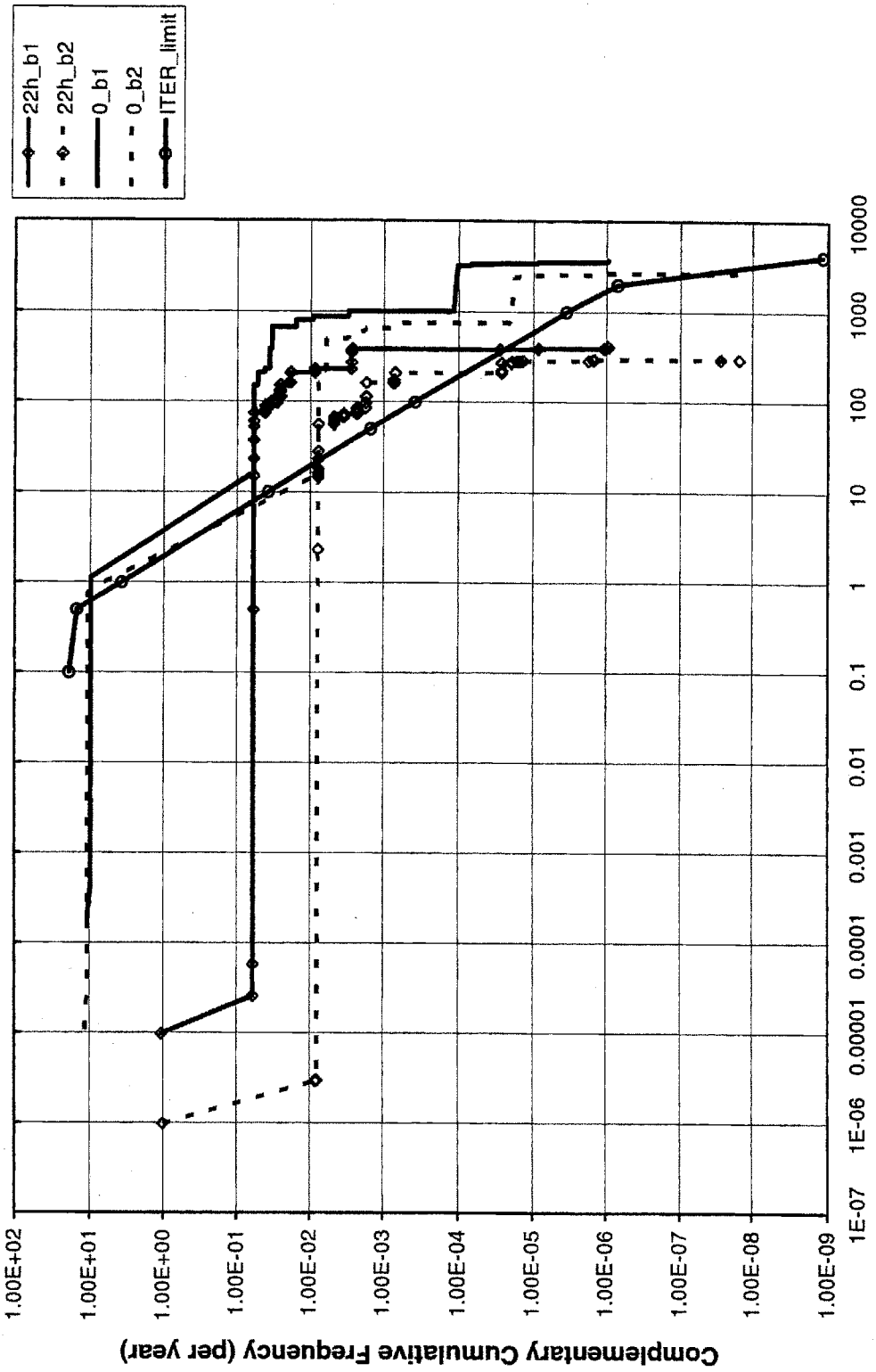

Figure 7-12: Sensitivity of CCF of Tritium Releases to the Vacuum Vessel Retention Factor (high limit)

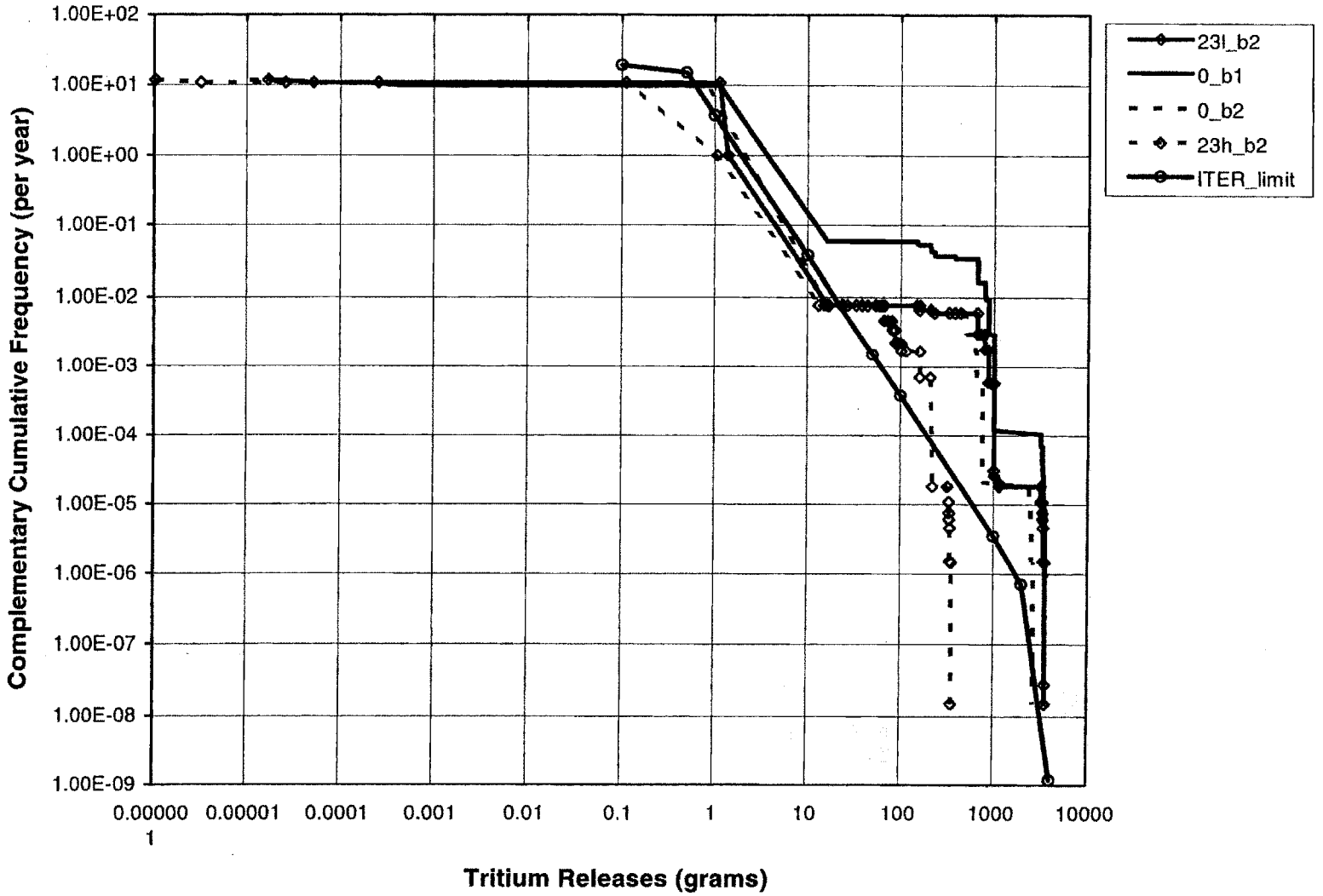

Figure 7-13: Sensitivity of CCF of Tritium Releases to the Cryostat Vessel Retention Factors

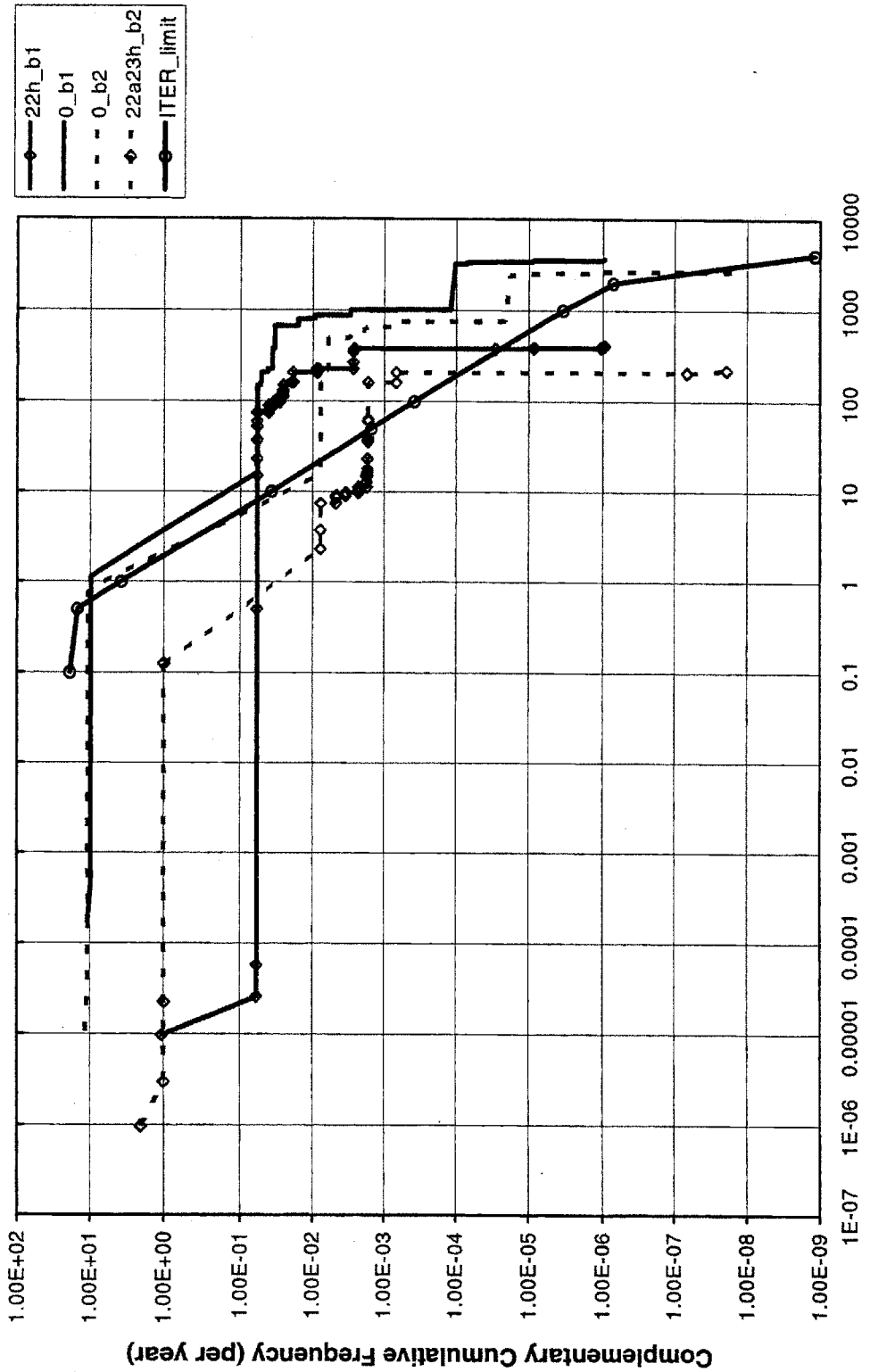

Figure 7-14: Sensitivity of CCF of Tritium Releases to Vacuum Vessel and Cryostat Vessel Retention Factors

7.4 Analysis of the Complementary Cumulative Distribution Function of the First Confinement Barrier

As previous sections of this chapter show, the CCF for the first confinement barrier practically depends on three parameters only: the failure probabilities of the vacuum vessel due to arcing (number 7) and displaced magnet coil (number 9), and the vacuum vessel retention factor (number 22). The CCF of tritium releases is actually derived from the frequency distribution of tritium releases calculated by using the probabilistic model developed in the previous chapters. Therefore, the frequency distribution is a function of the above mentioned parameters: p7, p9, and rf22. So far we studied the sensitivity of the CCF of releases when changing each of these parameters to a low and a high value. It might be interesting to study the sensitivity to some intermediary values. However, running the DPL accident sequences models and the EXCEL model that integrates the results from all the accident sequences into a CCF curve is very time expensive. Thus, we thought about using response surface techniques [7-1, 7-2] to represent the consequences as a function of the input parameters p7, p9, and rf22.

A probability density function can be fitted to the overall frequency distribution function of releases for ITER. This can be done using the BestFit package, and the data is the frequency distribution of radioactive releases as obtained in EXCEL after combining all the initiating event models together. In BestFit, this type of data given in the form of (x, f) pairs is called density data. The frequency weight f specifies the relative height of the frequency curve at each x value of tritium releases. When running a BestFit calculation on density data, the program sorts the data, gathers statistics and normalizes the data to create a continuos probability density function (PDF) (i.e., the area under the curve is equal to 1). Therefore, the fitted density function corresponds to the normalized continuos PDF rather than to the discrete frequency distribution, and is characterized by a number of parameters (usually between one and three parameters) that define the form of the function. The parameters of the fitted distribution depend in turn on the uncertain parameters p7, p9, and rf22. Sensitivity analysis can then be performed on the parameters of the fitted distribution for the whole range of values of p7, p9, and rf22.

After previewing with RiskView the form of the distributions available in BestFit, we concluded that gamma distribution fits the input data most closely although not perfectly, as shown in Figures 7-15 and 7-16. However, that is not relevant when performing sensitivity analysis on the parameters.

The gamma density function has the following form:

$$f(x) = \frac{b^a \cdot x^{a-1} \cdot e^{-\frac{x}{b}}}{\Gamma(a)} \qquad (7\text{-}2)$$

where $\Gamma(a)$ is the gamma function. The parameters are a>0 and b>0, and the domain is x≥0, where x are the tritium releases in the present case. Each parameter a and b are functions on p7, p9, and rf22, and we use response surface method to define a and b as second order polynomial functions of those three parameters.

The DPL model that calculates the frequency distribution of tritium releases using the gamma distribution with parameters a and b given by response surface functions of p7, p9, and rf22 is given in Figures 7-17 and 7-18. The values for p7, p9 and rf22 are input in DPL and exported to an EXCEL file that contains the response surface functions for a(p7,p9,rf22) and b(p7,p9,rf22); thus, a and b are import variables from EXCEL, and the frequency distribution function is then calculated in DPL as gamma(a,b). Sensitivity analysis can then be performed in DPL on any of the parameters p7, p9, and rf22.

The second-order response surface for the approximation of a given consequence, $f(\bar{z})$, as a function of parameters $z_1, \ldots, z_n$, has the following functional form [7-1]:

$$f(\bar{z}) = A + \sum_{j=1}^{n}\left\{\left[B_j + C_j(z_j - z_{j0}) + \sum_{k=j+1}^{n} D_{jk}(z_k - z_{k0})\right](z_j - z_{j0})\right\} \tag{7-3}$$

To determine the unknown coefficients, a set of 1+2n+[n(n-1)/2] points, $\bar{z}$, is selected at which the approximation, $f(\bar{z})$, is made equal to the actual values of $f(\bar{z})$ calculated by the DPL-EXCEL model. The coefficients are basically calculated using the following set of equations:

$$A = f_0, \tag{7-4}$$
$$B_j = R_{j1}(z_{j0} - z_{j2}) + R_{j2}(z_{j0} - z_{j1}),$$
$$C_j = R_{j1} + R_{j2},$$

where

$$R_{j1} = \frac{f_1(j) - f_0}{(z_{j1} - z_{j0})(z_{j1} - z_{j2})},$$

$$R_{j2} = \frac{f_2(j) - f_0}{(z_{j2} - z_{j0})(z_{j2} - z_{j1})},$$

$$D_{jk} = \frac{f_0 + f_{11}(j,k) - f_1(j) - f_1(k)}{(z_{j1} - z_{j0})(z_{k1} - z_{k0})},$$

for all $j = 1,\ldots,n$ and selected pairs j, k.

where $\bar{z}_0 = (z_{10},\ldots,z_{n0})$ is the reference point, z_{j1} and z_{j2} are two other selected values of z_j for all $j = 1,\ldots,n$, and $f_0 = f(\bar{z}_0)$, $f_1(j) = f(z_j = z_{j1})$, $f_2(j) = f(z_j = z_{j2})$, $f_{11}(j,k) = f(z_j = z_{j1}, z_k = z_{k1})$.

The MATHCAD file that calculates the response surface coefficients for a(p7,p9,rf22) and b(p7,p9,rf22) is in Appendix G. Parameters a and b have to be positive, and they also should make

physical sense. The mean of the gamma distribution is equal to (ab), and the variance is (ab^2). As the failure probabilities p7 or p9 increase, the mean value of the consequences should decrease; also, as the VV retention factor increases, the mean value of the consequences should decrease. The resulting a and b functions of those three parameters should be checked against all these conditions, so that the DPL model in Figure 7-17 does not return error messages when sensitivity analysis on p7, p9, and rf22 is performed. Our analysis shows the following results:

- a>0 for any p7, and a is approximately constant (at 0.0055) for p7<0.01 (the reference value);
- a is approximately constant (at 0.012) for p9<0.02, but is negative for 0.102<p9<0.424; moreover, a increases fast with p9 for p9>0.424, which is the region of interest to us;
- a decreases with rf22 for 0<rf22<0.2; for the rest of the rf22 value (rf22>0.2), the a function as derived here cannot be used because a is negative for 0.2<rf22<0.8, and is an increasing function of rf22 for rf22>0.8, which is not physically correct;
- b is positive for any p7, p9, or rf22 when varied individually; also, b is an increasing function of p7 for p7<0.27, an increasing function of p9 for ant p9, and a decreasing function of rf22 for any rf22.

While considering these restrictions, sensitivity analysis was performed with DPL and the results are presented in Figures 7-19 to 7-21. For p7 in the range 0 to 0.7, the expected value (EV) of tritium releases does not vary much, while from 0.7 to 0.9 the EV increases by a factor of 3. The EV is more sensitive to p9, since in the range 0.43 to 1, the EV increases by a factor of magnitude. For the retention factor between 0 and 0.2, the EV decreases by an order of magnitude.

Performing this type of sensitivity analysis might be of help in finding inconsistencies in the accident sequences models. More insight could be gained if a more conservative distribution fit can be found. Also, the response surface method has various ways of calculating the coefficients. The design we used has two weaknesses: a single response surface is used over the entire space, and the interaction term is determined in one quadrant only. A second scheme provides additional points, so that separate response surfaces are generated for different ranges of the uncertain variables.[7-1]

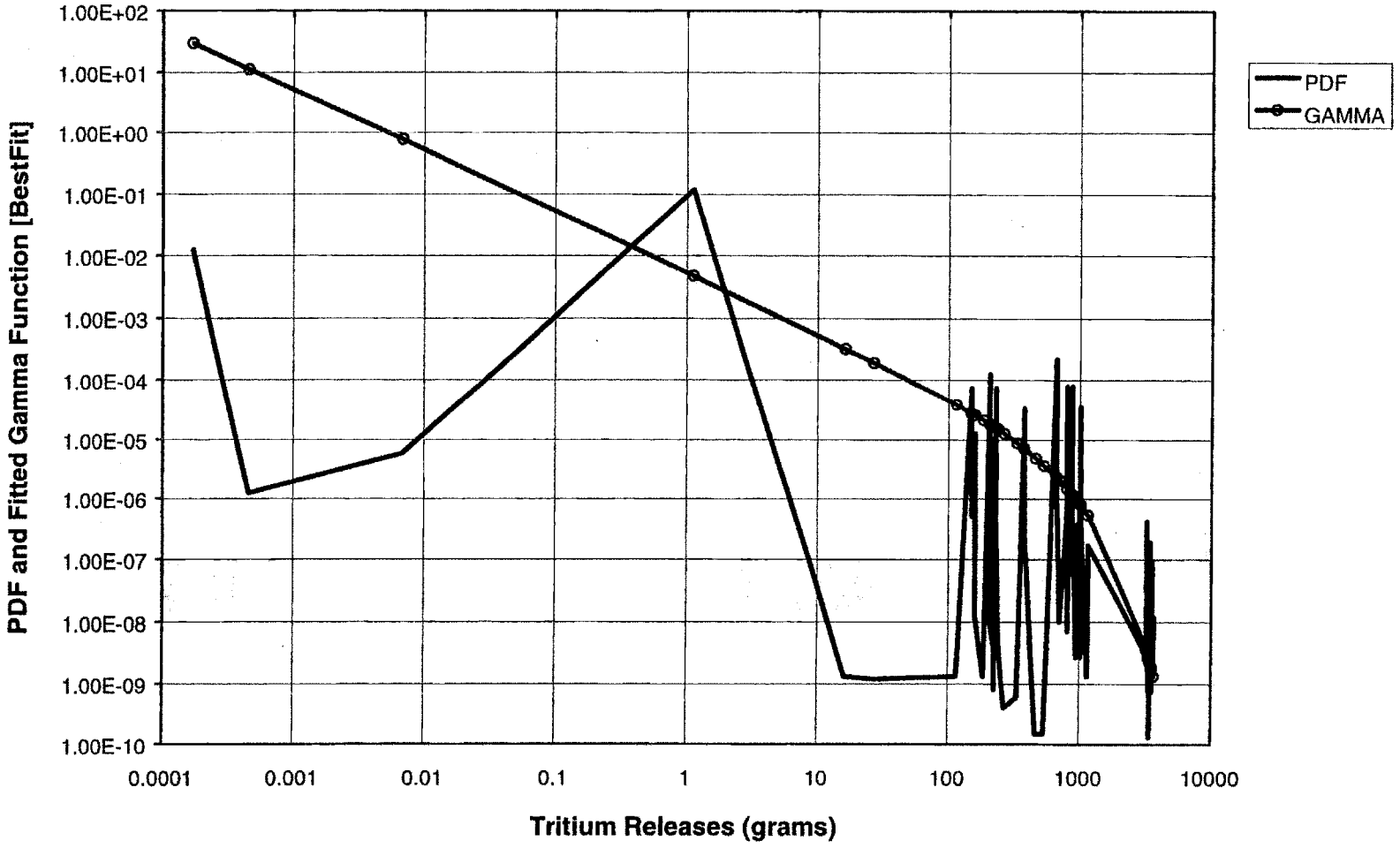

Figure 7-15: Fitted Gamma Distribution to the Frequency Distribution of Tritium Releases

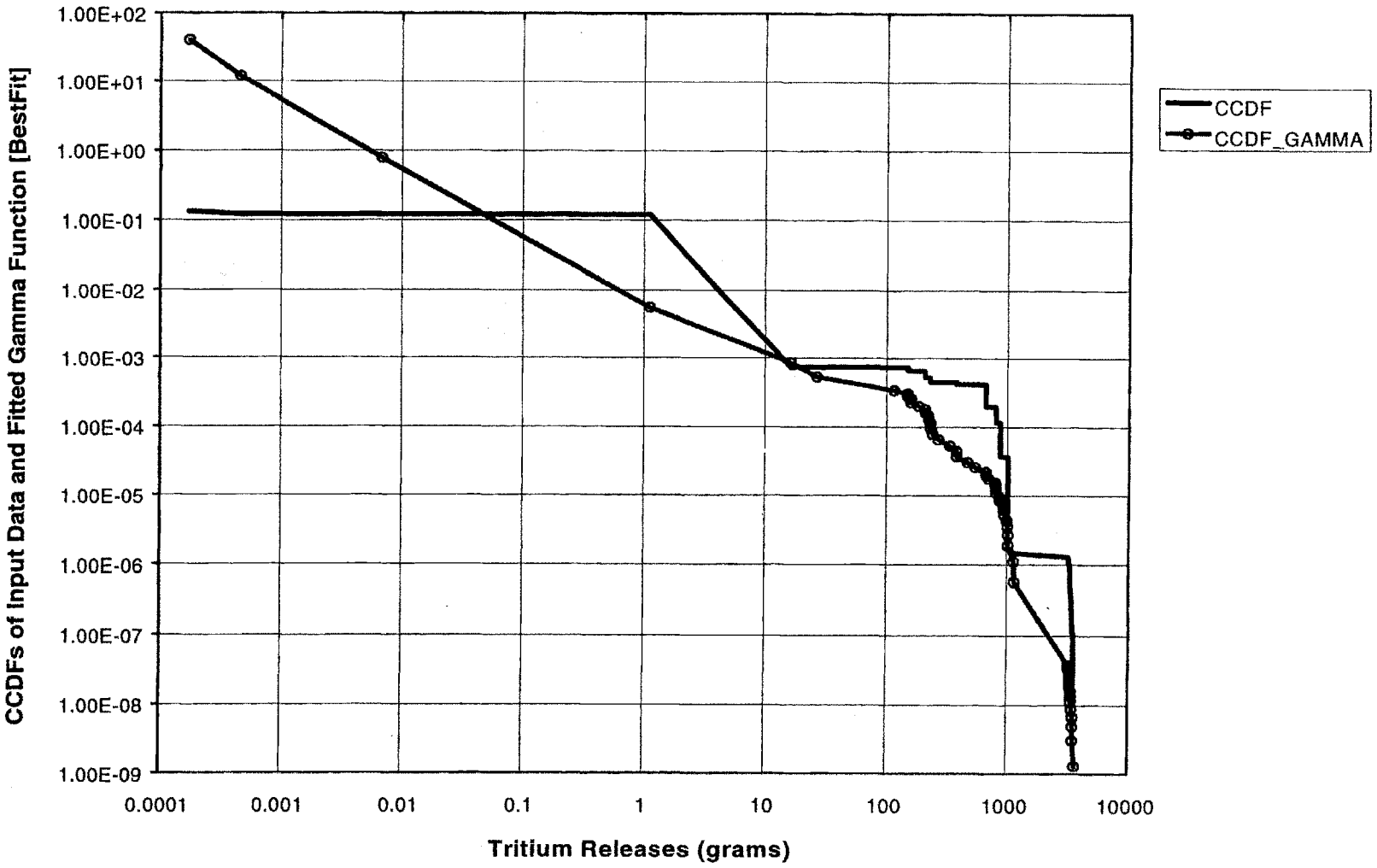

Figure 7-16: Fitted Gamma Complementary Cumulative Distribution to the Complementary Cumulative Frequency Distribution of Tritium Releases

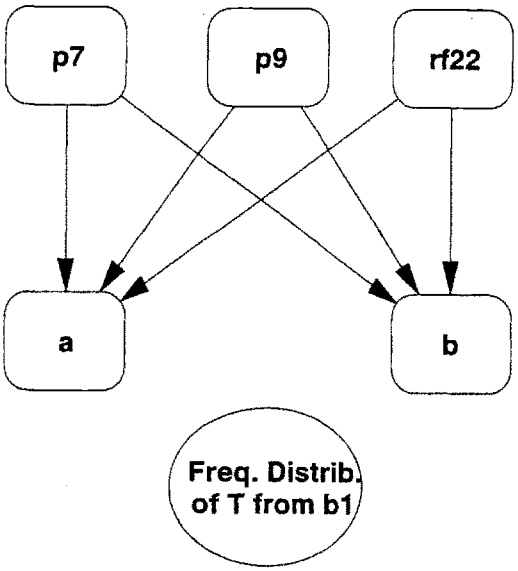

Figure 7-17: DPL Model for Frequency Distribution of Tritium Releases using Gamma Distribution

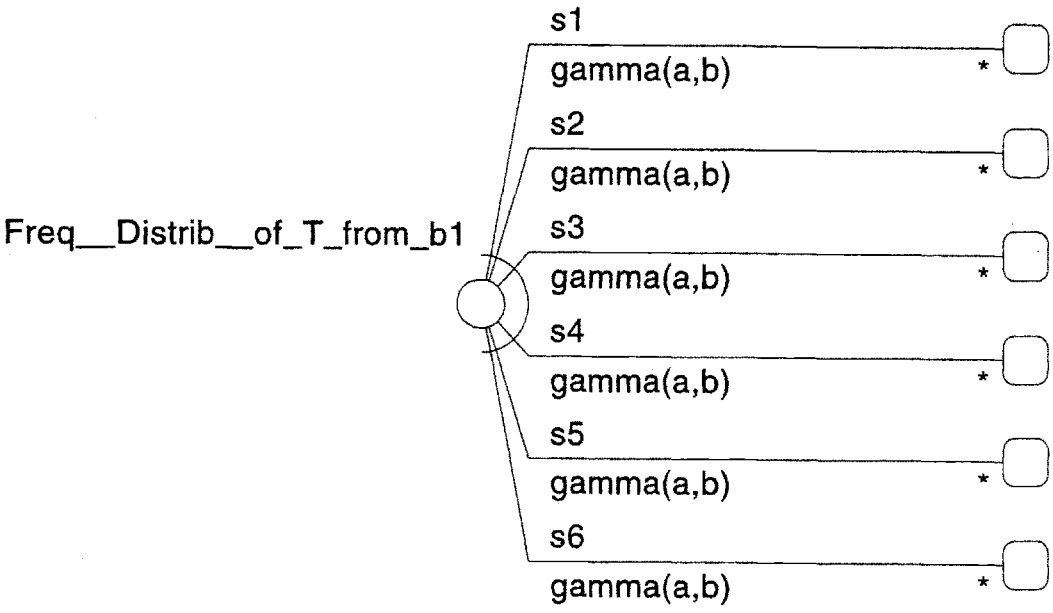

Figure 7-18: DPL Data Definition of the Frequency Distribution of Tritium Releases Chance Node of DPL Model in Figure 7-17

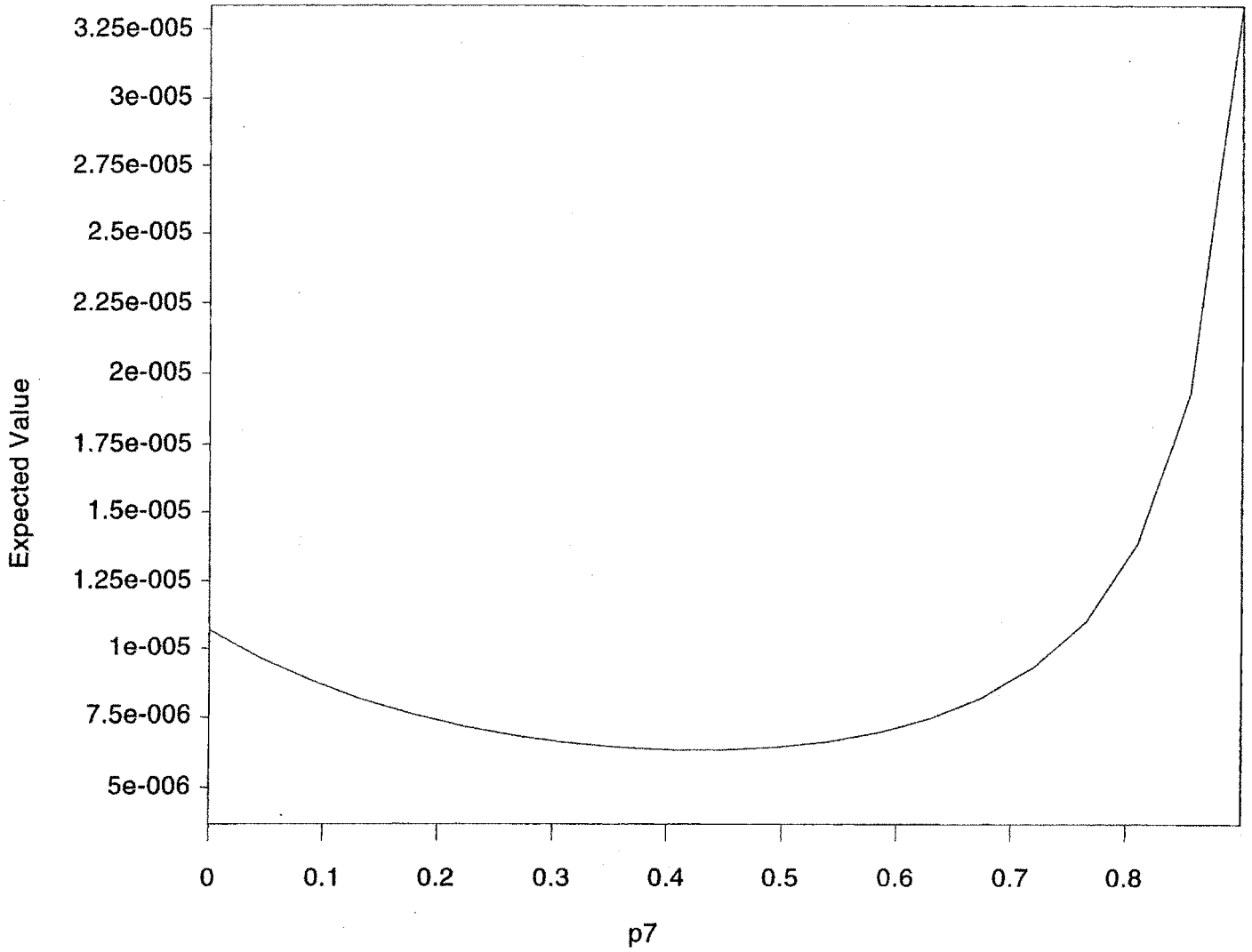

Figure 7-19: Sensitivity of Expected Value of Tritium Releases to p7

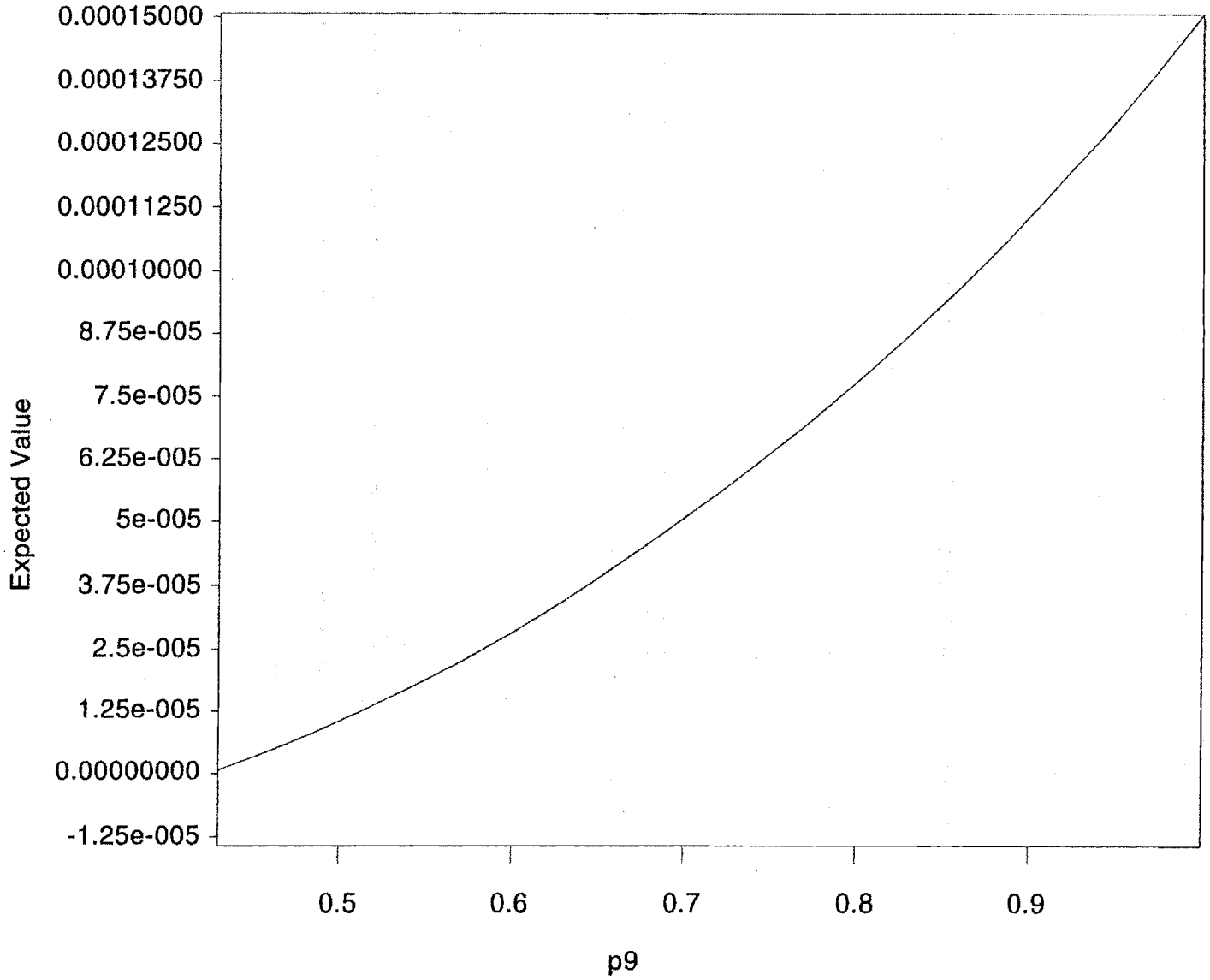

Figure 7-20: Sensitivity of Expected Value of Tritium Releases to p9

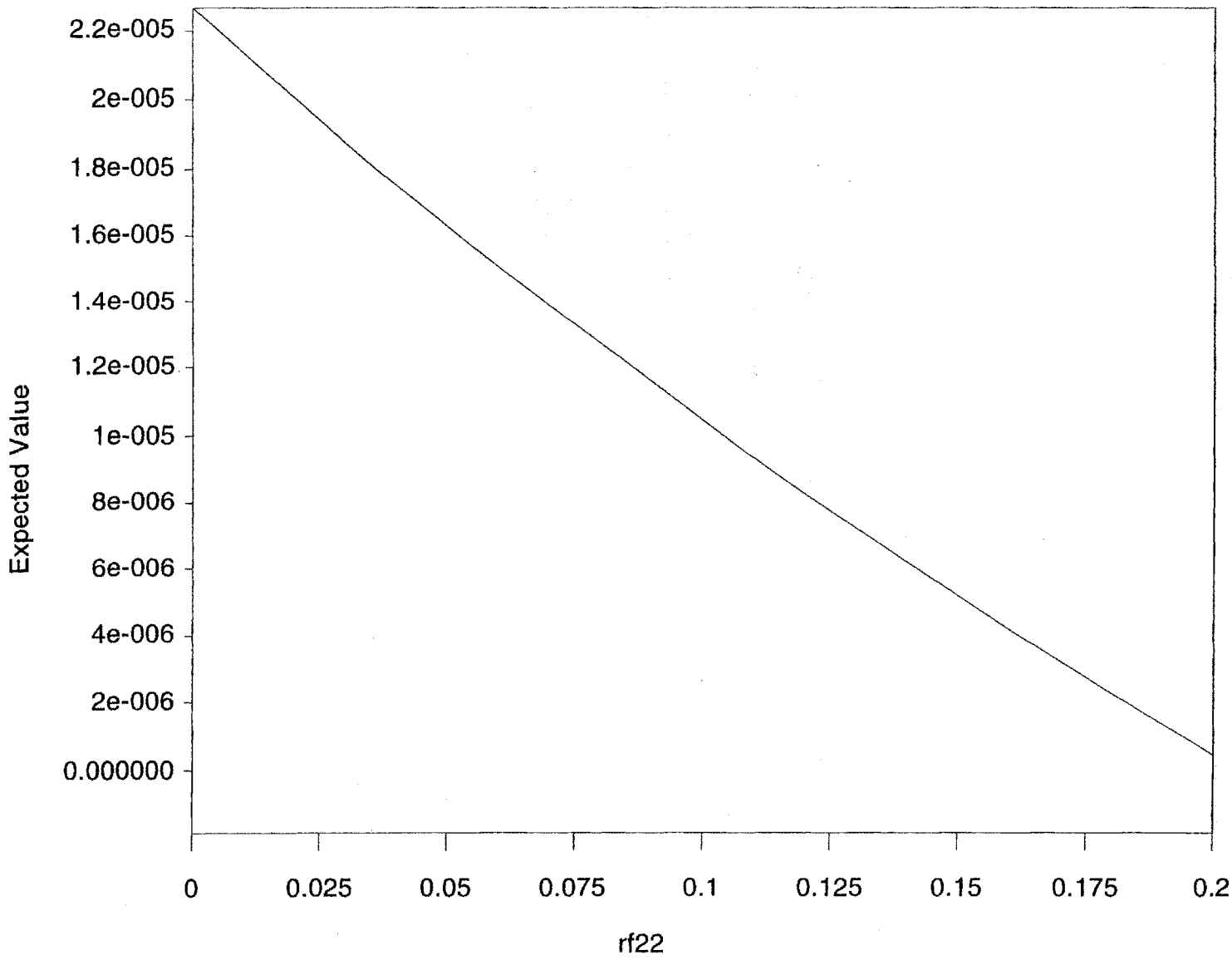

Figure 7-21: Sensitivity of Expected Value of Tritium Releases to rf22

8. Decision Model for the Type of Tokamak Building of ITER

The methodology developed in the previous chapters provides the means for deciding if a third confinement barrier is required to comply with the regulatory requirements. The results show that a third confinement barrier should be used to lower the releases of radioactive inventories to the environment under the desired limit. The tokamak building should play that role, but different designs could be used. The present chapter contains a decision model to help decide what type of tokamak building is the most appropriate from the designer's point of view. The model considers not only safety considerations, but also other important attributes such as construction cost, project completion time, technical feasibility and public attitude.

The ITER Joint Central Team is currently considering design changes for the tokamak building, but due to the time frame of our project, we will not include them in the present work. The design as described in the DDD 6.2 [8-16] is the first possible choice considered; it includes a filter/vent system that releases radioactive inventories through the stack to the atmosphere, and it does not withstand overpressures. The other option is to basically keep the same design for the tokamak pit, but to include a CANDU-type vacuum building that accommodates overpressure and radioactive inventories containment in case of accident. Other options, as they become of interest to the designer, can be easily included into the model.

The decision problem is inherently difficult because complex and developing technologies, as well as domestic and international economics and safety cultures are involved and highly intertwined. More specifically, the following characteristics of the problem complicate its analysis:

- large uncertainties: technological, economical, and political, partially due to the very long time into the future for which the decisions are relevant;
- multiple objectives: construction cost, technical performance (during sever accidents and external events), constructibility, construction schedule, design codes and regulatory concerns, safety and environmental impact, public fear and anxiety towards a new nuclear technology;
- multiple decision makers: fusion scientific community, utilities, general public, and governments.

The approach taken here is to construct a probabilistic model for the decision problem, construct a multi-attribute utility function to describe the stakeholder's preferences and conduct extensive sensitivity analysis with respect to the data that is most uncertain or subjective. The main goal of the analysis is to identify parameters, such as those related to costs, conditional probability distributions of the uncertain events, and preference structures of the decision makers that significantly affect the optimal strategies. The results will allow us to identify some key parameters that require a better assessment, or parameters to which the optimal strategy is insensitive.

Due to the complexity of the problem, we restricted the analysis to only one stakeholder group: the designers group. The main objective of the designer is to maximize the chance that the project is accepted by the other stakeholders and realized in practice. We assume here, for simplicity of the model, that the designer has to decide between two main options: the first is the current ITER tokamak building design as described in the Design Description Document [8-16]; the second is a CANDU type containment, as it was first proposed by Steven Piet in reference [1-1]. Because of the Canadian experience with tritium, the CANDU containment deserves some special attention among all the other types of fission reactor containments. The possibility of using a CANDU-style "vacuum building" for ITER has been discussed to accommodate accident overpressures, in lieu of a filter/vent system. The vacuum building for the existing CANDU power plants has a normal pressure of about 7 kPa, and it provides additional volume at low pressure for blowdown of pressurized water during LOCAs while keeping the pressure sub-atmospheric.

Chapter 2 described the current design for the ITER tokamak building, as well as the tritium confinement strategy. Table 2-9 presents the TB compartments parameters. The tokamak pit is a right circular cylinder, and the cryostat and tokamak are located in the center of the pit. The pit also contains all the components which must be in close proximity to the cryostat, such as diagnostics, plasma heating, plasma fueling, remote maintenance equipment, and a large number of penetrations in the cryostat. The upper part of the Tokamak Hall consists of a crane hall. The pit and the crane hall are separated by a floor made of movable sections. We will consider that only the tokamak pit is to be built as a CANDU containment in case that decision policy is preferred.

Table 8-1 presents the characteristics of the reactor buildings and vacuum buildings of the CANDU reactors in operation in Canada. The largest CANDU vacuum building is Darlington A as shown in Table 8-1. The ITER tokamak pit alone has a volume of 521,800 m^3, which is much bigger than the reactor building and vacuum building of Darlington taken together. The size of a vacuum building for ITER depends on details of LOCAs and subsequent pressurization within the ITER confinement.

The tokamak pit contains tritium bearing equipment, and therefore, it is provided with a separate ventilation system at negative pressure to the rest of the building. The HVAC system vents through the stack directly to the atmosphere. Reference [8-16] specifies the following pressure values :

- during operation, in the tokamak pit, outside the bioshield: -2 cm H_2O[1] (equal to 101.1 kPa);
- during operation, in the tokamak pit, inside the bioshield: -3 cm H_2O (equal to 101 kPa);
- during major maintenance, in the tokamak pit: atmospheric pressure.

A comparison of the characteristics of the ITER tokamak pit as given in [8-16], and the tokamak pit of a CANDU type is synthesized in Table 8-2, along with the characteristics of the Darlington CANDU containment. We assume that the volume of the tokamak pit is already minimized

[1] 1 atm = 101.3 kPa = 1033.2 cm H_2O

to provide enough room for all the equipment, so it would stay the same for any type of containment building being chosen. Although not clearly stated in DDD 6.2 [8-16], the current design pressure is the atmospheric pressure, since the pit is not designed to resist overpressures from LOCA accidents. Knief [8-17] gives a design pressure for a CANDU PHWR 600 MWe of 130 kPa. The ITER cryostat vessel includes a free volume of 18,600 m^3 with vacuum during normal operation which can accommodate some of the overpressure in case of LOCA. Thus, it is probably desirable to keep the design pressure of the tokamak pit of CANDU type at the atmospheric level, so that the cost does not increase considerably. The normal operation pressure for the current tokamak pit is 101 kPa, while for the Darlington CANDU building is 96 kPa.

Table 8-1: CANDU Containment Parameters [8-8]

Station	Net Output (MWe)	Containment Reactor Building	Volumes (m^3) Vacuum Building	Reactor Building Design Pressure (kPa)
Pickering A	4 x 520	51,000 each	82,000 serves all	41
Pickering B	4 x 520	51,000 each	8 units	41
Bruce A	4 x 750	92,500 shared (4 vaults + ducts)	62,000	69
Bruce B	4 x 850	95,000 shared	62,000	83
Darlington A	4 x 880	140,000 shared	95,000	96

Table 8-2: Comparison of Tokamak Pit DDD versus Tokamak Pit CANDU Type Containment

	Tokamak Pit DDD	**Tokamak Pit CANDU**	**Darlington CANDU**
Filter/Vent System	yes	none	none
Vent to	Stack to atmosphere	Vacuum Building	Vacuum Building
Vacuum Building	none	yes	yes
Tokamak Pit Total Volume (m^3)	521,800	521,800	140,000
Tokamak Pit Free Volume (m^3)	85,000	85,000	NA
Cryostat Vessel Volume (m^3)	31,400	31,400	none
Cryostat Vessel Free Volume (m^3)	18,600	18,600	none
Vacuum Building Volume (m^3)	0	(*1)	95,000
Primary Coolant Volume (m^3)	2593	2593	1408
Tokamak Pit Design Pressure (kPa)	101.3	101.3 (*2)	130
Tokamak Pit Normal Operation Pressure (kPa)	101	101 (*3)	96
Vacuum Building Normal Operation Pressure (kPa)	none	> 7 kPa (*4)	7 kPa
Primary Coolant Pressure (MPa)	2 - 4 (*5)	2 - 4	10

(*1) The required volume of the vacuum building should be calculated considering the possible LOCA events and the fact that the cryostat vessel already has a 18,600 m^3 of vacuum to suppress the overpressure.

(*2) The tokamak design pit pressure could be kept at the atmospheric level, and the overpressure released to the vacuum building. The Joint Central Team currently considers changing the design of the tokamak building to a strong barrier designed for overpressures of 3.5 to 5 psi (design pressure of 125.5 to 135.8 kPa). The new idea under exploration is to contain and condense steam releases, not to filter and vent them.[4-13]

(*3) The pit normal operation should be left at the current level so that no additional pumping power is required.

(*4) The required vacuum pressure in the vacuum building should be calculated along with its volume according to the possible LOCA accidents for ITER.

(*5) The primary heat transfer systems are under different pressures in the range given as follows: the first wall/shield blanket - 3 MPa, the divertor - 4 MPa, the vacuum vessel - 2 MPa.

8.1 Method of Solution for the Decision Problem

The interested parties in this decision are identified. They include all individuals and groups which may have an impact on deciding the TB safety role or which may be affected by it in some way.

The ITER is a joint project of the United States of America, the Russian Federation, Japan, and the European Community (which includes Canada) developed under the auspices of the International Agency for Atomic Energy (IAEA). In deciding upon the design of the TB, the interested parties would be as follows:

- the regulatory commission of the country of site,
- the owner of the site,
- environmental and public interest groups,
- electric utilities and tax payers,
- IAEA,
- designer groups from the participating countries.

As mentioned before, for simplicity, we restricted the analysis to only one stakeholder group: the designers. When choosing the proper design strategy, the designer should consider several issues called "attributes". These attributes should be both comprehensive and measurable. An attribute is *comprehensive* if, by knowing the level of an attribute in a particular situation, the decision maker has a clear understanding of the extent that the associated objective is achieved. An objective generally indicates the direction in which we strive to do better (i.e., the objective is to minimize the cost, and the attribute is the cost of the building). An attribute is *measurable* if it is reasonable both (a) to obtain a probability distribution for each alternative over the possible levels of the attribute (or to assign a point value), and (b) to assess the decision maker's preferences for different levels of the attribute. In addition, the set of attributes chosen for a particular problem should be *complete*, so that it covers all the important aspects of the problem; *operational*, so that it can be meaningfully used in the analysis; *decomposable*, so that aspects of the evaluation process can be simplified by breaking it down into parts; *nonredundant*, so that double counting of impacts should be avoided; and *minimal*, so that the problem dimension is kept as small as possible.[8-10, 8-12]

We developed two separate models to describe the same decision problem: an influence diagram in DPL linked with EXCEL by Data Dynamic Exchange (DDE), and an EXCEL - @Risk model. The latter model is less time-expensive to run, since it uses a deterministic sensitivity analysis on each parameter by keeping the others (which are independent from that particular parameter) constant. Thus, it offers a preliminary understanding on the important parameters on which more time-expensive probabilistic sensitivity should be performed with the DPL - EXCEL model.

The analysis followed several steps:

- Specification of the attributes,

- Verification of assumptions,
- Elicitation of one-dimensional utilities $U(X_i)$,
- Measurement of scaling factors, k_i,
- Calculation of normalizing parameter, K,
- Determination of multi-attribute utility function, U(X),
- Sensitivity analysis.

Specification of the Attributes

Let us choose a set of attributes, and then define the range of interest for each of them. The levels of each attribute which are most and least preferred should be identified for each one-dimensional utility. The following five attributes were included in the model:

X_1 = Tokamak Pit Construction Cost,
X_2 = Constructibility,
X_3 = Project Completion Time,
X_4 = Public Attitude,
X_5 = Radiological Confinement.

Three of these attributes are objective (as opposed to subjective) in nature. That means that there already exists a commonly understood scale for that attribute and its levels are objectively measurable. However, there are objectives for which no objective index exists, and in such cases a subjective index must be constructed. The two subjectively assessed scales in the present work are those of the attributes 'Public Attitude' and 'Constructibility'.

Tokamak Pit Construction Cost (X_1): For the current ITER option, we use estimates available in reference [8-3]. The evaluated Joint Central Team (JCT) estimate is given as a 1989 kIUA value within the uncertainty range.[2] Whether the estimated value will grow toward the high side of the range or reduce toward the lower cost depends on many factors, such as: commercial competition reducing cost, actual conditions of procurement increasing cost, control of vendor cost adopted by the project management organization, a "design-to-cost" approach whereby design changes are made to maintain costs within the budgeted amount, to ensure that the range is not exceeded. The JCT estimate for the ITER buildings structures (including cranes) as given in Table 3.3.1 [8-3] is 891 kIUA with an uncertainty of +45 / -90 kIUA. We assume that the construction cost of the tokamak pit is directly proportional to the volume of the building, and the volume of the tokamak pit represents about

[2] 1 IUA = 1,000 US $ (January 1989 buying power). The cost in currency in 1995 is converted to January 1989 using a de-escalation factor of 1.2415.[8-3]

20% of the total volume of the tokamak building. Thus, the best estimate for the tokamak pit cost is about $220 million, with minimum and maximum values of $207 and $240 million respectively. Having three estimated values only, we assume the cost to be distributed according to a triangular distribution[3]: Triangular(207, 240, 220), where $220 million is the peak (mode) of the distribution. Similarly, the CANDU option has an associated distribution for the construction cost as follows: Triangular(300, 480, 350). The peaks of these triangular distributions are controlled by nodes A1_1 and A1_2 in the DPL influence diagram presented in Figure 8-1.

Constructibility (X_2): Constructibility refers to the technical feasibility of the proposed confinement design. We defined a "feasibility scale" from 0 to 5. Zero on this scale would be for a type of technical solution which is used and works well on a 'regular' basis. Five would be assigned to a technical solution not yet demonstrated and generally considered to have very small chances of being successful in practice. A 'technical feasibility factor' was associated to each type of containment. This factor is allowed to vary according to a triangular distribution. The peaks of these triangular distributions are controlled by nodes A2_1 and A2_2 in Figure 8-1. (Example: the technical feasibility factor associated with the CANDU option is generated from the distribution Triangular(0, 5, A2_1) with a minimum value of 1, a maximum value of 4 and mode of A2_1).

Project completion time (X_3): We felt that the project total completion time might be an important attribute for the designer. In general, the shorter the duration of the project, the better. In addition, shorter duration of the project would reduce the chances of being interrupted by external factors (e.g. court actions by public groups). We considered 'time until completion' to be distributed according to an exponential distribution[4]. The reason for choosing this type of distribution is its

---

[3] This distribution has three parameters: a, b, and c. The distribution extends from a to b and peaks at c (which must lie between a and b). The only restriction on the parameters is that a<c<b. The distribution is as follows:

$$f_t(x|a,b,c)=\begin{cases}\dfrac{2(x-a)}{(b-c)(c-a)} & \text{for } a\le x\le c,\\ \dfrac{2(b-x)}{(b-a)(b-c)} & \text{for } c\le x\le b,\\ 0 & \text{otherwise.}\end{cases}$$

where a<c<b. DPL refers to this distribution as triangular(a, b, c). The equations for the mean and var are:

$$\text{mean}=\frac{a+b+c}{3},$$

$$\text{var}=\frac{a^2+b^2+c^2-ab-ac-bc}{18}.$$

[4] Exponential Distribution is defined for all positive values of x and declines exponentially. Its only parameter is λ, which must be positive. The distribution is as follows:

$$f_e(x|\lambda)=\lambda e^{-\lambda x}$$

where x>0 and λ>0. DPL refers to this distribution as Exponential(y). The equations for mean and variance are:

'memory-less' property. The mean time of the project completion (equal to the inverse of the 'lambda' parameter) for the two options is controlled by nodes T1 and T2 in Figure 8-1.

Public attitude ***(X_4)***: This attribute refers to the public fear and anxiety due to the new technology, which is the risk as perceived by the public, be it scientifically based or not. We assigned a scale from 1 to 10 to this attribute. Ten would be the measure associated with a technology which generates a lot fear, anxiety and implicit hostility of the public; one would be the kind of technical solution which would even generate a mild support from the public side. Triangular distributions where also used in this case. The peak values of these distributions are controlled by nodes A4_1 and A4_2 in Figure 8-1.

Radiological Confinement (X_5): We used the radioactive releases of tritium to the environment as a measure of the radiological confinement performance. The frequency distribution of the tritium releases to the environment was obtained from the probabilistic methodology developed as the main goal of this project. Chapters 4 and 5 described the method for obtaining frequencies distributions of releases out of the first and second confinement barriers respectively. As for the third confinement barrier represented by the tokamak building, we attached a chance event 'Tokamak Pit integrity' to the sequences where the second confinement failed. A more sophisticated method that divides this event into several failure modes of the building is recommended, but it is outside the scope of the present work. The DPL model was run for both of the options, CANDU and the current one, by considering different probabilities of failure and retention factors as shown in the EXCEL database in Appendix D.

Named probability distribution functions were then fit to the frequency histograms obtained above, to be used in the DPL decision problem for the attribute 'Radiological confinement'. The software package used for fitting the distributions is BestFit.[8-13] This software package includes RiskView, which allows a preview of all types of distributions and gives a sense of which of them might fit our data. That is how we decided to try the following distributions: negative binomial, Poisson, Rayleigh, triangular, Weibull and lognormal. The best fit is the triangular distribution with the following parameters: Triangular(0, 1910, 0.21)[5] for the CANDU option, and Triangular(0, 3230, 0.42) for the current option. The original distributions, the best fit and the lognormal distribution fitted to the data are presented in Figures 8-3 and 8-4 at the end of this chapter.

$$\text{mean} = \frac{1}{\lambda},$$

$$\text{var} = \frac{1}{\lambda^2}.$$

The mean must be positive.

[5] The values represent grams of tritium released to the environment.

Verification of Assumptions

The theory of multi-attribute utility is based on two assumptions about the structure of preferences which refer to the way a person values the interaction between attributes. The two assumptions are:

- preferential independence (PI)
- utility independence (UI)

If both of them hold, then we have a practical means to obtain the multi-attribute utility with a reasonable computational effort.

Preferential independence means that the ranking of preferences over any pair of attributes is independent of the other attributes. This implies that the order of ranking between two attributes does not change because of changes in the level of the other attributes, which does not mean that one does not care about the other attribute. Formally, the assumption of preferential independence is as follows: if for any pair of attributes, say X_1 and X_2, one combination is preferred to another $(X_1', X_2') > (X_1'', X_2'')$ for some level of the other attributes, say X_3 to X_N, then the order of this preference will be maintained for all other levels of the other attributes.

Returning to our problem, the five attributes specified above seem to satisfy the preferential independence assumption from the point of view of the designer. His goal is to perform a design with low cost, high constructibility, short project completion time, high public acceptance, and good radiological confinement. After testing for the requirements specified in the definition of the Preferential Independence, we concluded that it is reasonable to assume that X_1, X_2, X_3, X_4, X_5 are indeed preferentially independent of each other.

Utility independence concerns the intensity of preferences, not just their relative order as does PI. The UI assumption is that the indifference between a lottery and a certain equivalent for any attribute does not depend on the levels of the other attributes. Formally, the assumption of utility independence is as follows: if for any given level of attributes X_j other than X_i, there is an indifferent statement between several levels of X_i: $X_i' \sim (X_i'', P; X_i''')$ for one set of X_j, $j \neq i$, then this indifference holds for all levels of X_j, $j \neq i$.

Because the verification of the utility independence requires at least portions of the one-dimensional utility functions, we found more convenient to check this assumption as part of the assessment of these utility functions.

For our problem, we first assessed the single-attribute utility functions by the certainty equivalent (CE) method. The scale for the utility functions was set between 0 and 1 as follows: $U(X_\cdot) = 0$ and $U(X^*) = 1$, where $X_\cdot$ is the least desirable value of the attribute, and X^* is the most desirable value in the range considered. Once we obtained the single-attribute utility functions, we checked the UI assumption for each attribute as follows: assume that, for the attribute X_1, the interviewed person makes the statement: \$300M ~ (\$250M, 0.8; \$450M). Specifically,

$$U(\$300M) = 0.8\ U(\$250M) + 0.2\ U(\$450M) \qquad (8\text{-}1)$$

The person is utility independent for the construction cost (X_1) if the same statement is valid for any other value of radiological and public attitude, etc.

Elicitation of One-dimensional Utilities $U(X_i)$

It is very probable that the majority of the allegedly interviewed designers are "risk averse" for the attributes we have considered. We define the independent utility functions for all five attributes as being monotonically decreasing functions of the respective attributes for construction cost, radiological confinement defined in terms of releases to the environment, and project completion time. That is a intuitively understandable assumption since the designer prefers those attributes to be as small as possible (utility should be equal to one for the minimum value, and equal to zero for the maximum value of the attribute). As for constructibility and public attitude, we define the scales so that the minimum value of the scale corresponds to maximum utility, and the maximum value to minimum utility. That way we will only deal with decreasing utility functions.

For monotonically decreasing preferences, a person is *risk averse* if he prefers the expected consequences of any nondegenerate lottery[6] to that lottery. Then, if the utility function represents such preferences, the utility of the expected consequences must be grater than the expected utility of the lottery. If one prefers (is indifferent to) every nondegenerate lottery to its expected consequence, then he is said to be *risk prone* (*risk neutral*). It can be demonstrated that a decision maker is risk averse (risk prone, risk neutral) if and only if his monotonically decreasing utility function is concave (convex, linear).

There are many techniques for evaluating utility functions depending on the particular decision maker and on the context of the problem. The basic steps, however, that one uses to assess a utility function are essentially the same: preparing for assessment, identifying the relevant quantitative characteristics, specifying quantitative restrictions, choosing a utility function, checking for consistency. Instead of going through the elicitation work with the designer to evaluate his/her individual utility functions for each attribute, we chose to define risk averse functions for all five attributes, and then perform sensitivity analysis on the functions' parameters to explore the possible policy change when the designer becomes risk neutral or prone towards any of the attributes. Each individual utility function is defined as a sum of a line and a triangle with parameters a, b, r, and c, where a and b are the minimum and maximum value of the attribute, r indicates the position of the triangle peak between a and b, and c gives the height of the triangle. The parameter c determines the concavity of the utility

[6] A nondegenerate lottery is one where no single consequence has a probability one of occurring.

function as follows: $-1 < c < 0$ for the risk prone attitude, $c = 0$ for risk neutral, and $0 < c < 1$ for risk averse one. The analytical function is defined in Visual Basic as shown in Appendix E and can be used with EXCEL to generate values depending on the attributes' values.

Measurement of scaling factors (k_i)

The method used for finding each scaling factor was to obtain an indifference statement of the form: $(X_i^*, X_{j\cdot}) \sim (X^*, P_i; X_\cdot)$, $j \neq i$. These indifference statements were developed by varying the probabilities P_i. The probability P_i is actually the scaling factor k_i. References [8-12] and [8-14] explain and exemplify the method for obtaining the scaling factors. The basic idea is to obtain a set of independent equations in a number equal to the number of the scaling factors representing the unknown values and to solve for them. These equations can be generated from certainty considerations, probabilistic considerations or both. It is not easy to interpret the scaling factors since they depend on the minimum and maximum desirable values of the attributes and those depend on the possible consequences of the problem. The values of the k_i's are stored in the nodes k1 through k5 in the DPL diagram in Figure 8-1, and sensitivity analysis was performed on each of them.

Calculation of Normalizing Parameter (K)

The normalizing factor, K, is determined from the formula:

$$K + 1 = \prod_{i=1}^{n} (K k_i + 1) \tag{8-2}$$

In general, this expression, an (n-1)-dimensions polynomial, must be solved by trial and error. The determination of K is facilitated by the fact that its value is bounded by $\sum k_i$ as follows: $K > 0$ for $\sum k_i < 1$; $-1 < K < 0$ for $\sum k_i > 1$; K degenerates for $\sum k_i = 1$, and in that case the multi-attribute function is the simple additive model: $U(X) = \sum k_i U(X_i)$.

Returning to our problem, we have five attributes, so the equation to be solved is:

$$K + 1 = (K k_1 + 1)(K k_2 + 1) \ldots (K k_5 + 1) \tag{8-3}$$

A Visual Basic function [8-14] can be used in EXCEL applications to solve the equation (8-3) for the non-negative value of K. The function is presented in Appendix F.

Determination of multi-attribute utility, U(X)

The multi-attribute utility (MAU) for a stakeholder group U(X) is obtained from the formula:

$$K\,U(X) + 1 = \prod_{i=1}^{n} (K\,k_i\,U(X_i) + 1) \qquad (8\text{-}4)$$

where $U(X_i)$ are the one-dimensional utilities for each X_i. The Visual Basic function used for the calculation of MAU is presented in Appendix F. The cumulative distribution functions (CDFs) and the expected values of MAU for both tokamak pit options are presented in Figure 8-5, which shows that the CANDU option is clearly dominated by the current design with an expected value of 0.846.

Sensitivity Analysis

A thorough value sensitivity analysis was performed with respect to most of the parameters influencing the expected multi-attribute utility function. The EXCEL - @Risk model is less time-expensive because it changes only the parameter on which the sensitivity analysis is performed and the dependent parameters, and does not perform Monte Carlo simulations on the attributes' values as DPL - EXCEL model does. Therefore, we first used the first model to check which parameters lead to a change in policy, and then used the latter model to perform 'Rainbow Sensitivity Diagrams' that give a more precise value of the parameter where the policy changes.

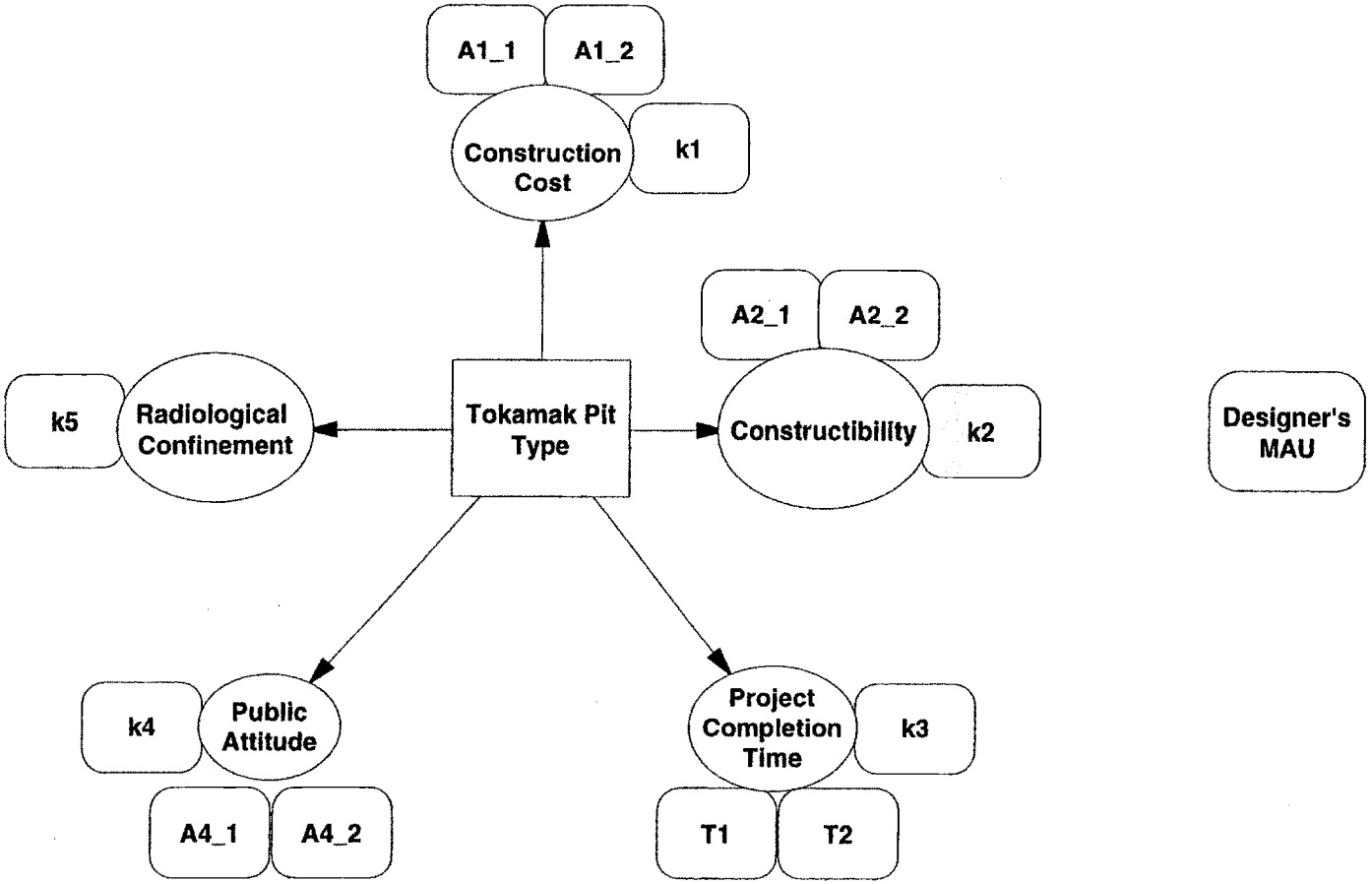

Figure 8-1: DPL Influence Diagram for the Type of Tokamak Pit Decision Problem

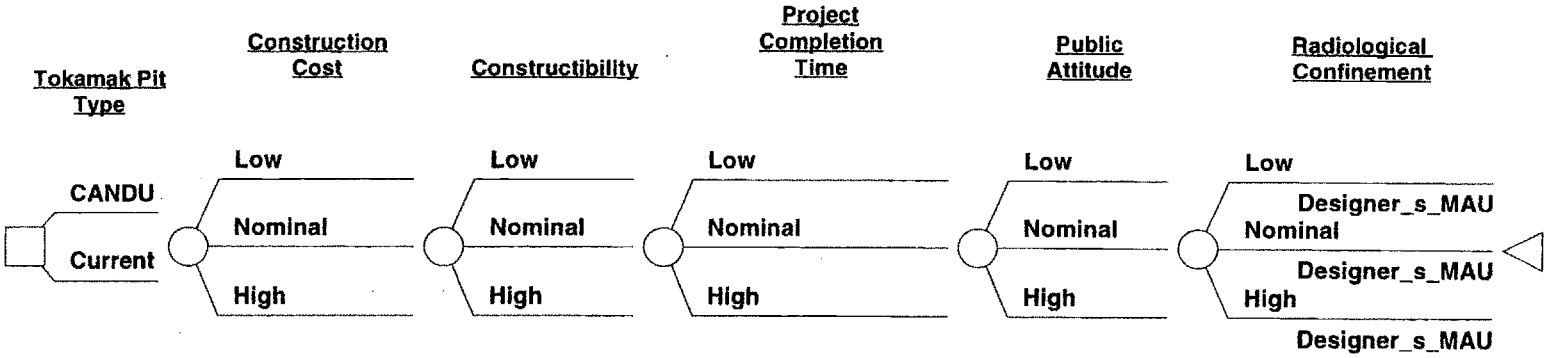

Figure 8-2: DPL Decision Tree for the Type of Tokamak Pit Decision Problem

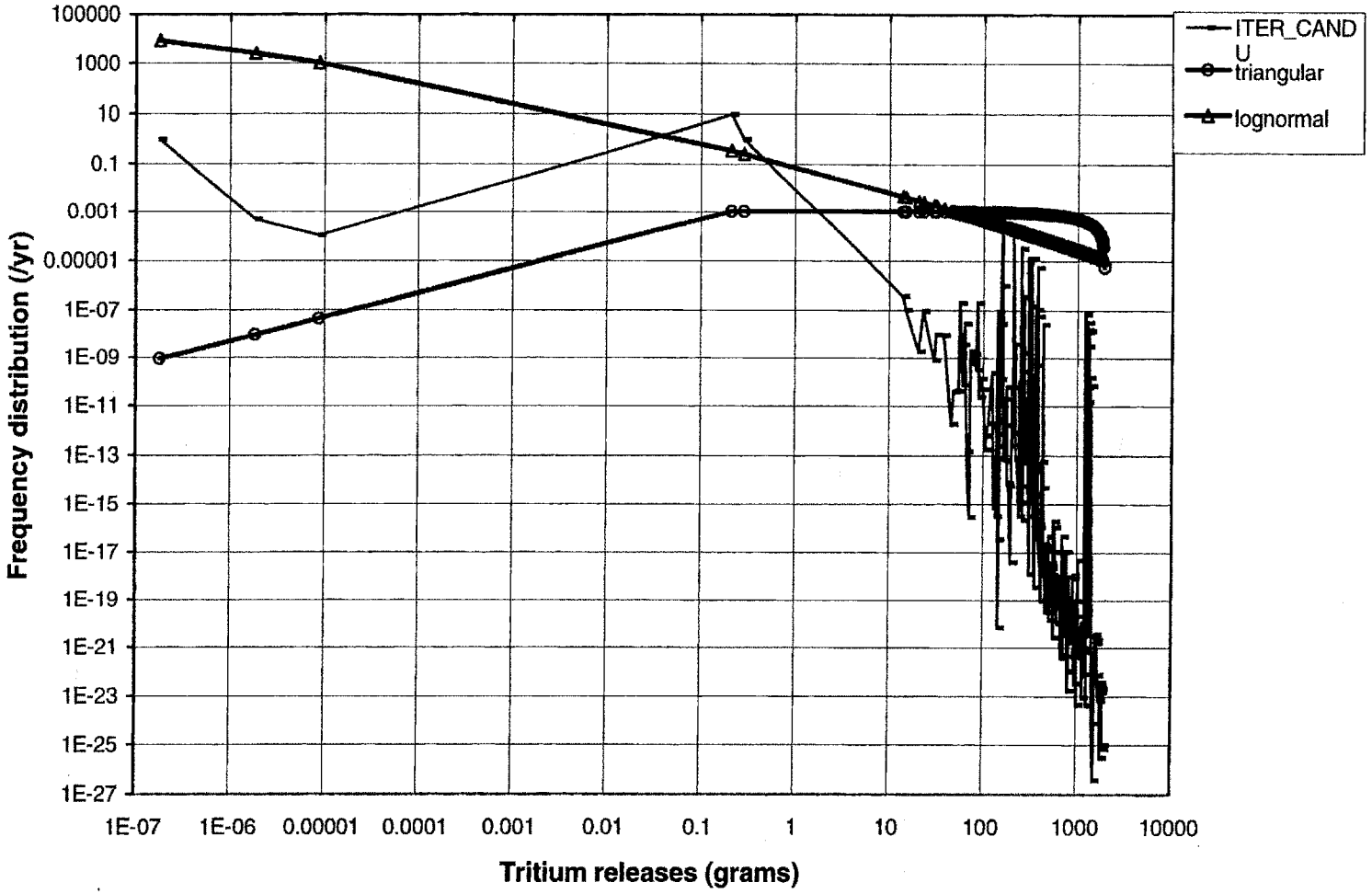

Figure 8-3: Frequency Distribution of Tritium Releases for CANDU Radiological Confinement

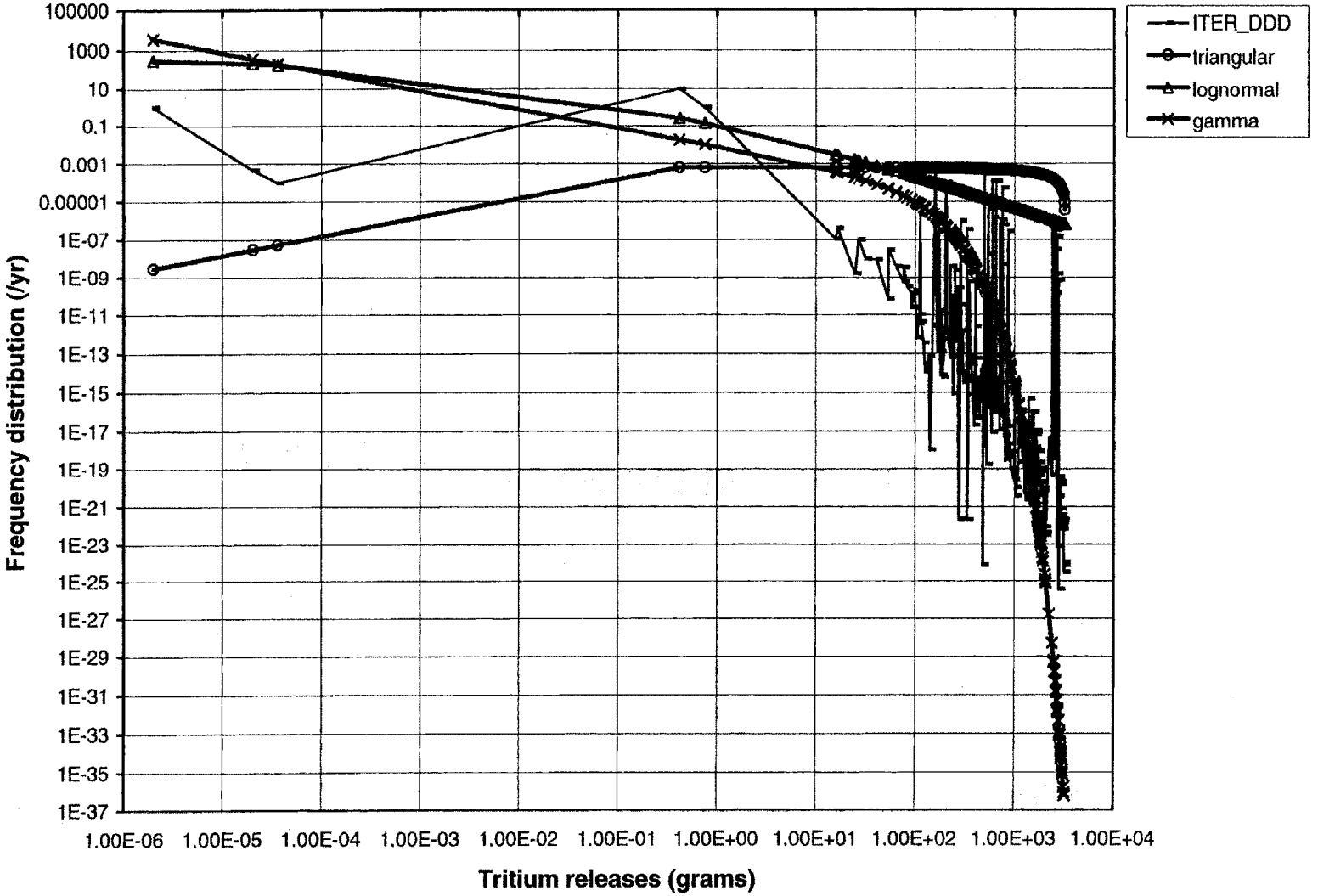

Figure 8-4: Frequency Distribution of Tritium Releases for ITER Current Design Radiological Confinement

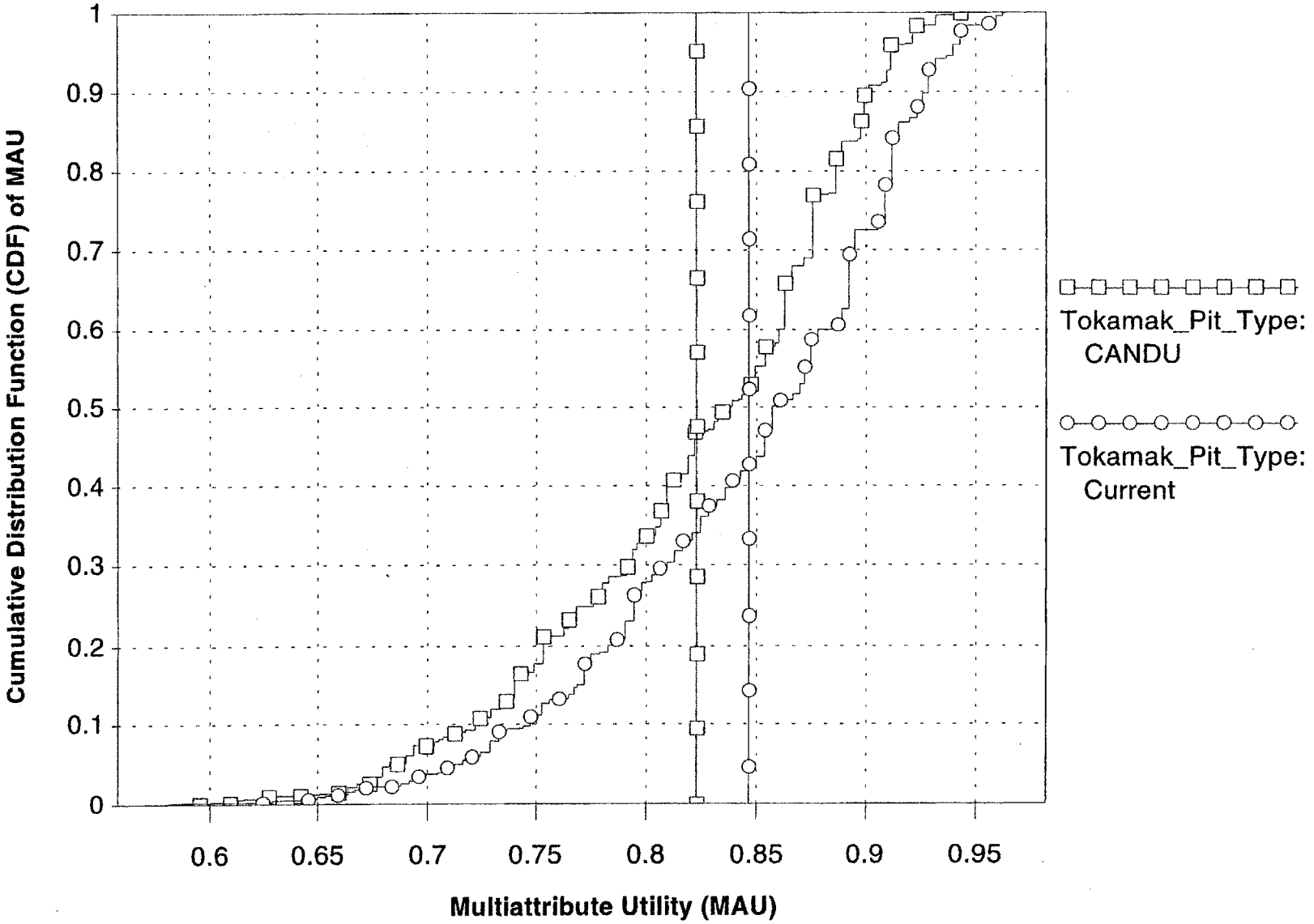

Figure 8-5: Multi-attribute Utility Functions CDFs for the Two Tokamak Pit Options

8.2 Summary of Results

We found that the alternative with the highest expected multi-attribute utility value is the current ITER design as shown in Figure 8-5, but, as the results of the sensitivity analysis show, the ranking of the options might change for relatively small variations in the input parameters.

Sensitivity analysis was performed on the following three types of parameters:

- **k_i factors**: The scaling factors considered for the reference case are as follows:

$$(k_1, k_2, k_3, k_4, k_5) = (0.3, 0.2, 0.2, 0.2, 0.4). \quad (8\text{-}5)$$

Figures 8-6 to 8-10 represent the sensitivity analysis on these five factors. The vertical bar marks the place where a change in the optimal decision choice occurs. In Figure 8-6, the reference value for k1 is equal to 0.3, value situated on the right of the vertical bar at 0.22; thus, all the values of k1 higher than 0.22 lead to recommending the current ITER DDD choice as the optimal solution. As the construction cost becomes more important to the designer's decision making process, k1 increases, and the ITER DDD design gets more credit, which is reflected in an increased MAU expected value of this choice. Also, Figure 8-6 shows that the CANDU option becomes the preferred one if k1 decreases bellow 0.22 (meaning that the importance that the designer gives to the construction cost decreases). For k1 < 0.2, the expected MAU remains approximately constant implying that, if the importance of the attribute decreases even more, the overall satisfaction level remains the same.

Figures 8-7 and 8-8 indicate that the expected value of MAU is an increasing function of k2 and k3, so if the importance of constructibility or project completion time increases, the current ITER DDD option becomes even more preferred over the CANDU option, and the recommended decision choice does not change over the entire range of these two attributes.

The sensitivity of the MAU expected value to the public attitude attribute, as shown in Figure 8-9, expresses the following behavior: while k4 decreases from 0.28 to 0, representing a decreasing concern of the designer towards the public attitude, the expected value of MAU increases for the currently preferred choice (i.e., current ITER DDD); however, at k4 = 0.28, the preferred decision policy changes to the CANDU option, and, as the public attitude weights more and more in the designer's decision making process, his expected MAU for the CANDU option increases with k4 almost linearly.

For radiological confinement attribute, the sensitivity analysis is represented in Figure 8-10. The designer's satisfaction level is increased by the increased value of the k5 factor for any of the tokamak pit design choice. A k5 higher than 0.68 will change the optimal policy from the current ITER DDD to CANDU.

- **the parameters[7] of the probability distribution functions associated to each of the five attributes**: The sensitivity of the MAU expected value on the construction cost PDF parameters is represented in Figures 8-11 and 8-12. It should be reminded that the PDF for the cost attribute is a triangular distribution, and sensitivity analysis of the MAU expected value on the mode of the distribution is performed for each of the two decision policies. With the information currently available, the MAU expected value corresponding to the ITER DDD optimal policy remains constant if the most probable cost of the CANDU-type building (A1_1) varies between the minimum and maximum limit, and decreases with the increase of the most probable cost of the current ITER DDD building (A1_2) (in other words, the designer's satisfaction decreases as the most probable cost of the ITER DDD building increases). None of these two parameters variation within the considered ranges lead to a change of the decision policy.

  The constructibility attribute is also given by triangular distributions for each of the decision policies. As a remainder, a zero value represents perfect constructibility, and a five value represents a not yet demonstrated feasibility, so that the lower the value the better. The mode of the CANDU constructibility PDF (A2_1) does not affect the MAU expected value for the ITER DDD choice (Figure 8-13). As for A2_2 (Figure 8-14), corresponding to the ITER DDD constructibility mode, its reference value is equal to 1, and the MAU expected value of the ITER DDD policy decreases with an increased value of A2_2, as expected. Moreover, for A2_2 $\geq$ 3.8, CANDU option becomes the choice with the higher MAU expected value. In other words, if some kind of unforeseen problem occurs in the current design, then the CANDU choice might become dominant.

  Varying the project completion time PDF parameter of any of the two options (Figures 8-15 and 8-16) does not change the expected value of MAU, and no change of policy is recommended.

  Finally, the sensitivity of the MAU expected value on the mode of the PDF associated with the public attitude towards the two policies is represented in Figures 8-17 and 8-18. In both cases, this parameter does not seem to cause a change in the preferred design, which is an interesting result because it gives the designer more freedom in the decision making process.

- **parameter 'c' of the single attribute utility functions, determining the designer attitude towards each attribute (risk averse, neutral, or prone):** The sensitivity was only performed with the EXCEL - @Risk model. Each of the Figures 8-19 to 8-23 represents the MAU expected value for both design options as a function of c corresponding to each attribute. The two MAU functions do not intersect in any of the cases, meaning that the change of the designer attitude towards the attribute does not lead to a change of his preferred option.

[7] The parameters for the chosen probability distribution functions of the five attributes are explained in the subsection 'Specification of the Attributes' of the present chapter.

Intuitively, CANDU type containment has the major advantage of being perceived as more reliable by the public, and provides a better radiological confinement. The major disadvantage is the cost. A better estimation of the construction costs is required.

A more advanced analysis should definitely take into account the location of the facility. (For example building construction costs as well as feasibility factors might depend strongly on the seismicity of the zone.)

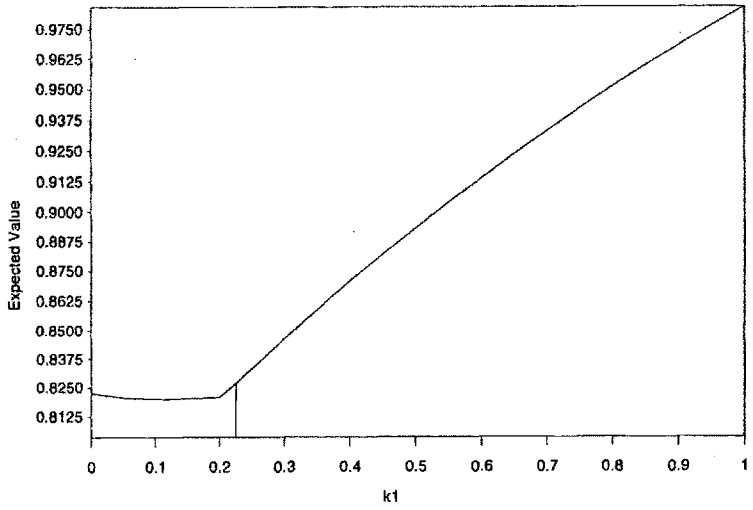

Figure 8-6: Sensitivity of MAU Expected Value to k1

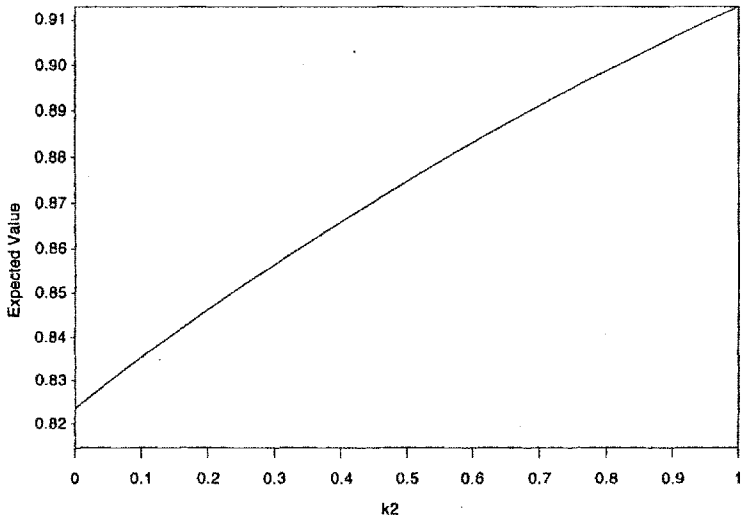

Figure 8-7: Sensitivity of MAU Expected Value to k2

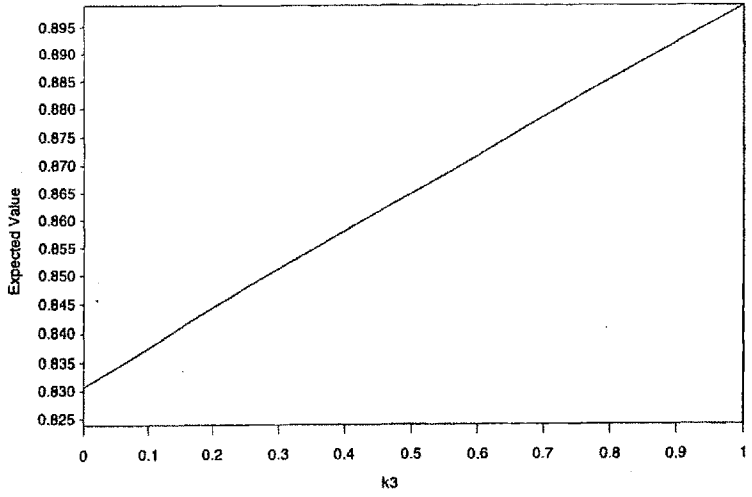

Figure 8-8: Sensitivity of MAU Expected Value to k3

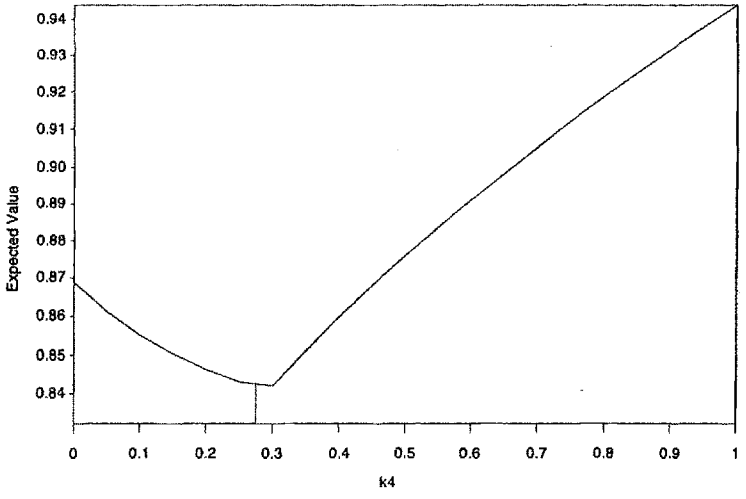

Figure 8-9: Sensitivity of MAU Expected Value to k4

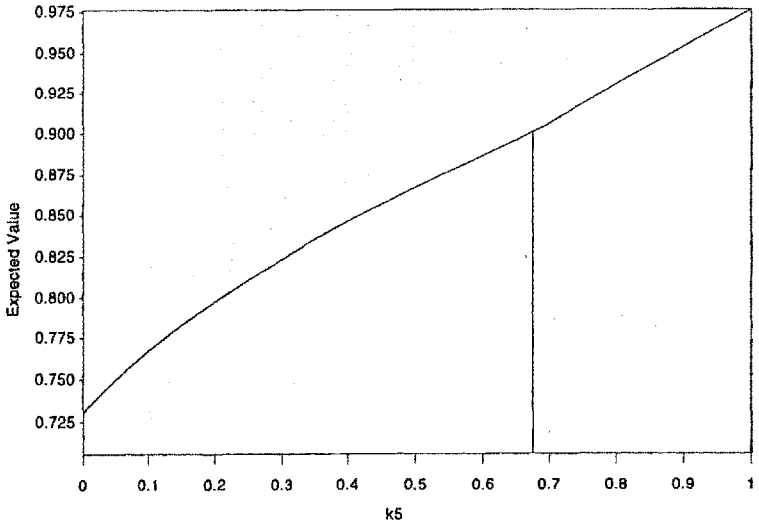

Figure 8-10: Sensitivity of MAU Expected Value to k5

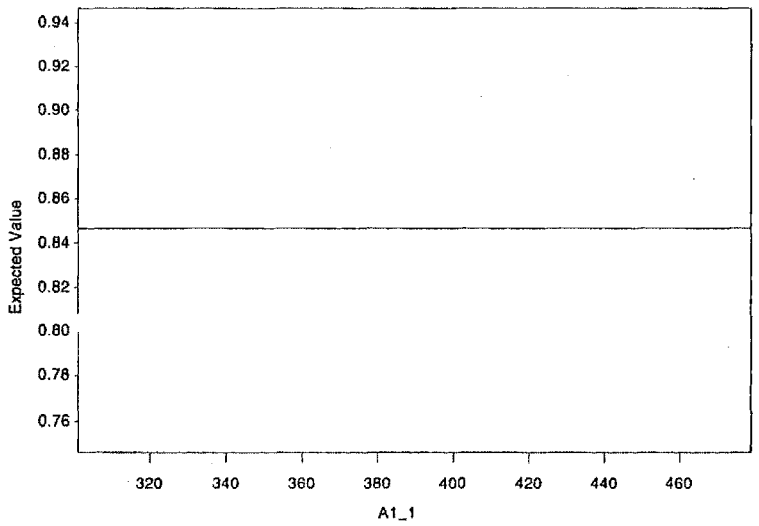

Figure 8-11: Sensitivity of MAU Expected Value to the Mode of PDF for CANDU Construction Cost

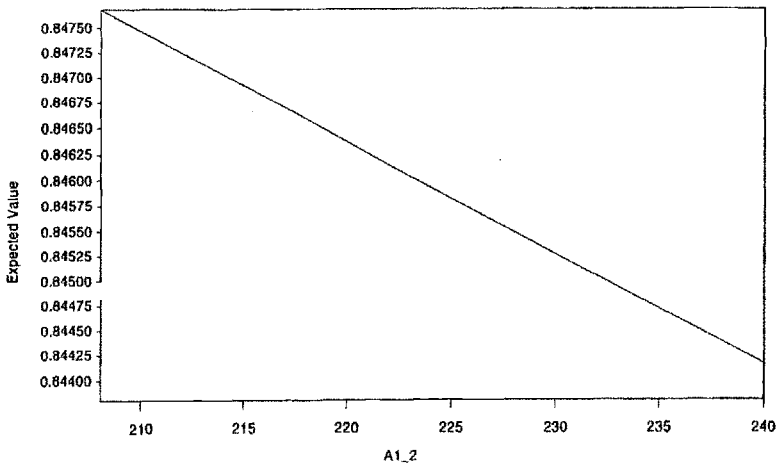

Figure 8-12: Sensitivity of MAU Expected Value to the Mode of PDF for Current Option Construction Cost

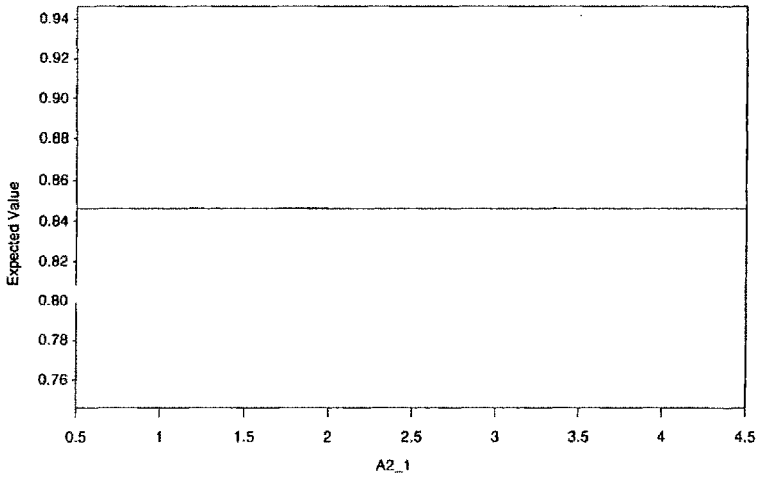

Figure 8-13: Sensitivity of MAU Expected Value to the Mode of PDF for CANDU Constructibility

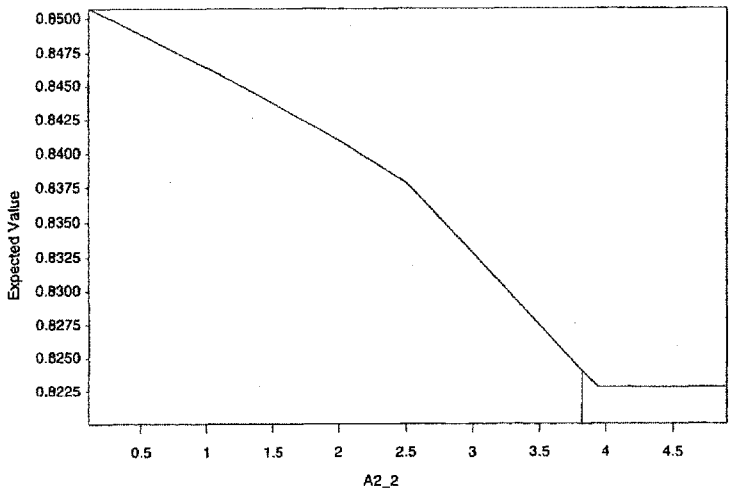

Figure 8-14: Sensitivity of MAU Expected Value to the Mode of PDF for Current Option Constructibility

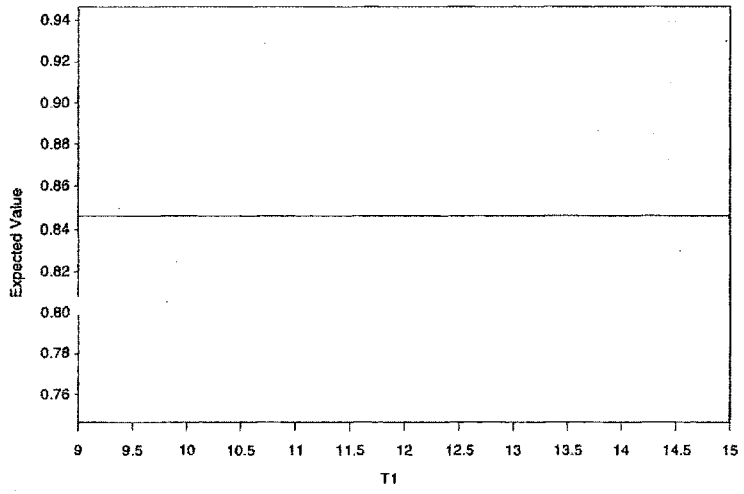

Figure 8-15: Sensitivity of MAU Expected Value to the Project Completion Time for CANDU Option

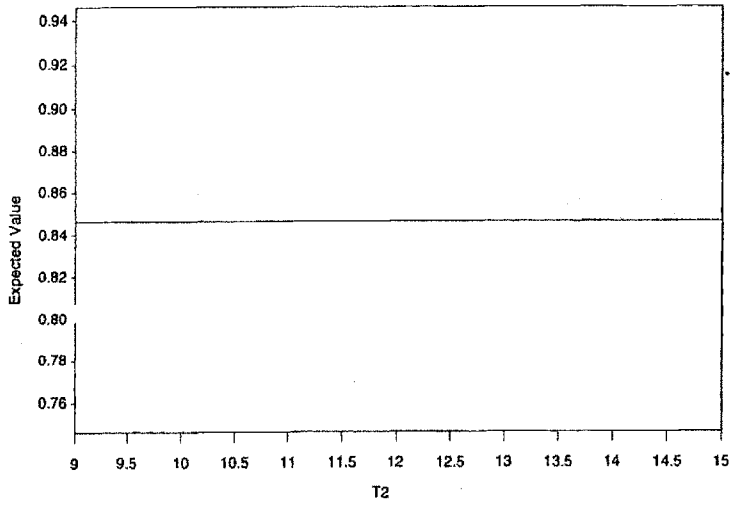

Figure 8-16: Sensitivity of MAU Expected Value to the Project Completion Time for Current Option

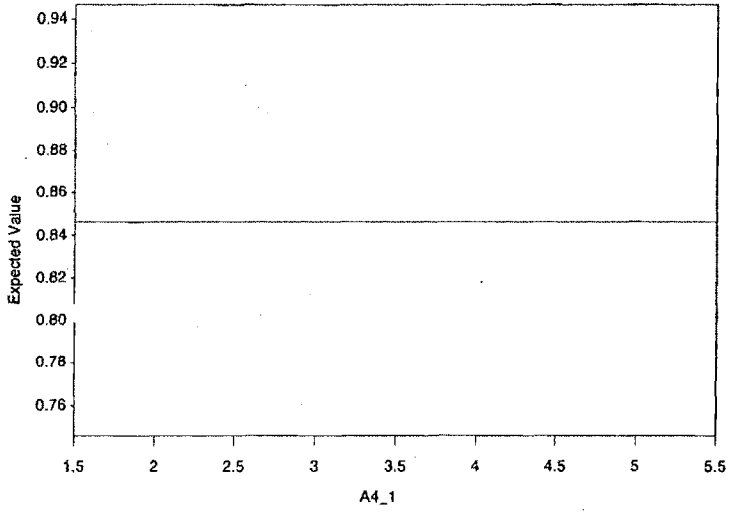

Figure 8-17: Sensitivity of MAU Expected Value to the Mode of PDF for Public Attitude towards CANDU Option

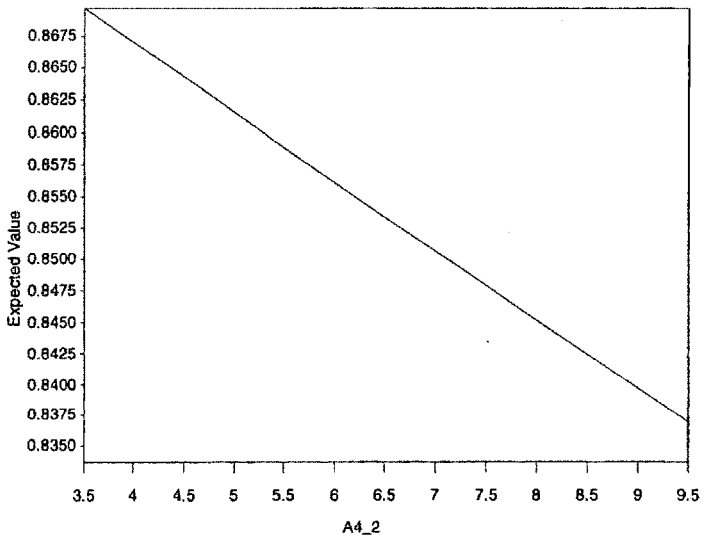

Figure 8-18: Sensitivity of MAU Expected Value
to the Mode of PDF for Public Attitude towards Current Option

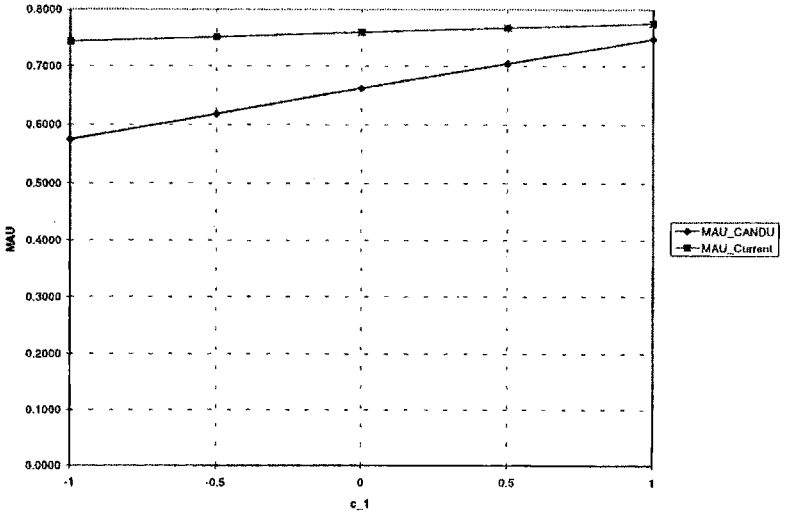

Figure 8-19: Sensitivity of MAU Expected Value
to the Construction Cost Utility Function Form

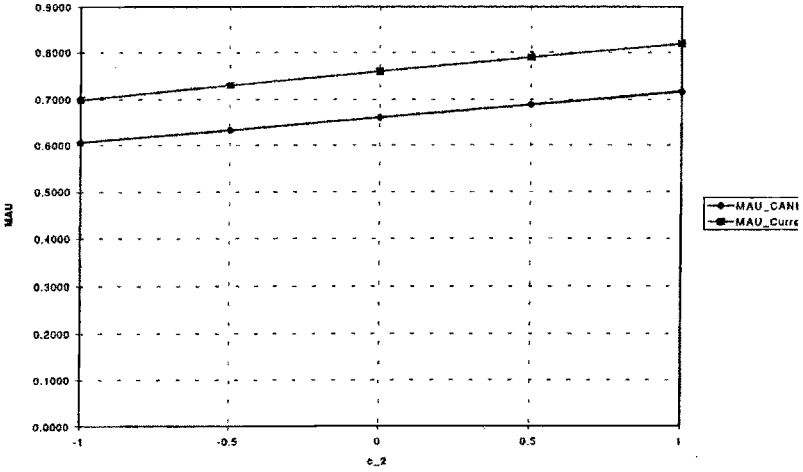

Figure 8-20: Sensitivity of MAU Expected Value
to the Constructibility Utility Function Form

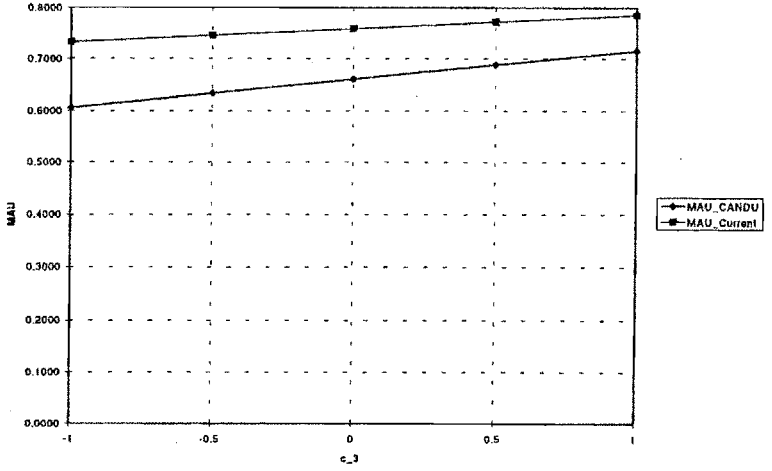

Figure 8-21: Sensitivity of MAU Expected Value
to the Project Completion Time Utility Function Form

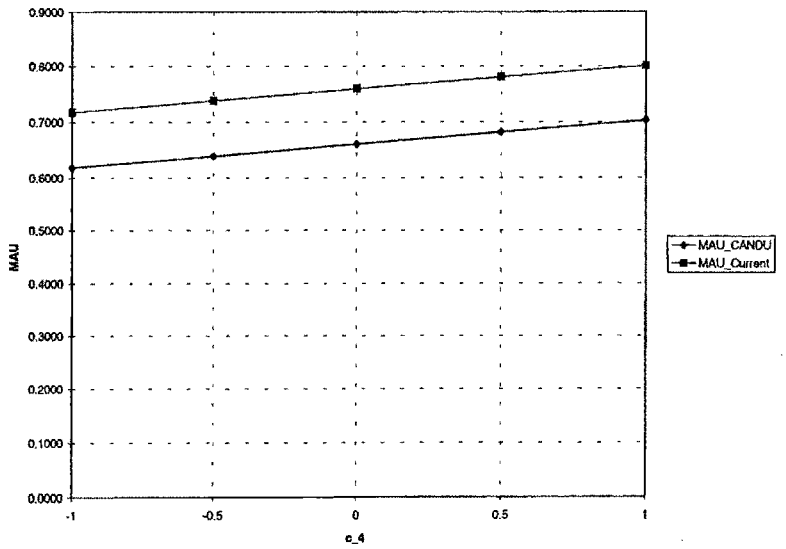

Figure 8-22: Sensitivity of MAU Expected Value to the Public Attitude Utility Function Form

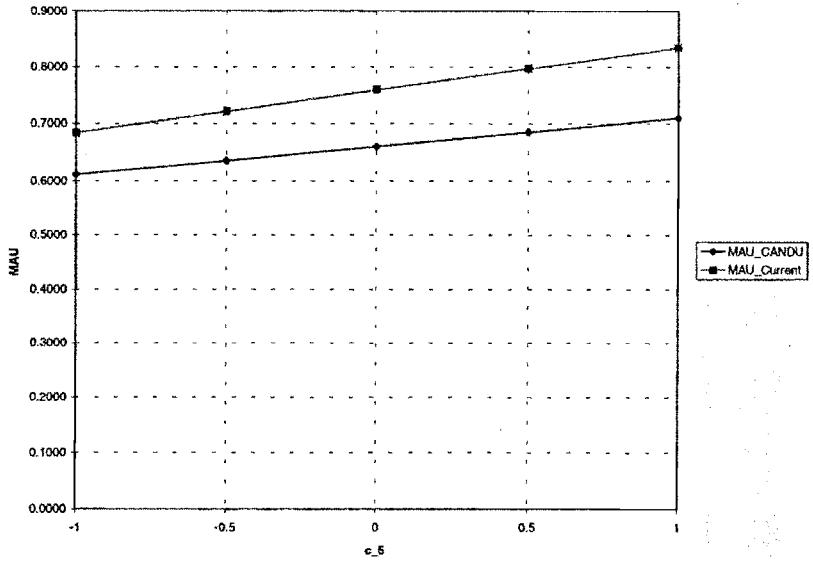

Figure 8-23: Sensitivity of MAU Expected Value to the Radiological Confinement Utility Function Form

9. Conclusions and Recommendations

9.1 Concluding Remarks

The overall objective of this work was to develop a methodology that evaluates the performance of the radiological confinement barriers for a tokamak reactor, recommending the number of barriers required to comply with the design requirements, and the type of the last confinement barrier to the environment. We decided to call this methodology as a whole the **Enhanced Probabilistic Decision Analysis (EPDA).**

In the first part of the present study, a probabilistic methodology was developed to assess the performance of the first and second confinement barriers. The models include only the accident sequences derived from six initiating events, each occurring in a different system of ITER: primary coolant systems, magnet systems, fuel systems, plasma vacuum chamber, cryostat vessel, and electric power supply system.

The accident sequences were developed using influence diagrams/event tree models in DPL [3-11], by defining all the system failures in an influence diagram, and constructing the time sequence in a system event tree. This method is suitable for large accident sequence models, because it separates the data definition including conditional events in the influence diagram and the time sequence in the event tree. The result of running a DPL accident sequences model is a frequency distribution of consequences, which is what was needed for our work. A drawback of using DPL for accident sequence modeling is that the accident sequences are not given explicitly with their corresponding frequency and consequence, which is desirable for a Probabilistic Risk Assessment study.

A database with failure probabilities of various systems failure modes as defined in this study was developed in EXCEL 5.0. Dynamic Data Exchange (DDE) was used between the DPL accident sequence models and the EXCEL database, to assure consistency: the same event might occur in several DPL models, but its probability is only changed once in the database, and all the models will get that new value when run. Some of the probabilities used were taken from the available references as indicated, but others are purely judgmental since no data is available. As more data becomes available, the database should be improved.

The safety design requirements currently recommended for ITER are setting limits on individual accident sequences in terms of both frequency and consequence. In our opinion, a complementary cumulative frequency (CCF) of radioactive releases form is more appropriate since it can take into consideration overall risk aspects and uncertainties can also be integrated. An analytical form of such a line was derived for ITER in the present study, based on criteria such as risk aversion, limit the risk from the low consequence - high frequency accidents, and limit the overall risk of the

fusion plant. The case of no risk aversion (a=1) was also analyzed and compared against the current ITER limit line, because we were not certain if that line already incorporates a risk aversion attitude or not. Our observation is that it might incorporate a risk aversion corresponding to a slope of -1.5.

Figures 3-12 and 3-13 in Chapter 3 show families of curves for different values of parameter 'a' for a proposed limit line in the form of a frequency distribution and a complementary cumulative frequency of tritium releases respectively. Nuclear fission power industry usually employs limit lines with a risk aversion corresponding to a slope of -1.2 to -1.5. However, ITER is a fusion machine still at the design stage, whose safety goal is to demonstrate no evacuation requirements. For that reason, and also because society tends to be more risk averse towards new technologies, we choose a limit line with a higher risk aversion than for fission reactors. That line corresponds to a parameter a=3, and is included in all of the figures representing results in graphs CCF versus tritium releases in Chapter 7. The results for the reference case, as well as for the sensitivity analyses on the confinement barriers failure modes are presented along with the proposed limit line. Only one probability of failure was changed at a time to a low or high value while keeping the others at the reference level. One exception is Figure 7-3 which also includes a limit line corresponding to a=1.5, for exemplification purposes. In case the regulation committee chooses such a line with lower risk aversion, it might be that no strong third confinement barrier is required, as Figure 7-3 implies.

Once the decision is made from a safety point of view that a strong third confinement barrier is required to comply with the design requirements, the type of the building has to be chosen. A decision model was developed to chose the appropriate ITER tokamak building while considering several attributes such as: safety, cost, project completion time, public attitude, and technical feasibility. A designer utility function was defined for each of the attributes, and multi-attribute utility function theory was used to combine the single attribute functions in a single one. The decision option which maximizes the multi-attribute utility is chosen. Our model currently considers two options for the ITER tokamak pit: the current design as given in the design Description Documents [8-16], and a CANDU design. More options can be easily implemented into the model as they become of interest.

9.2 Limitations

The completion of the present work required the adoption of a multitude of assumptions. They were usually specified along the thesis as they occurred, but we give some examples below:

- in the decision model for the type of tokamak building, the two assumptions about the structure of preferences which refer to the way a person values the interaction between attributes (preferential independence and utility independence) were both considered to hold; however, an extensive interviewing process with the stakeholders should be undertaken;
- the form of the singe-utility functions and the corresponding scaling factors were assigned forms and values without discussions with the designer groups, as it should be done;

- the accident sequence models were not exposed to peer reviews, which could have resulted in modifications performed during an iterative process;
- the database for the probabilities of failures by experts.

It is important to recognize that the value of this study is in providing a methodology that can be useful in making decisions during the design of the radiological confinement barriers of a tokamak reactor. At the present stage of development, our model cannot give definite answers about the safety of the ITER reactor. Considerable work should be added to complete the model with all the necessary details, but that is outside the scope of our project.

9.3 Recommendations for Further Work

A Probabilistic Risk Assessment (PRA) study for a nuclear power plant is a project undertaken by a large group of analysts, each specialized in a particular area. The present work involves using several PRA tools, yet it is essentially the product of one person. Thus, building a complete model that gives meaningful results for ITER confinement design was not possible. It should be noted that the development of the framework of a methodology was the main focus of this work. More work has to be added in several areas so that design recommendations can be made for ITER confinement strategy. Some of these areas are as follows:

- all the conceivable accident sequences should be included in the overall complementary frequency for the first and second confinement barriers;
- human errors should be included in the accident sequences;
- external events should be analyzed once a site is selected;
- the EXCEL database for probabilities of failure should be improved by performing a comprehensive fault-tree analysis for the systems involved;
- common cause failures should be more carefully analyzed, and the influence diagram can be a useful tool to explicitly represent events that can lead to the simultaneous failure of several systems;
- releases of other radioactive inventories should be analyzed with the same model;
- the definition of the systems failure modes should be checked against the latest designs;
- sensitivity should be performed on failure probabilities when changing more than one value at a time;
- the decision model for the type of tokamak building should be updated with the ITER choices under consideration;
- similar decision models for the type of tokamak building should be developed for other stakeholders interested in the ITER project, then their choices should be considered together for making a final decision (e.g., using game theory).

Appendix A: EXCEL Macro for First Confinement Barrier CCDF

```
Sub Macro_FirstBarrier()
  Sheets("LFO2").Select
  Workbooks.Open Filename:="LFO2.CSV"
  With ActiveWorkbook
    .Title = ""
    .Subject = ""
    .Author = "Ruxandra Golinescu"
    .Keywords = ""
    .Comments = ""
  End With
  ActiveWorkbook.SaveAs Filename:="LFO2.XLS", FileFormat:=xlNormal, _
    Password:="", WriteResPassword:="", ReadOnlyRecommended:=False _
    , CreateBackup:=False
  ActiveWorkbook.Close
  Range("A1:B92").AdvancedFilter Action:=xlFilterCopy, CriteriaRange _
    :=Range("D1:D2"), CopyToRange:=Columns("F:G"), Unique:=False
  Sheets("MPO1").Select
  Workbooks.Open Filename:="MPO1.CSV"
  With ActiveWorkbook
    .Title = ""
    .Subject = ""
    .Author = "Ruxandra Golinescu"
    .Keywords = ""
    .Comments = ""
  End With
  ActiveWorkbook.SaveAs Filename:="MPO1.XLS", FileFormat:=xlNormal, _
    Password:="", WriteResPassword:="", ReadOnlyRecommended:=False _
    , CreateBackup:=False
  ActiveWorkbook.Close
  Range("A1:B92").AdvancedFilter Action:=xlFilterCopy, CriteriaRange _
    :=Range("D1:D2"), CopyToRange:=Columns("F:G"), Unique:=False
  Sheets("TVP1").Select
  Workbooks.Open Filename:="TVP1.CSV"
```

```
With ActiveWorkbook
    .Title = ""
    .Subject = ""
    .Author = "Ruxandra Golinescu"
    .Keywords = ""
    .Comments = ""
End With
ActiveWorkbook.SaveAs Filename:="TVP1.XLS", FileFormat:=xlNormal, _
    Password:="", WriteResPassword:="", ReadOnlyRecommended:=False _
    , CreateBackup:=False
ActiveWorkbook.Close
Range("A1:B15").AdvancedFilter Action:=xlFilterCopy, CriteriaRange _
    :=Range("D1:D2"), CopyToRange:=Columns("F:G"), Unique:=False
Sheets("OP").Select
Workbooks.Open Filename:="OP.CSV"
With ActiveWorkbook
    .Title = ""
    .Subject = ""
    .Author = "Ruxandra Golinescu"
    .Keywords = ""
    .Comments = ""
End With
ActiveWorkbook.SaveAs Filename:="OP.XLS", FileFormat:=xlNormal, _
    Password:="", WriteResPassword:="", ReadOnlyRecommended:=False _
    , CreateBackup:=False
ActiveWorkbook.Close
Range("A1:B92").AdvancedFilter Action:=xlFilterCopy, CriteriaRange _
    :=Range("D1:D2"), CopyToRange:=Columns("F:G"), Unique:=False
Sheets("VCS").Select
Workbooks.Open Filename:="VCS.CSV"
With ActiveWorkbook
    .Title = ""
    .Subject = ""
    .Author = "Ruxandra Golinescu"
    .Keywords = ""
    .Comments = ""
End With
```

```
    ActiveWorkbook.SaveAs Filename:="VCS.XLS", FileFormat:=xlNormal, _
        Password:="", WriteResPassword:="", ReadOnlyRecommended:=False _
        , CreateBackup:=False
    ActiveWorkbook.Close
    Range("A1:B19").AdvancedFilter Action:=xlFilterCopy, CriteriaRange _
        :=Range("D1:D2"), CopyToRange:=Columns("F:G"), Unique:=False
    Sheets("LOSP").Select
    Workbooks.Open Filename:="LOSP.CSV"
    With ActiveWorkbook
        .Title = ""
        .Subject = ""
        .Author = "Ruxandra Golinescu"
        .Keywords = ""
        .Comments = ""
    End With
    ActiveWorkbook.SaveAs Filename:="LOSP.XLS", FileFormat:=xlNormal, _
        Password:="", WriteResPassword:="", ReadOnlyRecommended:=False _
        , CreateBackup:=False
    ActiveWorkbook.Close
    Range("A1:B22").AdvancedFilter Action:=xlFilterCopy, CriteriaRange _
        :=Range("D1:D2"), CopyToRange:=Columns("F:G"), Unique:=False
    Sheets("ALL1").Select
    ActiveSheet.PivotTables("PivotTable2").RefreshTable
    Sheets("ALL2").Select
    ActiveSheet.PivotTables("PivotTable1").RefreshTable
    Sheets("ALL3").Select
    ActiveCell.Select
    Selection.Sort Key1:=ActiveCell, Order1:=xlAscending, Header:= _
        xlGuess, OrderCustom:=1, MatchCase:=False, Orientation:= _
        xlTopToBottom
    Sheets("CCDF").Select
End Sub
```

Appendix B: Analysis of Accident Sequences that affect the Integrity of the First Confinement Barrier[1]

This appendix will discuss the accident sequences that affect the integrity of the first confinement barrier grouped in six categories as describes in Chapter 3. Six of the initiating events from the list presented in Table 2-2 (those in bold face) were analyzed in Chapter 4, because they were the ones we used to develop our methodology for evaluating the performance of the confinement barriers. The accident sequences in this appendix should be eventually included in the model for completeness, but that is outside the scope of the present study. However, we hope that this appendix can be a useful reference for further work in the ITER safety analysis.

B.1 Coolant Accidents

This section contains eight representative accidents in the primary coolant systems of the plasma facing components and the vacuum vessel. These systems are in operation both during the pulse and the dwell time. We will mention our assumptions as we go along in describing the accident sequences.

B.1.1 LBV1: Small in-vessel LOCA from FW/SB PHTS

This IE is representative for a family of IE's: small in-vessel LOCA through an opening of 1-2 cm^2 in one of the cooling systems: first wall, blanket, divertor, vacuum vessel. We develop the accident sequences deriving from a small leakage in the blanket cooling system. The frequency of this IE is estimated at 0.2/yr.[4-1] The relatively large frequency is what makes this event and the corresponding aggravating failures important to study. Figure B-2 and Figure B-3 represent the influence diagram/event tree model for accident sequences deriving from LBV1.

As described in Chapter 1, ITER is a pulsed machine with pulse duration of 1000 seconds, and nominal repetition time of 2200 seconds. We assume that the IE occurs during a plasma pulse, while the plasma is producing nominal fusion power.

A very small breach may be choked up by the freezing of the liquid water due to absorption of the latent heat of evaporation from itself, and ingress stops. We assume that the breach is not that

[1] Only six initiating events will be analyzed in this chapter, the rest will be attached Appendix A. The reason is that the construction of our probabilistic model is based only on these six events, eventually allowing for the inclusion of the others. However, this last part is outside the scope of the present study.

small. Due to the water ingress, the plasma disrupts almost immediately, and fusion reaction is shutdown.

The expected sequence developing from LBV1 is as follows:

- the water ingress into the VV causes a plasma shutdown by disruption;
- disruption causes runaway electrons and electromagnetic loads that challenge the integrity of the plasma facing components and corresponding PHTS loops, as well as the integrity of diagnostics windows; the electromagnetic loads might also cause the failure of the VV;
- the pressure rises in the VV;
- chemical reactions of water/steam with PFC metal produce hydrogen.

The safety functions which are challenged by the events following LBV1 are:

1. **decay heat removal**: The global decay heat at the time of shutdown is 20 MW (1.33% of the nominal fusion power of 1.5 GW), and it decreases to 1.2 MW after one week.[4-2, 4-3] There is no dedicated decay heat removal system, instead ITER uses its many normal operation cooling systems to remove heat. LBV1 means damage to one of those systems, which degrades the decay removal function. However, most of the safety burden is on the vacuum vessel cooling system, which has natural circulation capability and is divided into two fully independent loops with 100% capacity. Furthermore, we assume that the amount of radioactive inventories mobilized from the plasma facing components depends on the success of the coolant systems operation.
2. **overpressure relief**: Following the water ingress inside the VV, evaporation is caused by two effects: the PHTS water temperature is greater than the water saturation temperature at the pressure inside the VV (initially vacuum); water impinging on the PFC walls evaporates because the wall is hot. Pressure in the VV increases with evaporation up to the saturation value of the water temperature. Experimental results [4-4] show that the VV pressurization rate increases proportionally with the water injection pressure. The vacuum vessel has rupture disks set to open when the vacuum vessel pressure exceeds 0.2 MPa. The rupture disks will burst and vent steam to the relief tank where it is condensed. The vacuum vessel is designed for 0.5 MPa and calculations show that, although 0.2 MPa could be exceeded because of finite blowdown capacity, 0.5 MPa is sufficient even for an in-vessel LOCA with a total break size > 0.5 m^2 involving all first wall coolant systems.[4-3]
3. **bypass isolation**: There are hundreds of windows for plasma diagnostics between the vacuum vessel and the diagnostic lines. We consider three possible causes for windows break: run-away electron damage or electromagnetic loads following the disruption, overpressure caused by water ingress in the plasma chamber. A window integrity loss may lead to two undesired consequences: bypass of both the VV and CV directly into the diagnostics room, and air ingress into the VV. However, we give credit for the closure of active isolation valves providing the secondary confinement by assuming that there is a probability that the leak is detected and isolated before RI bypasses the confinement barriers.

4. **first barrier of radioactivity confinement**: The first confinement barrier consists of VV and all the PHTSs boundary (piping and systems). Since the leakage from PFC PHTSs is inside the VV, although the first confinement barrier has been broken (FW/SB PHTS), the radioactive inventories (RI) are still inside the first barrier. Therefore, the first confinement barriers whose performance is of interest is the VV, the plasma facing components and diagnostic windows.[2] The plasma disruption caused by the water ingress can damage the PFCs (first wall and divertor) as well as the diagnostics windows via two mechanisms: runaway electron damage and induced currents and loads.[3] Structural failure of the VV is possible due to: induced currents and loads in conducting structures [4-6], failure of the overpressure suppression system, or hydrogen explosion/detonation.

We defined conditional probabilities that, given a disruption induced by LBV1, FW, DIV, and diagnostics windows are damaged by RAE and/or by electromagnetic loads. The integrity of the plasma facing components directly affects the operation of the cooling systems, which should fulfill their decay heat removal function. Moreover, a PHTS loop has an independent probability of failure since it has active components that might happen to fail due to other causes which are not included in these accident sequences. The independent probabilities as well as the conditional probabilities of failure for the FW PHTS and DIV PHTS were calculated using a fault tree approach. Common cause failures were included. The success criterion of a PHTS refers to the successful removal of the decay heat, since the fusion power has been terminated by disruption. The fault tree for the calculation of the probability of failure of DIV PHTS is given in Figure B-1. We assume that the FW/SB PHTS damaged loop fails its heat removal function, therefore we question only the operation of the other three loops. The success of VV PHTS is given by the operation of at least one of the two loops, and we assume that the VV PHTS is not affected directly by LBV1 (only independent probability considered).

The vacuum pumps should have an isolation systems which should be activated when the plasma disrupts. If the isolation is not successful, the tritium in the cryogenic panels will become mobilized in the VV and will add to the rest of RI available inside the VV.

Another safety concern following from LBV1 is the hydrogen explosion hazard in the vacuum vessel. Three ingredients are necessary for a detonation[4] to occur: hydrogen and oxygen in the appropriate mixtures, and an ignition source. Generally, direct initiation of hydrogen-air mixtures is possible with about 1 gram of high explosive, equivalent to about 4 kJ of energy.[4-23] Since the plasma typically contains much higher levels of stored energy, it should be assumed that a point

---

[2] We separate windows from VV because a windows failure has the potential to lead to bypass of both VV and CV.

[3] The LBV1 sequences developed in ESECS do not consider the disruption effects on plasma facing components and windows integrity. Their argument is that those effects are covered in the ex-vessel LOCA analysis, but that initiating event has much lower frequency, and therefore the corresponding accident sequences will have lower frequencies.

[4] A detonation is defined as a flame front that is supersonic relative to the burned gas flowing toward the unburned gas. There is a significant increase in pressure as the front passes a stationary observer.[5-22]

ignition source is always present during normal operation and wall conditioning. The factors determining the likelihood of the detonation are then the availability of hydrogen isotopes and oxygen.

There are several sources of hydrogen in the ITER torus, including leakage of hydrogen isotopes from plasma fueling systems or discharge cleaning systems; dissociation of water leaking onto hot reactive metals (e.g., beryllium), and reaction of water leaking into hot graphite. Hydrogen isotopes are present in the solid matrix of the plasma facing components at substantial levels. This is not ordinarily available for combustion or detonation although a portion (including tritium) may be released if a detonation occurs. Since hot plasma facing components and the vacuum vessel are cooled with water, a leak could result in the generation of hydrogen from chemical reactions of water/steam with beryllium, graphite or tungsten.

Be-steam reactions and the subsequent H_2 production is a major concern for ITER safety. Be-water (and Be-air) reactions are exothermic:

$$Be + H_2O = BeO + H_2 + Q \qquad \text{(B-1)}$$

with $Q = 377\ kJ/g-mole$ of Be reacted with water

To develop into self sustained reactions the energy release by the chemical reaction needs to be larger than the energy removed from the plasma facing beryllium. This border line between both regimes presents a typical cliff edge effect: if self-sustained reactions develop, the amount of hydrogen produced will become very large (> 100 kg); if thermal relaxation is fast enough the amount of hydrogen produced will be negligible.

The reaction rates are strong functions of the temperature (thus, the PHTSs operation, especially the VV PHTS, is very important) and pressure (thus, the rupture disk successful opening is important), as well as the physical condition of the beryllium. The exothermic character of the Be-steam reactions leads to the possibility of self-sustained Be-steam reactions (beryllium fire).

Although endothermic and therefore not prone to self-sustained reactions, steam-graphite reactions would also lead to potential hazardous H_2 production. An air ingress might lead to potential self-sustained graphite air reactions but several studies have shown that for the temperature ranges expected for ITER such a scenario is not credible.

The tungsten-steam reaction for first wall/divertor coating of tungsten is not of concern.

Oxygen in the ITER torus would probably come from one of two sources: air entering through a broke component (e.g., pipe, window or bellows) or dissociation of water by hot metal or graphite. Dissociation of water is not a significant source of oxygen because reactive materials are also strong reduction agents, and will getter (react with) all the oxygen.

The flammability limit for H_2-O_2 reactions is about 10 kg inside the vacuum vessel, and 100 kg inside the cryostat. Detonation limits are about a factor 2.5 larger.[4-22]

An example of a sequence of events leading to detonation in the ITER vacuum vessel is as follows:

1. with the torus at its operating pressure of 10^{-6} torr, water leaks into the torus impinging on the hot plasma facing components;
2. a steam-beryllium (or graphite) reaction occurs;
3. either the resulting overpressure in the torus causes the torus to vent to atmosphere, or water on a hot component (e.g., window or pipe) causes structural failure and admits air into the torus;
4. the vacuum port gate valves close;
5. mixing of reactants and air occurs on the cooled side, away from the hot initiating source;
6. reactants contact the initiating source and detonation occurs.

From this sequence, it is evident that two events are necessary before a detonation can occur: a water leak followed by a vent to atmosphere. Note that these are not necessarily independent failures, since an initial water leak could lead to a vent to atmosphere. A time delay in ignition of the fuel-air mixture is required for a full-blown detonation; without such a delay, there could be multiple point ignition resulting in less violent events such as deflagration or graphite fires.[4-22]

We assume that the failure probabilities of the plasma diagnostic system and the plasma mitigation systems (fueling: gas puffing and pellet injector, heating/current drive, magnets) are low enough so that these events are not considered. Their introduction in the event sequences would lead to very low probability sequences which are BDBA ($< 10^{-8}$).

Relative to the consequences in term of radioactive releases out of the first confinement barrier, if a PFC is damaged, all the RI in that PFC PHTS loop will enter VV. The RIs in the PFCs may become mobilized depending on the temperature of that PFC; in turn, the temperature depends on the success of the PHTSs operation. All these RIs, which may become mobilized inside the VV, could get outside the first confinement barrier through different ways: leak through the VV walls cracks when the VV structural integrity is lost (electromagnetic loads or overpressure), bypass of both VV and CV via a diagnostics line when a window integrity is lost, and, the most undesirable of all: a hydrogen explosion/deflagration causing extensive damage to the VV.

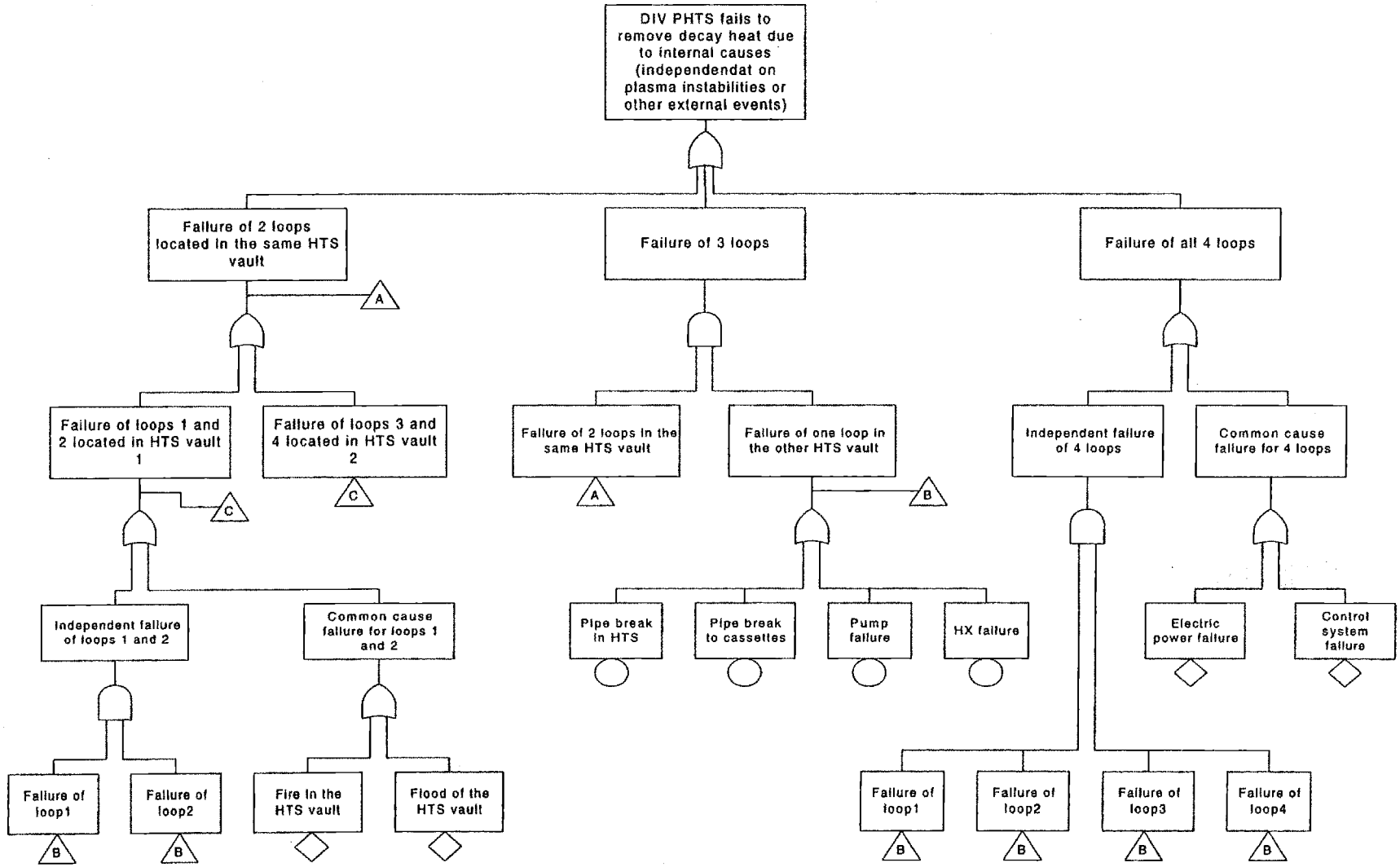

Figure B-1: Fault Tree for DIV PHTS Failure

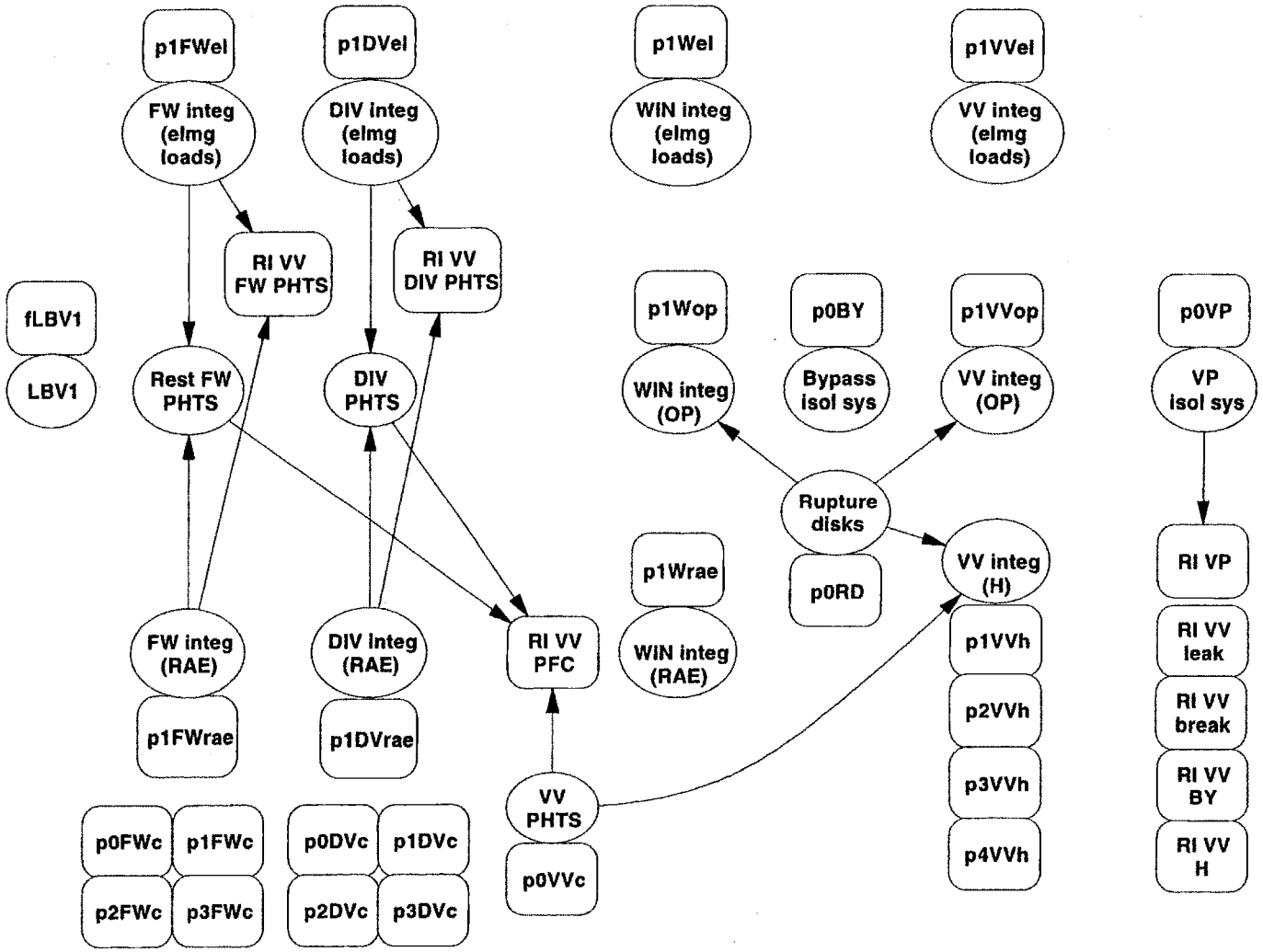

Figure B-2: Influence Diagram for the Initiating Event LBV1

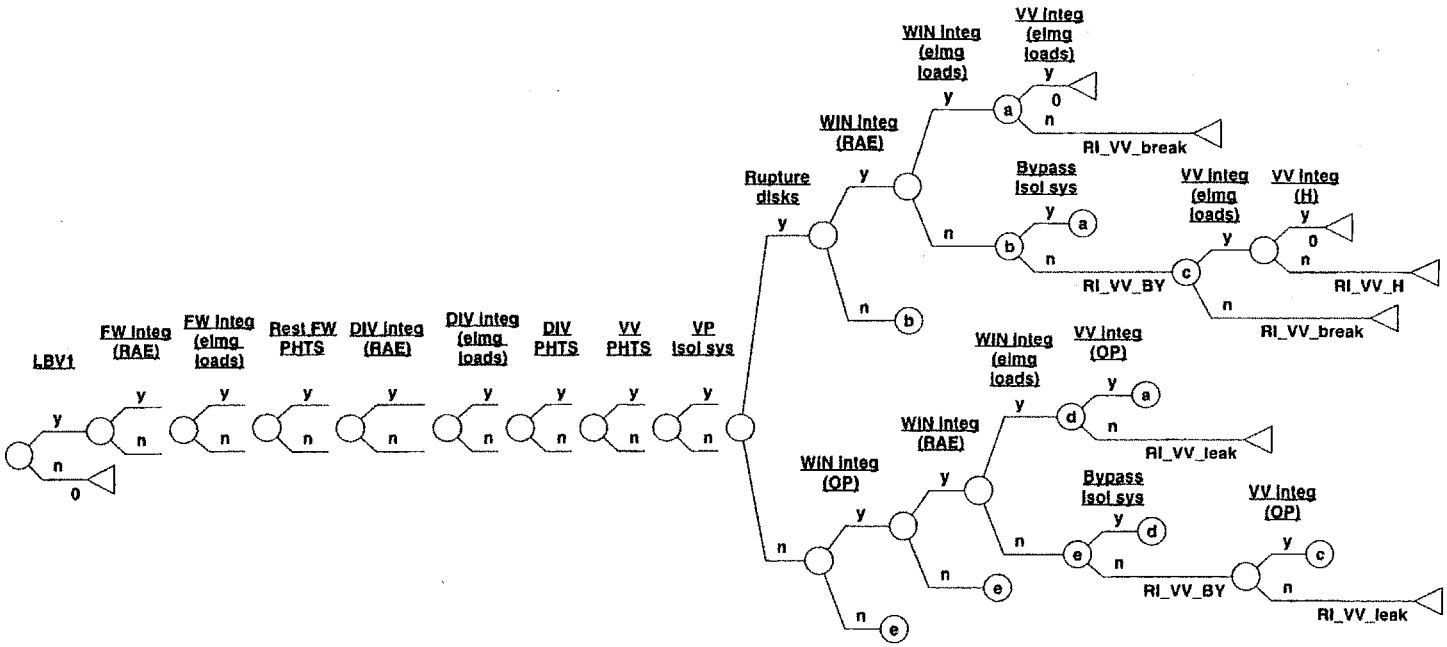

Figure B-3: Event Tree for the Initiating Event LBV1

B.1.2 LDO1: Ex-vessel LOCA in the divertor coolant loop

The IE is a rupture of a divertor primary coolant pipe inside the pipe guard or HTS vault. Figures B-4 and 4-5 represent the ID/ET model for the accident sequences following LDO1.

The pressure in the vault rises until the setpoint for venting is reached (0.17 MPa). In the current design, the initial pressure is released via a filter-vent system directly to the stack. ESECS notes that this initial relief path will be closed, and subsequent venting will occur into a pressure suppression tank and filter system. However, at the beginning of the sequence, releases of RI from the broken loop go directly to the environment. A pressure relief tank designed to suppress the initial and subsequent bursts is a better solution from a safety point of view, even if its price is higher. A decision regarding this matter is still pending.

For the purpose of this section, which estimates the frequency histogram of releases out of the first barrier, the RI in the DIV coolant of the broken loop will be considered first. The in-vessel part of the divertor in that loop becomes then the first confinement barrier.

Since the divertor is exposed to high heat load, the plasma must be rapidly shut down to avoid overheating and burn through the divertor coolant channels. Different loop parameters (e.g. pressure, flow) are suitable for detecting the accident conditions and to ask for a safety plasma shutdown. Without shutdown, the cooling channels of the divertor plate will reach a temperature value of 1000°C in about 3 seconds (and 2000°C in about 10 seconds). It should be noted that the conditions for the divertor are different than for FW due to the large heat loads. That leads to much shorter time scales to reach melting temperature. Therefore, we assume that, if safety shutdown fails, divertor surface melts with 100% probability, causing a plasma disruption by water ingress. On the other hand, also due to the short time, by the time in-vessel LOCA from the damaged loop occurs, there will still be a large amount of water in the loop.

The most challenged function in the case of LDO1 is the **fast plasma shutdown**. The fusion power termination systems are described in [4-5]. The safety shutdown system is one of several defense layers for active plasma shutdown. An interlock system is included for machine protection in cases where the normal plasma control function fails. The safety shutdown system backs up the normal plasma control and interlock systems. This shutdown system has a target unavailability of 10^{-2}/demand. The required time to shutdown in order to prevent the in-vessel component melting vary in the range 10-100 seconds, but for high heat flux components (divertor, baffle, limiters) the time could be of the order of a few seconds. Since the divertor temperature rises so fast after a LDO1, the safety shutdown system will be challenged.

We make the assumption that the divertor surface does not fail (melting or structural failure due to thermal stresses) when the safety shutdown is successful. This is based on thermohydraulic transient analysis that has shown that fast thermal relaxation occurs after melting of copper.[4-7] That is the result of the residual cooling capacity of the broken loop, which is sufficient to cool down the hot

structures.[5] The VV PHTS operation is also desirable but its probability of failure is so low that the sequence is beyond the design basis accident (BDBA).

What makes LDO1 interesting is that the ex-vessel LOCA might be followed by an in-vessel LOCA from the same DIV loop. This sequence creates a bypass of both VV and CV, and all the RI available inside the VV can go directly to the HTS vault. This situation can be aggravated by the ingress of air into the VV once the broken loop is depleted. The conditions for hydrogen explosion/deflagration are then in place: hydrogen from Be-steam reaction and air.

The water ingress into the VV challenges **the pressure relief function**. If the rupture disks (RD) fail to open at their setting point, VV might fail structurally leading to leaks into the CV or diagnostics room (if windows break). Note that here we do not separate between leakage coming from the VV walls or windows.[6]

The initial in-vessel LOCA from the damaged DIV loop is a small one, but it causes a disruption which may lead to an extended in-vessel LOCA (caused by RAE or electromagnetic loads to the PFCs). In terms of probability, these damages condition the operation of the PFCs PHTSs. In terms of consequences, they condition the values of RI from the water coolant into the plasma chamber. In turn, the operation of the PFCs PHTSs, as well as VV PHTS, determine the amount of RI mobilized from the PFCs into the VV.

We assume that the independent failure of VV has a very small probability, so it leads to a BDBA sequence. Thus, we will consider only the failure modes of the VV which can be caused by this particular IE:

1. VV might fail due to electromagnetic loads following a disruption;
2. VV might fail due to overpressure following in-vessel LOCA in the case RD fails;
3. VV might fail due to hydrogen deflagration/explosion following in-vessel LOCA and air ingress.

---

[5] ESECS considers that, even if fast plasma shutdown is triggered, there is a real possibility that the in-vessel divertor channels will undergo damage. It is not clear if the term 'triggered' means 'successful operation', or it might be the case that the signal went through, but without the desired response.

[6] In the LBV1 case, we differentiated between them because the windows failure leads to air ingress into the VV via a bypass sequence.

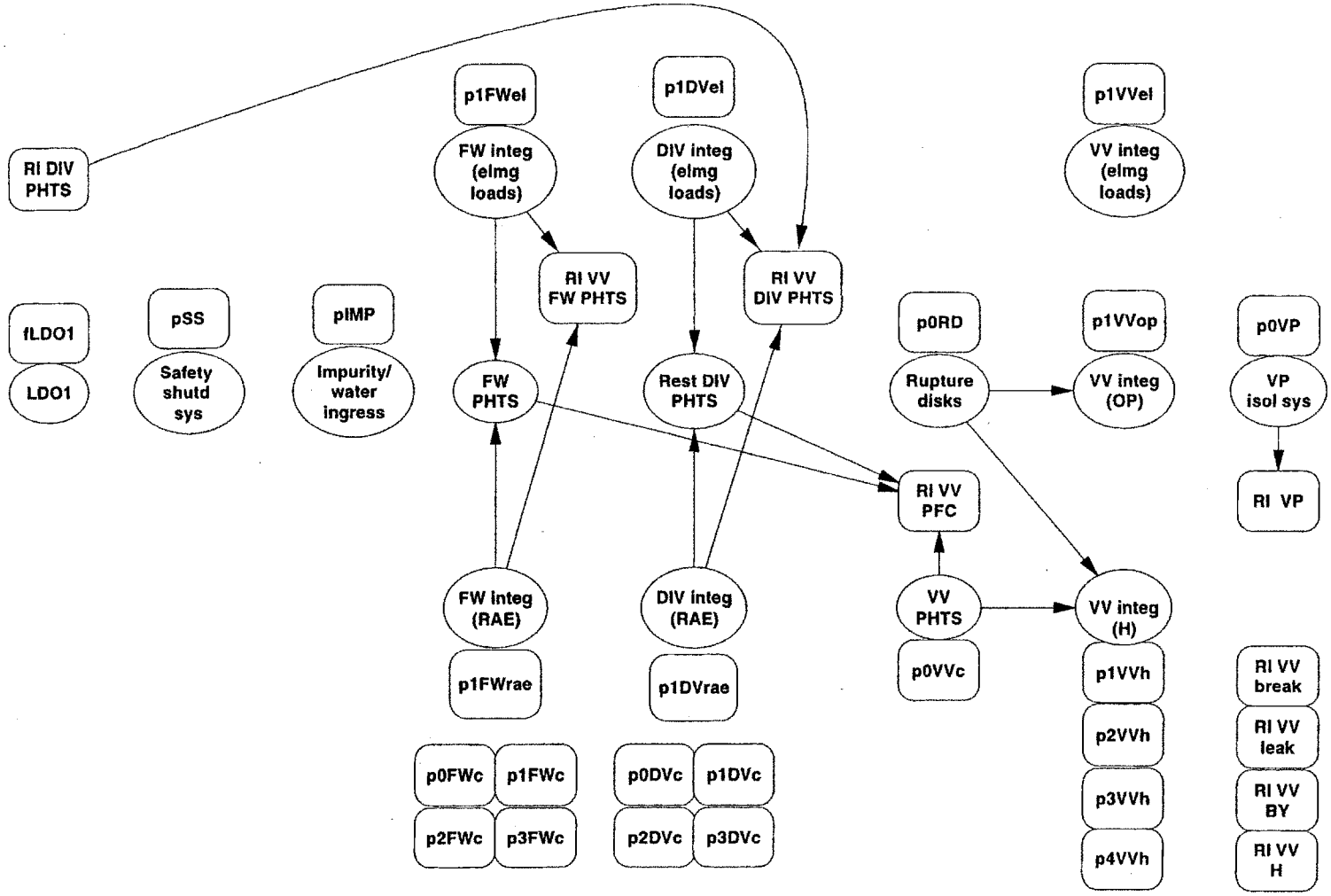

Figure B-4: Influence Diagram for the Initiating Event LDO1

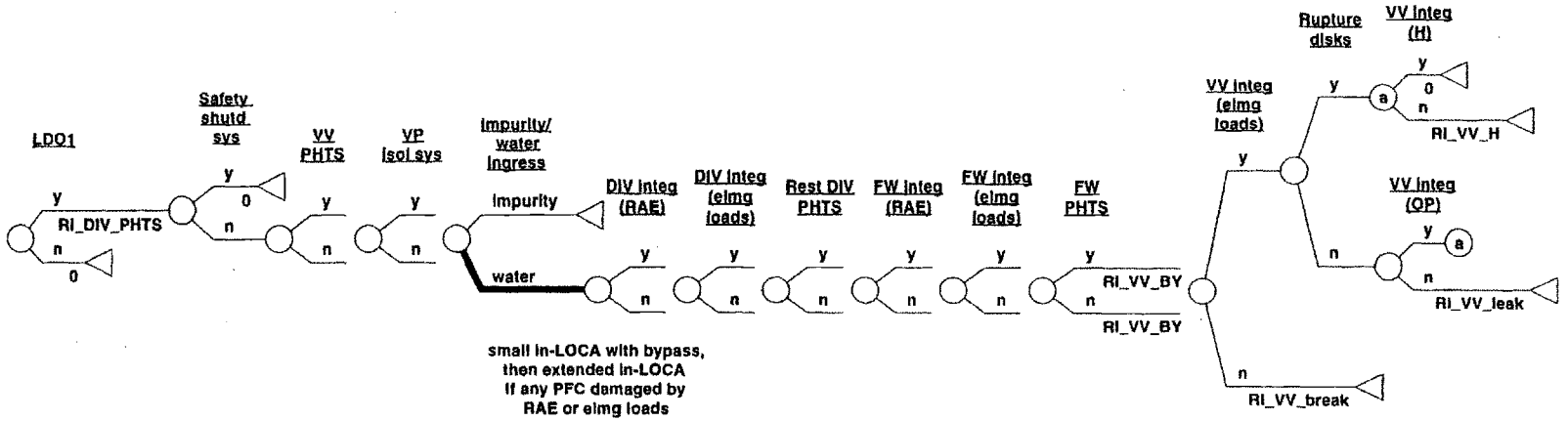

Figure B-5: Event Tree for the Initiating Event LDO1

B.1.3 LFO3: Heat exchanger tube rupture in a FW/SB coolant loop

The IE represents the rupture of a tube in a primary heat exchanger. The ID/ET model is shown in Figures B-6 and 4-7. It is anticipated that the first wall (baffle and limiters) and divertor will either have intermediate coolant loops so that no release to the environment would occur, or alternatively, isolation valves must be provided. In the latter case, the affected primary loop must be cooled down so that the rupture can be isolated from the environment by using isolation valves on the secondary loop.[7] The time needed to achieve that is estimated to be around 20 minutes. The **cooldown of the primary loop and the subsequent isolation** represent therefore an important safety function called by LFO3.[8] It is assumed that the tritium and activation products that are blown into the secondary loops before isolation are released to the environment. We will here analyze the case assuming no intermediate loops would be present. The radioactive inventories that leak from the steam generator (SG) of the primary loop are out of the primary confinement barrier.

The **plasma shutdown** is challenged since we need to start cool down of the primary loop as soon as possible in order to be able to isolate the secondary loop. We assume that as long as the plasma is not shutdown, the isolation system does not work. Plasma shutdown makes the cooling of the PHTS loop with the broken SG possible. Hence, the pressure in that PHTS decreases and allows the isolation system to operate. However, the isolation system might fail; causes for this include stuck isolation valves or late detection of leakage. There are many signals that could help detect leakage (monitoring of secondary loop water, pressure indication in the primary loop, level indication in the pressurizer), so that eventually the leak would be detected. The event of SHTS isolation success/failure is in any case conditioned by the cooldown of the primary loop due to the pressure difference of the two loops. After plasma shutdown, decay heat removal (DHR) in the broken loop should be performed by VV PHTS, so the success of SHTS isolation depends on the success of DHR by VV PHTS. In turn, the SHTS isolation conditions determine the amount of coolant which is lost through the SG tube break: SHTS isolation success means only 0.3 g-T is released, while failure means 100 g-T released.

This IE implies lower temperature transients, since only one SG tube is involved as opposed to a large ex-vessel LOCA in the LFO2 case. Thus, it is assumed that when the plasma shutdown system fails, the plasma will be terminated by one of the following causes:

1. FW tubes of the damaged loop will melt, leading to a in-vessel LOCA, disruption, and bypass sequence;

---

[7] The secondary loop is not designed to withstand the primary pressure.

[8] In the ID/ET model of LFO3, we represent this safety function by a single event: 'Secondary HTS (SHTS) Isolation System'. The cooldown of PHTS should therefore be included in the fault tree calculating the probability of failure for SHTS isolation valve.

2. end of the normal fusion pulse - this was not possible in the cases of LDO1 and LFO2 due to faster temperature transients of the PFCs.

We make the following assumptions:

- if plasma shutdown system succeeds immediately after the IE happens, FW surface melting is not an issue (ESECS considers that, even if the plasma shutdown system is successful, there is a risk that the disturbed loop is overheating with resulting damage to the in-vessel part, and consequently a bypass from the vacuum vessel to the environment can result);
- in the case 2 above, FW surface does not melt after the end of the pulse if VV PHTS continues to remove the decay heat.

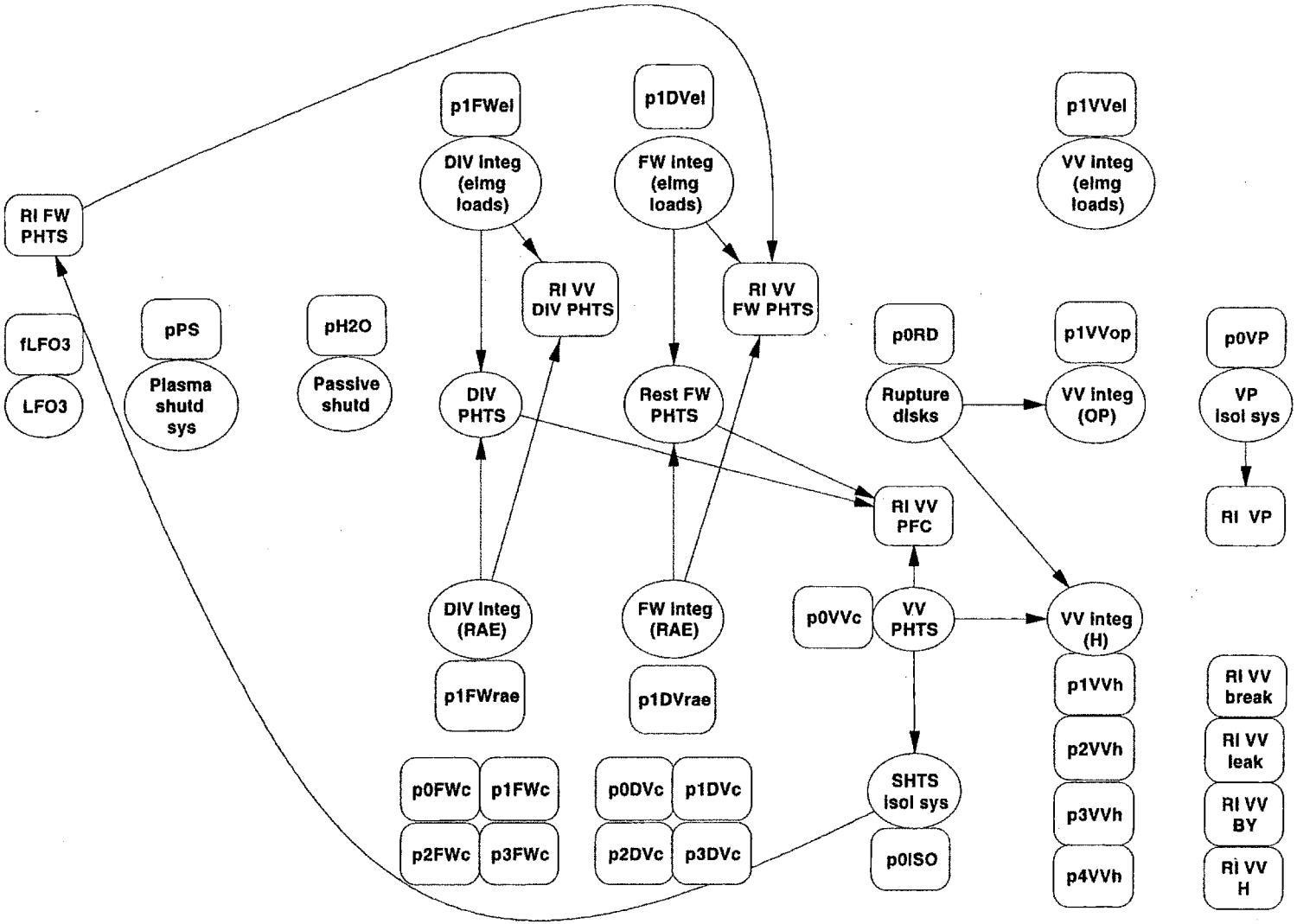

Figure B-6: Influence Diagram for the Initiating Event LFO3

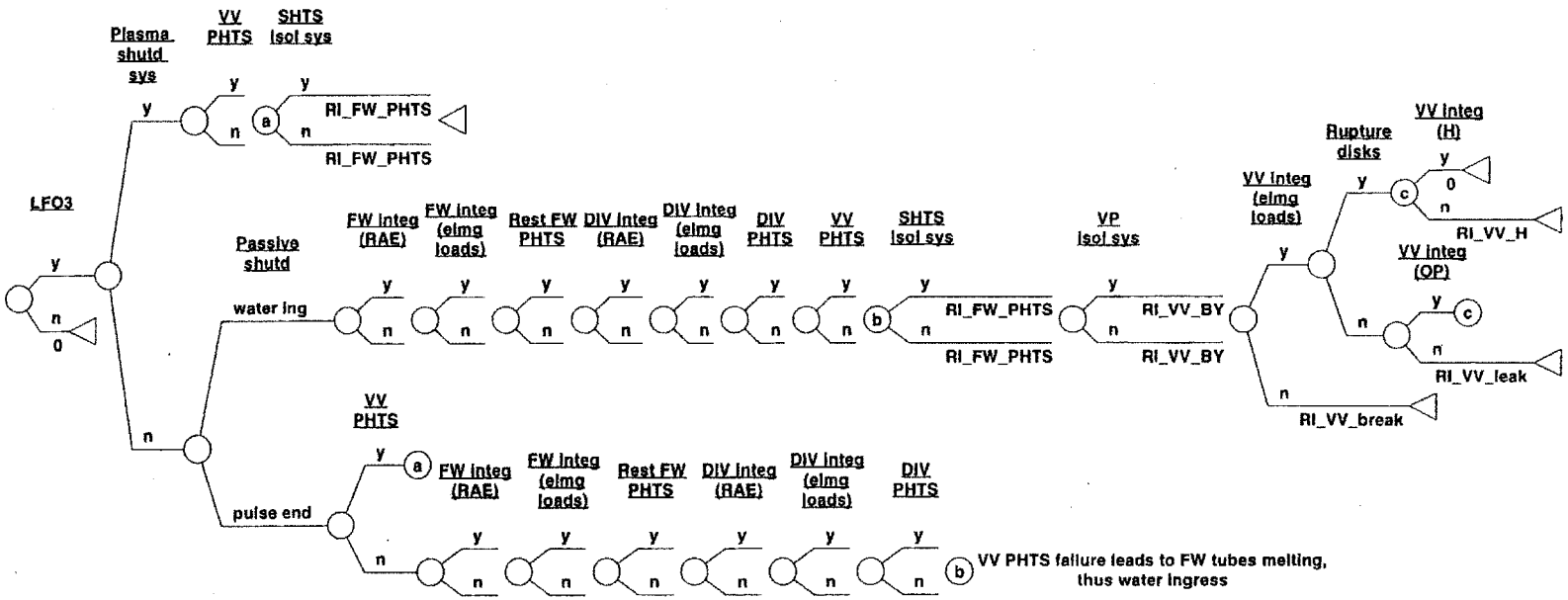

Figure B-7: Event Tree for the Initiating Event LFO3

B.1.4 LFV99: Large in-vessel LOCA from a FW/SB loop

The initiating event is a plasma wall interaction inducing generalized damage to the first wall. The corresponding accident sequences are developed in Figures B-8 and B-9. The underlying causes of such an event could be phenomena like disruptions with a fast decay of plasma current and significant production of runaway electrons, or a vertical displacement episode (VDE). The first wall segments will then leak into the vacuum vessel and the equivalent leak size is of the order of 0.5 m^2 area. The vacuum vessel will rapidly pressurize up to the pressure at which the rupture disks will open and coolant will blow off to the pressure suppression tank.

In the sequences following LFV99, there may be some dependencies between the IE and failure of the coolant systems of DIV and VV. Independent failures are also possible, although of low probability. Examples of dependencies are:

- a leak of the DIV or VV inside the plasma chamber could lead to the described disruption followed by runaway electrons, and thus be the underlying cause (the accident sequences describing this situation are encompassed in the analysis of the IE small in-vessel LOCA followed by an extended in-vessel LOCA);
- the transient following the global damage to the FW is sufficiently violent that subsequent damage to the DIV (RAE or electromagnetic loads) or VV (electromagnetic loads, overpressure, hydrogen deflagration/explosion) cannot be excluded.

From the point of view of the consequences, an immediate effect of the IE is that the RI of all the FW PHTS loops will go into the VV, so that the performance of the **VV as confinement barrier** will become even more important. The performance of the DIV and VV PHTSs has an effect on the temperature of the PFCs and hence on the amount of RI mobilized into the VV.

The **overpressure** shock in the VV could damage the VV walls as well as the windows. If the rupture disks to the suppression pool do not work as designed, VV and/or windows might fail due to overpressure. The result of VV walls failure would be that (part of) the steam would be blown into the cryostat rather than to the pressure suppression pool. Loss of integrity of a window can lead to a bypass of both the VV and the CV directly into a diagnostics room, if the isolation system fails; this also creates an air ingress path, and thus an increased chance of hydrogen deflagration/explosion. However, credit is taken for the case when the bypass is isolated.

In the case that the rupture disk does work, the steam will blow into the suppression tank. Due to the abrupt pressure rise, there is a probability that the suppression tank itself will leak. The pressure suppression tank is actually a sub-component of the VV system, making it part of the first confinement barrier.[4-8]

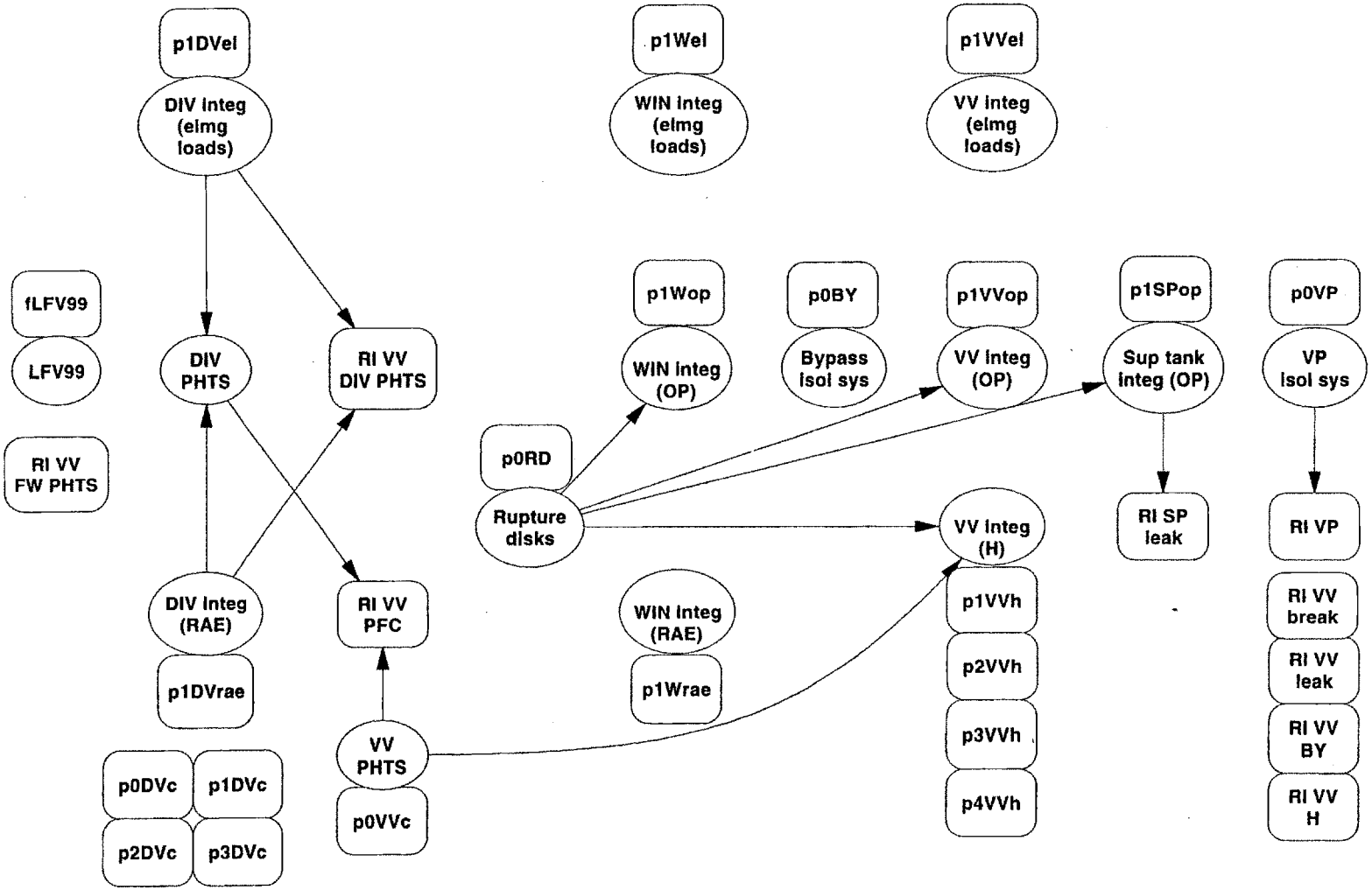

Figure B-8: Influence Diagram for the Initiating Event LFV99

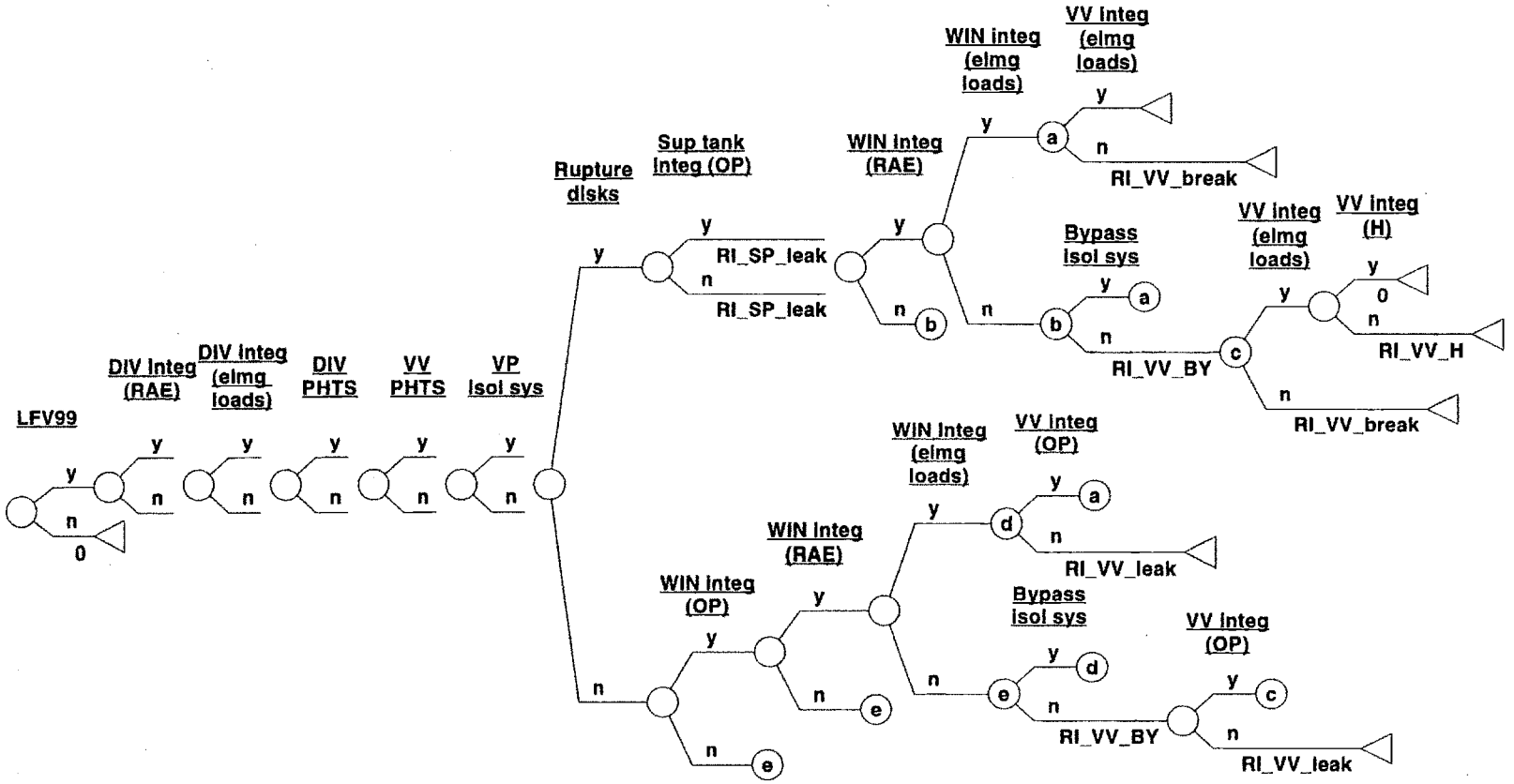

Figure B-9: Event Tree for the Initiating Event LFV99

B.1.5 LGC: Generalized rupture of coolant lines in cryostat

The initiating event is a displacement of the vacuum vessel or of the magnets rupturing multiple coolant lines and their guard pipes inside the cryostat vessel. All active cooling is interrupted and decay heat removal must rely on radiation, conduction and natural convection. The water lost in the cryostat will first freeze on the cold surfaces and the pressure transient will be relatively mild. The loss of the water coolant can happen with or without simultaneous release of cryogenic helium. Figures B-10 and B-11 contain the ID/ET model for this IE.

In this IE, the PFC tubes facing the plasma chamber become the first confinement barrier. That is why the PFC integrity is important. The rapid plasma shutdown is important for the temperature transients, given that all the PHTSs including those of VV are lost.

Even when safety shutdown is successful, there is a probability of melting of the PFCs. PFCs damage creates a bypass path for the RI outside the VV into the CV. We assume that the amount of water ingress into the VV following PFC melting is quite small, so there is no overpressure challenge for the VV. However, there is still a potential for Be-steam reaction that might cause a hydrogen deflagration and affect the VV integrity.

In the case safety shutdown fails, DIV surface will melt with probability 1, due to the high heat load and lack of any active heat transfer.

This IE seems to be the most severe of the coolant accidents from the point of view of consequences, due to the complete loss of active cooling to remove the decay heat.

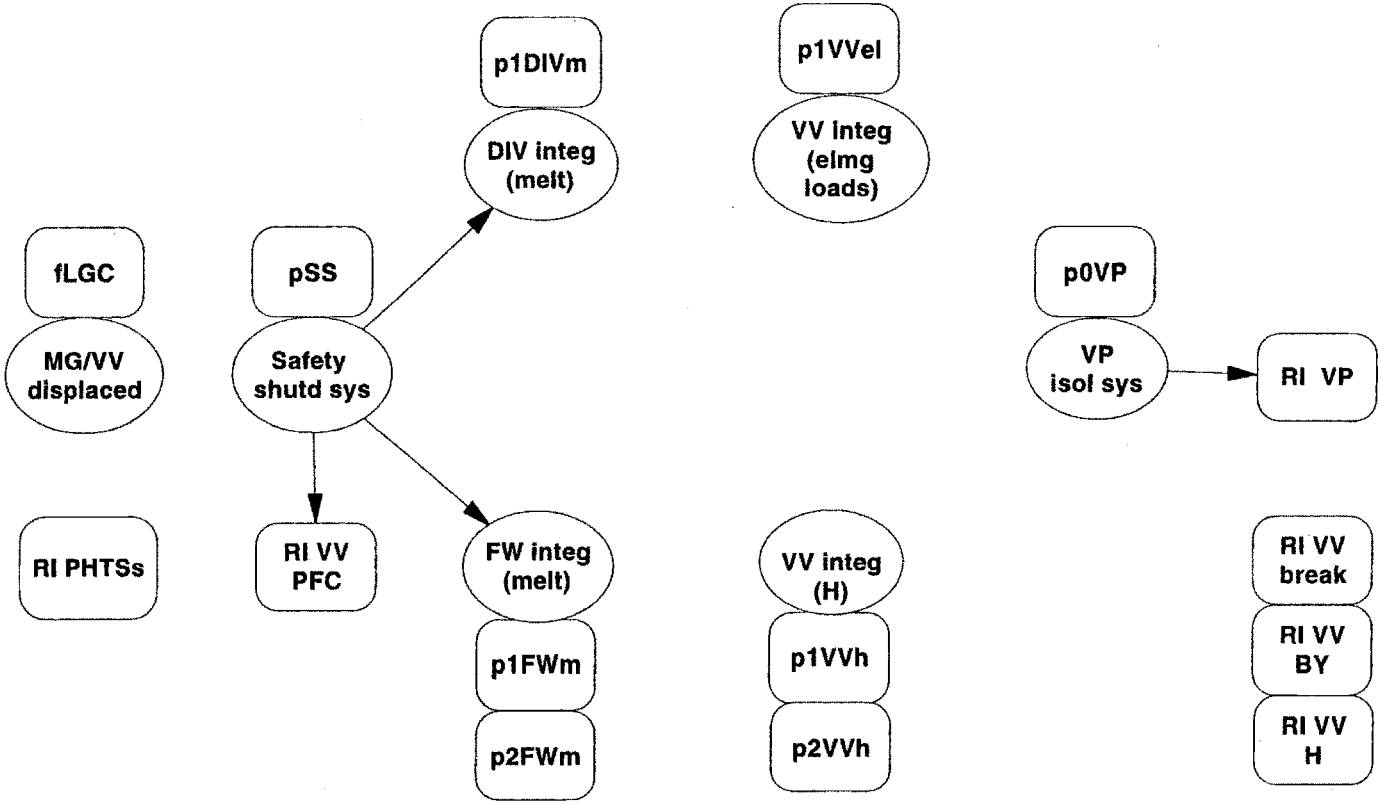

Figure B-10: Influence Diagram for the Initiating Event LGC

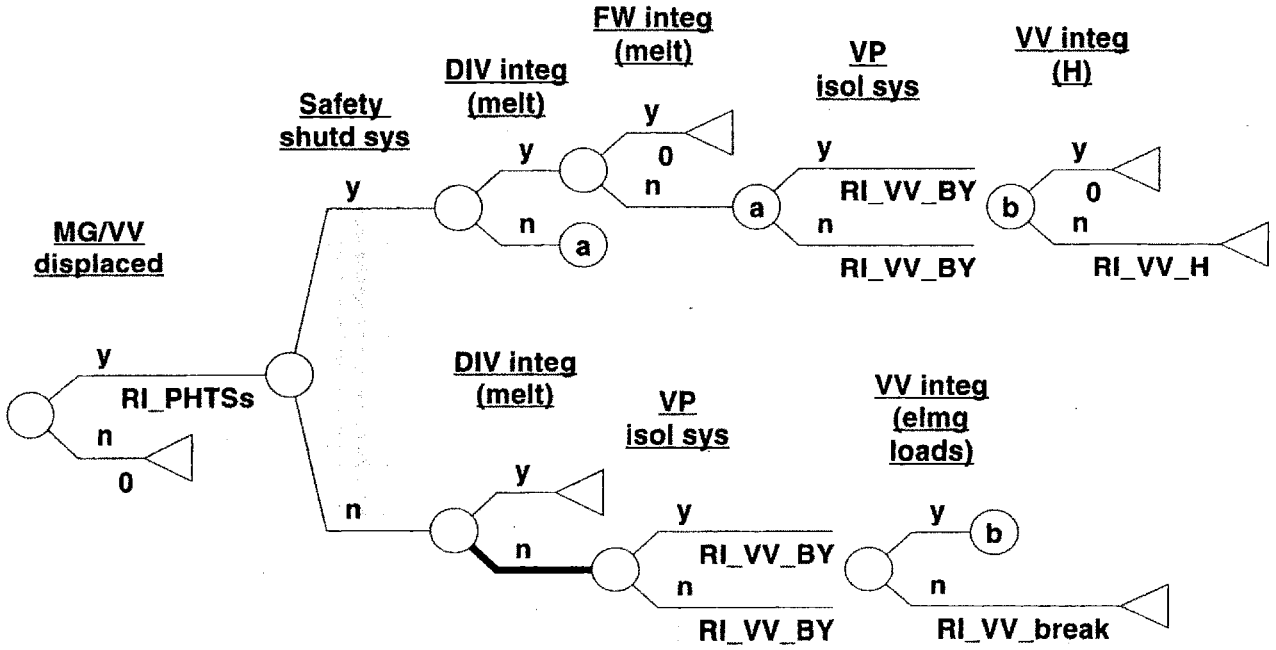

Figure B-11: Event Tree for the Initiating Event LGC

B.1.6 FF2: Loss of flow in a FW/SB coolant loop

FF2 refers to a loss of flow in a FW/SB coolant loop because of pump seizure. A loss of flow in one of the DIV PHTSs loops would have similar consequences. It leads to the increase of the FW and water temperature in the affected loop and possibility of in-vessel LOCA with initial temperature > 200°C. **Plasma shutdown** is a very important safety function to stop the heat flux to the PFCs. One specific problem is the **LOFA detection**. In conclusion, there are two systems whose operation is challenged by LOFA occurrence: LOFA detection system and the plasma shutdown system.

If plasma shutdown is not achieved actively, then the water temperature and pressure rise up to the setpoint of the safety valves on the loop. On the plasma side, the FW surface temperature will increase up to the point where disruption occurs due to either impurity or water ingress.

It is important to separate window performance from VV walls performance, because, if isolation fails, the former can lead to a bypass sequence of both the VV and the CV directly into a diagnostics room with air atmosphere.

When disruption is caused by impurity ingress, and no damage is caused to the PFCs by RAE or electromagnetic loads, VV can only be damaged by the electromagnetic loads. If a window's integrity is lost in that situation, the RI composed from PFC and vacuum pump (VP) inventories (each conditioned by events like PHTSs operation, VP isolation) can get out of the VV via the bypass sequence to a diagnostics room. Failure of PFCs will add the overpressure challenge of VV. Moreover, if air ingress through a damaged window is an issue, there is also a possibility of hydrogen deflagration/explosion in the VV.

The accident sequences are represented in Figures B-12 and B-13.

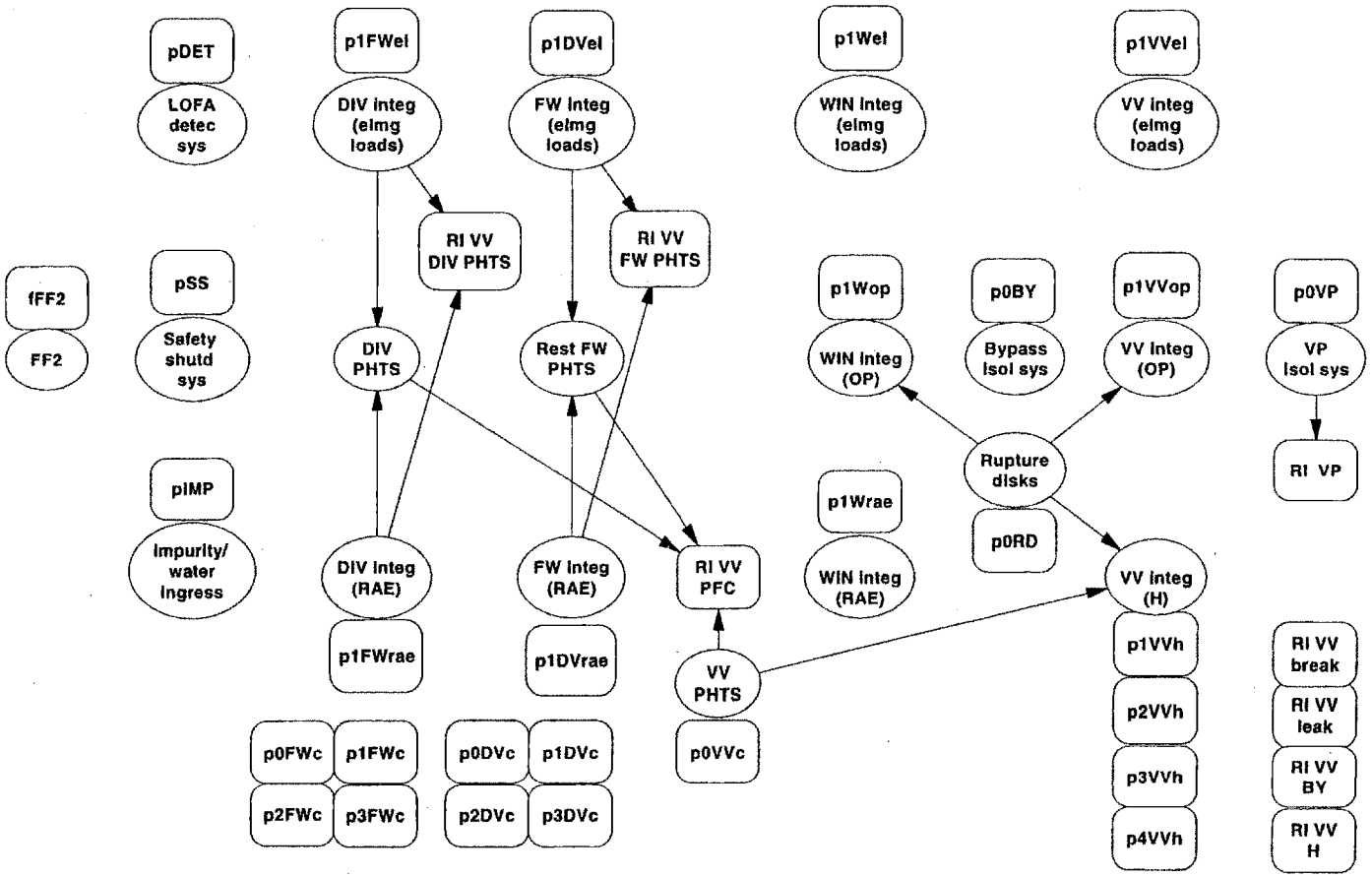

Figure B-12: Influence Diagram for the Initiating Event FF2

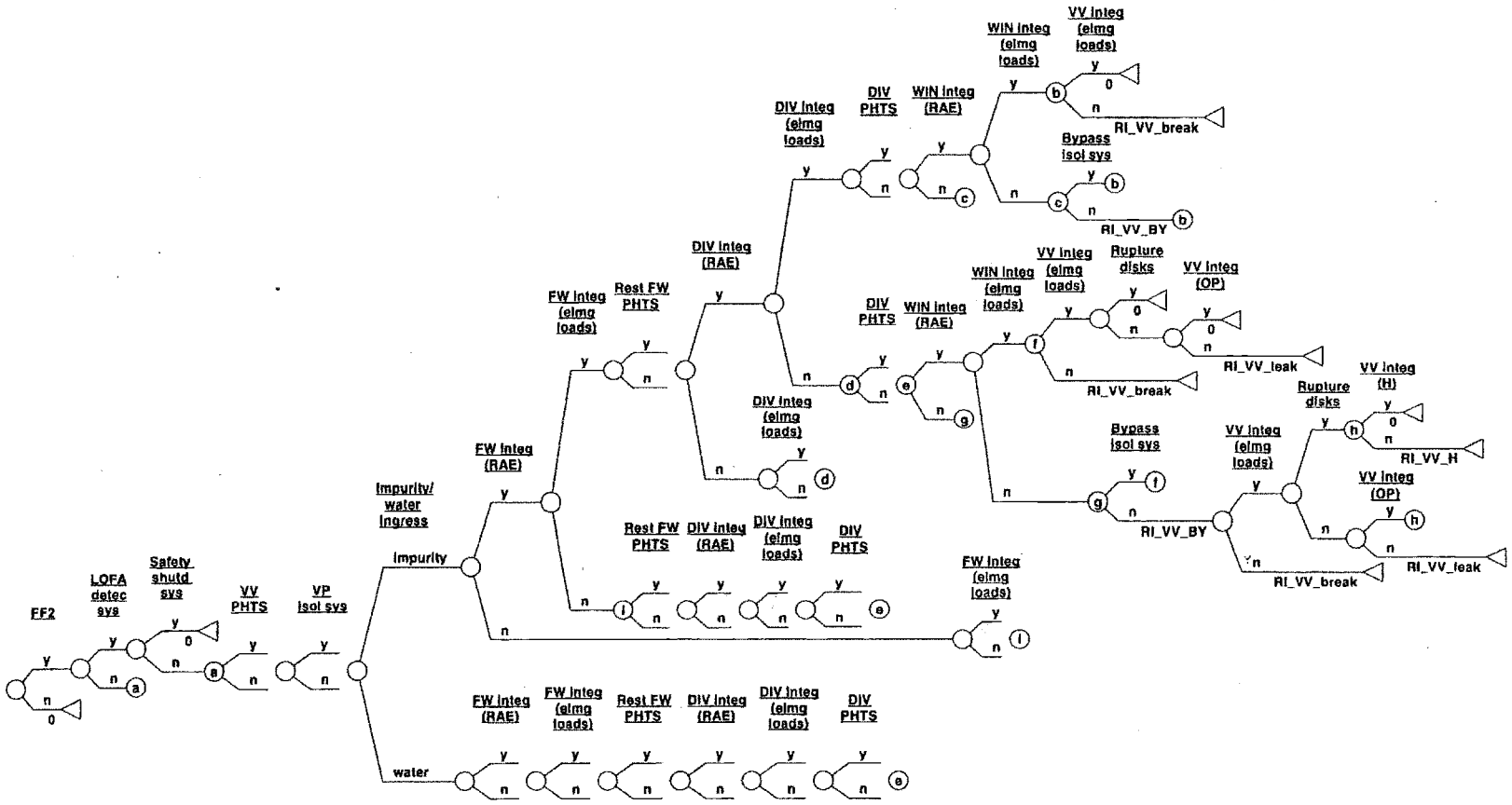

Figure B-13: Event Tree for the Initiating Event FF2

B.1.7 HB99: Loss of heat sink to divertor, blanket, and first wall

It is assumed that the first wall, blanket/shield and divertor will have a common heat sink, and that the vacuum vessel coolant loops will have two independent heat sinks by virtue of their decay heat removal function. A credible event is the ultimate loss of the heat sink system causing loss of heat sink to the first wall, blanket/shield and divertor loops. Figures B-14 and B-15 present the ID/ET model for this IE.

The immediate consequence will be the generalized heat-up of FW/SB and DIV coolants. Thus, pressure will rise, and safety valves on the pressurizers should open. Failure of the safety valves is a possible event, but is probably a beyond design basis accident (BDBA). Combination with no plasma shutdown needs to be investigated.

Loss of heat sink in the divertor is expected to lead to similar sequences as a large ex-vessel LOCA due to the small margin against departure from critical heat flux. Given the large thermal capacity of the cooling water, the time scales involved are rather long. Depending on the acceptable temperature increase inside the primary cooling loops, the time available is in tens of seconds before fusion power shutdown is needed. Without plasma shutdown, 1000 seconds of plasma burn would evaporate about 1100 m^3 of coolant.

Two safety systems are challenged by this IE: **the safety plasma shutdown** and **the safety valves to the PHTS loops pressurizers**. If the safety plasma shutdown works, only the decay heat remains to be removed and the VV PHTS should do that successfully, no matter what happens with the safety valves. If the safety plasma shutdown fails, the plasma power is higher than the VV PHTS heat removal capacity, thus the heat and pressure in PHTSs will raise. If all the safety valves open, the accident sequences are identical to those in ex-vessel LOCA case (PHTSs overpressurization is not an issue). If any of the safety valves fails, that PHTS loop is overpressurized and in- and/or ex-vessel LOCA can occur. Therefore, the probability of water ingress inside the VV is higher in this case. The sequence including ex-vessel LOCA event has a probability of the order of 10^{-8}, which means BDBA, and therefore we do not extend the analysis further.

Remind that the design option studied here is the one with integrated FW/BS PHTSs. The FW/BS and DIV PHTSs each have four loops, and each loop has its own pressurizer. Thus, there is a total of eight safety valves. When calculating the probability that any of the safety valves fails, common cause failures (design, manufacture, maintenance, valves in the same HTS) should be considered. For the present work, we assumed that the valves failures are independent.

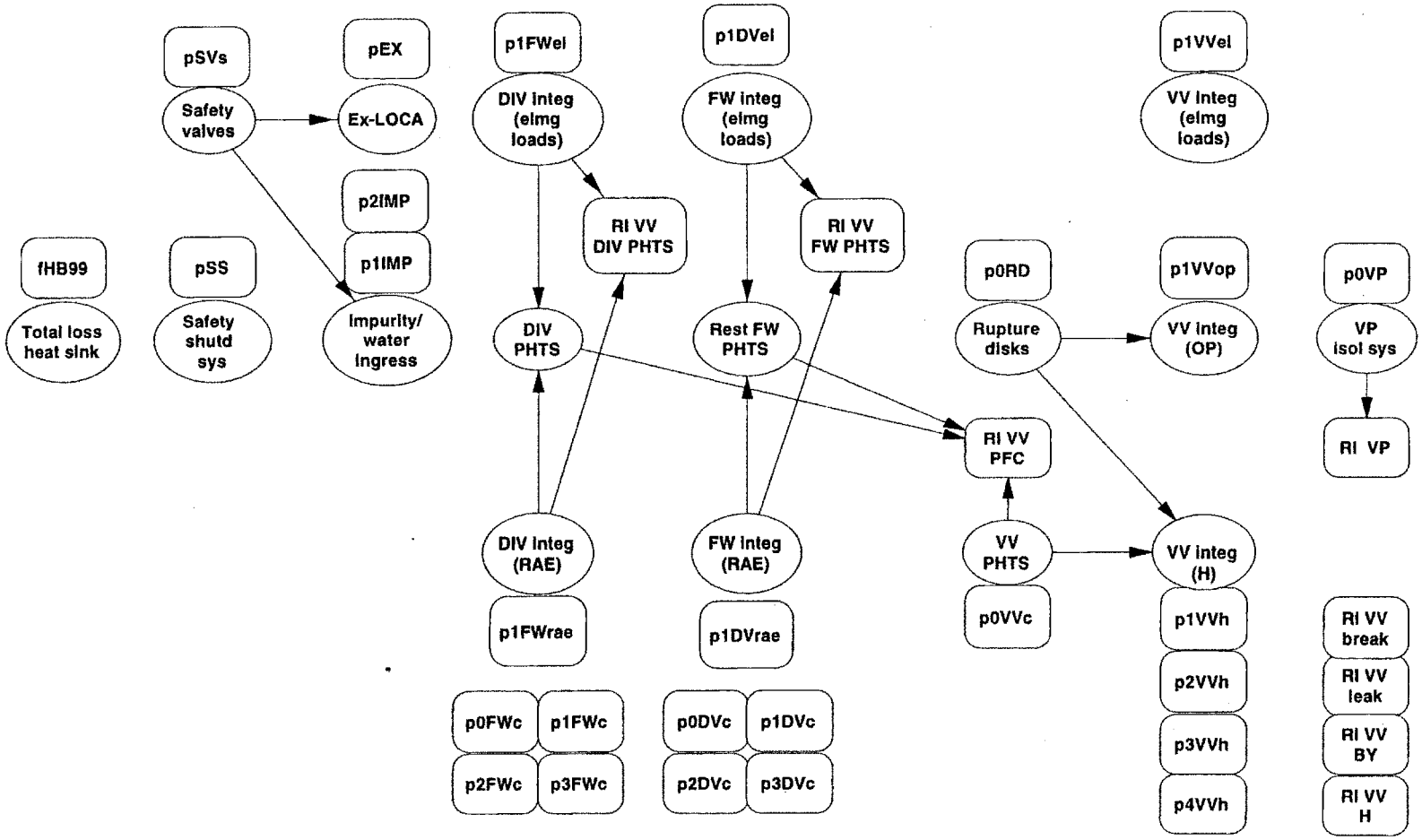

Figure B-14: Influence Diagram for the Initiating Event HB99

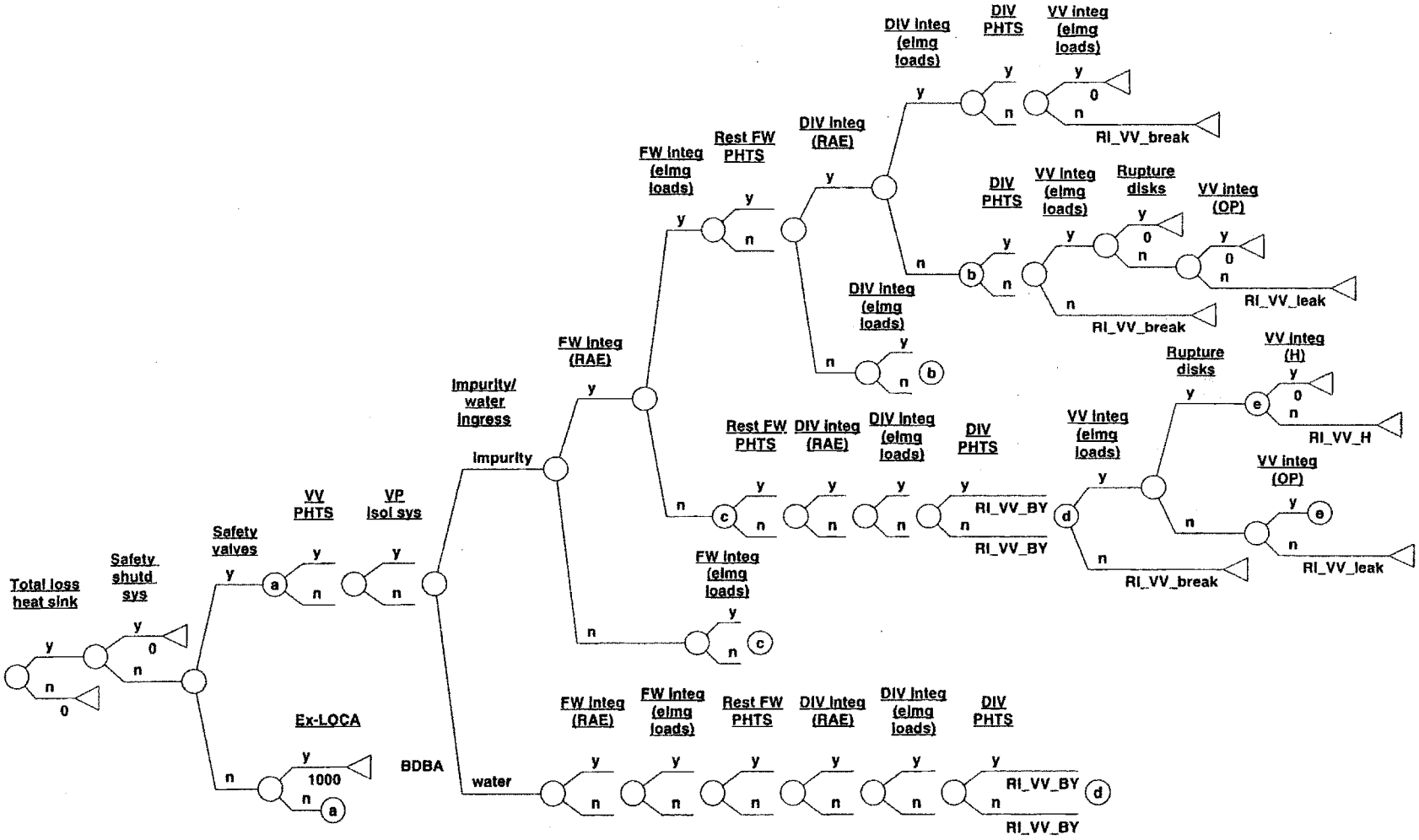

Figure B-15: Event Tree for the Initiating Event HB99

B.2 Magnet Accidents

The magnet systems do not contain any radioactivity by themselves, but they store high amount of energy that has the potential to damage the structures or components that are used for confinement of radioactive inventories. Thus, it is important to understand not only the design and operation of the magnet systems but also the possible interactions of the magnets with all the other tokamak systems.

The literature available so far contain accidents that might happen in magnet systems, but not accident sequences developed to determine the effect on confinement barriers, and that is what we try to do in the present section. Reference [4-9] contains the results of a survey conducted among the majors centers of large magnet development and operation in USA to obtain information on magnet system failure and accident events. It is useful to check the credibility of the sequences developed here against events that happened in reality.

Data about probability of events in the magnet systems is very scarce due to the fact that ITER magnets will be the first superconducting magnets of such large dimensions. Reference [4-10] contains data on probabilities of failure of the magnet systems for NET. Sensitivity analysis on the probability of events can offer more insight into the importance of magnet related events.

The type of damage due to an initiating event occurring in the magnet systems can be categorized as follows:

- Structural damage:
  - ◊ overcurrents in coils cause large in-place forces;
  - ◊ off-normal currents in PF coils result in large vertical forces;
  - ◊ of-normal out-of-plane forces on TF due to exceptional PF currents;
  - ◊ faulted TF coil or faulted TF coil busbars/power supply causes exceptional loads on out-of-plane support structure;
  - ◊ large scale crack failure of TF coil case;
- Thermal damage:
  - ◊ shorts or open circuits causes overheating and arcing on busbars external to cryostat;
  - ◊ distributed heating of winding pack material (jacket and/or plates) from an overcurrent level;
  - ◊ local heating of winding pack material from discharge failure;
  - ◊ local melting or vaporization from short/arc inside a coil;
- Fluid damage:
  - ◊ coil quench after a cryostat loss of vacuum;
  - ◊ cryostat pressure increase after coil helium leak.

The damage from several potential accidents is analyzed to determine if radiological confinement barriers could be affected.

B.2.1 MPO2: CS/PF coil overcurrent

Overcurrent in individual central solenoid (CS) or PF coils, or exceptional combinations of currents in sets of coils can cause off-normal patterns in the out of plane forces on the TF coils. That can overload the support structure or the coil cases themselves. Full assessment of all possible combinations requires extensive calculations with a finite element model to determine the worst PF coil current combinations. ESECS cites preliminary assessment results using the out of plane forces and moments compared to the values in normal operation.[4-1] The PF coil faults have been limited to an increase in current to critical conditions for one coil while the remainder stay at the normal (start of flat top) operating condition. Consistently with the coil overcurrent, the forces increase by up to 80%. In the critical inner leg region, as expected, the CS and PF 2 and 7 faults have the most impact, whereas the outer coils dominate the outer region.

Combinations of current in different CS/PF coils may also create vertical forces on other PF coils. The PF coils are supported onto the TF coils by a link at each coil. These links are sized on the basis of the vertical loads in normal operation: towards the machine (compressive static limit) or away (tensile fatigue limit). An abrupt increase in load by up to a factor of two could cause one of the twenty supports to fail (probably by yielding if an initial crack already extends to a substantial fraction of the area), but simultaneous failure of several supports is seen as a very low probability event.

Reference [4-9] mentions that shorted PF coils were analyzed. The variable current combinations and different mutual inductances mean that a shorted coil, with all other coils discharged at any point in the scenario, only exceeds its maximum operating current by 1 or 2 kA (i.e. up to 45 kA). This does not represent a safety issue and is not considered further.

When the fast discharge systems fail to respond on demand, damage to the magnet systems may occur and can lead to undesired consequences to the confinement barriers.

The development of the accident sequences in terms of effects on confinement barriers for CS/PF coil overcurrent is very similar to the TF coil overcurrent case described in the previous section. The differences between TF and PF systems will cause some components to be more challenged, for instance the torsion cylinder, crown rings' keyways, and PF supports on the TF case. Thus, the probability of damage due to missile generation and coils displacement should be higher.

Figures B-16 and B-17 represent the ID/ET model for MPO2, which includes the accident sequences inside the plasma vacuum chamber.

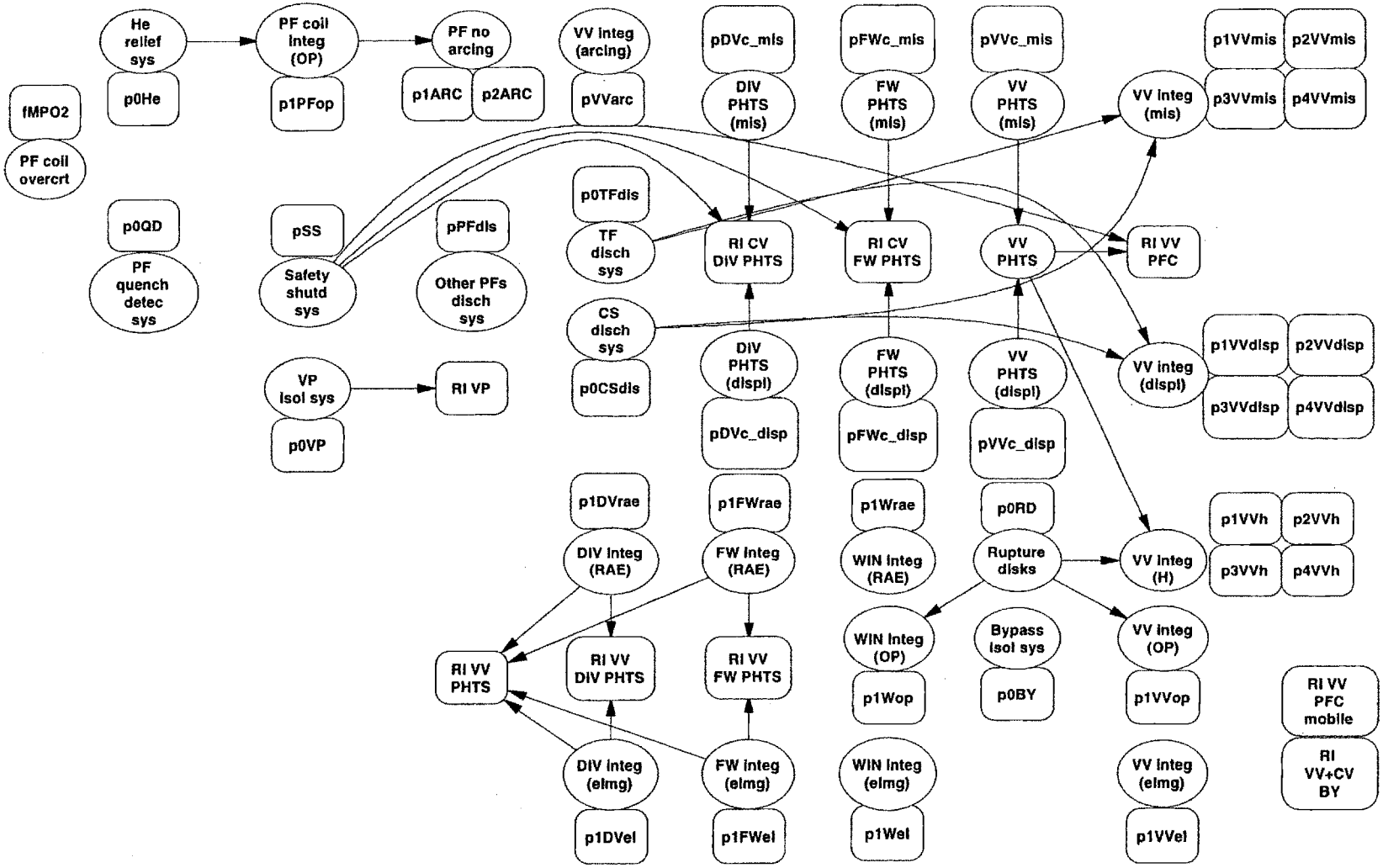

Figure B-16: Influence Diagram for the Initiating Event MPO2

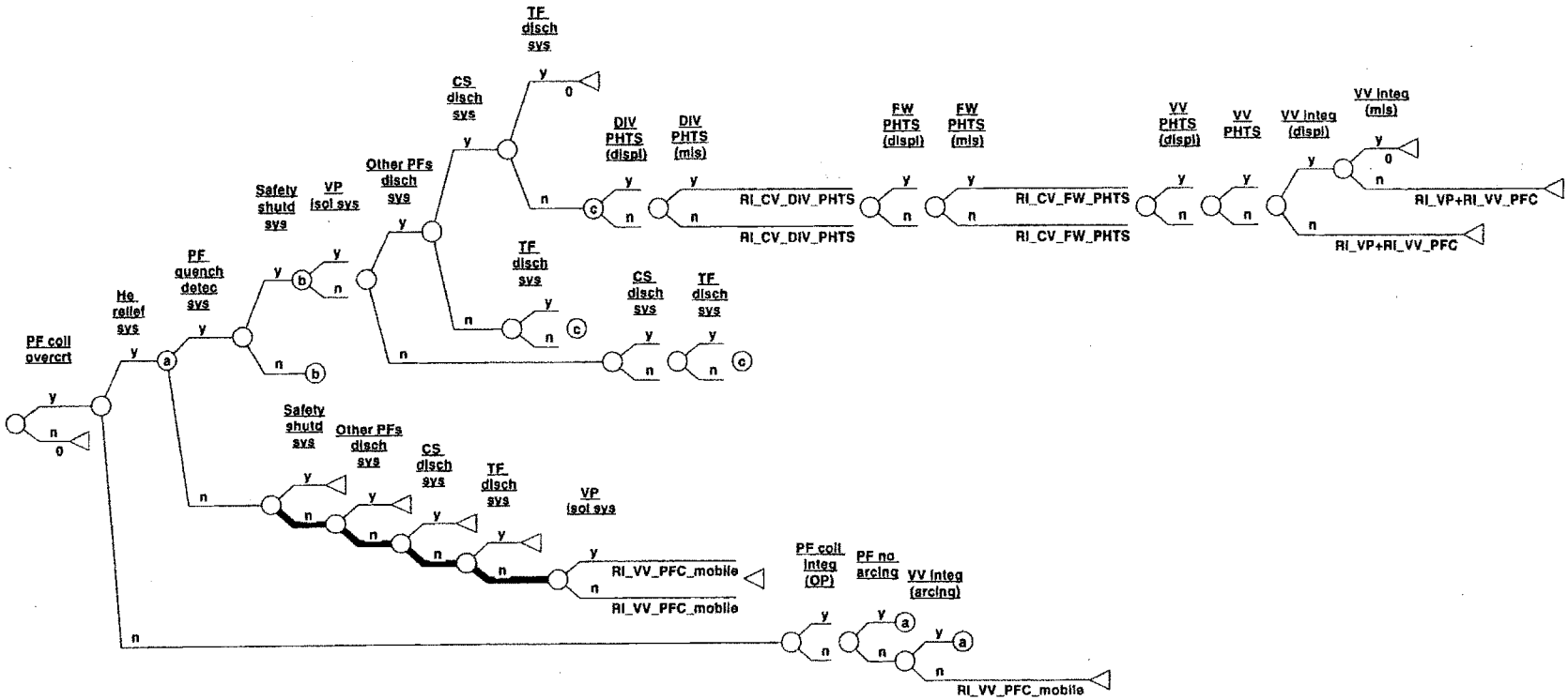

Figure B-17: Event Tree for the Initiating Event MPO2

B.2.2 MS: TF coil case failure from initial defect

A similar accident is described in [4-9]: an initially localized structural failure leads to sequential overloading and fracture of other structural components. The primary cause appears to have been design flaws relative to structural details and the load distribution in localized areas. The conversion of the stored magnetic energy to kinetic energy of the fractured components is a source of missile generation and coils displacement.

The structural material areas in one of the TF coils at the equatorial cross-section are: case 0.37 m^2, jacket and radial plates 0.42 m^2.

Deterministic calculations referred to in ESECS concluded that complete structural failure of the coil cross-section (plates and case) is not possible.[4-1] However, insulation damage, particularly of the ground insulation at the break point, is probable. Current flows at the short are generally restricted by the use of ground resistors, and development of an arc is not likely. The break would probably generate sufficient mechanical heat to quench the coil (thus causing a fast discharge to be initiated) even if the movement due to the break is not detected.

The ID/ET model for MS is shown in Figures B-18 and B-19, and includes the accident sequences inside the plasma vacuum chamber.

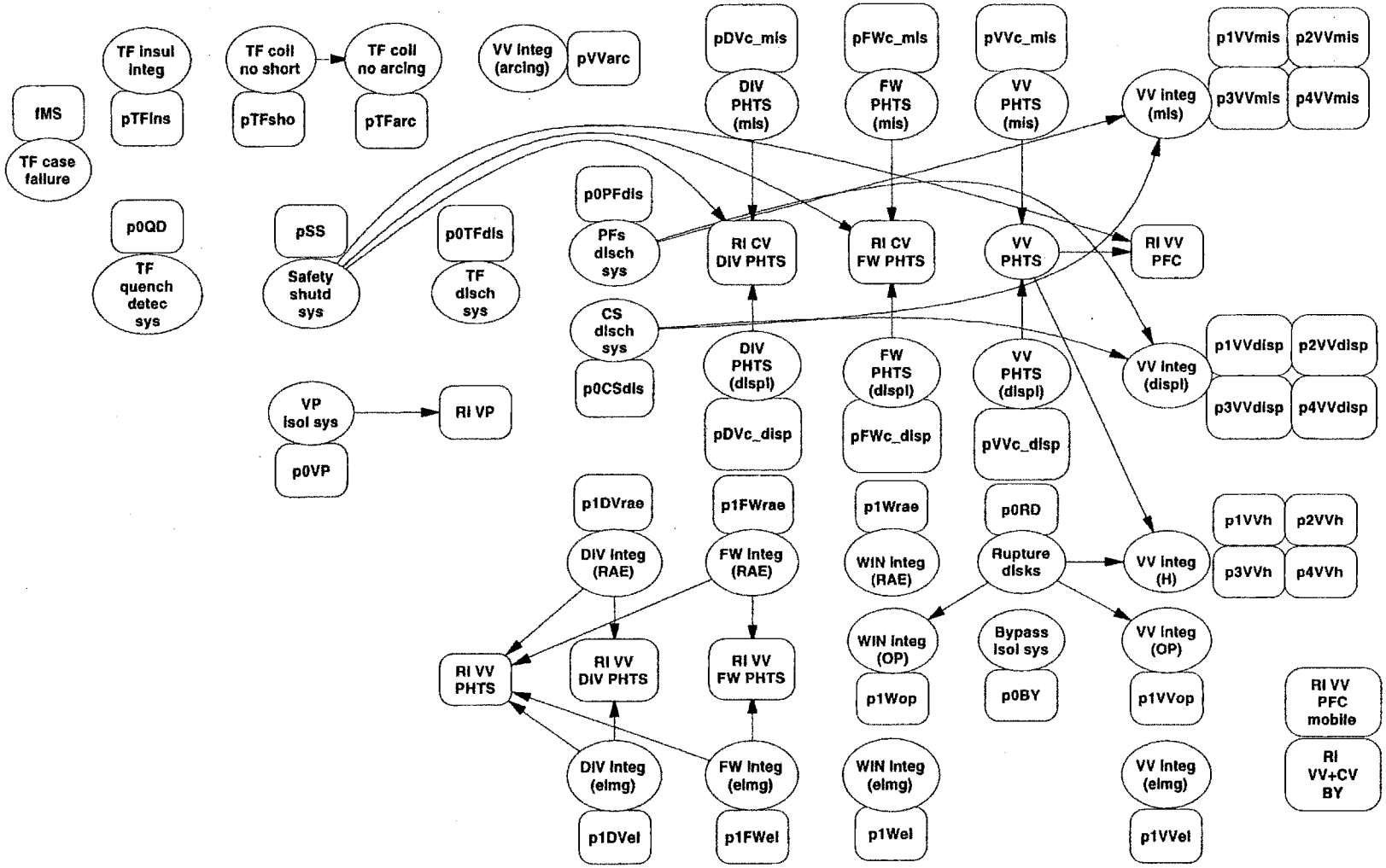

Figure B-18: Influence Diagram for the Initiating Event MS

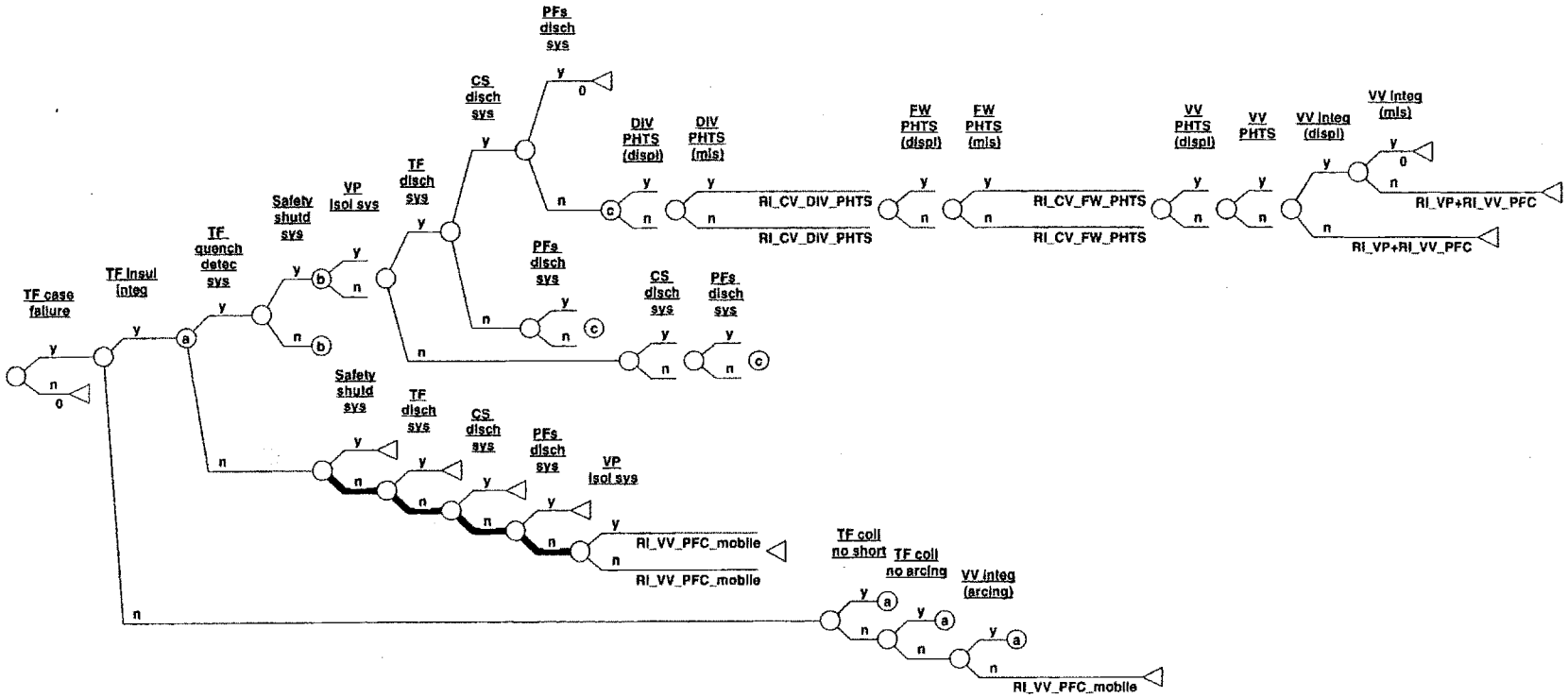

Figure B-19: Event Tree for the Initiating Event MS

B.2.3 MAC: Short between busbars outside the cryostat vessel

Since there is no direct link back to the cryostat (even after several minutes) to cause a coil quench through loss of vacuum, there is the possibility to dissipate almost the whole TF coil energy (100 GJ) at the short. The coils cannot be discharged without driving a substantial fraction of the energy into the shorted coil, probably resulting in the permanent damage of this coil and increasing (at least temporarily) the arc current.

If the fast discharge system fails, off-normal currents and forces create the potential for coil melting, helium release, and arcing. The most significant difference from the previous magnet accidents is the possibility of shorted coil melting which can damage the VV vessel.

Although from the safety viewpoint the coil could withstand these forces, it seems desirable to eliminate the possibility of this fault by ensuring that the two terminals of each coil are widely separated in the busbar runs, preferably in different containments. It is acceptable to pair the terminals of adjacent coils.

The ID/ET model for MAC is shown in Figures B-20 and B-21, and includes the accident sequences inside the plasma vacuum chamber.

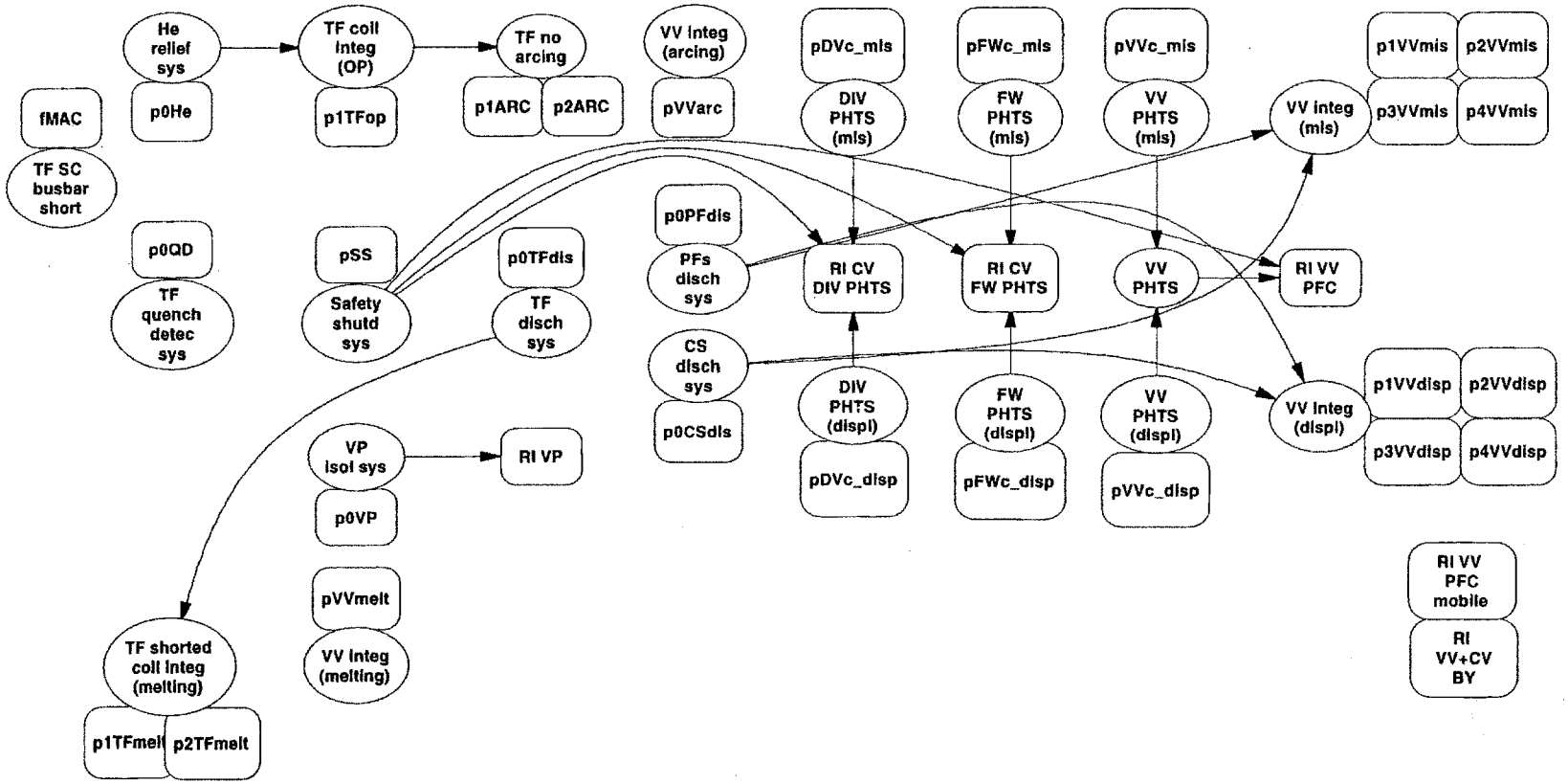

Figure B-20: Influence Diagram for the Initiating Event MAC

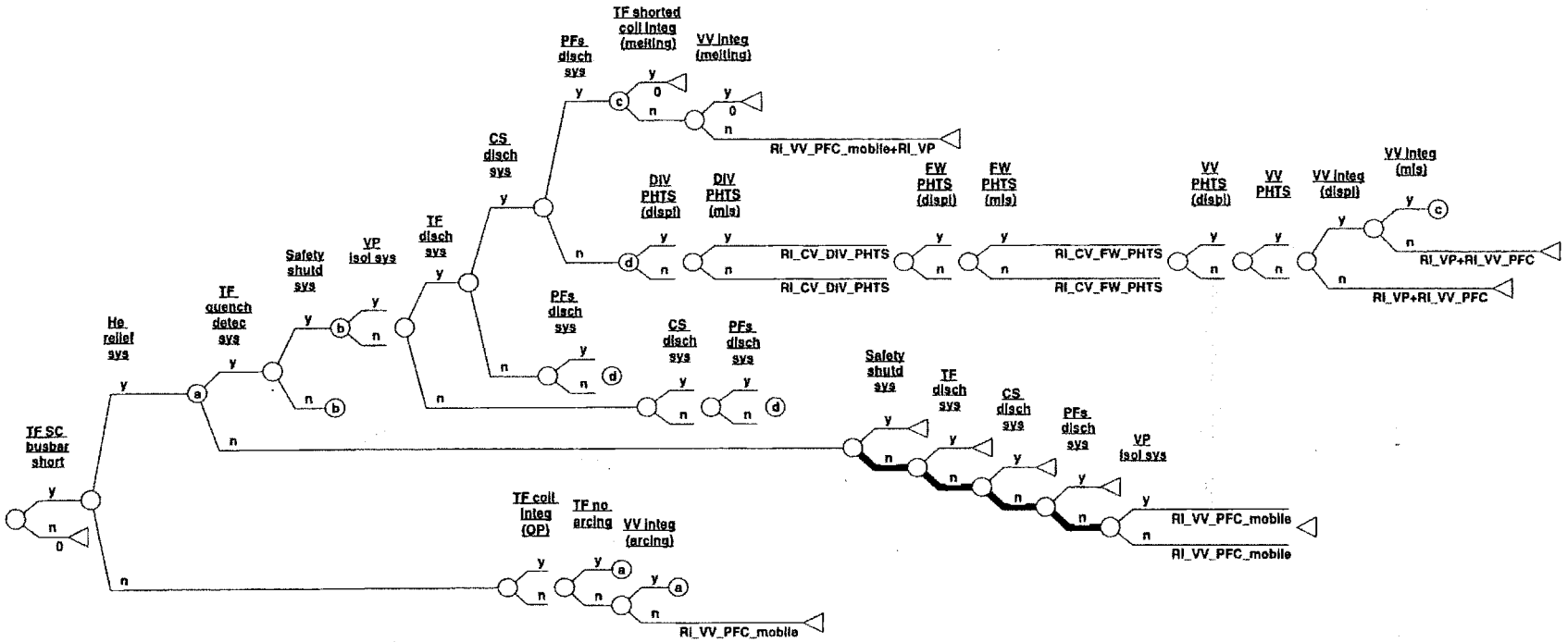

Figure B-21: Event Tree for the Initiating Event MAC

B.2.4 MI: Insulation failure (turn and pancake arcs)

A major source of internal heating is an internal arc. Besides acting as an initiator of a quench, the arc itself can dissipate significant heat in the winding. Internal shorts in coils develop at a rate determined by the external voltage applied to the coil (i.e. from a resistive discharge) and by the propagation of the coil quench initiated by the heat from the short which greatly modifies the coil resistance.

Simultaneously with the initiation of the coil discharge and the development of a coil voltage, current begins to flow in the short. After the shorting piece of metal evaporates, an arc is formed with a voltage drop related to the length, power, and area. The arc voltage has little impact on the initial current build up in the short. The current buildup is determined primarily by the short resistance and the mutual inductance of the shorted loop with the rest of the coil and the self inductance of the shorted loop. The induced current can rise significantly above the critical current leading in the high field zone to an immediate quench. Additionally, the energy of the arc heats the conductor and reduces the critical current. The quench develops as a time dependent resistance in the shorted loop and propagates very rapidly. In less than a second, the resistance forces the short current to decay.

Eventually the short current reaches zero and then, assuming the destruction of the conductor is limited, the short is either evaporated and a gap is formed, or the shorting piece is still there providing a parallel path around the shorted turn. Alternatively, if the arc energy in the area has melted through the conductors, an in-line or bypass arc could develop.

It appears that for all except a narrow range of values for the initial short resistance, the associated conductor quench is sufficiently rapid to give only a limited energy release in the coil, not sufficient to cause significant structural damage. The case of the short resistance that can generate in-line and bypass arcs requires further calculation; the worst case energy release requires many assumptions about the ability of arcs to reignite after the current passes zero. However, even in this worst case, the energy deposition in the coil is less than 50 MJ, still insufficient to cause structural damage.

In the case of the TF coils, the conductor case could contain any helium release from damage to the surface conductors. For the CS and PF, a helium release to the cryostat could occur.

The ID/ET model for MI is shown in Figures B-22 and B-23, and includes the accident sequences inside the plasma vacuum chamber.

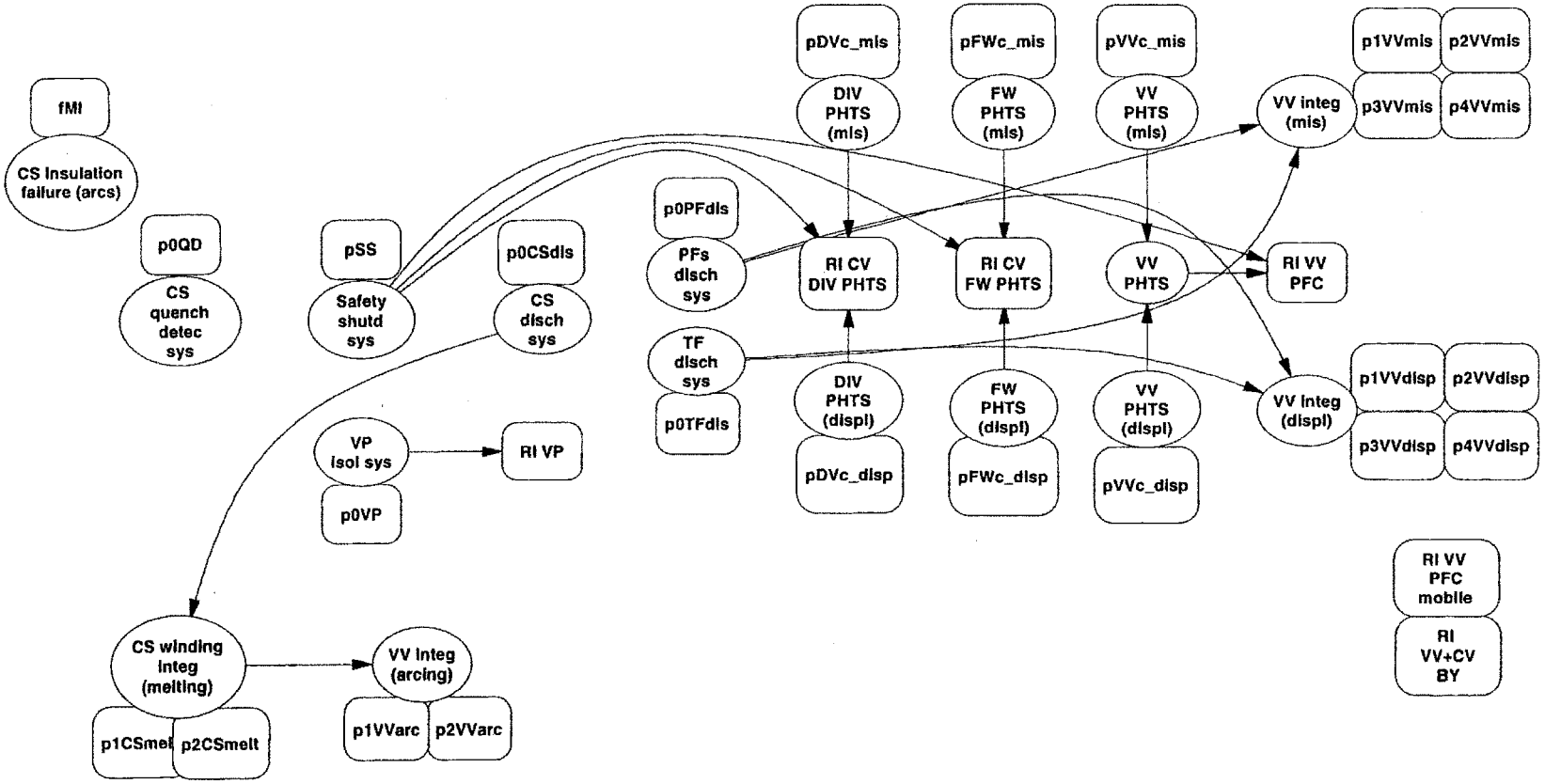

Figure B-22: Influence Diagram for the Initiating Event MI

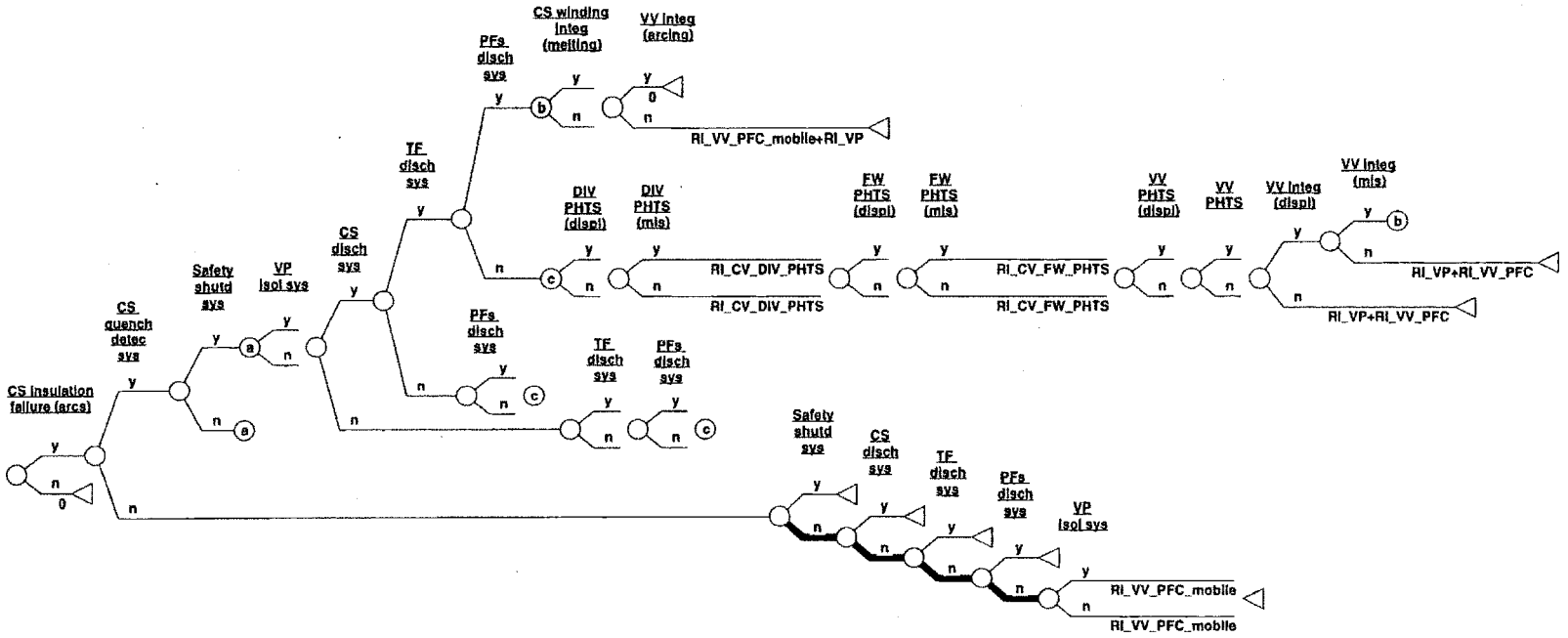

Figure B-23: Event Tree for the Initiating Event MI

B.2.5 MCC1: Cryogen leaks in cryostat

A cryogen release into the cryostat will lead to coil quench and fast discharge, and to cryostat pressurization. The worst case for the cryostat overpressure is the **complete break of the helium lines to all TF coils simultaneously**, with the loss of 96 m^3 of liquid helium. The coils undergo a fast discharge and eddy current heating of the steel in the coils occurs, to about 50 K in 20 s.

The first step of our analysis is concerned with the performance of the first confinement barrier (VV + PHTSs). We will look at the potential of this IE to damage the magnets and furthermore the VV and/or PHTSs. The cryostat pressurization will be studied during the second step concerned with the performance of the second confinement barrier. An emergency atmosphere detritiation system with a capacity of about 5000 m^3/h is foreseen to cope with the pressure transient. Using this system, the cryostat pressure can be brought to atmospheric pressure in about 7 hours.[4-1] In case the detritiation system would not be available for accidents involving cryostat pressurization, a relief line with rupture disks venting directly to the stack is foreseen. The helium is not causing any significant concern from the radiological releases point of view.

The ID/ET model for MCC1 is shown in Figures B-24 and B-25, and includes the effects on the PHTSs, but it does not include the disruption model on the three branches indicated.

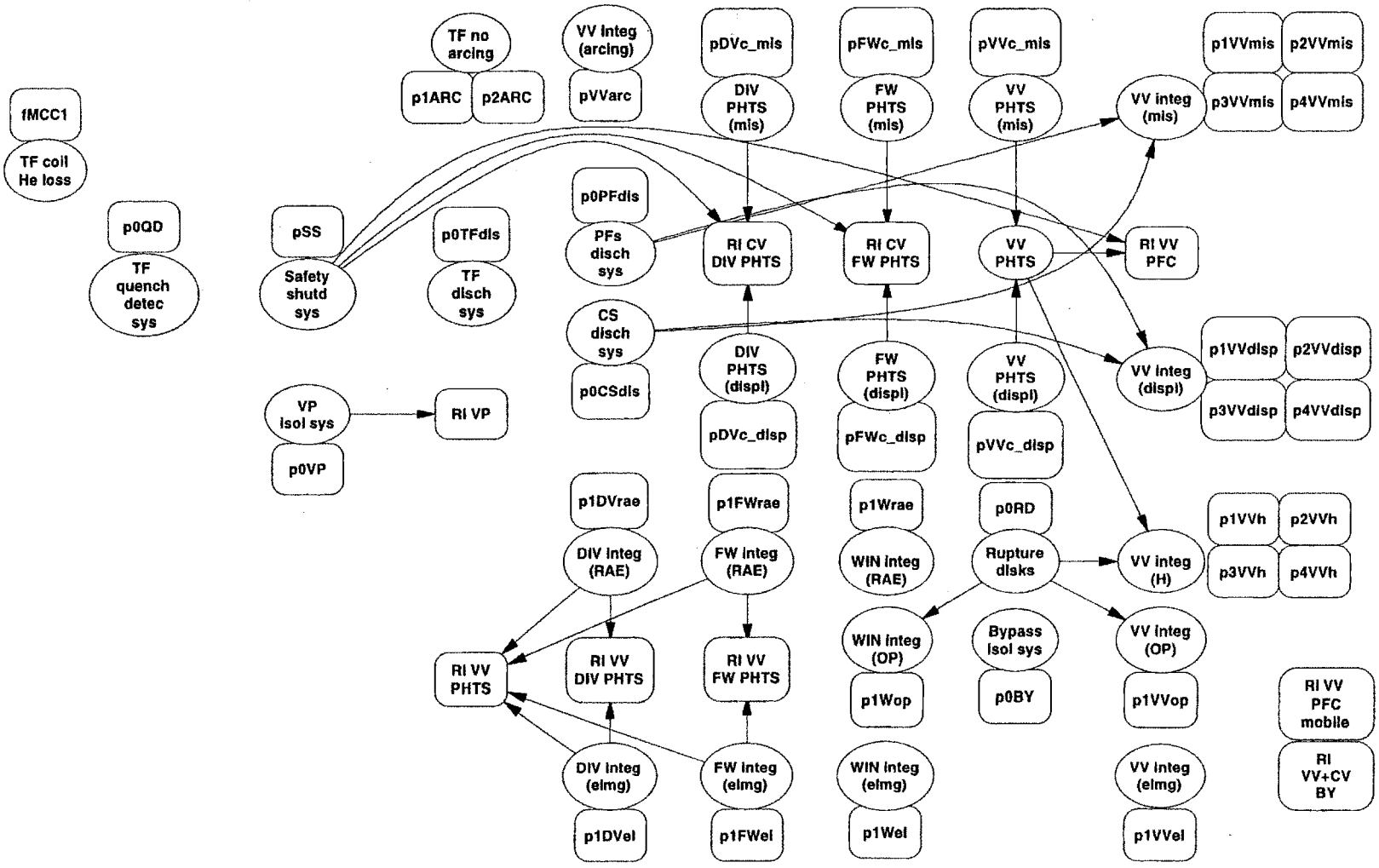

Figure B-24: Influence Diagram for the Initiating Event MCC1 without Disruption

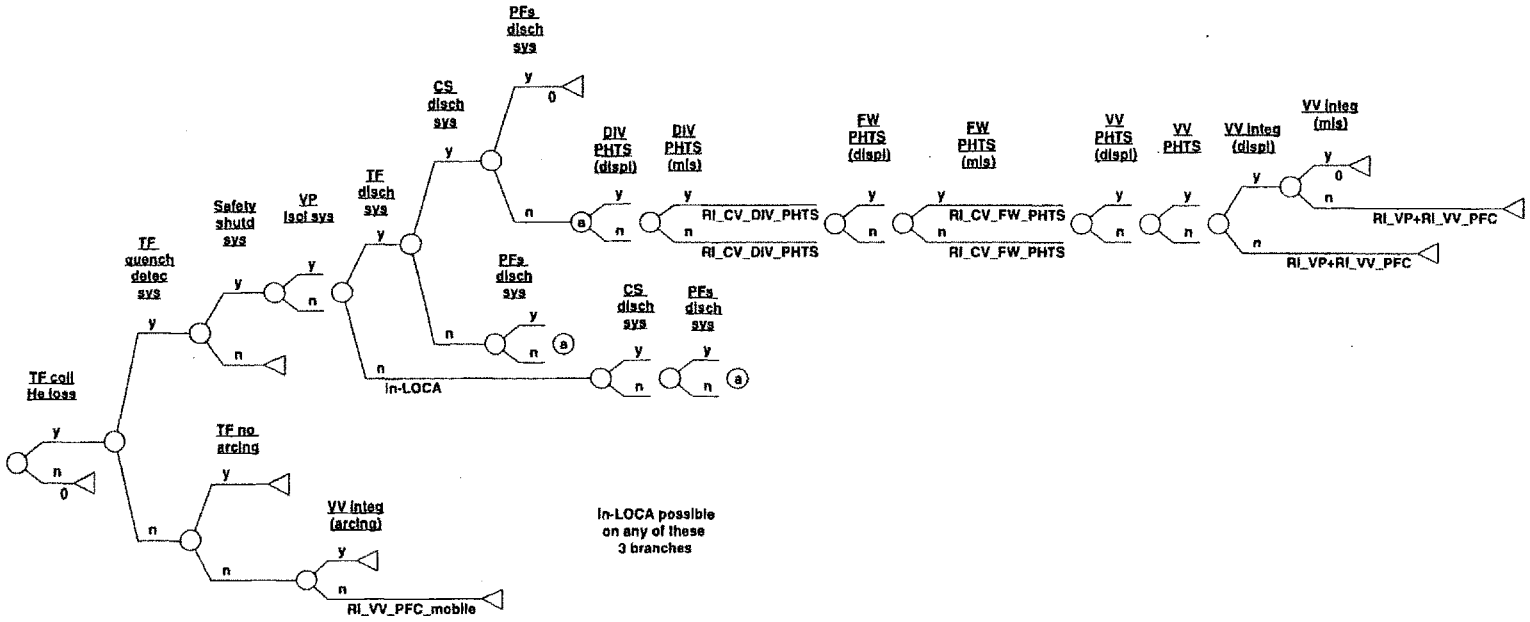

Figure B-25: Event Tree for the Initiating Event MCC1 without Disruption

B.3 Fuel Systems Accidents

Accidents in the fueling and fuel processing systems can occur in the torus pumping system, the impurities processing system, the isotope separation system, the on-line storage system and the fueling systems (gas puffing and pellet injection). There are many process lines that connect the various components, and these lines are also potential accident initiators.

The scope of the present study refers to the confinement barriers inside the tokamak building only, therefore we will not analyze the IEs affecting confinement barriers in the tritium building.

B.3.1 TGP3: Failure of gas puffing valves in open position

There are three major components inside the gas puffer room: a) the buffer tank, b) the process piping, and c) the gas puffing valves. A process boundary failure in a) or b) will lead to a release of DT inside the gas puffer room; and failure of the gas puffing valves (e.g., valve sticks in the open position) could lead to the injection of a large quantity of DT gas in the vacuum vessel.

It is assumed that 1 kg of tritium gas is mobilized from the plasma facing components, by the in-vessel LOCA, but because the diameter of the gas puffing line is small (a few millimeters), compared to the diameter of the rupture disks in the vacuum vessel pressure relief system, only minute quantities of tritium would be transported, by steam flow, into the gas puffing room. Hence, the environmental releases are negligible.

The immediate consequence of a stuck-open gas puffing valve is a continuos injection of DT gas into plasma. This may cause plasma quench or overpower. If the plasma instability is detected, a safety shutdown could be successful with no further consequences. Otherwise, a disruption due to impurity or water ingress can lead to in-vessel LOCA. Also, the pressure in the VV can become high enough to get radioactive inventories out into the gas puffing room via the stuck-open valve.

Figures B-26 and B-27 describe the IT/ET model for TGP3 without disruption.

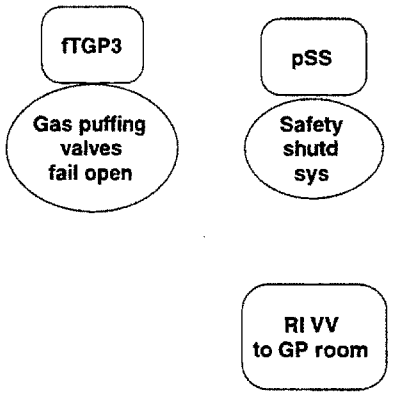

Figure B-26: Influence Diagram for the Initiating Event TGP3 without Disruption

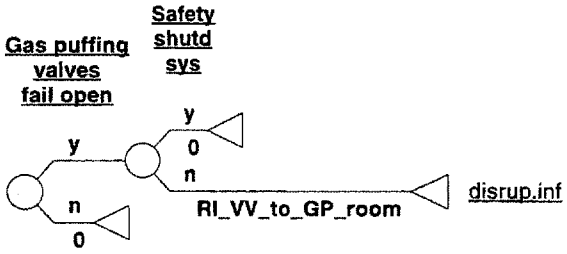

Figure B-27: Event Tree for the Initiating Event TGP3 without Disruption

B.5 Loss of Secondary Vacuum Accidents

ESECS estimates that the loss of primary vacuum (vacuum vessel) is not of concern from a safety point of view. Hence, we only analyzed the secondary vacuum loss accidents (cryostat vessel) in Chapter 4.

B.5.1 VCL: Large leakage of air in the cryostat vessel

A large air ingress in the cryostat will lead to generalized quench of coils due to generalized overheating of the coils. If the quench protection system does not work, there is a potential for arcing and consequential damage of the vacuum vessel. However, conditions for fractional air condensation would not exist for a long time, so that ozone explosion does not seem likely. This is covered by the magnet accident analysis chapter, thus **we will not analyze this IE here.**

B.6 Loss of Auxiliary Systems

This category of initiating events includes the different loss of electrical power events, as well as events related to the loss of other service systems (cryogenics, ventilation, compressed air, etc.). The loss of site power was analyzed in Chapter 4.

B.4 Plasma Accidents

There are several events related to plasma anomalies, but their effects are more severe when coupled with the occurrence with other IE's in the coolant, magnet, or fueling systems, context in which we have already analyzed plasma disruptions, run-away electron damage. The following is a description of these events:

1. **Plasma disruptions**: they are part of the normal operation events. The systems in ITER are designed to withstand a large number of disruptions: for the BPP, the requirements stipulate 3000 disruptions of which 500 at full current and full energy. The most important safety parameter is the bulk temperature of the FW. Thus, the most dangerous situation is when the bulk first wall and blanket temperatures are high for another reason (e.g. LOCAs or LOFAs) and therefore the reaction front temperature cannot be rapidly relaxed. These cases have been analyzed in the coolant accidents section.
2. **Run-away electron damage**: Disruption of the ignited plasma has the potential to vaporize a large amount of plasma facing material and result in a fast decay of the plasma current. This leads to a strong electric field in which electrons could be accelerated and escape in the form of run-away electrons that could damage the plasma facing components as they strike in a toroidally symmetric way.
3. **Vertical Displacement Events**: they are part of the normal operation events for ITER. During a VDE, the plasma becomes vertically unstable and comes into contact with the first wall and/or the divertor while moving rapidly upwards or downwards along with the major axis of the machine. This induces a localized heat load and poloidal currents (halo currents) which produce significant structural loading on the components in contact with the plasma. The machine will be designed to withstand the effects of the worst VDE, but, for machine protection reasons, a mitigation strategy based on initiating a fast disruption may be included in the design.
4. **Overpower transient**: This is the only IE among the plasma anomalies that we will analyzed in more detail in Chapter 4.

Appendix C: Accident Sequences including the Second Confinement Barriers Models

This appendix presents the accident sequences including the second confinement barriers for the six initiating events analyzed in Chapter 4. The figures were explained in Chapter 5.

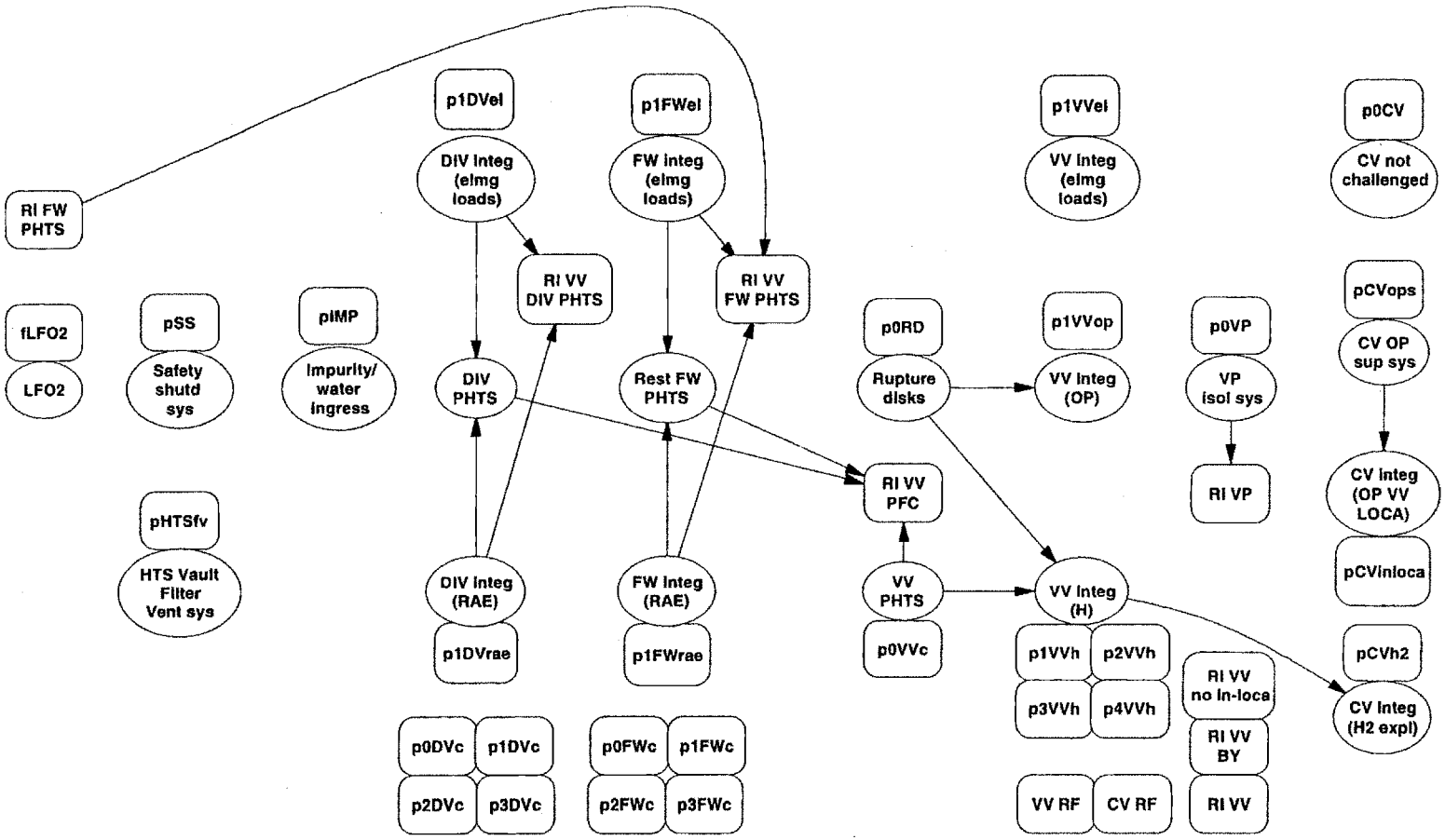

Figure C-1: LFO2 Influence Diagram with Second Confinement Model

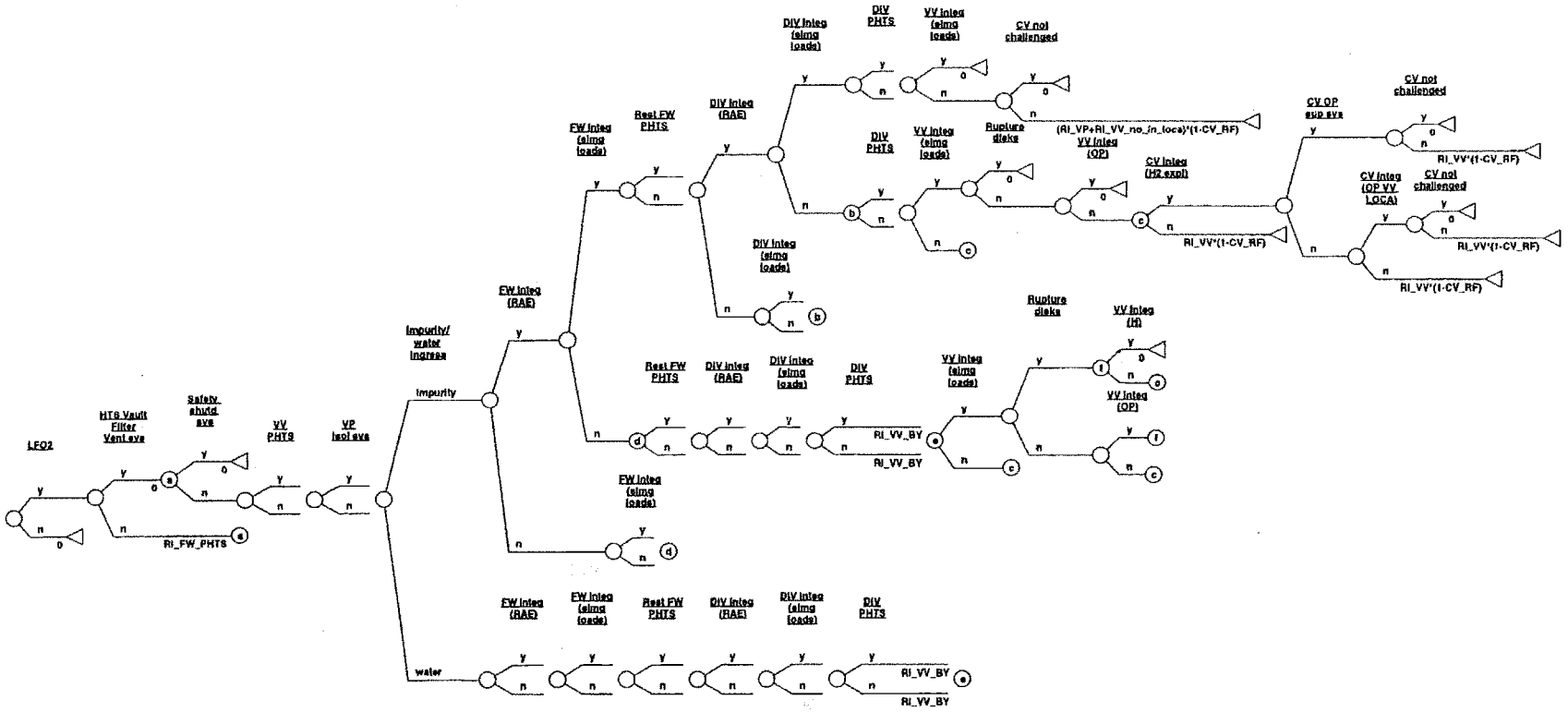

Figure C-2: LFO2 Event Tree with Second Confinement Model

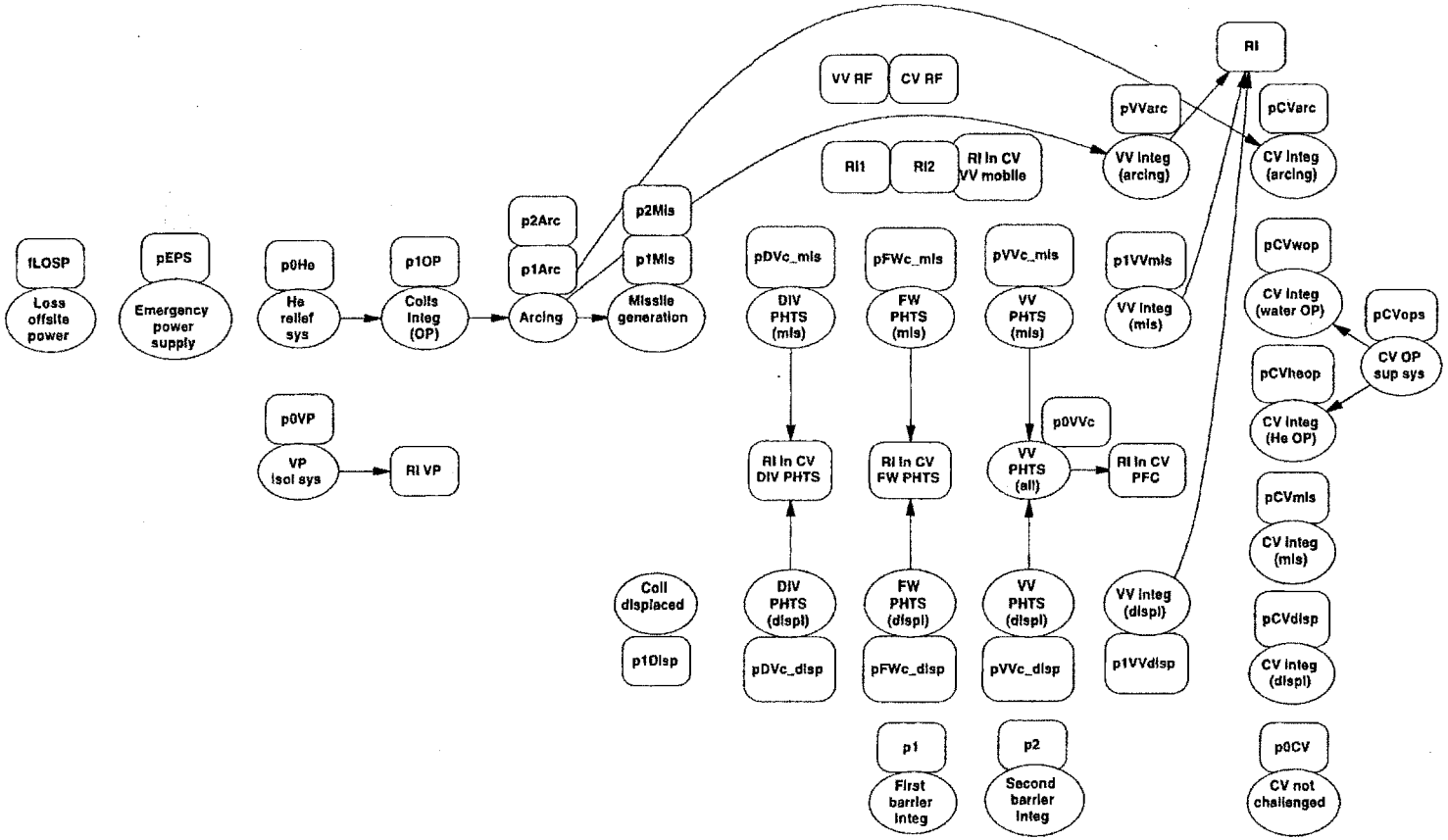

Figure C-3: LOSP Influence Diagram with Second Confinement Model

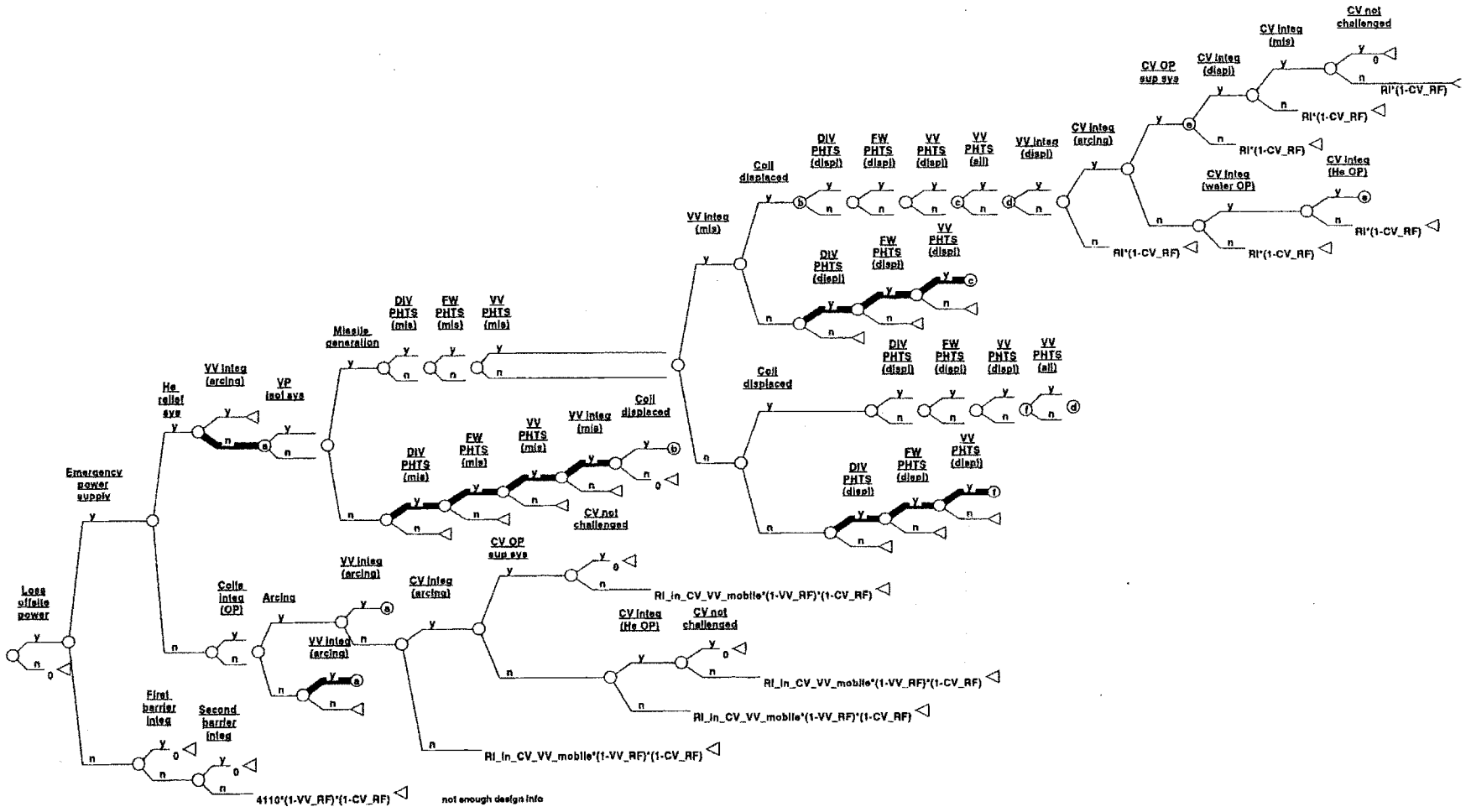

Figure C-4: LOSP Event Tree with Second Confinement Model

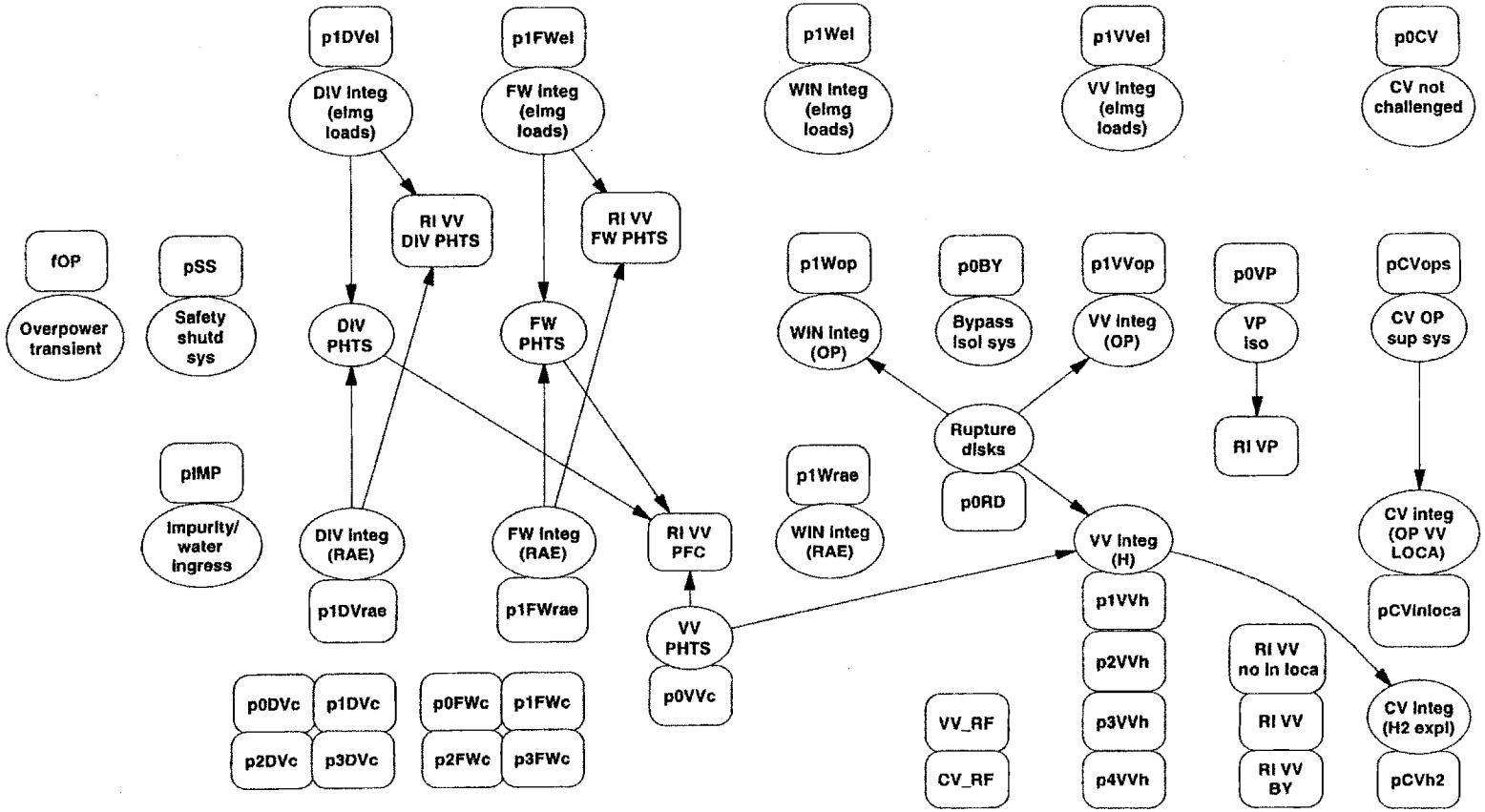

Figure C-5: OP Influence Diagram with Second Confinement Model

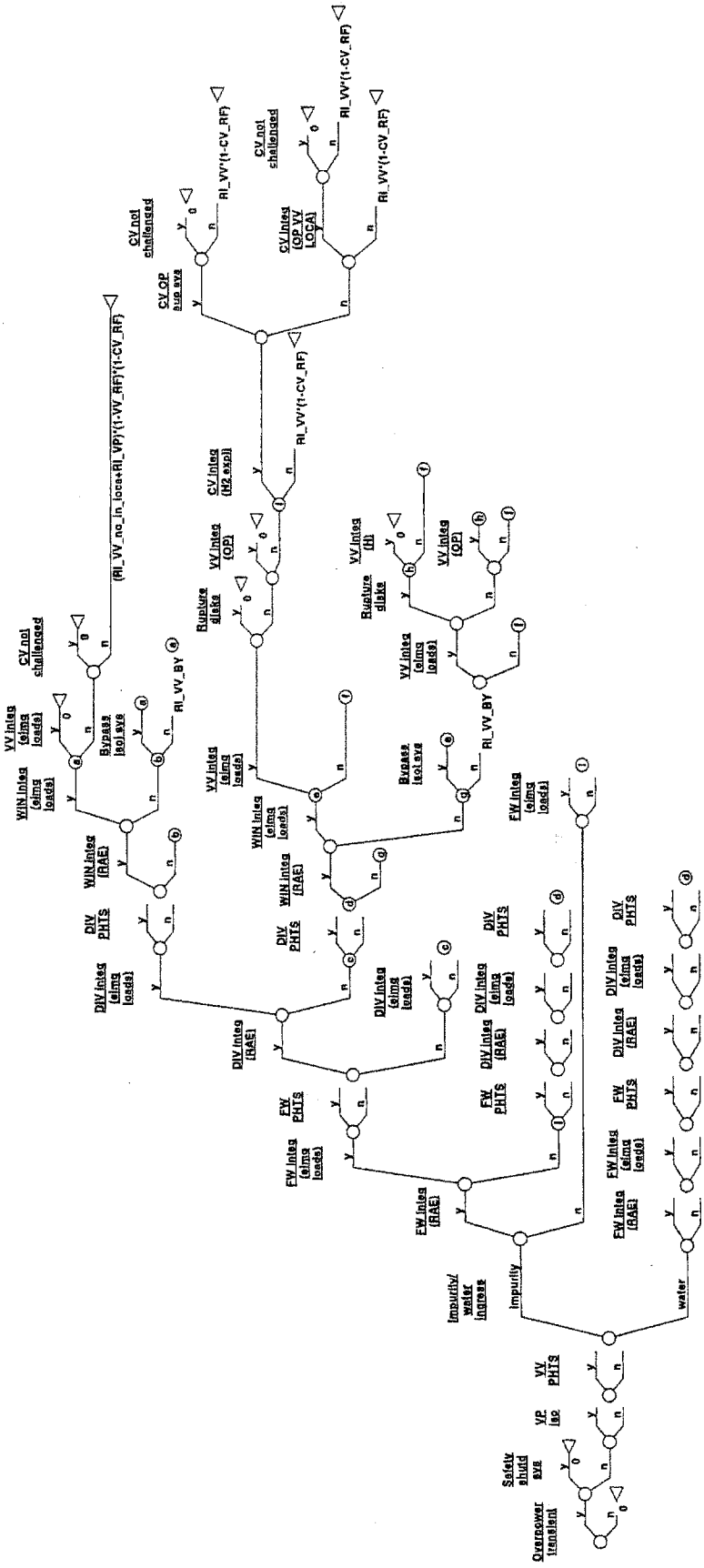

Figure C-6: OP Event Tree with Second Confinement Model

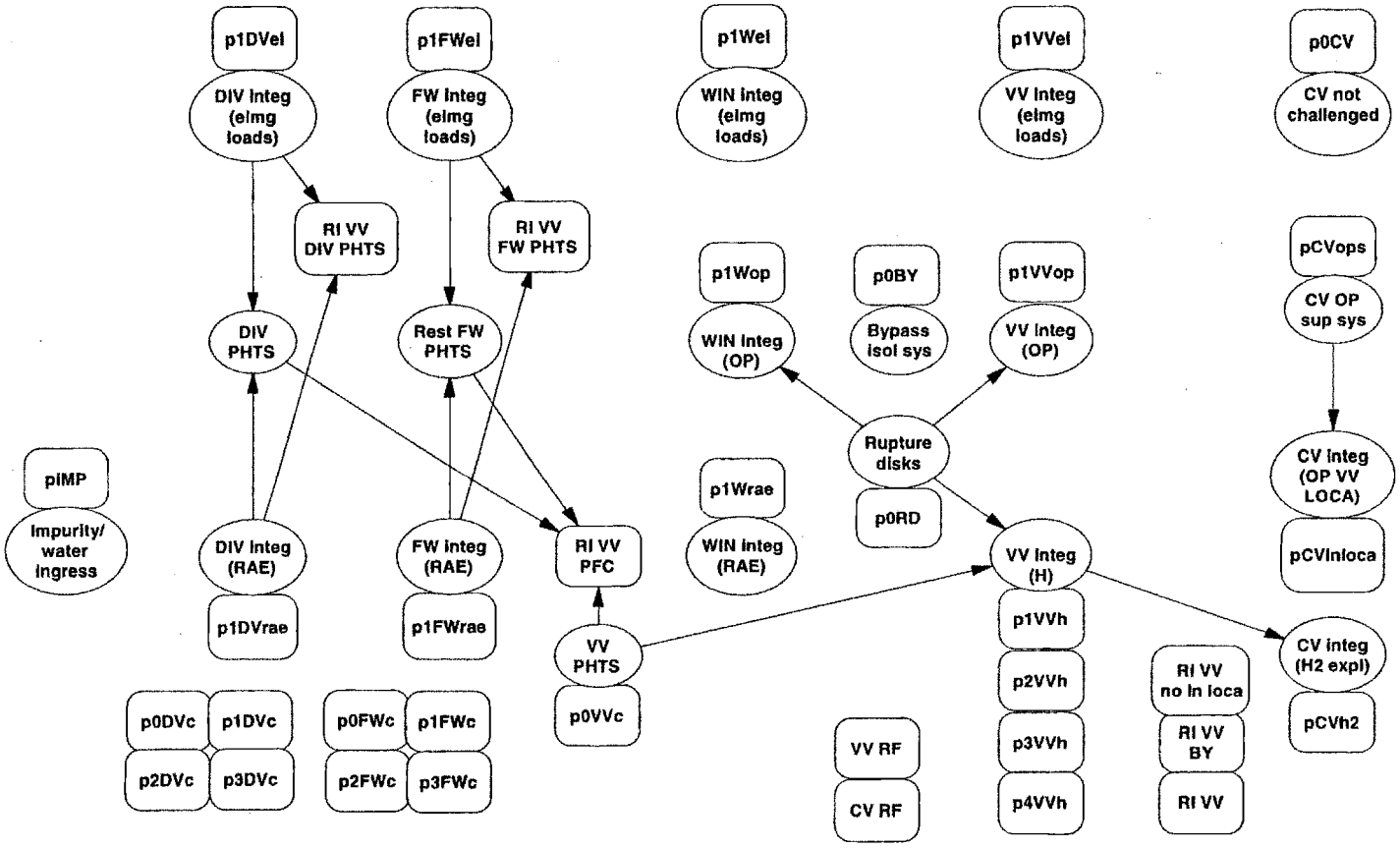

Figure C-7: Disruption Influence Diagram with Second Confinement Model

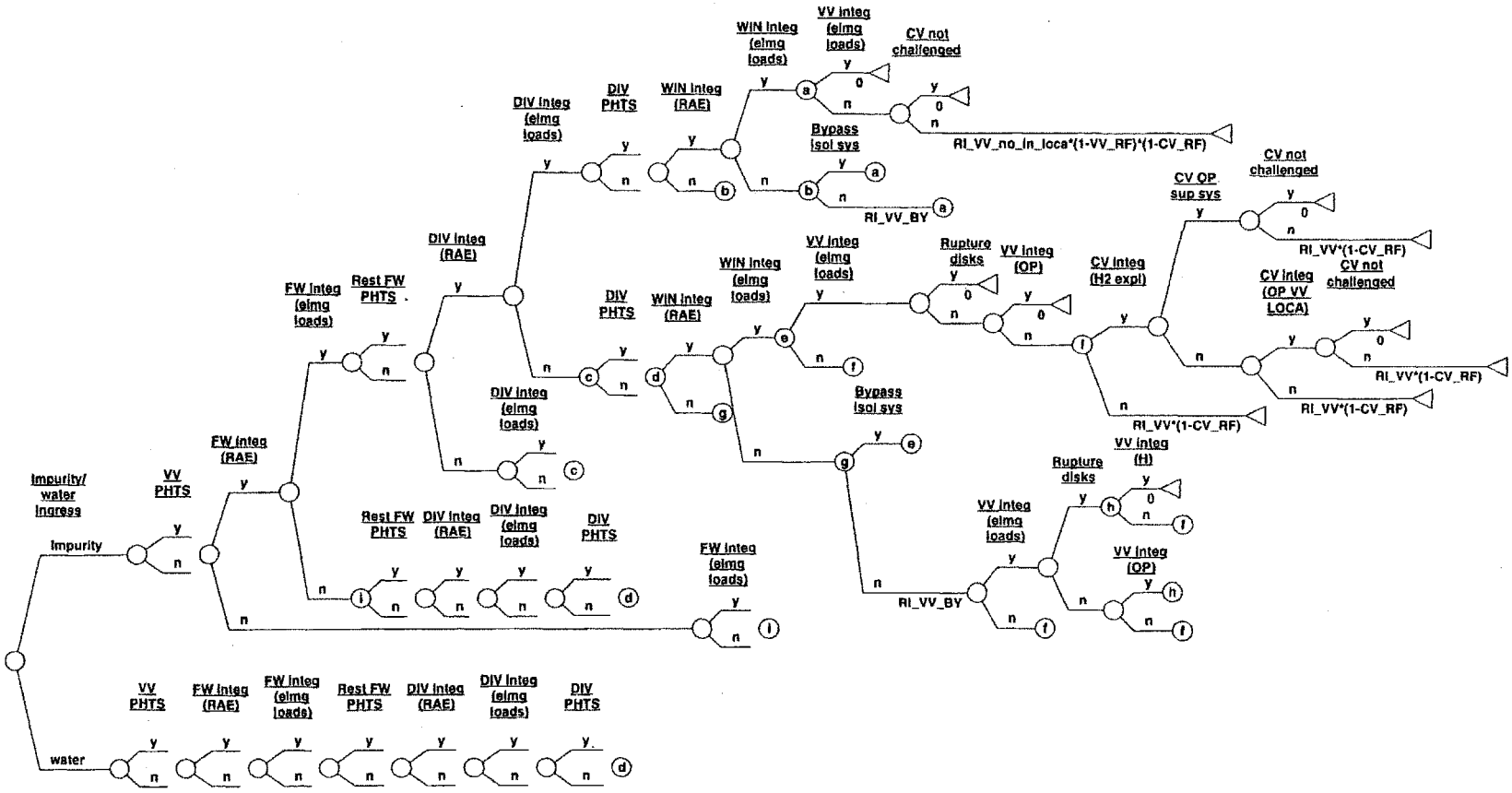

Figure C-8: Disruption Event Tree with Second Confinement Model

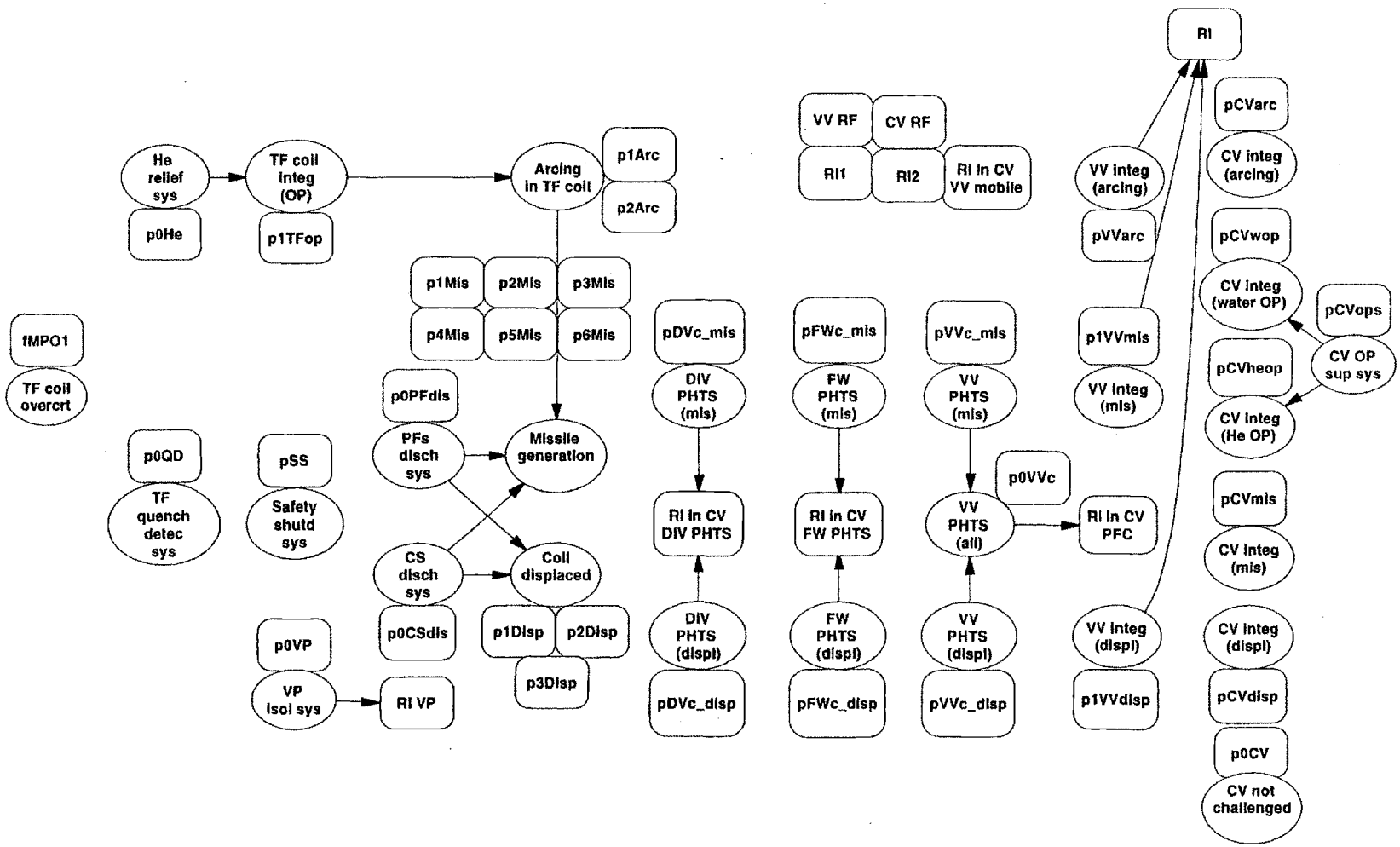

Figure C-9: MPO1 Influence Diagram with Second Confinement Model

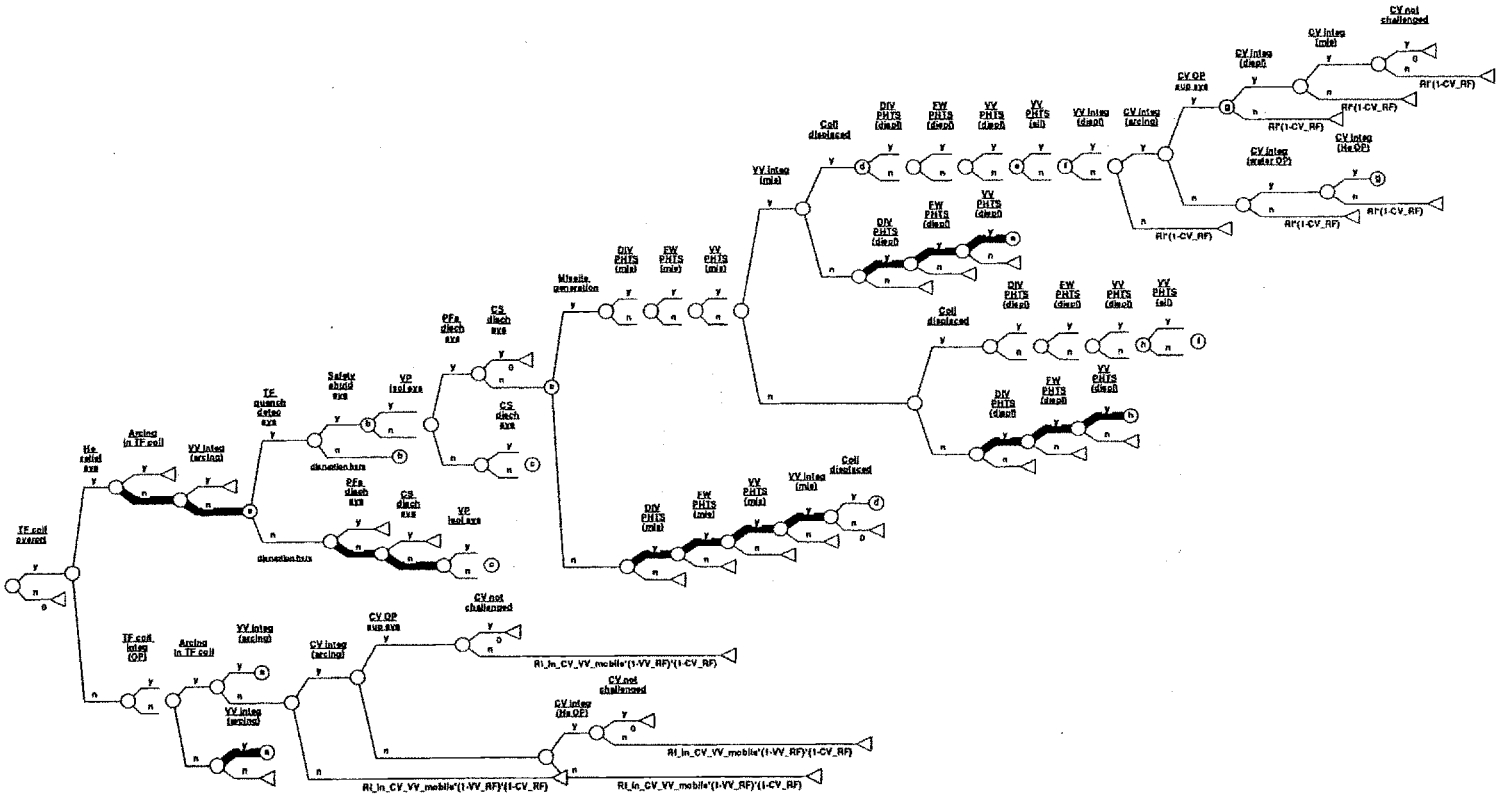

Figure C-10: MPO1 Event Tree with Second Confinement Model

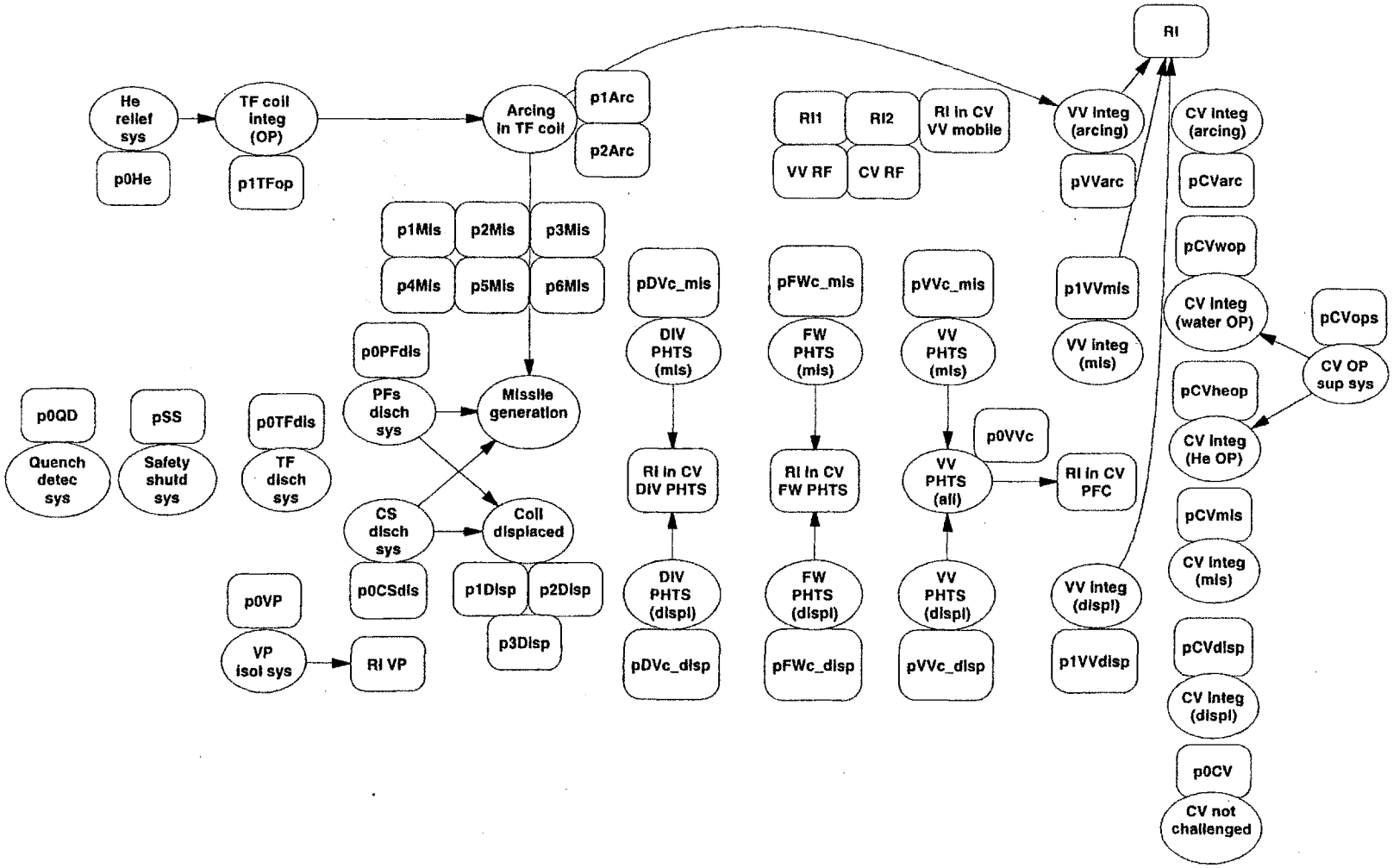

Figure C-11: Quench Influence Diagram with Second Confinement Model

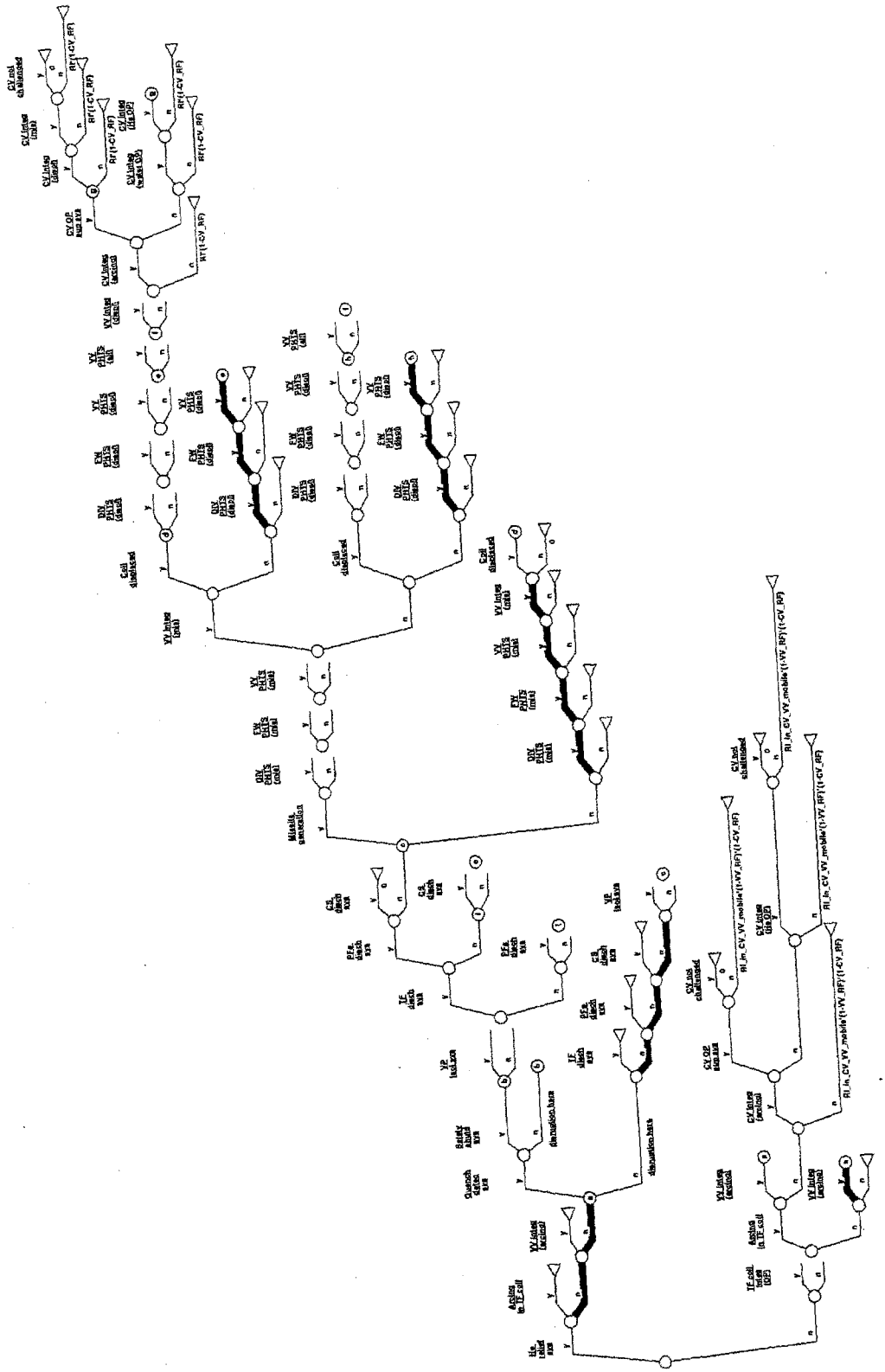

Figure C-12: Quench Event Tree with Second Confinement Model

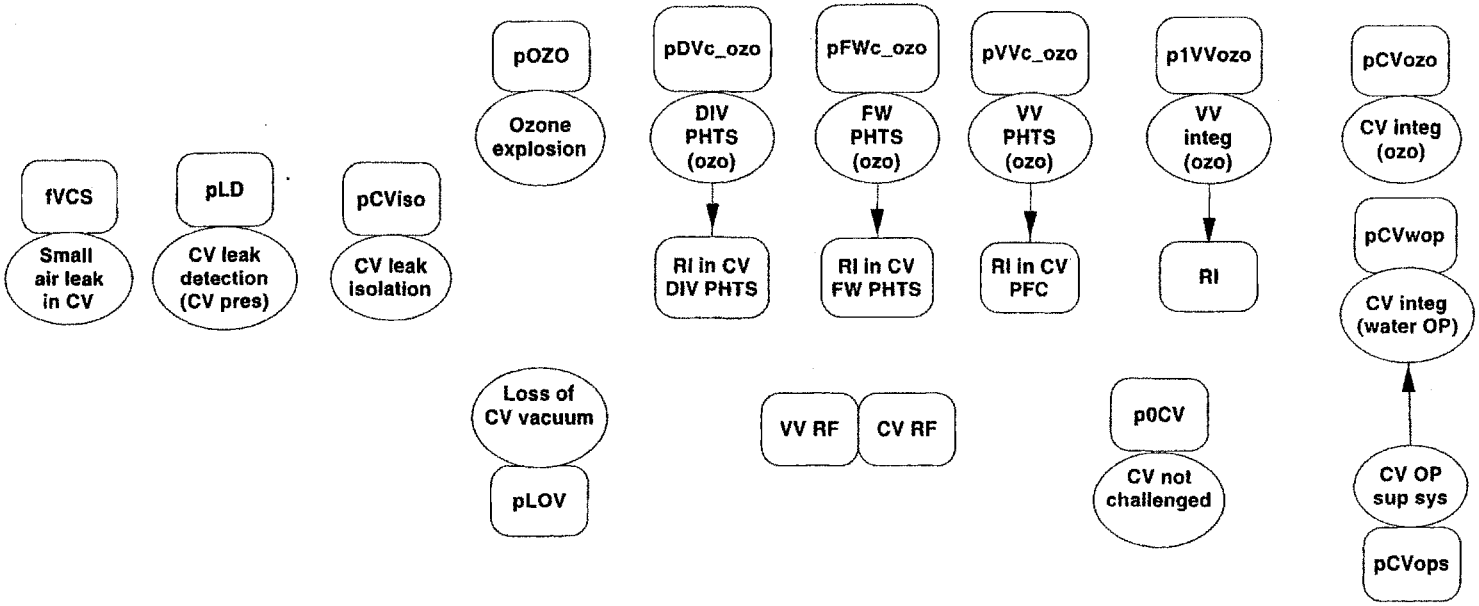

Figure C-13: VCS Influence Diagram with Second Confinement Model

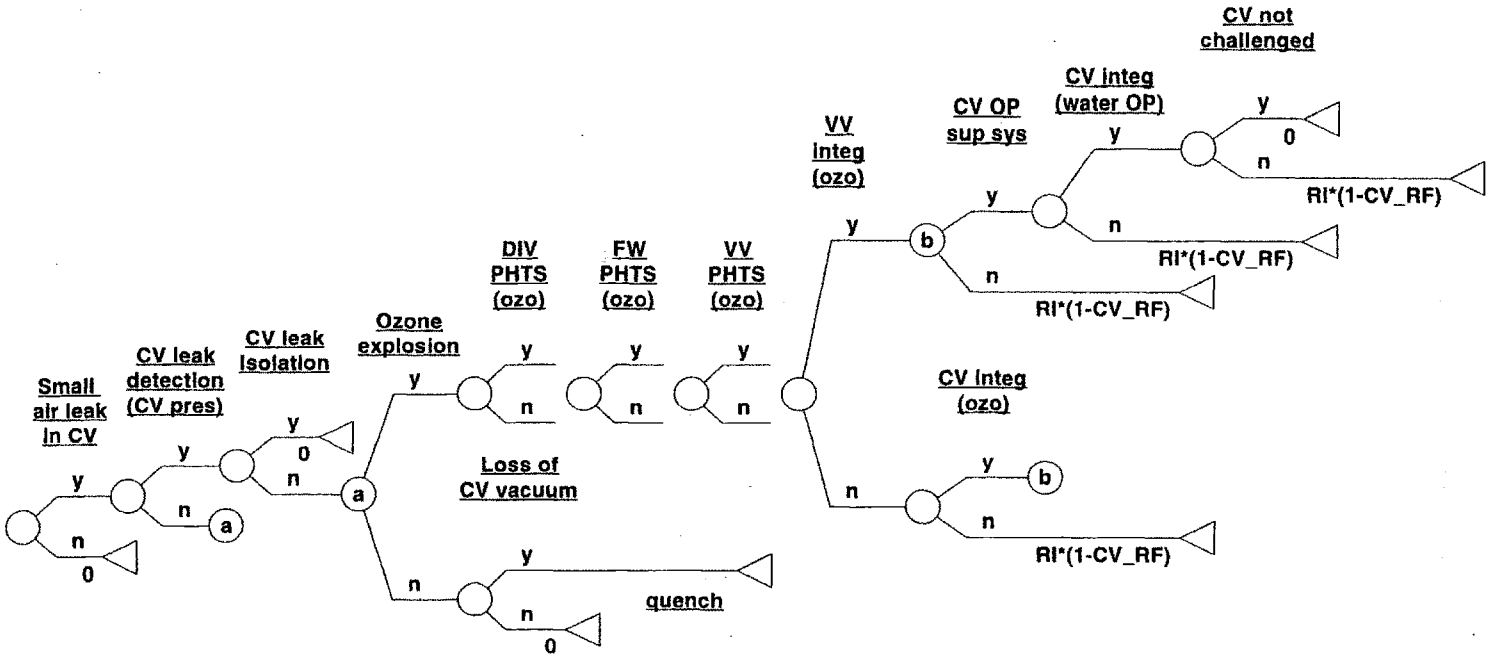

Figure C-14: VCS Event Tree with Second Confinement Model

Appendix D: EXCEL Database

The data is grouped by categories of systems: values extracted from references are written in italics and values for events that have not been found as such in references are given in bold. Some that the definitions for systems failure events, especially conditional events, do not correspond to any of the events found in the references. However, we believe that the definitions are reasonable and their probabilities could be more precisely estimated upon further deterministic analysis and operational experience. Sensitivity analysis particularly for these type of events will be undertaken to study their influence on the results of the systems model.

In DPL, the definition of events is given in terms of the success of a system to fulfill its intended mission. Each event has to states: yes - meaning successful operation; no - meaning system failure. The sum of the probabilities of the two states is equal to 1 (complementary states)[1]. Thus, estimating the probability of systems failure is sufficient, and these failure probabilities are centralized in the EXCEL database. In conclusion, the events defined in EXCEL are in fact the complementary events of those defined in DPL.

The attempt of the present work was not to develop a comprehensive failure rates data base, but only to centralize data for the events defined in the six initiating events models for accident sequences that are included in the probabilistic model for studying the confinement barriers.

Initiating Events

Six initiating events were picked from the comprehensive list studied in Chapter 4, each starting in a different part of the plant. It is simpler to develop a model by using a minimal number of initiating events, and then implement the rest of the initiating events.

LFO2 (ex-vessel LOCA in a FW/SB coolant loop) frequency can be estimated using pipe failure data, and depends on the size of the pipe: for medium size piping (typically 160 mm diameter), the break frequency is between 10^{-3} and 10^{-2}/a; for large pipes (800 mm diameter), the frequency is 10^{-4}/a.[4-11]

MPO1 (TF coil overcurrent) frequency was estimated from [4-10], where the TF coil system is broken down into assemblies and aggregates as follows: superconducting coil, cryogenic cooling, energy supply, protection devices including instrumentation. We assume that TF coil overcurrent is the result of a failure of one of the electrical components: electrical connection between double pancakes with helium passage and one helium pipe connection (GA1), electrical connections without helium passage and with two helium pipe connections (GA2), current leads (GD), pancakes (GM). The failure

[1] No partial fulfillment of mission is considered in the present study. See [4-17] for three-state model: normal, degraded and failed states.

rates of these components are given in [4-10] Table III. The MPO1 frequency is calculated as the sum of these failure rates per year, assuming that the TF coil system is kept energized at all times. The estimated frequency for MPO1 initiating event is 10^{-1}/a.

$$f_{MPO1} = (\lambda_{GA1} + \lambda_{GA2} + \lambda_{GD} + \lambda_{GM})[/hr]\, 8760[hr / yr] \quad \text{(D-1)}$$
where $\lambda_{GA1} = 1.26E-07 / hr$, $\lambda_{GA2} = 3.4E-08 / hr$,
$\lambda_{GD} = 1.0E-05 / hr$, $\lambda_{GM} = 1.0E-06 / hr$

TVP1 (Vacuum pump process boundary failure) frequency is taken from ESECS [4-1], and it is assumed to be 10^{-1}/a, given the large number of process lines inside the vacuum vessel boundary.

OP (Overpower transient) occurs due to failure of the fuel injection systems (fuel pellet injection or fuel gas injection). The two systems are independent, so the possibility of common cause failures is quite small. The result is about 9.6 events/year. The frequency value is introduced in DPL as the branch probability that the initiating event occurs, and DPL can only work with values between 0 and 1 for the probability. Therefore, we use a value of 1 for the frequency of OP as DPL insert variable, and we multiply the resulting accident sequences frequencies by the real OP frequency value of 9.6/a. This trick does not affect the results.

$$f_{OP} = (\lambda_{PI} + \lambda_{GI})[/hr]\, 8760[hr / yr] \quad \text{(D-2)}$$
where $\lambda_{PI} = 1.0E-03 / hr$, $\lambda_{GI} = 1.0E-04 / hr$

VCS (Small leakage of air in the cryostat vessel) frequency value is extracted from [4-11], where the initiating event 'vacuum leak at bellows' has a frequency of 0.2/a.

LOSP (Loss of offsite power) data for power plants indicate that the frequency of this event is between 10-3/a and 10-6/a, depending on the duration of the loss of power: the higher value is for short duration events (typically under 2 hours), and the lower value for events with a duration up to 10 hours.[4-1] Reference [4-11] gives data from various US utilities, of the order of 0.1/a. To be on the conservative side, we will use a frequency of 0.1/a for LOSP initiating event.

Plasma Facing Components Primary Cooling Systems

The PFC PHTSs are not designed as safety systems, but they are assumed to play a role in removing the decay heat from the plasma facing components. The ITER decay heat is about 20 MW right after plasma shutdown, and it decreases to about 1 MW after the first week. So, we assume a mission time for the decay heat removal of one week after the plasma shutdown.

Table D-1: ITER Decay Heat

Time after shutdown (days)	Global decay heat (MW)
1.16E-05	20
0.007	14
0.042	9.5
0.417	1.9
1	1.6
7	1.2
31	1

The failure causes for the PFC PHTSs loss of integrity are:

- independent failure, meaning that PFC PHTS fails to causes unrelated to the accident sequence events;
- runaway electron damage to PFC penetrates the PHTS tubes;
- electromagnetic loads damage PFC and penetrates the tubes;
- magnet coils displacement cause break of PFC PHTS;
- missile generation cause break of PFC PHTS;
- ozone explosion in cryostat vessel cause break of PFC PHTS.

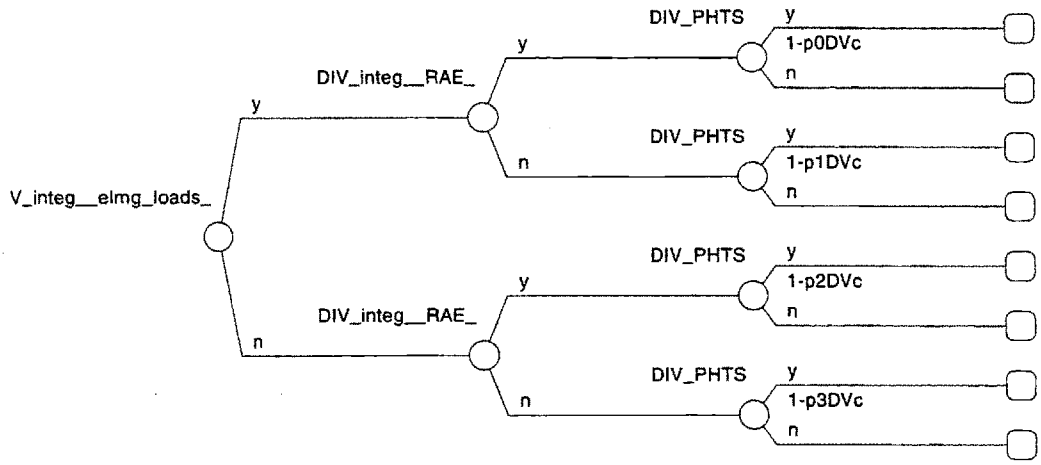

Figure D-1: DPL Probability Data for DIV PHTS Success/Failure Event

The following four situations can be distinguished for the capability of DIV PHTS to remove the fusion decay heat for one week after plasma shutdown:

1. The divertor plates are not damaged by disruption effects. Then, DIV PHTS can still fail due some independent causes such as sub-component failures or common causes. We developed a fault tree with the top event "DIV PHTS fails to remove decay heat during one week after shutdown due to causes unrelated to plasma instabilities" to calculate the failure probability p0DVc in Figure D-1. The DIV PHTS has four loops situated in two HTS vaults; the two loops in the same HTS vault can be interconnected in case one of them fails. Hence, the success criterion for the fault tree top event refers to the operation of at least one loop in each HTS vault. The corresponding failure criterion is failure of at least two loops in the same vault, and the three situations when that happens are described in the fault tree. The failure rates for the basic events (identified by circles) and for events which are not developed further (identified by rhombus) are taken from [4-10, 4-11].

Table D-2: Failure rates for basic events in DIV PHTS failure fault tree

Event name	**Event symbol**	**Failure Rate**	**[4-11] page no.**
Pipe break in one HTS loop	PIHTS	10^{-4}/yr	50
Pipe break to cassettes	PICAS	10^{-3}/yr	50
Pump failure	PUMP	10^{-5}/hr	53
Heat exchanger failure	HX	10^{-6}/hr	50
Fire in one HTS vault	FIRE	$3x10^{-2}$/yr	60
Bad maintenance, high humidity, bad coolant chemistry	MAIN	$1.1x10^{-6}$/hr	50
Electric power failure	ELPO	$9x10^{-2}$/yr	60
Control system failure	CONSY	10^{-6}/hr	55

For the event 'Bad maintenance, high humidity, bad coolant chemistry', we used the beta factor method to calculate the common cause failure rate:

$$\beta = \frac{\lambda_c}{\lambda_c + \lambda_i} = \frac{\lambda_c}{\lambda_t} \qquad \text{(D-3)}$$

where λ_c is the failure rate of both loops due to the common cause, λ_i is the independent failure rate of one loop due to the same cause, β is the beta factor, usually estimated from previous experiences. A reasonable value for β is 0.1. Hence, λ_c can be evaluated as follows:

$$\lambda_c = \lambda_i \frac{\beta}{1-\beta} \qquad \text{(D-4)}$$

For $\lambda_i = 10^{-5}/\text{hr}$, $\lambda_c = 1.1 \cdot 10^{-6}/\text{hr}$.

Boolean algebra is then used to calculate the top event probability of occurrence:

GO1= GO2+GA1+GO3 (D-5)
GO2= GO4+GO4
GO4= GA3+GO7
GA3= GO5·GO5
GO7= FIRE + MAIN
GA1= GO2·GO5
GO5= PIHTS + PICAS + PUMP + HX
GO3= GA2+GO6
GA2= GO5·GO5·GO5·GO5
GO5= ELPO + CONSY

where GO is an 'OR' gate, and GA is an 'AND' gate. With a mission time for DIV PHTS of one week, the probability p0DVc is 0.0034.

2. DIV plates are damaged by runaway electrons (RAE), but are not damaged by electromagnetic loads. Hence, the DIV PHTS will either fail independently or due to RAE penetration of DIV plate cooling tubes. The failure probability of DIV PHTS is p1DVc in this case, and it is in fact a conditional probability:

p1DVc = Pr(DIV PHTS fails independently OR due to RAE damage to DIV tubes | RAE damage to DIV plates) (D-6)
p1DVc = Pr(DIV PHTS fails independently | RAE damage to DIV plates) + Pr(DIV PHTS fails due to RAE damage to DIV tubes | RAE damage to DIV plates)
p1DVc = Pr(DIV PHTS fails independently) + Pr(DIV PHTS fails due to RAE damage to DIV tubes | RAE damage to DIV plates)
p1DVc = p0DVc + Pr(DIV PHTS fails due to RAE damage to DIV tubes | RAE damage to DIV plates)

Two probability theory concepts were used in (D-4):

- p(A or B|C)=p(A|C)+p(B|C), if A and B are mutually exclusive events;
- =p(A), if A and C are independent events.

Runaway electron damage is a toroidally symmetric event, so it has the capability of damaging all four DIV PHTS loops simultaneously. To estimate a value for Pr(DIV PHTS fails due to RAE damage to DIV tubes | RAE damage to DIV plates) more detailed analysis should be performed, which is outside the scope of the present work. For now, we assume that in 2 out of 100 disruptions (0.02 probability) causing RAE damage to the divertor plates, DIV PHTS fails due to RAE damage to DIV tubes. Thus, p1DVc = 0.0034+0.02.

3. DIV plates are not damaged by runaway electrons (RAE), but are damaged by electromagnetic loads. The failure probability of DIV PHTS is p2DVc in this case, and it is again a conditional probability. Everything we said in part 2 applies here, except that the failure cause is electromagnetic loads to DIV plates instead of RAE. We assume that in 1 out of 100 disruptions (0.01 probability) causing electromagnetic loads damage to the divertor plates, DIV PHTS fails due to electromagnetic loads damage to DIV tubes. Thus, p2DVc = 0.0034+0.01.

4. DIV plates are damaged by both runaway electrons (RAE), and electromagnetic loads. The failure probability of DIV PHTS is p3DVc in this case, and it is a conditional probability. We believe that the effect is more than cumulative, and assume a probability of 0.06 (6 out of 100) that DIV PHTS fails due to the damage to DIV plates by RAE and Electromagnetic loads.

For the similar events referring to the FW/SB PHTS, the same types of calculations should be performed. Some basic events failure probabilities might be different, since the design of the FW/SB PHTS is not identical with DIV PHTS in terms of thermohydraulic parameters, piping dimensions and configuration. However, the number of loops is also four, and we will assume the same values for the events probabilities as for DIV PHTS failure, at least for the time being.

The LFO2 initiating event represents a break in one loop of the FW/SB PHTS. Therefore, only three loops are left to remove the decay heat from the FW. We called the event "Rest of FW PHTS failure" to refer to the three loops unaffected by LFO2, and we considered the independent failure to have a probability equal to the probability at gate GA1 in Figure D-3.

Missile generation, magnet coil displacement, and ozone explosion in the cryostat vessel are three other causes for PFC PHTS failure that we considered in this study. We calculated the conditional probabilities of DIV and FW PHTS failures given any of these events based on the same considerations as in Equations (D-4). We again estimated some rough values for the probabilities of PHTS damaged by these events, and the values are shown explicitly in the EXCEL database. As an example, we assumed that, given a missile was generated, the probability that a PFC PHTS is damaged is of the order of 0.1 (in 1 out of 10 events with missile generation, the PFC PHTS is damaged by that missile). Further research should be performed for a more reliable estimation.

ITER Safety Systems

The safety systems for ITER include:

- off-normal fusion power shutdown;
- pressure suppression systems to protect confinement barriers;
- vacuum vessel cooling system used for decay heat removal, and having the capability for natural circulation;
- magnet quench detection and discharge systems;
- isolation valves;
- emergency power supply.

Reference [4-10] gives a generic failure rate for the Engineered Safety Features of 10^{-4}/hr with a Mean Downtime (MDT) of 1.1 hours.

Similarly to the possible damage causes for the PFC PHTS, we defined the event that the VV PHTS fails independently with a probability of 2×10^{-4}, and the conditional events that the VV PHTS fails given missile generation, coil displacement, or ozone explosion in the cryostat vessel.

For failure to respond on demand of fusion shutdown system, a probability of 10^{-3} was considered , as in [4-12].

The connection between the vacuum vessel and its pressure suppression tank is made by four ducts, each of diameter 1 m^2, fitted with rupture disks which isolate them during normal operation. The success criterion for pressure release is when at least one disk breaks on demand, so the failure of pressure releases occurs when all four disks fail simultaneously. The probability of failure on demand for one disk, as given in ESECS [4-1] is 10^{-3}. Hence, the simultaneous independent failure is quite small, but common cause failure is a possibility; we assume a beta factor of 0.1, leading to a probability of failure of 10^{-4} for the rupture disks system.

The plasma vacuum pumping in ITER is part of the exhaust system, and it contains radioactive inventories. The vacuum pumps should be therefore isolated form the plasma chamber following plasma shutdown, to avoid the transport of the radioactive inventories between the two systems. Fast acting valves are located upstream the cryopumps to isolate the vacuum lines from the plasma chamber, if needed. Reference [4-12] estimates the probability of failure on demand of the vacuum pumps isolation system at 4.8×10^{-3}.

The initiating event TVP1 consists in boundary failure of the vacuum pump. Credit is taken for the break isolation, and ESECS [4-1] assumes a probability of 10^{-2} for the failure of vacuum pump boundary break isolation to respond on demand.

The superconducting magnets should not damage safety functions leading to a release of radioactivity in excess of specified limits. Emphasis is placed on magnet design concepts that preclude catastrophic structural failure or thermal conditions that could damage confinement barriers, and include safety features of the structure, conductor, insulation, cryogenics, power supplies.

The cryogenic plant supplies helium to the coils, busbars, and current leads. In the event of a fast discharge, much of the helium is expelled from the coils, because the heating of the coolant causes a fast pressure rise. A system of relief valves and a relief tank will capture the helium. We do not have more information about the system at this time, and [4-15] gives a probability of failure of 10^{-1} for Cryogenic helium relief.

The magnet conductor is designed to tolerate a range of disturbances without initiating a quench[2] (in particular disruptions and limited mechanical motion). The copper in the cable provides a limited degree of thermal protection, but, to prevent local overheating and possible coil damage, the coil affected must be discharged with a time constant of about 20 seconds. The primary quench detection system relies on voltage balance between similar conductors to exclude inductive voltages and reliably detect the small resistive voltage that characterizes the start of a quench. There is a backup system that acts on a larger time scale and uses the pressure wave from a quench for detection. An estimate for the TF coil quench detection system failure rate is taken form [4-10]: $8 \cdot 10^{-7}$/hr. The probability of failure (0.003) is calculated for a mission time equal to the Basic Performance Phase (BPP) time: 13000 pulses, each pulse of 1000 seconds. Reference [4-15] gives a probability of failure per demand of 0.01 for the coil quench detection system.

If quench is detected, the magnet coil discharge system should be activated not only in the coil system where a defect occurred, but also in the other coil system due to mutual forces among magnet coils. The failure rate of discharge system equal to 10^{-7}/hr is taken from [4-11], and a mission time equal to BPP is assumed. The seven PF coils have separate power supplies, and the failure criterion is that at least one PF coil is not discharged; hence, the PF coils discharge system has a probability of failure of about seven times the probability of failure of TF or CS coil system (simultaneous failure of two or more PF coils and common cause failures are not considered, they are assumed to have a relatively low probability).

Reference [4-12] contains data on air leak detection and isolation in the cryostat vessel as follows: for leak detection, a failure rate of 10^{-6}/hr (mission time equal to BPP), and for leak isolation, a failure on demand of 10^{-3}.

A disruption has the potential to damage diagnostics windows which are numerous in the plasma chamber. Such an event would lead to bypass of both of the confinement barrier: vacuum vessel and cryostat vessel, to the diagnostics room. However, credit is taken for the isolation of the bypass. We found a probability of failure of isolation valves of 6×10^{-6}/hr in [4-10], and using a mission time equal to BPP, a probability of failure of 0.021 was obtained.

---

[2] When a conductor loses its superconducting properties locally, its resistance increases rapidly and the resistive spot becomes an internal heat source. This heating could lead to propagation of the resistive zone along the conductor, which is called a quench. This can be avoided in some cases when the conductor is cryogenically stable: a stabilizer (copper or aluminum, or another material whose resistivity is lower than that of the superconducting material when it is resistive) is needed to carry the coil current for the time the superconductor need to cool down and recover, so that the superconductor can carry the current again.

An emergency power supply system could consists of two redundant Diesel generators. The probability of failure on demand for one Diesel generator is 0.03 as given in [4-11], so the probability that both fail at the same time is $(0.03)^2$.

Plasma Facing Components

The plasma facing components are: divertor, first wall, and diagnostics windows. They could be damaged by disruption effects such as runaway electron damage and electromagnetic loads. We assume that the effect of runaway electrons on the plasma facing components is different for a disruption caused by impurity ingress or water ingress in the plasma chamber. So, we estimate different values for conditional probabilities of PFC failure in these two situations. We also estimate a probability that diagnostics window fail due to overpressure, since that can lead to an aggravating sequence such as bypass of two confinement barriers.

In the case of a fusion tokamak reactor, the occurrence of an accident will lead directly or indirectly to the plasma shutdown: directly - the initiating event causes plasma disruption, e.g. in-vessel LOCA from plasma facing components; indirectly - the detection of the accident should activate the safety plasma shutdown system. However, even if the plasma safety shutdown system fails to respond quickly, the accident sequence eventually leads to an increase of the temperature of the plasma facing components. The effect will be impurities ingress into plasma, and even water ingress if the heat load on the component is very high and the melting is so rapid that a disruption due to impurity ingress does not have enough time to happen. In conclusion, if the shutdown system fails, the events 'Impurity ingress' and 'Water ingress' are complementary, which means that their probability sum to 1.

The event 'DIV damaged by electromagnetic loads given disruption' is a conditional event which could be further decomposed as follows:

Pr(DIV damaged by electromagnetic loads I disruption) = Pr(DIV damaged by electromagnetic loads I electromagnetic loads) Pr(electromagnetic loads I disruption) (D-7)

For the present time, 50% of disruptions are assumed to produce severe electromagnetic loads, and in 1 in 100 cases when electromagnetic loads are produced, they actually damage the PFC (DIV, FW or windows).

Runaway electrons are generated during plasma disruptions that produce conditions of low density and low plasma temperature. Experience from JET is used to estimate the number of impurity caused disruptions generating significant quantities of runaway electrons as being 15%; in other words, Pr(RAE I disruption by impurity ingress) = 0.15. The coolant ingress-induced plasma disruptions are likely to be two or three times more intense than typical disruptions or disruptions caused by impurity

ingress; 90% of these disruptions are assumed to be able to produce energetic runaway electrons: Pr(RAE | disruption by water ingress) = 0.9. We assume that, given runaway electrons are produced, there is a probability of 0.5 that DIV or FW is damaged by RAE, and a probability of 0.01 that diagnostics windows are damaged by RAE.

Pr(DIV/FW damaged by RAE | disruption by impurity ingress) = Pr(DIV/FW damaged by RAE | RAE) Pr(RAE | disruption by impurity ingress) = (D-8)

0.5 x 0.15 = 0.075

Pr(DIV/FW damaged by RAE | disruption by water ingress) = Pr(DIV/FW damaged by RAE | RAE) Pr(RAE | disruption by water ingress) =

0.5 x 0.9 = 0.45

Pr(Windows damaged by RAE | disruption by impurity ingress) = Pr(Windows damaged by RAE | RAE) Pr(RAE | disruption by impurity ingress) =

0.01 x 0.15 = 0.0015

Pr(Windows damaged by RAE | disruption by water ingress) = Pr(Windows damaged by RAE | RAE) Pr(RAE | disruption by water ingress) =

0.01 x 0.9 = 0.009

By tradition, designers of building windows use a probability of window failure of 0.008[3] over the life of the building (20 to 25 years), when the windows are designed to accommodate ambient conditions as well as pressure loads from high velocity winds. That is a failure rate of $4 \cdot 10^{-4}$/yr. For overpressure demand (usually less than one atmosphere differential pressure), the building windows have to meet the 50 year storm wind loading demand, which gives a probability of failure of 0.02/demand[4] of window.

The view port windows for ITER are generally smaller, and use higher grade materials, but the overpressure loading is 0.5 to 0.8 MPa, or even 2 MPa differential pressure possible in some ITER scenarios. Therefore, we assume a failure rate for diagnostics windows in ITER equal to the one for building windows at 0.02/demand for 5 to 8 atmospheres overpressure. [4-13]

[3] 8 out of 1000 windows failed during the 20 - 25 years period.

[4] $(4 \cdot 10^{-4}$ / yr) (50 years / demand) = 0.02 / demand

Vacuum Vessel Confinement Barrier

The behavior of the vacuum vessel as the first confinement barrier for radioactive inventories is the main interest of the present work. The following events can cause the loss of VV integrity: electromagnetic loads following disruptions, overpressure when the rupture disks fail to open towards the pressure suppression tank, hydrogen explosion[5], arcing, missile generation, magnet coil displacement, ozone explosion in the cryostat vessel.

For the electromagnetic loads effect, we assume the same values as in (D-5):

Pr(VV damaged by electromagnetic loads | disruption) = Pr(VV damaged by electromagnetic loads | electromagnetic loads) Pr(electromagnetic loads | disruption) = 0.01 x 0.5 = 0.005 (D-9)

For the VV failure due to overpressure given rupture disks fail to open, a probability of 0.5 was estimated in [4-14], where this conditional event is called CRYOBOUND: Primary boundary failure towards the cryostat. That value probably refers to an overpressure higher than the VV design pressure of 0.5 MPa. The rupture disks should open at about 0.2 MPa. For a steam overpressure of 0.5 MPa, Lee Cadwallader suggested a probability of failure of 10^{-4} per demand.

For the hydrogen detonation/explosion event, the probability of VV failure can be written as follows:

Pr(VV damaged by H detonation/explosion | state[VV PHTS] and state[RDs]) = (D-10)
Pr(VV damaged by H detonation/explosion | H detonation/explosion) x
Pr(H detonation/explosion | state[VV PHTS] and state[RDs])

where 'state[event_name]' can be either success or failure.

Among all the events defined for the VV confinement barrier, the failure due to overpressure was the only one that we found in the literature. All the other events' probabilities are guessed values, and sensitivity analysis should give a sense of which failure causes have relatively higher effect on the confinement function of the vacuum vessel.

[5] Hydrogen is produced by the reaction of water/steam with plasma facing materials, and depends on the quantity of steam and the plasma facing materials temperature. Thus, we assume that the probability of hydrogen explosion depends on the VV PHTS successful operation for heat removal, and on the rupture disks response on demand.

Magnet Systems

The major concern about magnet transients is the potential for propagating faults to other components of the fusion machine. The magnet faults of concerns from an off-normal event propagation viewpoint are off-normal forces that would produce large coil displacements, break off magnet pieces, pull ferrous missiles from other areas, or arcs that could produce melting and volatilization in other components. In ITER, these events could have the potential to damage the vacuum vessel, ducts and piping from the vacuum vessel, and the cryostat and potentially result in radioactivity releases. Off-normal forces could arise from shorts in coils, faults in the discharge system, or power supply faults. Arcs between coils, arcs to ground, and arcs at open leads could lead to melting and/or volatilization. Arcs could arise from insulation faults, gas ingress, over-voltage, or other causes.

At this point in time, there is no reliable data available for ITER magnets, as they are much bigger than the other experimental tokamak machines. The Japanese team is currently building a model coil for tests that could produce more reliable data. Reference [4-9] presents the results of a survey conducted among the major centers of large magnet development and operation in the USA to obtain information on magnet system failure and accident events, and it contains a brief summary of 31 such events. Reference [4-15] contains accident scenarios for three initiating events: puncture of coil insulation, local loss of superconductivity, and loss of cryostat vacuum. The event trees contain probabilities of failure on demand for the systems involved.

The probabilities we need to estimate for the events occurring in the magnet systems or caused by magnet systems are all conditional probabilities. For instance, we assume that the probability of missile generation depends on the discharge of the all the magnet coils and of arcing, as shown in Figure D-2. Reference [4-15] gives an estimate for the probability of arcing of 0.1.

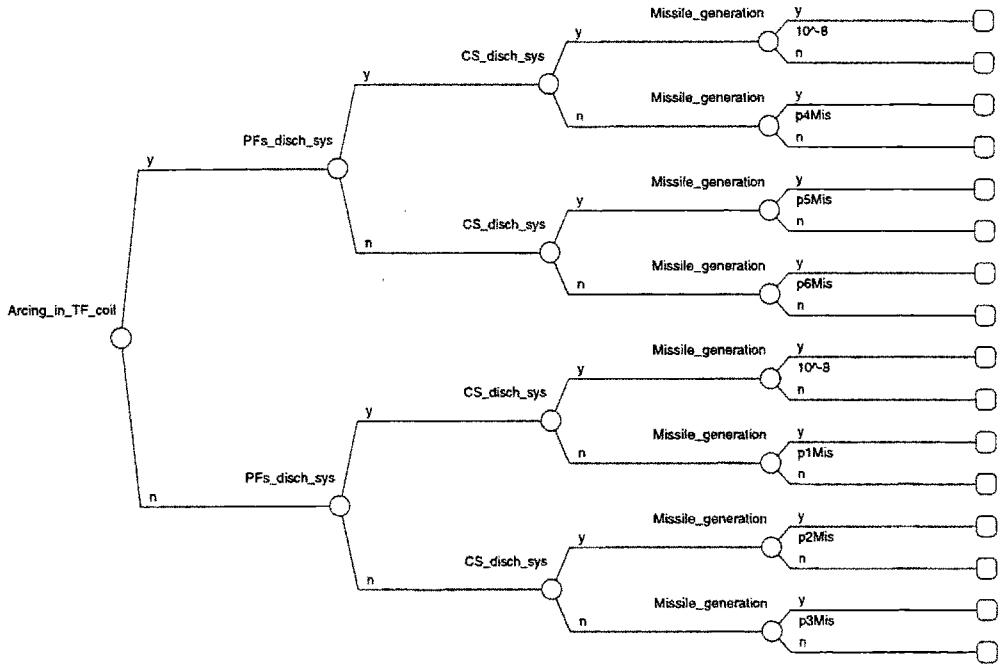

Figure D-2: DPL Probability Data for the 'Missile Generation' Event

Cryostat Vessel Confinement Barrier

The cryostat vessel is a containment building, and hence it is subject to leaks. ITER has no reliability data for this vessel yet, and ESECS uses generic data such as 10^{-1} - 10^{-2} failure probability per demand. Sensitivity analysis will be performed to study the effects of using probabilities of failure for the cryostat of different orders of magnitude. Similarly to the vacuum vessel case, we defined events for the cryostat integrity loss due to several failure causes: arcing, overpressure from in-vessel LOCA, water LOCA in the cryostat, or loss of cryogen in the cryostat, missile generation, coil displacement, ozone explosion, hydrogen explosion propagating from the vacuum vessel.

For the event 'Cryostat vessel fails without being challenged by off-normal events', we assumed a failure rate of 10^{-3}/yr (Lee Cadwallader proposed a value of 10^{-5}/yr for the vacuum vessel), resulting in a probability of failure during BPP of 4×10^{-4}.

Table D-3: Failure Rates Database

IEs	Frequency [/a]	
Ex-vessel LOCA of the FW/SB coolant loop	0.01	
TF coil overcurrent	0.1	
Vacuum pump process boundary failure during regeneration at power	0.1	
Overpower transient	1	9.6
Small leakage of air in the cryostat	0.2	
Loss of offsite power	0.1	

PFC PHTSs	Probab. of failure
DIV PHTS fails independently	0.0034 [24]
DIV PHTS fails given DIV damaged by RAE	0.0234 [25]
DIV PHTS fails given DIV damaged by electromagnetic loads	0.0134 [26]
DIV PHTS fails given DIV damaged by RAE + electromagnetic loads	0.0634
DIV PHTS fails given missile generation	0.1034
DIV PHTS damaged by missile given missile generation	0.1 [27]
DIV PHTS fails given displaced coil	0.3034
DIV PHTS damaged by displaced coil given displaced coil	0.3 [28]
DIV PHTS fails given ozone explosion in CV	0.2034
DIV PHTS damaged by ozone explosion in CV given ozone explosion	0.2 [29]
Rest FW PHTS fails independently	0.0026
Rest FW PHTS fails given FW damaged by RAE	0.0326
Rest FW PHTS fails given FW damaged by electromagnetic loads	0.0226
Rest FW PHTS fails given FW damaged by RAE + electromagnetic loads	0.0826
FW PHTS fails independently	0.0034
FW PHTS fails given FW damaged by RAE	0.0234
FW PHTS fails given FW damaged by electromagnetic loads	0.0134
FW PHTS fails given FW damaged by RAE + electromagnetic loads	0.0634
FW PHTS fails given missile generation	0.1034
FW PHTS damaged by missile given missile generation	0.1
FW PHTS fails given displaced coil	0.3034
FW PHTS damaged by displaced coil given displaced coil	0.3
FW PHTS fails given ozone explosion in CV	0.2034
FW PHTS damaged by ozone explosion in CV given ozone explosion	0.2

SAFETY SYSTEMS	
Plasma safety shutdown system fails to respond on demand	0.001
Rupture disks from VV to suppression tank fail to open on demand	0.0001
Vacuum pumps isolation system to VV fails to respond on demand	0.0048
Vacuum pumps process boundary break fails to be isolated from Tritium plant	0.01
VV PHTS fails independently	0.0002
VV PHTS fails given missile generation	0.0102
VV PHTS damaged by missile given missile generation	0.01
VV PHTS fails given displaced coil	0.0502
VV PHTS damaged by displaced coil given displaced coil	0.05
VV PHTS fails given ozone explosion in CV	0.0202
VV PHTS damaged by ozone explosion in CV given ozone explosion	0.02
Cryogenic He relief system fails	0.1

TF coil quench detection system fails	0.003	[5-15] 0.01
TF discharge system fails	0.0004	
PF coils discharge systems fail	0.0025	
CS discharge system fails	0.0004	
Bypass of VV & CV (diagnostics window) isolation system fails on demand	0.021	
Air leak detection in CV	0.004	
Air leak isolation from CV	0.001	
Emergency power supply system fails to activate on demand	0.0009	
HTS boundary fails to retain radioactive inventories	0.067	

PLASMA FACING COMPONENTS

Impurity ingress	0.6	
Water ingress	0.4	
DIV damaged by electromagnetic loads given disruption	0.005	
DIV damaged by RAE given disruption by impurity ingress	0.075	
DIV damaged by RAE given disruption by water ingress	0.45	
FW damaged by electromagnetic loads given disruption	0.005	
FW damaged by RAE given disruption by impurity ingress	0.075	
FW damaged by RAE given disruption by water ingress	0.45	
Windows damaged by electromagnetic loads given disruption	0.005	
Windows damaged by RAE given disruption by impurity ingress	0.0015	
Windows damaged by RAE given disruption by water ingress	0.009	
Windows fail due to overpressure given rupture disks fail to open	0.02	

MAGNET SYSTEMS

TF coil fails due to overpressure given He relief system fails	0.5	
Arcing in TF coil given TF coil structure does not fail due to He overpressure	0.1	
Arcing in TF coil given TF coil structure fails due to He overpressure	0.2	
Missile generation given no arcing + PFs discharged + CS undischarged	0.1	
Missile generation given no arcing + PFs undischarged + CS discharged	0.3	
Missile generation given no arcing + PFs and CS undischarged	0.5	
Missile generation given arcing + PFs discharged + CS undischarged	0.2	
Missile generation given arcing + PFs undischarged + CS discharged	0.4	
Missile generation given arcing + PFs and CS undischarged	0.6	
Coil displacement given PFs discharged + CS undischarged	0.5	[5-15] 0.1
Coil displacement given PFs undischarged + CS discharged	0.6	
Coil displacement given PFs and CS undischarged	0.7	
Any coil fails due to overpressure given He relief system fails	0.5	

VACUUM VESSEL CONFINEMENT BARRIER

VV fails due to electromagnetic loads given disruption	0.0001 [1]	
VV fails due to overpressure given rupture disks fail to open	0.5 [2]	[5-13]0.0001
VV fails due to H detonation/explosion given VV PHTS and RDs succeed	0.005 [3]	
VV fails due to H detonation/explosion given VV PHTS succeeds and RDs fail	0.01 [4]	
VV fails due to H detonation/explosion given VV PHTS fails and RDs succeed	0.015 [5]	
VV fails due to H detonation/explosion given VV PHTS and RDs fail	0.02 [6]	
VV fails due to arcing given arcing	0.01 [7]	
VV damaged by missile given missile generation	0.1 [8]	

VV damaged by displaced coil given displaced coil	0.5 [9]
VV damaged by ozone explosion in CV given ozone explosion	0.2 [10]

CRYOSTAT VESSEL CONFINEMENT BARRIER	
Ozone explosion	0.0004
Loss of CV vacuum given unisolated small air leakage in the CV	0.5 [11]
CV fails due to arcing given arcing	0.1 [12]
CV fails due to overpressure from LOCA (water) inside the cryostat	0.01 [13]
CV fails due to overpressure from cryogen release inside the cryostat	0.01 [14]
CV fails due to missile given missile generation	0.01 [15]
CV fails due to displaced coil given displaced coil	0.01 [16]
CV overpressure suppression system fails	0.0001 [17]
CV fails without being challenged by off-normal events	1.0E-03 [18]
CV fails due to overpressure from in-vessel LOCA given CV OP sys fails	0.95 [19]
CV fails due to hydrogen explosion in VV (VV integrity lost)	0.001 [20]
CV integrity lost due to ozone explosion given ozone explosion	0.5 [21]

CONFINEMENT BARRIERS RETENTION FACTORS	
Vacuum Vessel	0.1 [22]
Cryostat Vessel	0.25 [23]
Tokamak Pit, CANDU	0.5
Tokamak Pit, current	0

TOKAMAK PIT	
Tokamak Pit, CANDU fails	0.01
Tokamak Pit, current fails	0.1

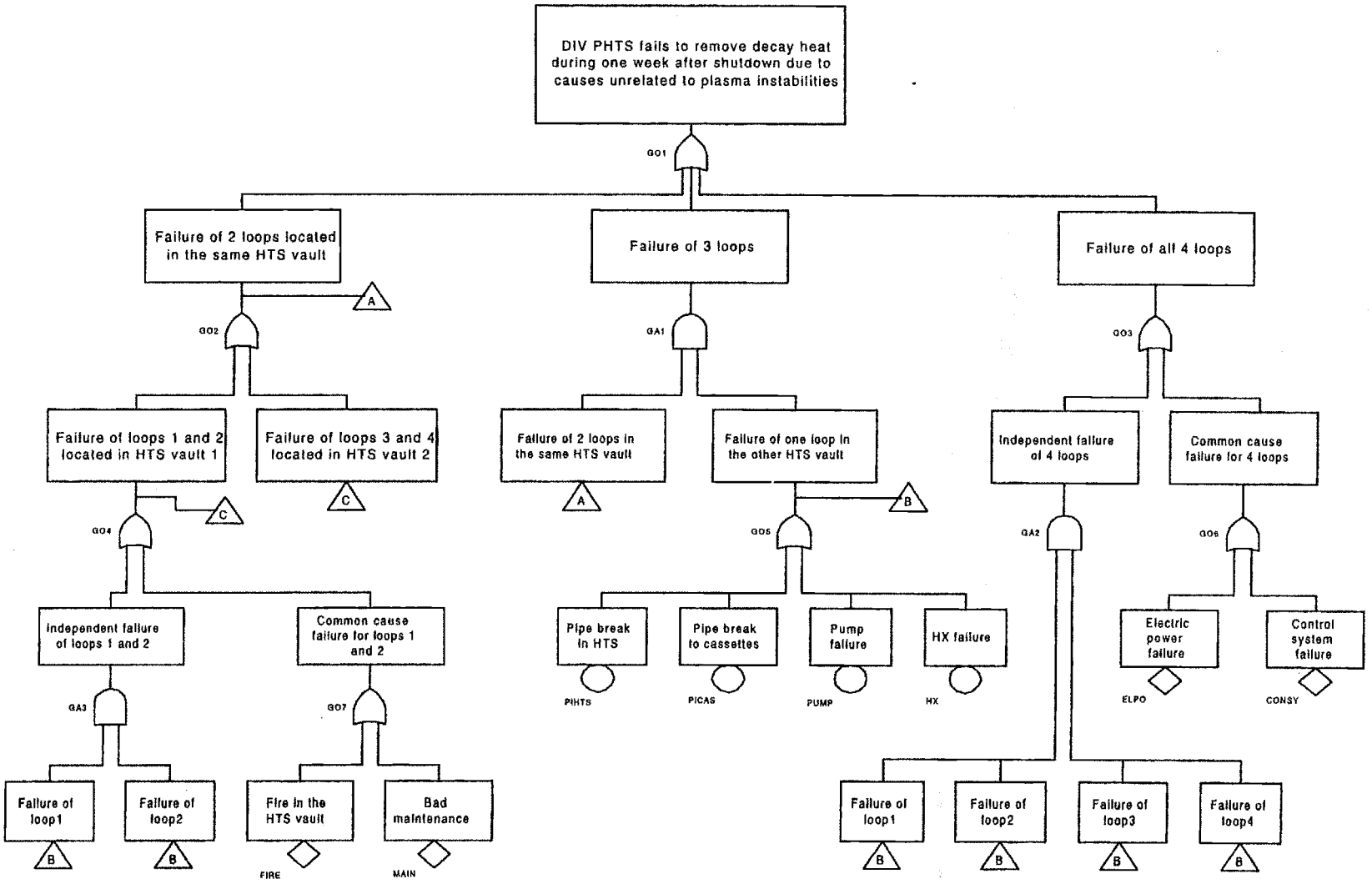

Figure D-3: Quantified Fault Tree for DIV PHTS Failure

Appendix E: Single Attribute Utility Functions

The single attribute utility function in Visual Basic language is defined below [8-14]:

```
Function utility(x, a, b, r, c)
If ((b - a) < 0 Or r < 0 Or r > 1 Or c < -1 Or c > 1 Or b < 0 Or a < 0) Then
utility = "check parameters"
Else
   M = a + r * (b - a)
   '
   If c < 0 Then
      h = c * (1 - r)
   Else
      h = c * r
   End If
   '
   If x < a Then
      linear = 1
   Else
      If (x > b) Then
         linear = 0
      Else
         linear = 1 - (x - a) / (b - a)
      End If
   End If
   '
   If ((x < a) Or (x > b)) Then
      triang = 0
   Else
      If (x < M) Then
         triang = h * ((x - a) / (M - a))
      Else
         triang = h * ((b - x) / (b - M))
      End If
   End If
   '
   utility = linear + triang
   '
End If
End Function
```

Construction Cost

Table E-1: Single Attribute Utility Function Parameters for Construction Cost

Single Attribute Utility Function Parameters	
a	200 [$M]
b	500 [$M]
r	0.5
c	0.5

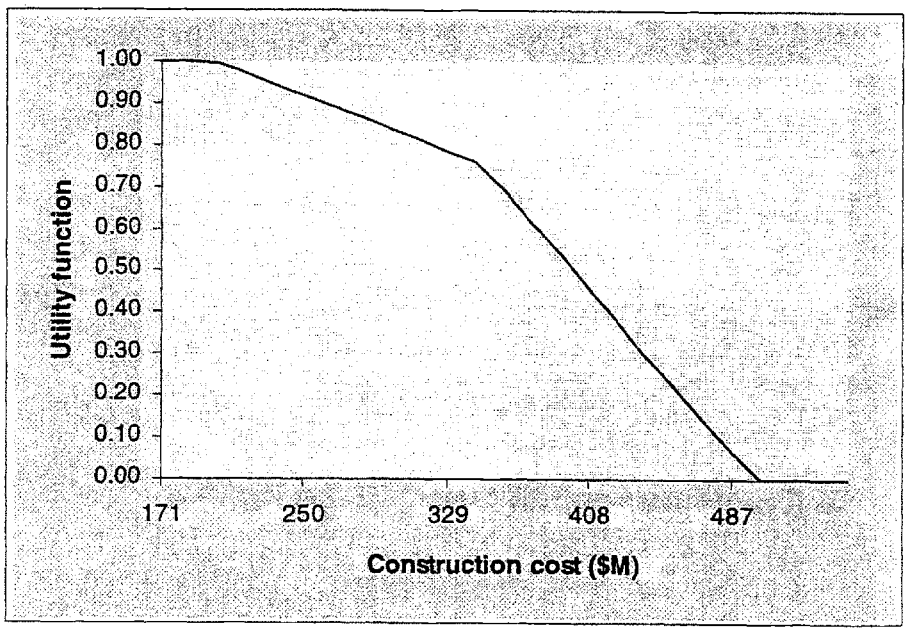

Figure E-1: Utility Function for Construction Cost

Constructibility

Table E-2: Single Attribute Utility Function Parameters for Constructibility

Single Attribute Utility Function Parameters	
a	0
b	5
r	0.5
c	0.5

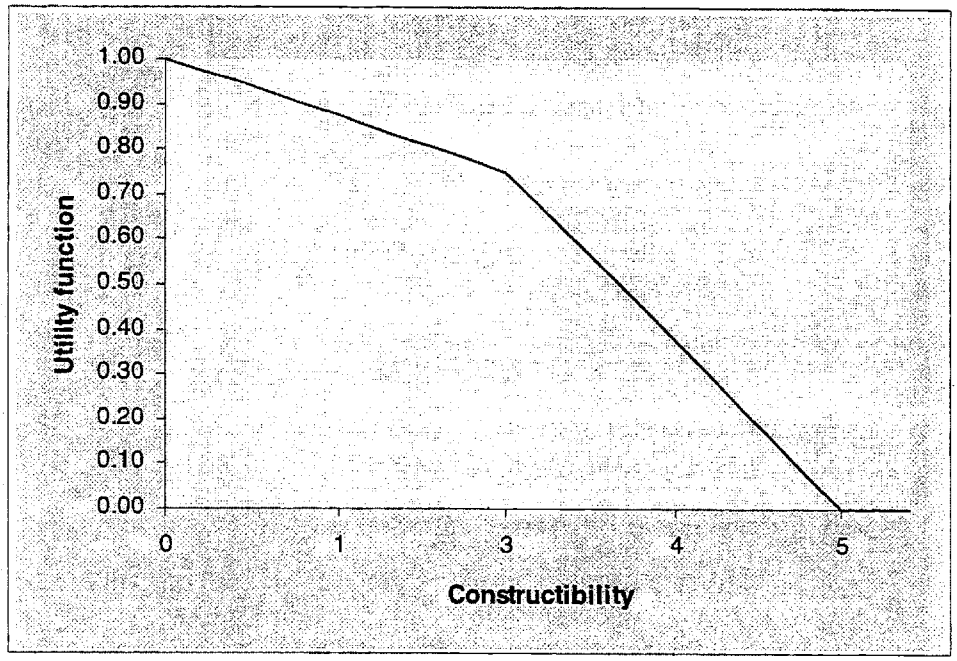

Figure E-2: Utility Function for Constructibility

Project Completion Time

Table E-3: Single Attribute Utility Function Parameters for Project Completion Time

Single Attribute Utility Function Parameters	
a	9 [yr]
b	15 [yr]
r	0.5
c	0.5

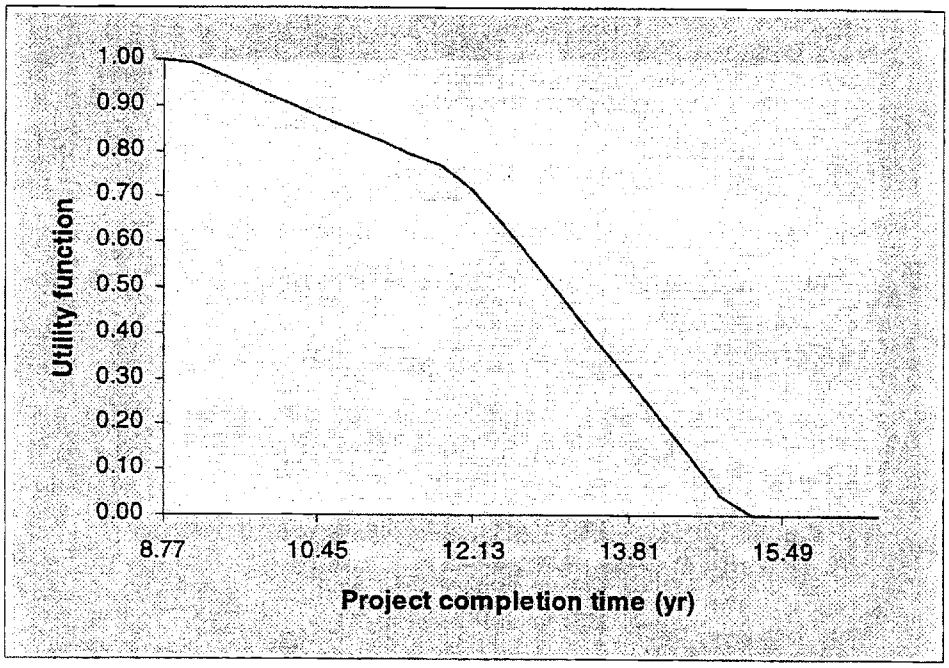

Figure E-3: Utility Function for Project Completion Time

Public Attitude

Table E-4: Single Attribute Utility Function Parameters for Public Attitude

Single Attribute Utility Function Parameters	
a	1
b	10
r	0.5
c	0.5

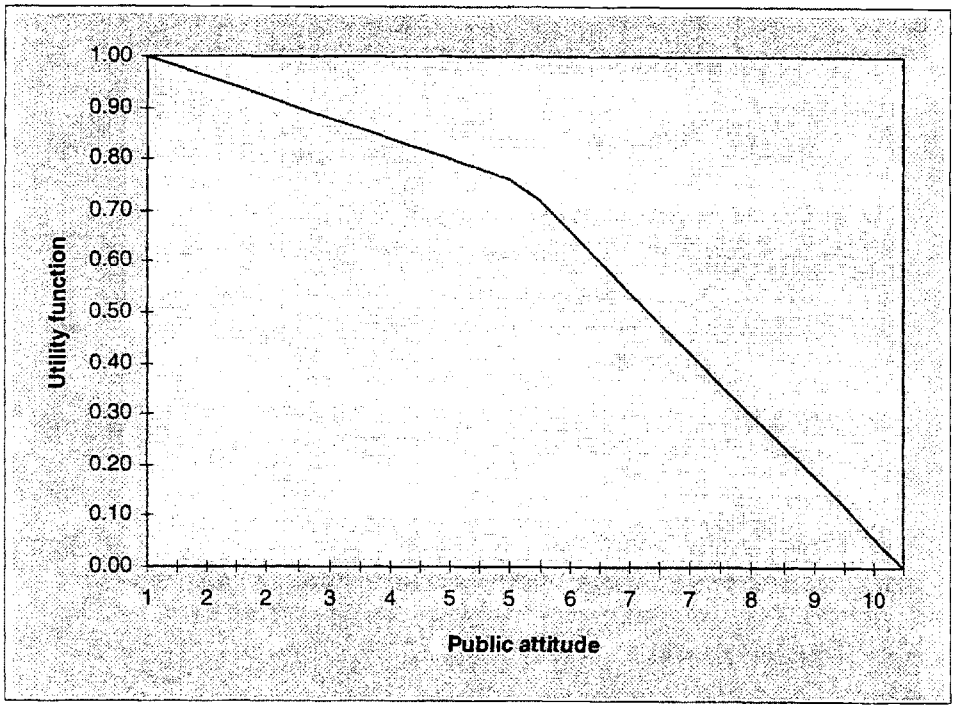

Figure E-4: Utility Function for Public Attitude

Radiological Confinement

Table E-5: Single Attribute Utility Function Parameters for Radiological Confinement

Single Attribute Utility Function Parameters	
a	0 [grams]
b	4110 [grams]
r	0.5
c	0.7

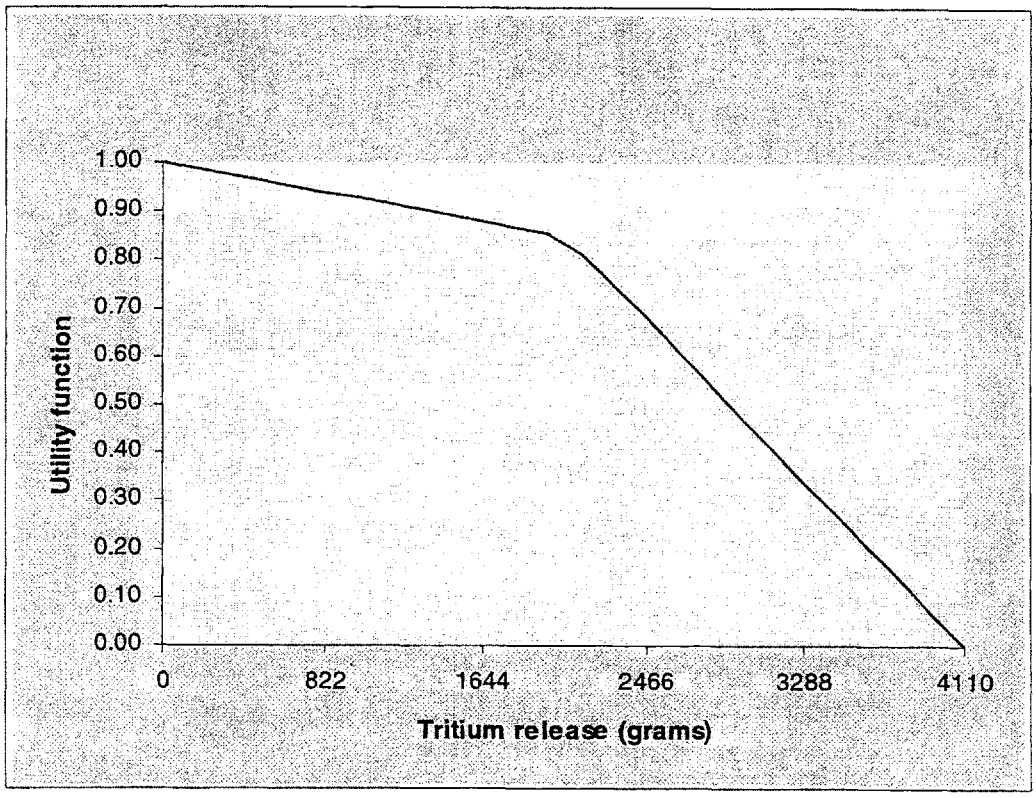

Figure E-5: Utility Function for Radiological Confinement

Appendix F: Visual Basic Functions for K Factor and Multi-attribute Utility Function

The K factor is calculated in EXCEL as a function of k_i factors using the following Visual Basic function:

```
Function findK(kArray)
   xacc = 0.0000001
   xacc2 = 0.02
   MAXIT = 500
   a = -1.000000001
   b = -0.00001
   c = 0.000001
   d = 100000

theSum = Application.Sum(kArray)
If theSum <= (1 - xacc2) Then
fl = bigK(c, kArray)
Do While fl * bigK(d, kArray) < 0
d = 0.8 * d
Loop
d = d / 0.8
findK = findBigK(c, d, kArray, MAXIT, xacc)
Else
   If theSum >= (1 + xacc2) Then
   findK = findBigK(a, b, kArray, MAXIT, xacc)
   Else
      If Abs(theSum - 1) < xacc2 Then findK = 0
   End If
End If
End Function

Function bigK(K, kArray)
Product = 1
For Each x In kArray
Product = Product * (K * x + 1)
Next x
bigK = K + 1 - Product
End Function

Function findBigK(x1, x2, kArray, MAXIT, xacc)


   fl = bigK(x1, kArray)
   fh = bigK(x2, kArray)
If (fl * fh > 0) Then
findBigK = "Root must be bracketed in findBigK"
Else
   If (fl < 0) Then
      xl = x1
      xh = x2
```

```
    Else
       xl = x2
       xh = x1
       swap = fl
       fl = fh
       fh = swap
    End If
    dx = xh - xl
    j = 1
    Do While j <= MAXIT
       rtf = xl + dx * fl / (fl - fh)
       f = bigK(rtf, kArray)
       If (f < 0) Then
          del = xl - rtf
          xl = rtf
          fl = f
       Else
          del = xh - rtf
          xh = rtf
          fh = f
       End If
       dx = xh - xl
       If ((Abs(f) < xacc * xacc) Or Abs(del) < xacc) Then
       findBigK = rtf
       Exit Do
       Else
       findBigK = "Maximum number of iterations exceeded in findBigK"
       End If
       j = j + 1
     Loop

End If
End Function
```

The MAU function is calculated in EXCEL as a function of K and k_i factors using the following Visual Basic function:

```
Function MAU(kArray, uArray, K)
  If K = 0 Then
    N = 0
    For Each x In kArray
      N = N + 1
    Next x
    MAU = 0
    i = 1
    For i = 1 To N Step 1
      MAU = MAU + (kArray(i) * uArray(i))
    Next i
  Else
    N = 0
    For Each x In kArray
      N = N + 1
    Next x
    MAU = 1
    i = 1
    For i = 1 To N Step 1
      MAU = MAU * (K * kArray(i) * uArray(i) + 1)
    Next i
    MAU = (MAU - 1) / K
  End If
End Function
```

Appendix G: MATHCAD File for Response Surface Coefficients of Gamma Distribution Parameters for Frequency Distribution of Tritium Releases

$p0\_7 := 0.01$ $p0\_9 := 0.5$ $rf0\_22 := 0.1$

$p1\_7 := 10^{-6}$ $p1\_9 := 10^{-6}$ $rf1\_22 := 0$

$p2\_7 := 0.9$ $p2\_9 := 0.9$ $rf2\_22 := 0.9$

$a0 := 0.00548$ $b0 := 525$

$a1\_7 := 0.00554$ $b1\_7 := 518$

$a2\_7 := 0.0034$ $b2\_7 := 102$

$a1\_9 := 0.00793$ $b1\_9 := 188$

$a2\_9 := 0.0693$ $b2\_9 := 625$

$a1\_22 := 0.0122$ $b1\_22 := 538$

$a2\_22 := 0.00406$ $b2\_22 := 160$

$a11\_7a9 := 0.00855$ $b11\_7a9 := 173$

$a11\_7a22 := 0.00546$ $b11\_7a22 := 577$

$a11\_9a22 := 0.00809$ $b11\_9a22 := 196$

$Aa := a0$ $\quad Aa = 0.00548$

$$R1\_7a := \frac{a1\_7 - a0}{(p1\_7 - p0\_7)\cdot(p1\_7 - p2\_7)} \quad R1\_7a = 0.006667$$

$$R2\_7a := \frac{a2\_7 - a0}{(p2\_7 - p0\_7)\cdot(p2\_7 - p1\_7)} \quad R2\_7a = -0.002597$$

$$R1\_9a := \frac{a1\_9 - a0}{(p1\_9 - p0\_9)\cdot(p1\_9 - p2\_9)} \quad R1\_9a = 0.005444$$

$$R2\_9a := \frac{a2\_9 - a0}{(p2\_9 - p0\_9)\cdot(p2\_9 - p1\_9)} \quad R2\_9a = 0.177278$$

$$R1\_22a := \frac{a1\_22 - a0}{(rf1\_22 - rf0\_22)\cdot(rf1\_22 - rf2\_22)} \quad R1\_22a = 0.074667$$

$$R2\_22a := \frac{a2\_22 - a0}{(rf2\_22 - rf0\_22)\cdot(rf2\_22 - rf1\_22)} \quad R2\_22a = -0.001972$$

$B\_7a := R1\_7a\cdot(p0\_7 - p2\_7) + R2\_7a\cdot(p0\_7 - p1\_7)$ $\quad B\_7a = -0.00596$

$B\_9a := R1\_9a\cdot(p0\_9 - p2\_9) + R2\_9a\cdot(p0\_9 - p1\_9)$ $\quad B\_9a = 0.086461$

$B\_22a := R1\_22a\cdot(rf0\_22 - rf2\_22) + R2\_22a\cdot(rf0\_22 - rf1\_22)$ $\quad B\_22a = -0.059931$

$C\_7a := R1\_7a + R2\_7a$ $\quad C\_7a = 0.004071$

$C\_9a := R1\_9a + R2\_9a$ $\quad C\_9a = 0.182722$

$C\_22a := R1\_22a + R2\_22a$ $\quad C\_22a = 0.072694$

$$D\_7a9a := \frac{a0 + a11\_7a9 - a1\_7 - a1\_9}{(p1\_7 - p0\_7)\cdot(p1\_9 - p0\_9)} \quad D\_7a9a = 0.112011$$

$$D\_7a22a := \frac{a0 + a11\_7a22 - a1\_7 - a1\_22}{(p1\_7 - p0\_7)\cdot(rf1\_22 - rf0\_22)} \quad D\_7a22a = -6.80068$$

$$D\_9a22a := \frac{a0 + a11\_9a22 - a1\_9 - a1\_22}{(p1\_9 - p0\_9)\cdot(rf1\_22 - rf0\_22)} \quad D\_9a22a = -0.1312$$

$$\begin{aligned} a(p7, p9, rf22) := {} & Aa \ldots \\ & + (B\_7a + C\_7a\cdot(p7 - p0\_7) + D\_7a9a\cdot(p9 - p0\_9) + D\_7a22a\cdot(rf22 - rf0\_22))\cdot(p7 - p0\_7) \ldots \\ & + (B\_9a + C\_9a\cdot(p9 - p0\_9) + D\_9a22a\cdot(rf22 - rf0\_22))\cdot(p9 - p0\_9) \ldots \\ & + (B\_22a + C\_22a\cdot(rf22 - rf0\_22))\cdot(rf22 - rf0\_22) \end{aligned}$$

$Ab := b0$ $\quad Ab = 525$

$$R1\_7b := \frac{b1\_7 - b0}{(p1\_7 - p0\_7)\cdot(p1\_7 - p2\_7)} \quad R1\_7b = -777.856428$$

$$R2\_7b := \frac{b2\_7 - b0}{(p2\_7 - p0\_7)\cdot(p2\_7 - p1\_7)} \quad R2\_7b = -528.090474$$

$$R1\_9b := \frac{b1\_9 - b0}{(p1\_9 - p0\_9)\cdot(p1\_9 - p2\_9)} \quad R1\_9b = -748.891219$$

$$R2\_9b := \frac{b2\_9 - b0}{(p2\_9 - p0\_9)\cdot(p2\_9 - p1\_9)} \quad R2\_9b = 277.778086$$

$$R1\_22b := \frac{b1\_22 - b0}{(rf1\_22 - rf0\_22)\cdot(rf1\_22 - rf2\_22)} \quad R1\_22b = 144.444444$$

$$R2\_22b := \frac{b2\_22 - b0}{(rf2\_22 - rf0\_22)\cdot(rf2\_22 - rf1\_22)} \quad R2\_22b = -506.944444$$

$B\_7b := R1\_7b\cdot(p0\_7 - p2\_7) + R2\_7b\cdot(p0\_7 - p1\_7)$ $\quad B\_7b = 687.011844$

$B\_9b := R1\_9b\cdot(p0\_9 - p2\_9) + R2\_9b\cdot(p0\_9 - p1\_9)$ $\quad B\_9b = 438.445253$

$B\_22b := R1\_22b\cdot(rf0\_22 - rf2\_22) + R2\_22b\cdot(rf0\_22 - rf1\_22)$ $\quad B\_22b = -166.25$

$C\_7b := R1\_7b + R2\_7b$ $\quad C\_7b = -1.30594710^{3}$

$C\_9b := R1\_9b + R2\_9b$ $\quad C\_9b = -471.113132$

$C\_22b := R1\_22b + R2\_22b$ $\quad C\_22b = -362.5$

$$D\_7a9b := \frac{b0 + b11\_7a9 - b1\_7 - b1\_9}{(p1\_7 - p0\_7)\cdot(p1\_9 - p0\_9)} \quad D\_7a9b = -1.6001631^{3}$$

$$D\_7a22b := \frac{b0 + b11\_7a22 - b1\_7 - b1\_22}{(p1\_7 - p0\_7)\cdot(rf1\_22 - rf0\_22)} \quad D\_7a22b = 4.600461^{4}$$

$$D\_9a22b := \frac{b0 + b11\_9a22 - b1\_9 - b1\_22}{(p1\_9 - p0\_9)\cdot(rf1\_22 - rf0\_22)} \quad D\_9a22b = -100.0002$$

$b(p7, p9, rf22) := Ab \ldots$
$+ (B\_7b + C\_7b\cdot(p7 - p0\_7) + D\_7a9b\cdot(p9 - p0\_9) + D\_7a22b\cdot(rf22 - rf0\_22))\cdot(p7 - p0\_7) \ldots$
$+ (B\_9b + C\_9b\cdot(p9 - p0\_9) + D\_9a22b\cdot(rf22 - rf0\_22))\cdot(p9 - p0\_9) \ldots$
$+ (B\_22b + C\_22b\cdot(rf22 - rf0\_22))\cdot(rf22 - rf0\_22)$

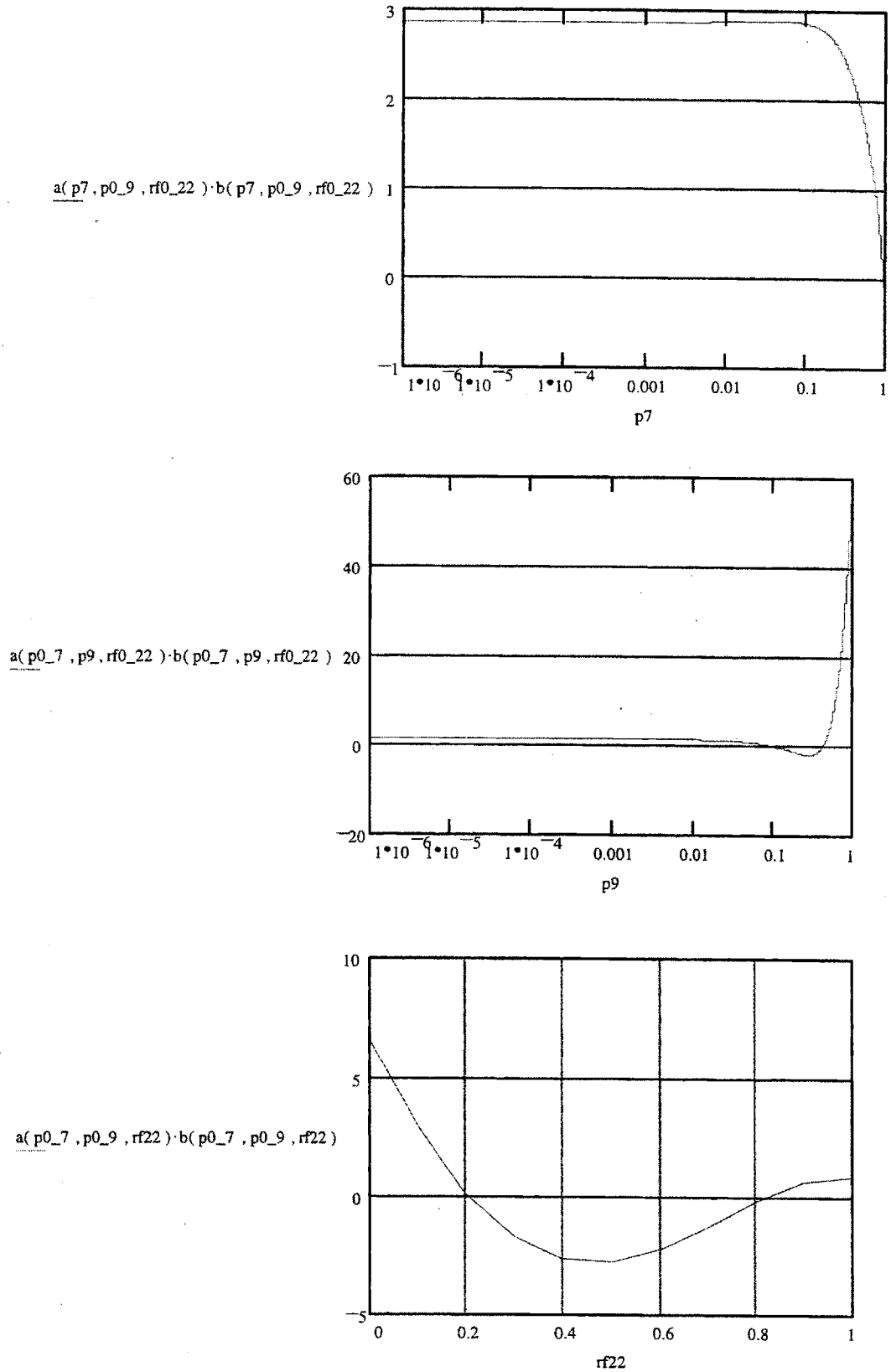

Figure G-1: Product (ab) versus each of the three parameters: p7, p9, rf22

References

1-1. S. J. Piet, S. J. Brereton, "Fusion Radioactivity Confinement and Application to Postulated ITER Accidents", EGG-FSP-9470, March, 1991;

1-2. S. J. Piet, "Implications of Probabilistic Risk Assessment for Fusion Decision Making", Fusion Technology, 1986, Vol. 10, Page 31;

1-3. "ITER Safety Approach and Systems", ITER EDA, June 5, 1995;

2-1. Interim Design Report - ITER Preliminary Safety Assessment, June 12, 1995;

2-2. Interim Design Report - ITER General Design Requirements, June 12, 1995;

2-3. Early Safety and Environmental Characterization Study (ESECS), S 81 RE 95-06-01 W 1.1;

2-4. ITER Design Description Document (DDD) 2.4 Cryostat, June 5, 1995;

2-5. ITER DDD 2.6 Primary Heat Transfer System (PHTS), June 5, 1995;

2-6. ITER DDD 1.5 Vacuum Vessel, June 5, 1995;

3-1. ITER EDA, "Early Safety and Environmental Characterization Study (ESECS)", S 81 RE 95-06-01 W 1.1, June 1995;

3-2. R. R. Fullwood, R. E. Hall, "Probabilistic Risk Assessment in the Nuclear Power Industry: Fundamentals and Applications", Pergamon Press, 1988;

3-3. A. Madrid, G. Apostolakis, R. W. Conn, "On the Development of Accident Sequences Involving Tokamak Impurity Control Systems", *Nuclear Technology/Fusion*, Vol. 4, Page 1135, September 1983;

3-4. W. M. Stacey, Jr., et al., "The US Contribution to the International Tokamak Reactor Phase 1-1 Workshop", INTOR/81-1, 1981;

3-5. "ITER Interim Design Report", June 12, 1995;

3-6. "ITER Design Description Documents", June 10, 1995;

3-7. M. Jae, G. E. Apostolakis, "The Use of Influence Diagrams for Evaluating Severe Accident Management Strategies", *Nuclear Technology*, Vol. 99, Page 142, August 1992;

3-8. Y. Hong, G. Apostolakis, "Conditional Influence Diagrams in Risk Management", *Risk Analysis*, Vol. 13, No. 6, Page 625, 1993;

3-9. R. D. Shachter, "Evaluating Influence Diagrams", *Operations Research*, Vol. 34, No. 6, Page 871, November-December 1986;

3-10. R. D. Shachter, "Probabilistic Inference and Influence Diagrams", *Operations Research*, Vol. 36, No. 4, Page 589, July-August 1988;

3-11. "DPL Advanced Version: Decision Analysis Software for Microsoft Windows", Users Guide, ADA Decision Systems, 1995;

3-12. F. R. Farmer, "Reactor safety and siting: a proposed risk criterion", *Nuclear Safety*, vol. 8, no. 6, pp. 539-547, Nov.-Dec. 1967;

3-13. J. H. Bowen, "Techniques for consequences assessment", *Nuclear Engineering and Design*, vol. 13, pp. 236-240, 1970;
3-14. D. Okrent, "On limit-line curves in risk evaluation", Letter to the Editor, *Nuclear Technology*, vol. 27, pp. 304, 1975;
3-15. S. Kaplan, B. J. Garrick, "On the quantitative definition of risk", *Risk Analysis*, vol. 1, no. 1, pp. 11-27, 1981;
3-16. U. S. Nuclear Regulatory Commission, "Reactor Safety Study: An assessment of accident risks in U. S. commercial nuclear power plants", WASH-1400, NUREG-75/014, Oct. 1975;
3-17. D. C. Cox, P. Baybutt, "Limit lines for risk", *Nuclear Technology*, vol. 57, pp. 320-330, June 1982;
3-18. G. Ballard, "Guest Editorial: Societal Risk - Progress since Farmer", *Reliability Engineering and System Safety*, No. 39, Page 123, 1993;
3-19. E. S. Beckjord, M. A. Cunningham, J. A. Murphy, "Probabilistic Safety Assessment Development in the United States 1972-1990", *Reliability Engineering and System Safety*, No. 39, Page 159, 1993;
3-20. M. F. Versteeg, "Showing Compliance with Probabilistic Safety Criteria and Objectives", *Reliability Engineering and System Safety*, No. 28, Page 39, 1992;
3-21. B. J. Garrick, "Recent Case Studies and Advancements in Probabilistic Risk Assessment", *Risk Analysis*, Vol. 4, No. 4, Page 267, 1984;
3-22. A. C. Cullen, "Measures of Compounding Conservatism in Probabilistic Risk Assessment", *Risk Analysis*, Vol. 14, No. 4, Page 389, 1994;
3-23. G. Apostolakis, S. Kaplan, "Pitfalls in Risk Calculations", *Reliability Engineering*, Vol. 2, Page 135, 1981;
3-24. G. Cambi, G. Cavallone, S. Ciattaglia, M. Costa, "ENEA Fusion Plant Safety Assessment (EFPSA) and General Methodology of Safety Analysis for Fusion Energy Systems (GEMSAFE) comparison", Doc FUS S+E TR 04/93, July 1993;
3-25. M. Modarres, "What Every Engineer should know about Reliability and Risk Analysis", New York M. Dekker, 1993;
3-26. "Probabilistic Risk Assessment (PRA) Procedures Guide", NUREG/CR-2300, Nuclear Regulatory Commission, 1983;
3-27. M. Meleis, R. C. Erdmann, "The Development of Reactor Siting Criteria Based upon Risk Probability", *Nuclear Safety*, Vol. 13, No. 1, January - February 1972;
3-28. F. R. Farmer, "Letters to the Editor", Nuclear Safety, Vol. 13, No. 5, September - October 1972;
4-1. Early Safety and Environmental Characterization Study (ESECS), ITER EDA, S 81 RE 95-06-01 W 1.1, June, 1995;
4-2. H-W. Bartels, "Decay Heat Removal and Related Design Requirements", ITER internal report, S71 RI2 27-Oct-94 W1.1, November 1994;
4-3. ITER Interim Design Report, page VI-23, June 12, 1995;
4-4. Ogawa, Kunugi, FED 29, 1995;

4-5. C. Gordon, "ITER Safety Approach and Systems", Draft for SEHD Review, June 5, 1995;
4-6. Nelson, B. Riemer, R. Sayer, D. Strickler, "Disruptions, Loads, and Dynamic Response of ITER", Paper presented at SOFE95;
4-7. M. Gaeta, "MELCOR ITER LOCA Sensitivity Calculations in Support of ESECS", ITER/US/95/TE/SA20, August 9, 1995;
4-8. ITER Design Description Document (DDD) 1.5, "Vacuum Vessel";
4-9. R. J. Thome, J. B. Czirr, J. H. Schultz, "Survey of Selected Magnet Failures and Accidents", *Fusion Technology*, Vol. 10, Page 1216, 1986;
4-10. R. Buende, "Reliability and Availability Assessment of the Next European Torus", *Fusion Technology*, Vol. 14, Page 197, 1988;
4-11. L. C. Cadwallader, S. J. Piet, "1989 Failure Rate Screening Data for Fusion Reliability and Risk Analysis", EGG-FSP-8709, September 1989;
4-12. G. Cambi, G. Cavallone, T. Palma, "Accident Scenarios for The In-Vessel Plant Area of NET-II/ITER", NET Task SEA 4.1, ENEA-DISP, 1991;
4-13. Lee Cadwallader, Personal Communications;
4-14. G. Cambi, G. Cavallone, S. Ciattaglia, "ENEA Fusion Plant Safety Assessment (EFSPA) and General Methodology of Safety Analysis for Fusion Energy Systems (t) comparison", DOC FUS S+E TR 04/93, July 1993;
4-15. L. Topilski, "Magnet System Accident Scenarios", Safety and Environment Homework Task 1, Kurchatov Institute of Atomic Energy, Moscow, July 1990;
4-16. S. Ciattaglia, G. Cambi, M. T. Porfiri, "Accident Scenarios Identification for the Main Reactor Systems", SEAFP/R-A1/6(94), Rev. 1, June 1994;
4-17. Y. Watanebe, C. W. Maynard, Z. Musicki, "Three-state Model for Fusion Reactor Plant Availability Analysis", Fusion Technology, Vol. 10, Page 1590, November 1986;
4-18. WASH-1400, "Reactor Safety Study: An Assessment of Accident Risks in Commercial Nuclear Power Plants", NUREG-75/014, October 1975;
4-19. R. R. Fullwood, R. E. Hall, "Probabilistic Risk Assessment in the Nuclear Power Industry", Pergamon Press, 1988;
4-20. C. Rizzello, T. Pinna, M. T. Porfiri, "Ozone Hazard in the ITER Cryostat", Paper presented at SOFE95;
4-21. T. Honda, T. Uda, K. Maki, T. Ozaki, Y. Seki, I. Aoki, "Comprehensive Safety Analysis Code System for Nuclear Fusion Reactors I: Model and Analysis of Overpower Events for the International Thermonuclear Experimental Reactor", *Fusion Technology*, Vol. 25, Page 451, July 1994;
4-22. P. L. Goranson, "Hydrogen/Hydrocarbon Explosions in the ITER Vacuum Vessel", *Fusion Technology*, Vol. 21, Page 2041, May 1992;
4-23. "A Summary of Hydrogen-Air Detonation Experiments", NUREG/CR-4961, May 1989;

4-24. J. Raeder, et al., "Safety and Environmental Assessment of Fusion Power", EURFUBRU XII-217/95, June 1995;

7-1. J. K. Vaurio, C. Mueller, "Probabilistic Analysis of Liquid-Metal Fast Breeder Reactor Accident Consequences with Response Surface Techniques", *Nuclear Science and Engineering*, Vol. 65, Page 401, 1978;

7-2. D. A. O'Brien, "Probabilistic Failure Analysis and its Application to Fusion Reactor First Wall Design", Ph.D. Thesis, Rensselaer Polytechnic Institute, December, 1987;

8-1. "ITER Interim Design Report", Executive Summary, June 16, 1995;

8-2. "ITER Interim Design Report", Chapter VII: ITER Construction Plan and Project Schedule, June 12, 1995;

8-3. "ITER Interim Design Report", Chapter VIII: ITER Project Cost Estimate, June 12, 1995;

8-4. The EBASCO Team, "Heavy Water Reactor Facility - Containment Analysis Report", RD Req. No. H564, H 585, U. S. Department of Energy;

8-5. "Final Report: Code Development Incorporating Environmental, Safety, and Economic Aspects of Fusion Reactors (FY 92-94)", Fusion Environmental and Safety Group, Berkeley Fusion Engineering, UC-BFE-043, November 1, 1994;

8-6. "Safety, Environmental Impact, and Economic Prospects of Nuclear Fusion", Plenum Press, New York, 1990;

8-7. "ITER Safety", *ITER Documentation Series*, No. 36, IAEA, Vienna, 1991;

8-8. G. D. Zakaib, P. D. Stevens-Guille, "Ontario Hydro's Containment Testing Program - Practice, Performance, and Direction", *Nuclear Containment - Proceedings of an International Conference organized by the Institution of Nuclear Engineers*, 1988;

8-9. R. T. Clemen, "Making Hard Decisions", PWS-KENT, 1990;

8-10. R. L. Keeney, H. Raiffa, "Decisions with Multiple Objectives", John Wiley & Sons, Inc., 1976;

8-11. K. L. Yuracko, "Transporting Spent Nuclear Fuel: A Framework for Decision-Making", Ph.D. Thesis, 1990;

8-12. R. de Neufville, "Applied Systems Analysis: Engineering Planning and Technology Management", McGraw-Hill, Inc., 1990;

8-13. "BestFit", Version 1.12a, September 1994, Palisade Corporation;

8-14. Florinel Morosan, "Evaluation of Hanford Defense Nuclear Waste Remediation Strategies", Ph.D. Thesis in progress, MIT;

8-15. Ruxandra Golinescu, Florinel Morosan, "What Type of a Containment Building should a Fusion Reactor have?", Decision Analysis (Course 15.065) Term Project, December 1994;

8-16. ITER DDD 6.2 Buildings, June 5, 1995;

8-17. R. A. Knief, "Nuclear Engineering: Theory and Technology of Commercial Nuclear Power", Hemisphere Publishing Corporation, Second Edition, 1992;